ISSN 2310-5607

PREMIER Publishing

Austrian Journal of Technical and Natural Sciences

Premier Publishing s.r.o.

2025
7-8

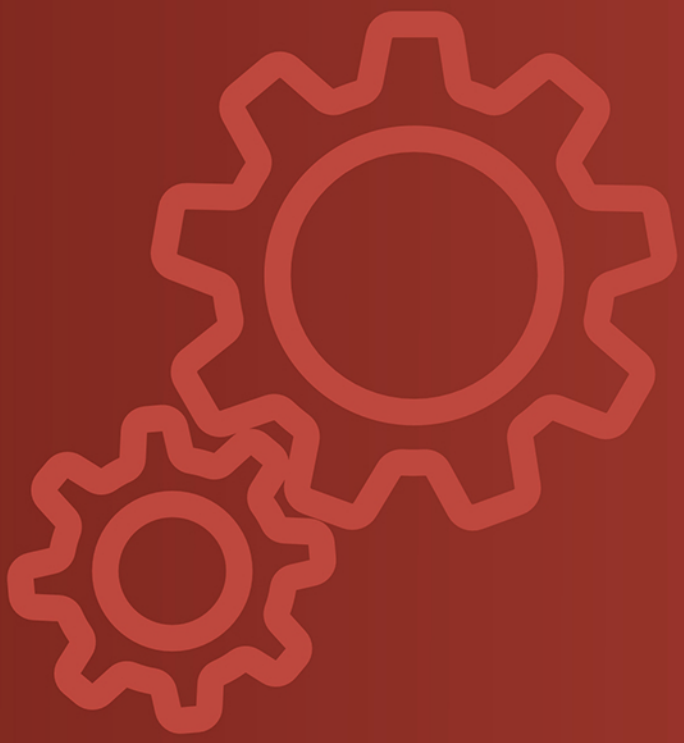

Austrian Journal of Technical and Natural Sciences

2025, No 7–8

PREMIER Publishing

Vienna
2025

Austrian Journal of Technical and Natural Sciences

Scientific journal

№ 7–8 2025

ISSN 2310-5607

Proofreading Kristin Theissen
Cover design Andreas Vogel
Additional design Stephan Friedman
Editorial office Premier Publishing s.r.o.
Praha 8 – Karlín, Lyčkovo nám. 508/7, PSČ 18600
E-mail: pub@ppublishing.org
Homepage: ppublishing.org

Austrian Journal of Technical and Natural Sciences is an international, English language, peer-reviewed journal. The journal is published in electronic form.

The decisive criterion for accepting a manuscript for publication is scientific quality. All research articles published in this journal have undergone a rigorous peer review. Based on initial screening by the editors, each paper is anonymized and reviewed by at least two anonymous referees. Recommending the articles for publishing, the reviewers confirm that in their opinion the submitted article contains important or new scientific results.

Premier Publishing is not responsible for the stylistic content of the article. The responsibility for the stylistic content lies on an author of an article.

Instructions for authors

Full instructions for manuscript preparation and submission can be found through the Premier Publishing home page at: http://ppublishing.org.

Material disclaimer

The opinions expressed in the conference proceedings do not necessarily reflect those of the Premier Publishing, the editor, the editorial board, or the organization to which the authors are affiliated.

Premier Publishing is not responsible for the stylistic content of the article. The responsibility for the stylistic content lies on an author of an article.

Included to the open access repositories:

TOGETHER WE REACH THE GOAL SJIF 2024 = 6.62 (Scientific Journal Impact Factor Value for 2024).

Included to the Uzbekistan OAK journals bulletin.

The Austrian Journal of Technical and Natural Sciences, No 7–8
ISSN 2310-5607

PREMIER Publishing
ppublishing.org

Section 1. Chemistry

DOI:10.29013/AJT-25-7.8-3-7

SYNTHESIS OF ORGANOSILICINE OLIGOMER BASED ON SODIUM SILICATE

Eshmurodov Khurshid Esanberdievich [1],
Turaev Khayit Khudaynazarovich [2], ***Djalilov Abdulakhat Turapovich*** [1],
Ashurova Muborak Sherali qizi [2], ***Xodjayev Akbarali Akhmedovich*** [2]

[1] Tashkent Scientific Research Institute of Chemical Technology, Republic of Uzbekistan, Tashkent Region, Tashkent District

[2] Termez State University, Termez

Cite: *Eshmurodov Kh.E., Turaev Kh.Kh., Djalilov A.T., Ashurova M.Sh., Xodjayev A.A. (2025). Synthesis of Organosilicine Oligomer Based on Sodium Silicate. Austrian Journal of Technical and Natural Sciences 2025, No. 7–8.* https://doi.org/10.29013/AJT-25-7.8-3-7

Abstract

In this work, a study was conducted on the synthesis of high molecular weight organosilicon oligomers such as oligoethylsiloxane based on 1,2-dichloroethane and sodium metasilicate. The synthesis was carried out via a three-step nucleophilic displacement and condensation reaction in the presence of ethylene glycol, in a dimethylsulfoxide (DMSO) solvent, and in an autoclave using potassium hydroxide as a catalyst. The structure of the resulting oligomer was confirmed by FTIR analysis, and its thermal stability was determined by TGA/DTA. The resulting oligomer has hydrophobic properties and can be used in the separation of oil-water mixtures and in the biomedical field.

Keywords: *1,2-dichloroethane, sodium silicate, ethylene glycol, organosilicon oligomer, oligoethylsiloxane, nucleophilic substitution, condensation reaction, dimethylsulfoxide (DMSO), potassium hydroxide (KOH), autoclave synthesis, thermal stability, hydrophobicity, FTIR spectroscopy, TGA/DTA, environmental safety*

1. Introduction

In recent years, the separation of oil-water mixtures has become a pressing global issue due to the severe environmental damage caused by oil pollution. To address this problem, various functional materials, particularly polyurethane and silicon-based nanocomposites, have been successfully developed. The affordability, durability, and excellent mechanical properties of these materials have further increased interest in them (Liu, Lb & Guo, Gailan & Dang, Zhao & Wenyuan, Fang. 2017). Silicon (IV) oxide nanoparticles, synthesized from materials

such as sodium silicate or tetraethoxysilane (TEOS) using the sol-gel method, are widely used to create hydrophobic and superhydrophilic surfaces. In this process, the influence of electrolytes on particle morphology, as well as the roles of surfactants and solvents, are of significant importance (Valdez salas, Benjamin & Salazar Navarro, Alexis. 2022, 7). For instance, amorphous silicon nanoparticles have been synthesized from sodium silicate in a water-ethanol mixture with low ethanol concentration, controlling the condensation rate, and the process was stabilized by boiling at 95°C for one hour, which does not require high temperatures ((Valdez salas, Benjamin & Salazar Navarro, Alexis. 2022). Additionally, hydrophobic silicon nanoparticles have been synthesized using sodium silicate and trimethylchlorosilane, applied to filter paper and polyurethane foams via a dipping technique, resulting in superhydrophobic/superoleophilic surfaces with water contact angles of ~155° and <5°, demonstrating high efficiency in gravitational oil-water separation (Zulfiqar, Usama & Hussain, Syed Zajif & Khan, Sharjeel Ahmed. 2017).

Furthermore, polyurethane-based materials are gaining special attention in oil-water separation due to their affordability, durability, and mechanical properties (Liu, Lb & Guo, Gailan & Dang, Zhao & Wenyuan, Fang. 2017). Hyperbranched polyurethane (HBPU) and fluorine-modified silicon (F-SiO_2) composite membranes, produced using electrospinning techniques, can transition from superhydrophobicity to superhydrophilicity through plasma treatment, exhibiting variable wetting properties. These membranes have proven effective in separating water-oil and oil-water emulsions stabilized with surfactants (Liu, Lb & Wenyuan, Fang & Guo, Gailan. 2017; Wenyuan, Fang & Liu, Lb & Guo, Gailan. 2017). Additionally, fluorine-free, pH-sensitive polymers and silicon-based coatings have been used for the continuous separation of three-phase oil-water-oil mixtures and emulsion filtration. These coatings stand out for their cost-effective preparation process and environmental friendliness (Dang, Zhao & Liu, Lb & Li, Yan & Xiang, Yu & Guo, Gailan. 2016).

Silicon nanoparticles are also widely applied in the medical field. For example, amorphous silicon nanoparticles have been synthesized through the hydrolysis of TEOS in ethanol, with their properties studied using surfactants such as cetyltrimethylammonium bromide (STAB) and polyvinylpyrrolidone (PVP). These particles, measuring 198 nm, have demonstrated biocompatibility and drug-carrier properties confirmed by MTT assays (Ashour, Mohamed & Soliman, Islam & Mabrouk, Mostafa & Beherei, Hanan & tohamy, Khairy. 2020). Furthermore, chitosan and its oligomer (COS) have been functionalized with silicon nanoparticles to synthesize nanosystems with antibacterial properties. COS-SiNPs systems, with sizes of 139–251 nm and zeta potentials of 30–34 mV, exhibited high antibacterial activity against Escherichia coli and Staphylococcus aureus (Salazar Navarro, Alexis & Rivera-Reyna, Nallely & gonzalez-mendoza, Daniel. 2023). Chitosan oligomers (OCS) were synthesized via microwave oxidation with hydrogen peroxide (H_2O_2), optimizing their molecular weight and deacetylation degree. The minimum inhibitory concentration (MIC) and minimum bactericidal concentration (MBC) of OCS ranged from 3.75––15 mg/ml, confirming their potential use in wound healing (Doan, Vinh & Ly, Loan Khanh & Tran, Nam & Ho, Trinh & Ho, Minh & Ngoc, Nhi & Chang, Cheng-Chung & Nguyen, Hoai & Phuong Thu, Ha & Tran, Quyen & Tran, Lam & Vo, Toi & Nguyen, Thi. 2021). These studies highlight the broad application of silicon-based materials in oil-water separation and biomedical fields, emphasizing their importance in ensuring ecological sustainability. The aim of this study was to synthesize organosilicon compounds, such as ethylsiloxane, using 1,2-dichloroethane ($C_2H_4Cl_2$) and sodium silicate (Na_2SiO_3).

2. Materials and methods

The study utilized 1,2-dichloroethane (99%), anhydrous sodium silicate (99%), ethylene glycol (99%), anhydrous dimethyl sulfoxide (DMSO, 99.8%) as a solvent, and copper (I) iodide and potassium hydroxide as catalysts. FTIR spectroscopy and thermogravimetric/differential thermal analysis methods were employed.

Experimental part. The synthesis of an organosilicon oligomer, specifically oligoethylsiloxane, was carried out via a nucleophilic substitution reaction between 1,2-dichloroethane ($C_2H_4Cl_2$) and anhydrous sodium silicate (Na_2SiO_3), with ethylene glycol as an additional monomer. The experiment was conducted in a 150 ml stainless steel autoclave capable of withstanding 10 atm pressure. Reagents were used in a 1,2-dichloroethane:sodium silicate:ethylene glycol molar ratio of 1:2:1. Initially, the reagents were dissolved in DMSO solvent and mixed for 15 minutes at 600 rpm using a magnetic stirrer to ensure a homogeneous reaction environment. The resulting mixture was placed in the autoclave, securely sealed, and maintained at 100 ± 5 °C under 3–5 atm pressure for 6–8 hours. After the reaction, the autoclave was cooled to room temperature, and the mixture was filtered using a vacuum filter, with sodium chloride residues washed away. The obtained product was dried in an oven at 80 °C for 12 hours. The bonds and functional groups in the oligomer product were analyzed using infrared spectroscopy, while its thermal stability was assessed with thermogravimetric/differential thermal analysis. The synthesis yielded oligoethylsiloxane with a 75–90% yield, exhibiting hydrophobic properties (contact angle >90°).

3. Results

The synthesis of oligoethylsiloxane resulted in a yield of 75–90%, exhibiting hydrophobic properties with a water contact angle of 92–110°. Table 1 presents the reaction conditions and results, with experiments conducted at 80 °C and 100 °C temperatures, using molar ratios of $C_2H_4Cl_2$:Na_2SiO_3:HO-CH_2CH_2-OH at 1:1:1 and 1:2:1, and 0.5% CuI as a catalyst. The optimal conditions, achieved at 100 °C with a 1:2:1 ratio over 6–8 hours, provided a 90% yield. FTIR spectroscopy revealed Si-O-C and Si-O-Si (1000–1050 cm^{-1}) bonds in the 1080––1100 cm^{-1} region. TGA/DTA analysis indicated a mass loss of less than 8% up to 300 °C, confirming high thermal stability (Figure 1). Hydrophobicity tests demonstrated that the oligomer achieved 95% efficiency in separating oil-water mixtures.

Table 1. *Reaction conditions and results*

Experiments	Mol ratio*	Temperature (°C)	Catalyst (CuI, %)	Reaction time (hours)	Yield (%)
1	1:1:1	80	0.5	6	75
2	1:1:1	100	0.5	6	80
3	1:2:1	80	0.5	6	82
4	1:2:1	100	0.5	8	90
5	1:2:1	80	0.3	8	78
6	1:2:1	100	0.3	8	85

** – ($C_2H_4Cl_2$:Na_2SiO_3:HO-CH_2CH_2-OH)*

As evident from Table 1, the 1:2:1 molar ratio at 100 °C with CuI catalyst over an 8-hour reaction provided the highest yield (90%). Lower temperature (80 °C) and reduced catalyst amount decreased the yield.

Figure 1 shows the TGA/DTA curves of oligoethylsiloxane. Three main temperature ranges were identified by TGA: a 16% mass loss at 25–267 °C, attributed to the evaporation of residual DMSO, moisture, and ethylene glycol; a 7.2% loss at 267–596°C, indicating the complete degradation of Si-O-C bonds and organic chains (1,2-dichloroethane and ethylene glycol residues); and a minimal 11.5% loss above 596°C, with 50–55% stable SiO_2 residues retained. These results confirm the oligomer's high stability up to 267 °C, making it suitable for use in coatings, adhesives, and composite materials.

Figure 1. *Thermal analysis of the synthesized organosilicon oligomer*

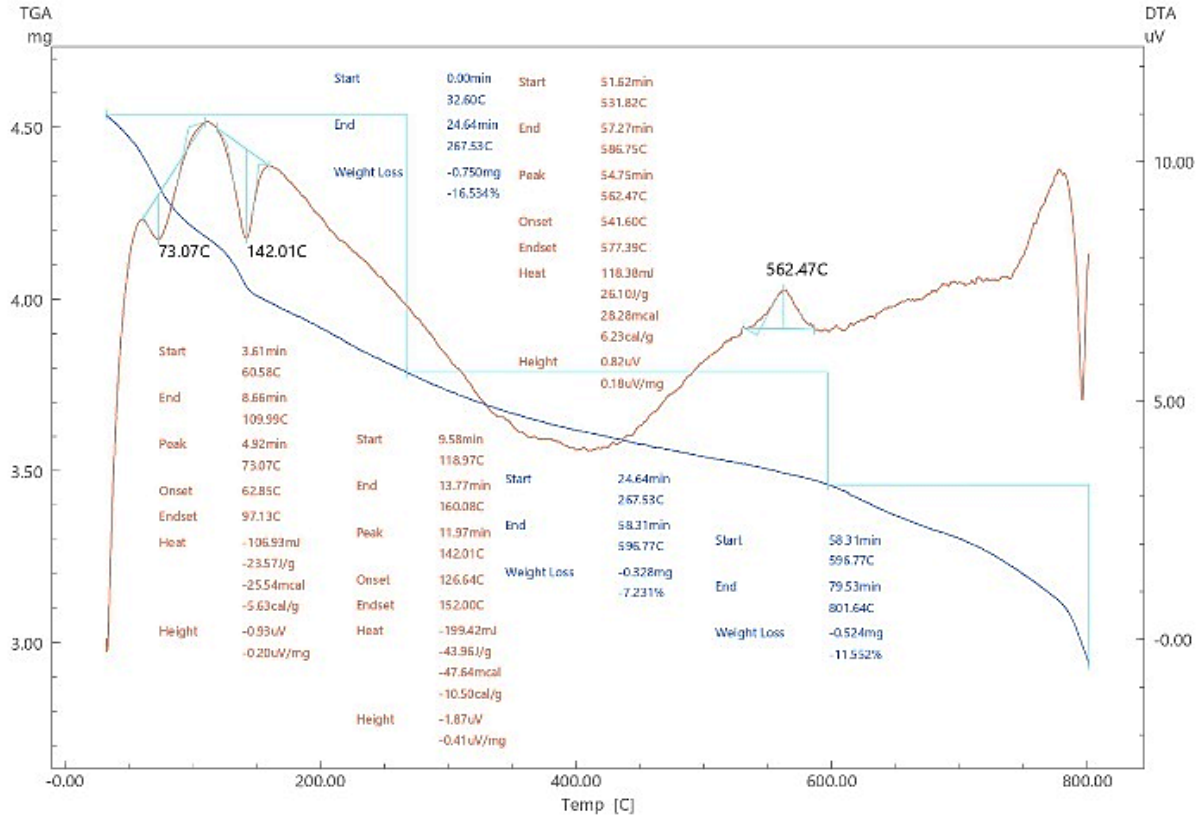

4. Discussion

The obtained oligoethylsiloxane exhibits high thermal stability and hydrophobic properties, achieving 95% efficiency in separating oil-water mixtures. These results indicate slightly lower hydrophobicity compared to silicon nanoparticles synthesized via the sol-gel method using sodium silicate (contact angle ~155°), but the absence of fluorine in this study provides an ecological advantage. The high yield (90%) of the nucleophilic substitution reaction is attributed to the effectiveness of CuI and KOH catalysts, enhanced by the high polarity of the DMSO solvent. FTIR analysis confirmed the presence of Si-O-C and Si-O-Si bonds, indicating the oligomer's siloxane chain structure.

5. Conclusion

An effective method for synthesizing oligoethylsiloxane based on 1,2-dichloroethane and sodium silicate was developed, involving nucleophilic substitution and condensation reactions conducted in an autoclave with CuI and KOH catalysts in DMSO. The resulting compound exhibits thermal stability up to 300°C and hydrophobic properties, achieving 95% efficiency in separating oil-water mixtures. FTIR analysis confirmed the siloxane structure of the new organosilicon compound.

References:

Valdez salas, Benjamin & Salazar Navarro, Alexis. (2022). Synthesis of silica nanoparticles from sodium metasilicate. International Journal of Nanoparticles. – 14. 1. 10.1504/IJNP.2022.10044641.

Zulfiqar, Usama & Hussain, Syed Zajif & Khan, Sharjeel Ahmed. (2017). Fabrication of superhydrophobic filter paper and foam for oil-water separation based on silica nanoparticles from sodium silicate. Journal of Sol-Gel Science and Technology. – 81. – P. 912-920. 10.1007/s10971-016-4250-6.

Liu, Lb & Guo, Gailan & Dang, Zhao & Wenyuan, Fang. (2017). Recent Progress of Polyurethane-Based Materials for Oil/Water Separation. Nano. – 12. 10.1142/S1793292017300018.

Liu, Lb & Wenyuan, Fang & Guo, Gailan. (2017). Tunable Wettability of Electrospun Polyurethane/Silica Composite Membranes for Effective Separation of Water-in-Oil and Oil-in-Water Emulsions. Chemistry (Weinheim an der Bergstrasse, Germany). – 23. 10.1002/chem.201701409.

Wenyuan, Fang & Liu, Lb & Guo, Gailan. (2017). Frontispiece: Tunable Wettability of Electrospun Polyurethane/Silica Composite Membranes for Effective Separation of Water-in-Oil and Oil-in-Water Emulsions. Chemistry - A European Journal. – 23. 10.1002/chem.201784764.

Dang, Zhao & Liu, Lb & Li, Yan & Xiang, Yu & Guo, Gailan. (2016). In Situ and Ex Situ pH-Responsive Coatings with Switchable Wettability for Controllable Oil/Water Separation. ACS Applied Materials & Interfaces. – 8. 10.1021/acsami.6b09381.

Ashour, Mohamed & Soliman, Islam & Mabrouk, Mostafa & Beherei, Hanan & tohamy, Khairy. (2020). Silica Nanoparticles as a Potential Carrier for Doxycycline Hyclate. Egyptian Journal of Biomedical Engineering and Biophysics. 10.21608/ejbbe.2020.40105.1034.

Salazar Navarro, Alexis & Rivera-Reyna, Nallely & gonzalez-mendoza, Daniel. (2023). Synthesis of silica chitosan oligosaccharides nanoparticles. Agro Productividad. 10.32854/agrop.v16i11.2728.

Doan, Vinh & Ly, Loan Khanh & Tran, Nam & Ho, Trinh & Ho, Minh & Ngoc, Nhi & Chang, Cheng-Chung & Nguyen, Hoai & Phuong Thu, Ha & Tran, Quyen & Tran, Lam & Vo, Toi & Nguyen, Thi. (2021). Characterizations and Antibacterial Efficacy of Chitosan Oligomers Synthesized by Microwave-Assisted Hydrogen Peroxide Oxidative Depolymerization Method for Infectious Wound Applications. Materials. – 14. 4475. 10.3390/ma14164475.

Mai, C., Militz, H. (2004). Modification of wood with silicon compounds. Treatment systems based on organic silicon compounds - a review. *Wood Sci Technol* – 37. – P. 453-461 URL: https://doi.org/10.1007/s00226-004-0225-9

Eshmurodov X.E., Turayev X.X., Djalilov A.T., Geldiyev Yu.A., Babamuratov B.E. (2020). Development of carbamide-formaldehyde resin-based glue compositions modified with silicon organic compounds // Austrian Journal of Technical and Natural Sciences. – No. 7-8.

submitted 04.08.2025;
accepted for publication 18.08.2025;
published 29.09.2025

Contact: khurshideshmurodov@mail.com; hhturaev@rambler.ru; gup_tniixt@mail.ru

The Austrian Journal of Technical and Natural Sciences, No 7–8
ISSN 2310-5607

PREMIER Publishing
ppublishing.org

DOI:10.29013/AJT-25-7.8-8-12

DEVELOPMENT OF A TECHNOLOGICAL SCHEME FOR THE SYNTHESIS OF PHENYL-3-METHYLPHENOXYPROPIONATE BY REACTION OF PHENYL-2-CHLOROPROPIONATE WITH 3-METHYLPHENOL

Ochilov Mansur [1], ***Abdushukurov Anvar Kabirovich*** [2],
Mamatkulov Nematillo Narzullaevich [2],
Rajabov Shohzodbek Holmuratovich [2]

[1] Almalyk Branch of Tashkent State Technical University named after I. Karimov, Almalyk, Republic of Uzbekistan

[2] Faculty of Chemistry, National University of Uzbekistan named after Mirzo Ulugbek, Tashkent, Republic of Uzbekistan

Cite: *Ochilov M., Abdushukurov A. K., Mamatkulov N. N., Rajabov S. H. (2025). Development of a Technological Scheme for the Synthesis of Phenyl-3-Methylphenoxypropionate by Reaction of Phenyl-2-Chloropropionate With 3-Methylphenol. Austrian Journal of Technical and Natural Sciences 2025, No 7–8.* https://doi.org/10.29013/AJT-25-7.8-8-12

Abstract

The article presents nucleophilic substitution reactions of phenyl-2-chloropropionate with 3-methylphenol under various conditions and a method for preparing phenyl-3-methylphenoxypropionate. Nucleophilic substitution reactions were carried out in the solvents benzene, acetone, dioxane, DMF (Dimethylformamide), and DMSO (Dimethyl sulfoxide). It was found that these solvents affect the duration and yield of the reaction. In the reaction, phenyl-3-methylphenoxypropionate was obtained in a DMSO solution with a yield of 83%. A technological scheme for the synthesis of phenyl-3-methylphenoxypropionate in acetone was developed. The reason is that acetone is a cheap solvent and is convenient for the industrial production of organic substances. The structure of the synthesized new organic substance, phenyl-3-methylphenoxypropionate, was confirmed using modern IR, ^{1}HyAMR and 13CYaMR spectra.

Keywords: *organic synthesis, 3-methylphenol, reagent, nucleophile, substitution, extraction, solvent, synthesis, analysis, chloroacetylation, technological scheme*

Introduction

Chemists are conducting scientific research to find a simple way to obtain new organic substances through simple and basic organic synthesis methods and to create a technology for their production.

Currently, one of the urgent problems facing specialists is the synthesis and production of nutritional yeasts, amino acids, vitamins, enzyme preparations, antibiotics, preparations for protecting plants from pests

and diseases, etc., for the microbiology industry through organic synthesis.

Through acylation reactions of aromatic hydrocarbons, preparations against microorganisms that cause corrosion in the oil and gas industry have been synthesized, and a production technology has been created and put into practice (Ochilov M., Mamatkulov N. N., Abdushukurov A. K., 2025).

It has been found that compounds obtained by the chloroacetylation reaction of aminophenols exhibit high biological activity against gram-positive bacteria (Bacillus subtilis and Bacillus thuringiensis), gram-negative bacteria (Escherichia coli and Pseudomonas aeruginosa), and fungi Fusarium oxysporum and Botrytis fabae (Abdushukurov A. K., Yusufov M. S., 2020).

Substances synthesized by chloroacetylation reactions of phenol and its derivatives have high biological activity and are widely used in pharmaceuticals as antibacterial, analgesic, and bactericidal drugs against pathogenic microorganisms (Abdushukurov A. K., Mamatkulov N. N., Ibragimov T. E., 2023). In medicine, these include immunostimulants, drugs with antidiabetic and anticancer activity (Mamatkulov N. N., Ochilov M., Tursunova D. R. 2023; Azomova G.Z., Yuldasheva M.R., Tadjimuhamedov K.S. 2020), as well as substances with high biological activity such as adrenaline, noradrenaline, and isradipine, which have been used as hormonal drugs in pharmaceuticals (Vartanyan R.S., 2005; Sibrikov S.G., 2022). Substances synthesized by acylation reactions of phenols are used in practice as stabilizers for polymers, pesticides, and dyes (Mamatkulov N.N., Yakubov L E., 2021; Mamatkulov N.N., Yakubov L. E. Madusmanova N.K., Khoshimkhanova M.A., 2021).

Materials and methods

Synthesis of phenyl-3-methylphenoxypropionate

Experiment No. 1. In a two-necked flask equipped with a reflux condenser and a stirrer, 30 ml of absolute benzene and 5.4 g (0.05 g-mol) of 3-methylphenol were dissolved. 1.15 g (0.05 g-mol) of sodium metal, free from oxide film, was added little by little to it. After the formation of sodium 3-methylphenolate slowed down, the reaction mixture was heated in a flask heater for 4 hours. Then, 9.2 g (0.05 g-mol) of phenyl-2-chloropropionate was slowly added, and the reaction mixture was boiled for 5 hours. The reaction mixture was washed with alkaline water, extracted three times with benzene, and dried with $CaCl_2$. After the benzene was pumped out in a water pump, the product was collected in a vacuum at 215-225 °C/10 mm. sim. overhead. The yield of phenyl-3-methylphenoxypropionate was 8.2 g (64%).

Experiment No. 2. 5.4 g (0.05 g-mol) of 3-methylphenol, 6.9 g (0.05 g-mol) of potassium carbonate, and 9.2 g (0.05 g-mol) of phenyl-2-chloropropionate taken for the reaction were placed in a two-necked flask equipped with a reflux condenser and a stirrer and boiled for 9 hours. A white precipitate of potassium chloride was formed during boiling. After the reaction was complete, the precipitate was separated, and the acetone was evaporated under normal conditions. The reaction mixture was washed with 5% alkaline water and extracted with benzene. After the benzene was evaporated, the reaction product was evaporated in vacuo. The yield of phenyl-3-methylphenoxypropionate was 8.4 g (66%).

Experiment No. 4. DMF was used as the solvent, and sodium 3-methylphenolate was synthesized by the reaction of 5.4 g (0.05 mol) of 3-methylphenol with 1.15 g (0.05 mol) of sodium metal. When 9.2 g (0.05 g-mol) of phenyl-2-chloropropionate was added to it, the reaction lasted for a short time of 1.5 hours. The sodium chloride salt was filtered off from the reaction mixture, and DMF was separated by distillation under normal conditions. Then the product was washed with 5% alkaline water, extracted with benzene, and dried with $CaCl_2$. First, the benzene was distilled off, then the product. The yield of phenyl-3-methylphenoxypropionate was 9.8 g (77%).

Experiment No. 5. The amount of reagents in the reaction was taken to be 0.05 mol. Sodium 3-methylphenolate was prepared in a DMSO solution. The reaction of phenyl-2-chloropropionate with 3-methylphenol lasted for 1.5 hours. After the reaction was complete, the sodium chloride was first filtered, and the DMSO was evaporated under normal conditions. The reaction product was washed with 5% alkaline water, extracted with benzene, and dried with $CaCl_2$. First, the

benzene was evaporated, then the product. The yield of phenyl-3-methylphenoxypropionate was 10.6 g (83%).

Phenyl-3-methylphenoxypropionate is a colorless liquid, and in the hexane: ethyl acetate: chloroform system in a volume ratio of 2:1:1, a single spot was observed on silifol UV-254, Rf=0.61. Its refractive index nD^{20} =

IR spectrum of phenyl-3-methylphenoxypropionate: $\nu_{C=0}$=766; $\nu_{C=C}$=592; ν_{C-O-C}=093, 1160, 1234; δ_{CH}=688 (mono alm. ben.); δ_{CH}=750 (1,3 alm. ben.); $\delta^{s}_{CH_3}$=1454; $\delta^{as}_{CH_3}$=1488; $\nu_{=CH}$=3052; $\delta^{as}_{CH_3}$=2935,2996.

1H NMR spectrum of phenyl-3-methylphenoxypropionate: δ 1.50 (3H, d, *J* = 6.9 Hz), 2.32 (3H, s), 4.82 (1H, q, *J* = 6.9 Hz), 6.79 (1H, ddd, *J* = 2.8, 2.0, 0.5 Hz), 6.85-6.99 (2H, 6.91 (ddd, *J* = = 8.0, 2.7, 2.0 Hz), 6.93 (dt, *J* = 8.2, 2.7 Hz)), 7.13-7.35 (4H, 7.20 (ddd, *J* = 8.2, 8.0, 0.5 Hz), 7.28 (tt, *J* = 7.6, 1.3 Hz), 7.29 (dtd, *J* = = 8.1, 1.3, 0.5 Hz)), 7.47 (2H, dddd, *J* = 8.1, 7.6, 1.5, 0.5 Hz).

13C NMR spectrum of phenyl-3-methylphenoxypropionate: δ 17.9 (1C, s), 21.3 (1C, s), 74.3 (1C, s), 112.4 (1C, s), 116.7 (1C, s), 121.3 (2C, s), 123.5 (1C, s), 126.2 (1C, s), 129.1 (1C, s), 129.5 (2C, s), 139.5 (1C, s), 150.6 (1C, s), 158.5 (1C, s), 168.4 (1C, s).

Results and discussion

Extensive efforts are being made worldwide to synthesize effective drugs for use in agriculture and medicine based on phenol and its derivatives, which, in turn, has led to significant progress in the creation of competitive drugs based on natural raw materials and synthetic organic chemical products, which is leading to intensive development of agriculture on a scientific basis. Scientific research has been carried out to synthesize similar competitive compounds.

Since there is no information in the literature on the nucleophilic substitution reactions of phenyl-2-phenoxypropionate with 3-methylphenol, this reaction was carried out for the first time. Benzene, acetone, dioxane, DMF DMSO were used as solvents. The reaction for the formation of phenyl-3-methylphenoxypropionate proceeded according to the following scheme:

$$3\text{-}CH_3\text{-}C_6H_4OH + 2Na \xrightarrow{\text{Solvent}} 3\text{-}CH_3\text{-}C_6H_4OH + 2Na$$

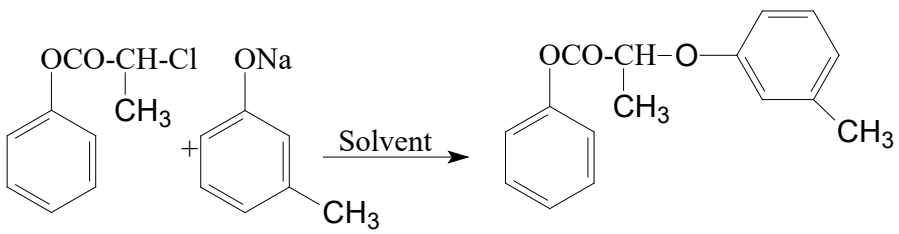

Solvent=Benzene, 1,4-Benzodioxane, DMFA,DMSO

When nucleophilic substitution reactions of phenyl-2-phenoxypropionate were carried out with 3-methylphenol in acetone solution in the presence of K2CO3, the reaction proceeded according to the following scheme.

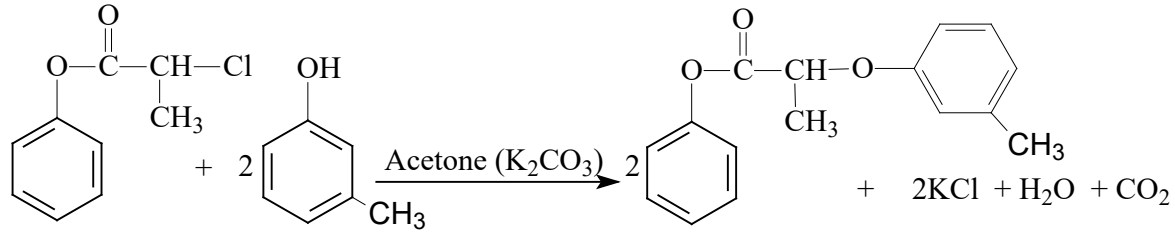

In the nucleophilic substitution reactions of phenyl-2-phenoxypropionate with 3-methylphenol, solvents affected the yield of the resulting product. In benzene solution, the reaction yield was 64%, while in DMSO solution, it was found that phenyl-3-methylphenoxypropionate was formed with a yield of 83%.

Figure 1. *Technological scheme for the synthesis of phenyl-3-methylphenoxypropionate in acetone solution*

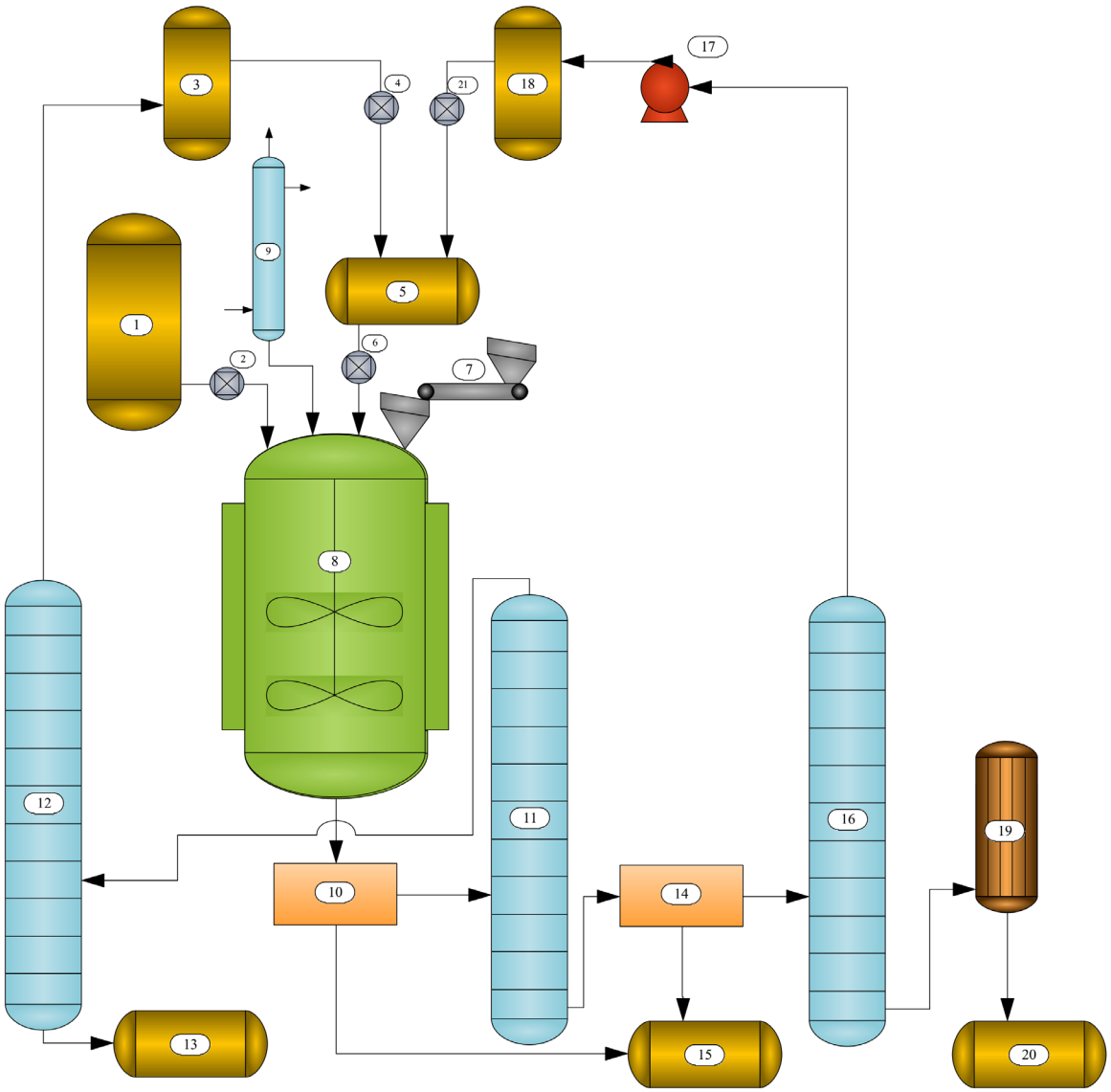

The technology of nucleophilic substitution reaction of phenyl-2-phenoxypropionate with 3-methylphenol in acetone solvent to form phenyl-3-methylphenoxypropionate was developed.

The synthesis of phenyl-4-methoxyphenoxypropionate was carried out according to the following technological scheme. Phenyl-2-chloropropionate is fed from the tank (pos 1) through a rheometer (pos 2) into a reactor (pos 8) equipped with a mixer. From the tank for acetone (pos 3) through a rheometer (pos 4), 4-methoxyphenol and acetone are fed from the mixing unit (pos 5) through a rheometer (pos 6) into the reactor (pos 8). Crushed K_2CO_3 is fed from the ribbon saturator (pos 7) through a funnel into the reactor (pos 8). During the reaction, volatile substances formed are cooled in a cooler (pos 9) installed at the top of the reactor (pos 8). The reaction mixture enters the filter (pos. 10) and from there passes to the distillation column (pos. 11).

From the top of the distillation column (pos. 11), the acetone and water mixture is sent to the next distillation column (pos. 12). From the distillation column (pos. 12), acetone is returned to the process, and the remaining water is collected in the water tank (pos. 13). The reaction mixture purified from acetone and water is transferred from the distillation column (pos. 11) to the

filter (pos. 14) and collected in the KCl tank (pos. 15). The reaction mixture is sent from the filter (pos. 14) to the distillation column (pos. 16). From the top of the column, 4-methoxyphenol is sent to the tank (pos. 18) via a pump (pos. 17) and 4-methoxyphenol is returned to the process. The remaining phenyl-4-methoxyphenoxypropionate from the distillation column (item 16) was purified by vacuum evaporation (item 19) and collected in a phenyl-4-methoxyphenoxypropionate (item 20) container.

References

Ochilov M., Mamatkulov N. N., Abdushukurov A. K. Synthesis, characteristics and development of a process flow chart for obtaining phenyl 2-phenoxypropionate in an acetone medium // Universum: technical sciences: electronic scientific journal. 2025. – 8(137). – P. 60-65. URL: https://7universum.com/ru/tech/archive/item/20690.

Abdushukurov A. K., Yusufov M. S. Study of the reaction of isomeric aminophenols with chloroacetyl chloride // Universum: Technical sciences: electronic scientific journal. 2020. – No. 3(72). – P. 74-75. URL: http://7universum.com/ru/tech/archive/item/9096.

Abdushukurov A. K., Mamatkulov N. N., Ibragimov T. E. 2-Isopropyl-5-Methylphenylchloroacetate Synthesis Method // Web of Synergy:International Interdisciplinary Research Journal. Volume 2. Issue 4. Year, 2023. – P. 687–691.

Mamatkulov N. N., Ochilov M., Tursunova D. R. 5- Methyl -2-(1-Methylethyl) Phenol with Chloroacetyl Chloride under Alkaline Conditions// Web of Semantic: Universal Journal on Ie Education. Volume 2. Issue 4. Year 2023. – P. 73-76.

Azomova G. Z., Yuldasheva M. R., Tadjimuhamedov K. S. Influnce of a nanostructural catalyst in the synthesis of allulnaphthols//Austrian jurnal of technical and natural sciences. №5-6. Vena, 2020. – P. 32-36.

Vartanyan R. S. Synthesis of essential drugs. – Moscow: MIA, 2005. – 180 p.

Sibrikov S. G. Pathways of pesticide transformation in living organisms. Moscow: – (reprinted 2022). – 220 p.

Mamatkulov N. N., Yakubov L E. Synthesis of o-tolylphenoxyastatin through a nucleophilic substitution reaction from o-toluoyl chloride and examination of its biological activity // Nat. Volatiles & Essent. Oils, 2021. – № 8(5). – P. 12125-12131.

Mamatkulov N. N., Yakubov L. E. Madusmanova N. K., Khoshimkhanova M. A. Method for the Synthesis and Bioavailability of Phenol-4-Methoxyphenoxy-acetate by Nucleophilic Exchange Reaction // Nat. Volatiles & Essent. Oils, 2021. – No. 8(5). – P. 12140–12144.

submitted 15.08.2025;
accepted for publication 31.08.2025;
published 29.09.2025

Contact: mansurochilov2003@gmail.com; abdushukurov-ximik@mail.ru;
nematillomamatqulov767@gmail.com; shohzodbekrajabov99@gmail.com

The Austrian Journal of Technical and Natural Sciences, No 7–8
ISSN 2310-5607

PREMIER Publishing
ppublishing.org

DOI:10.29013/AJT-25-7.8-13-17

SYNTHESIS OF AN INHIBITOR AND ANALYSIS OF ITS PROPERTIES FOR MITIGATING ACID CORROSION IN THE OIL AND GAS INDUSTRY

Olimov Bobir Bahodirovich [1]

[1] Bukhara state technical university, Department of technology of the chemistry

Cite: *Olimov B.B. (2025). Synthesis of an Inhibitor and Analysis of Its Properties for Mitigating Acid Corrosion in the Oil and Gas Industry. Austrian Journal of Technical and Natural Sciences 2025, No 7–8.* https://doi.org/10.29013/AJT-25-7.8-13-17

Abstract

This article presents the synthesis of a cost-effective, efficient, and environmentally friendly corrosion inhibitor, along with an analysis of its inhibitive properties. The inhibitor was synthesized using linear alkylbenzene sulfonic acid (LABSA), urea, and phosphoric acid. The resulting compound was tested for its ability to protect against acid-induced corrosion, particularly in hydrochloric acid (HCl) solutions, relevant to the oil and gas industry. The molecular weight of the synthesized substance was determined using the cryoscopic method, while its inhibitory performance was evaluated through gravimetric analysis. The inhibitor demonstrated high corrosion protection efficiency, and its synthesis from locally available raw materials makes it economically advantageous.

Keywords: *corrosion, inhibitor, LABSA (dodecylbenzenesulfonic acid), urea, phosphoric acid, weight loss, acidic medium*

Introduction

Corrosion is the degradation of metals resulting from chemical or electrochemical interactions with the surrounding environment, leading to significant economic losses in industrial settings. Equipment, pipelines, storage tanks, and heat exchangers operating in acidic environments are particularly susceptible to corrosion. Therefore, specific agents known as inhibitors are used to prevent or slow down this destructive process (El-Etre, A. Y., 2006; Ebenso, E. E., 2003).

In recent years, considerable attention has been given to the development of environmentally safe and economically efficient corrosion inhibitors. Traditional inhibitors often contain heavy metals, chlorinated organic compounds, and other toxic substances, which restrict their practical applications. This has created a pressing need for the development of biodegradable, inexpensive, and water-soluble inhibitors based on novel components (Quraishi, M.A., et al., 2011; Popova, A., 2007).

The literature reports various substances such as amines, phosphonates, benzotriazole derivatives, imidazoles, and surfactants as corrosion inhibitors. For instance, El-Etre (2006) reported high efficiency of urea and thiourea mixtures in hydrochloric acid media.

Additionally, the passivating properties of phosphoric acids function by forming a protective film on the metal surface. LABSA, containing sulfonic groups, adsorbs onto metal surfaces and contributes to surface coverage and protection (Niyozov, E., Razzakov, K., Nazarov, S., Olimov, B., & Gafurova, G., 2024; Kurbanov F. P., Axmedov V. N., Olimov B. B., Urinov X. X., Gafurova G. A., 2025).

However, there are no reports in the literature on the synthesis of a corrosion inhibitor composed of LABSA, urea, and phosphoric acid. Therefore, this study aims to develop a novel, cost-effective, and efficient inhibitor, investigate its synthesis process, and evaluate its anti-corrosive properties.

Materials and methods

In this study, to synthesize a novel corrosion inhibitor, the following raw materials were selected: LABSA (97%), urea (99%), phosphoric acid (85%), and distilled water.

Synthesis Procedure:

The synthesis of the compound was carried out in four main stages:

Stage 1: A total of 400 g of LABSA was placed into a 1000 mL three-necked round-bottom flask, followed by the addition of 100 mL of distilled water. The mixture was stirred using a magnetic stirrer for 10–15 minutes until a completely homogeneous solution was obtained. During this stage, the sulfonic acid group of LABSA becomes ionized, forming an active anion in the solution.

Stage 2: 200 g of urea was added gradually to the solution in 20 g portions. After each addition, the mixture was stirred for 5 minutes. The temperature was maintained at 30 °C using a water bath. Urea forms stable complexes with LABSA molecules through its ionized ammonium group in solution.

Stage 3: 150 g of 85% phosphoric acid was added dropwise to the solution using a pipette or burette. During this stage, the pH of the mixture dropped from 6 to approximately 2.5. Phosphoric acid reacts with urea to form several ionic complexes. Additionally, the phosphate groups act as active centers capable of further interaction with metal surfaces. The resulting mixture was kept at room temperature (20–25 °C) in a sealed container for 2 hours. During this process, ionic bonds are stabilized and macromolecular complexes are formed.

Stage 4: The final mixture was filtered through a 0.45-micron filter. The resulting viscous liquid acts as a surfactant. The substance was stored in an airtight container, protected from light, at 4–8 °C. Based on the isolated product's mass, the reaction yield was calculated to be 92%. The final product is a brown, homogeneous liquid with a characteristic odor and is completely soluble in water. It exhibits high surface activity and polyelectrolyte behavior, enabling efficient adsorption onto metal surfaces.

This step-by-step reaction process yields a multifunctional corrosion inhibitor. The synthesis can be carried out under simple laboratory conditions without the need for complex equipment, making it suitable for potential industrial application.

he structural formula of the synthesized compound is as follows:

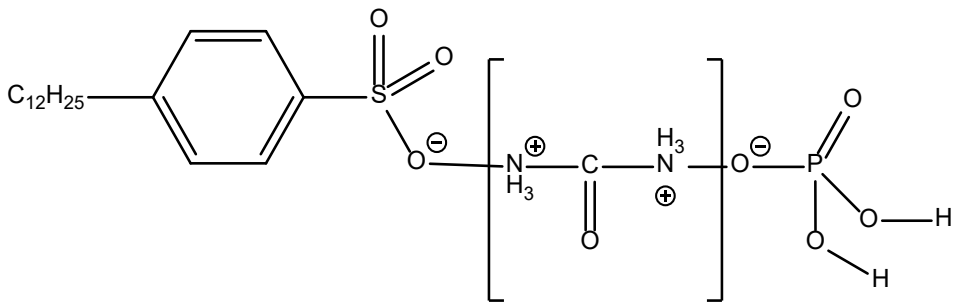

Due to the complex ionic structure of the synthesized compound, it was named according to IUPAC nomenclature as: bis(ammonium)urea dodecylbenzenesulfonate dihydrogen phosphate salt (BDDP)

Determination of the Molecular Weight of the Synthesized Compound by the Cryoscopic Method

The determination of the molecular weight of the synthesized compound by the cryoscopic method is based on the change in the freezing point of a pure solvent upon the addition of the compound. In this method, the freezing point of the pure solvent is first measured. In the present study, distilled water was used as the solvent, with a normal freezing point $T_{\text{pure sol.}}$=0 °C and a cryoscopic constant K_{water}=1.816

The measurement of the freezing point is carried out using a calorimeter, as shown in Figure 1. For the determination, 2–3 g of the test compound (accurately weighed to 0.0001 g) is placed into a long test tube (2). The solvent (water) is added in an amount 20–25 times greater than the mass of the test compound. A thermometer (4) and stirrer (3) are then inserted into the tube, which is sealed with a stopper. Care is taken to ensure that the thermometer does not touch the walls of the container and that the bulb of the thermometer is fully immersed in the solution.

Next, the test tube is placed into an ice bath (1). The solution is stirred continuously using the stirrer (3) to ensure uniform cooling. Once crystals begin to form, stirring is stopped. The temperature is recorded at regular intervals (every 8–10 seconds). A correction must be applied to the observed freezing point to account for the exposed mercury column of the thermometer. This correction is calculated using the following equation:

$$\Delta t = \text{k} \cdot \text{h} \cdot (t_0 - t_1)$$

where:

k – is the volumetric expansion coefficient of mercury in the thermometer tube, taken as 0.000159 °C per 10 °C,

h – is the length of the exposed mercury column, measured in thermometer scale divisions,

t_0 – is the observed freezing point,

t_1 – is the average temperature of the exposed mercury column, determined using an auxiliary thermometer attached to the main thermometer with a rubber band and positioned at the center of the mercury column.

The molecular weight is calculated using the following formula:

$$M = \frac{1{,}816 \cdot 1000 \cdot m}{m_s \cdot \left(t_s - \left(t_m + \Delta t\right)\right)}$$

where:

m – mass of the test sample (in grams);

m_s – mass of the water (solvent);

t_s – freezing point of pure water;

t_m – freezing point of the test solution;

Δt – thermometer correction factor.

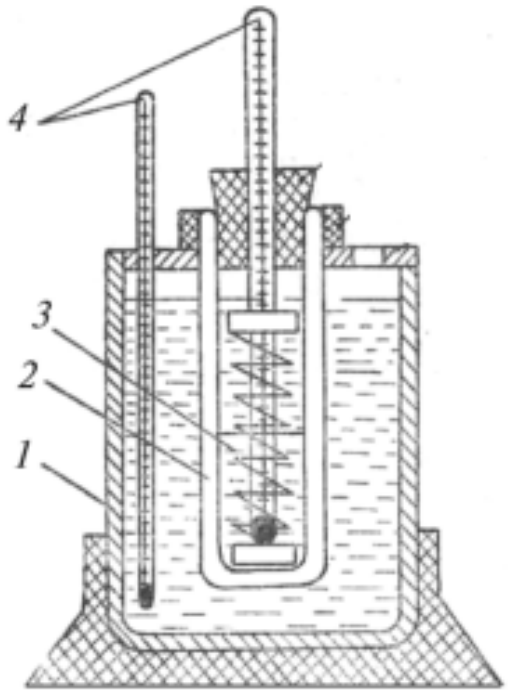

Figure 1. *Apparatus for Molecular Weight Determination by the Cryoscopic Method*

1. Dewar vessel mounted on a stand
2. Thick-walled test tube (150 mL volume)
3. Magnetic stirrer
4. Thermometers

To evaluate the inhibitory properties of the synthesized compound, the gravimetric analysis method was employed. In this method, steel samples (coupons) were exposed to various concentrations and ratios of the studied inhibitor in different environments. The corrosion rate and protection efficiency were determined within a specific temperature range.

The samples were immersed for 300 hours in acidic media, both with and without the inhibitor. After exposure, the samples were removed, cleaned, and weighed, and their final masses were compared with the initial masses. Based on these data, the corrosion rate (K) and inhibition efficiency (Z) were calculated using the standard gravimetric formulas:

$$K = \frac{(m_1 - m_2)\cdot 1000}{S\cdot \tau_1}$$

$$Z = 100\% - K$$

where:

m_1 – initial mass of the metal coupon (g);

m_2 – final mass of the metal coupon after the experiment (g);

S – surface area of the metal coupon (m^2);

τ_1 – duration of the experiment (days).

Results and discussion

In the cryoscopic analysis, 12 g of the synthesized compound was dissolved in 100 g of water. At the end of the process, crystal formation and freezing were observed at –0.446 °C. Based on the obtained data and the cryoscopic formula, the molecular weight of the compound was calculated to be 488.1 g/mol. This result is very close to the theoretical molecular weight of 484 g/mol.

The percentage of experimental error was calculated as follows:

$$\chi = \frac{(488.1 - 484)\cdot 100\%}{484} = 0.85\%$$

Thus, the measurement was conducted with an accuracy of:

100% – 0.85%=99.15%

This high level of accuracy indicates strong agreement between the theoretical and experimental results.

The corrosion inhibition performance of the synthesized compound in 15% HCl solution at concentrations ranging from 100 mg/L to 300 mg/L is presented in

Table 1. *Dependence of the corrosion inhibition efficiency of the synthesized inhibitor on its concentration*

Blank	S, 10^{-4} m^2	τ, hour	mass m_0, g	mass m, g	Δ m	Concentration of inhibitor, mg/l	Rate of corrosion	Z, %	γ
1	21	300	23,42	22,595	0,825	–	1,31	–	–
2	21	300	23,58	23,383	0,197	100	0,313	76,1	4,18
3	21	300	23,56	23,4	0,160	150	0,255	80,5	5,14
4	21	300	23,61	23,512	0,098	200	0,156	88,1	8,39
5	21	300	23,45	23,365	0,085	250	0,135	89,7	9,7
6	21	300	23,57	23,514	0,056	300	0,085	93,2	14,72

According to the results of the gravimetric tests, the optimum corrosion inhibition efficiency was achieved at a concentration of 300 mg/L. At this concentration, the inhibitor exhibited a protection efficiency of 93.2%, confirming its high inhibitory performance.

From an economic perspective, the cost of raw materials for producing 1 kg of the final product is approximately 11,000 Uzbek so‘m, which is 2–3 times cheaper than global market prices. In addition, local production and environmental safety make this inhibitor

highly competitive. Compared to the studies of El-Etre (2006), Ebenso (2003), Quraishi (2011), and others, the efficiency of this inhibitor is comparable or even superior, while also being environmentally friendly and industrially viable.

Conclusion

Within the scope of this study, the efficiency of a newly synthesized urea-based corrosion inhibitor was thoroughly investigated using various methods. The experimental molecular weight of the compound was determined to be 488.1 g/mol, which is very close to the theoretical value of 484 g/mol. Calculations showed a relative error of χ=0.85% indicating that the experiment was conducted with an accuracy of 99.15%. This small discrepancy confirms the strong agreement between theoretical and experimental values.

Corrosion tests using the gravimetric method were conducted in 15% HCl solution with inhibitor concentrations ranging from 100 to 300 mg/L. According to the data, the highest inhibition was observed at 300 mg/L, with a maximum protection efficiency of 93.2%. This result demonstrates that the synthesized compound possesses high efficiency and can effectively protect mild steel in aggressive acidic environments.

In summary, the results of this research indicate that urea-derived corrosion inhibitors combine high efficiency, low cost, environmental safety, and industrial applicability. Therefore, such compounds can be considered promising corrosion protection agents. Future studies will focus on developing even more effective modified derivatives and conducting extended trials under industrial conditions.

References

El-Etre, A. Y. (2006). Urea as a corrosion inhibitor. Corrosion Science, – 48(10). – P. 3255–3265.
Ebenso, E. E. (2003). Synergistic effect of halide ions on the corrosion inhibition of aluminium. Materials Chemistry and Physics, – 79(1). – P. 58–70.
Quraishi, M. A., et al. (2011). Green approach to corrosion inhibition. Journal of Applied Electrochemistry, – 41(1). – P. 15–27.
Popova, A. (2007). Effect of molecular structure on corrosion inhibition. Corrosion Science, – 49(5). – P. 2131–2143.
Niyozov, E., Razzakov, K., Nazarov, S., Olimov, B., & Gafurova, G. (2024). Investigation of physicochemical properties of guanidine-based corrosion inhibitor. In E3S Web of Conferences (Vol. 587, – p. 03004). EDP Sciences.
Kurbanov F. P., Axmedov V. N., Olimov B. B., Urinov X. X., Gafurova G. A. (2025). Investigation of the degree of inhibitor protection relative to conditions at different depths. AIP Conf. Proc. 21 July 2025; – 3304 (1): 040081. URL: https://doi.org/10.1063/5.0269249

submitted 12.07.2025;
accepted for publication 26.07.2025;
published 29.09.2025

Contact: 2927@mail.ru

The Austrian Journal of Technical and Natural Sciences, No 7–8
ISSN 2310-5607

PREMIER Publishing
ppublishing.org

DOI:10.29013/AJT-25-7.8-18-24

ENHANCING THE COHESION PROPERTIES OF 60/90 ROAD BITUMEN USING GOSSYPOL RESIN AS A SUSTAINABLE MODIFIER

Rajapbayev Xamza Zaripbayevich [1],
Gulomov Shuxratqodir Tashmatovich [1]

[1] Uzbek Scientific Research Institute of Chemistry and Pharmaceutics of name A. Sultanov

Cite: *Rajapbayev X.Z., Gulomov Sh.T. (2025). Enhancing the Cohesion Properties of 60/90 Road Bitumen Using Gossypol Resin as a Sustainable Modifier. Austrian Journal of Technical and Natural Sciences 2025, No 7–8.* https://doi.org/10.29013/AJT-25-7.8-18-24

Abstract

This study explores the effect of gossypol resin – an underutilized by-product of the cottonseed oil industry – on the cohesion behavior of 60/90 penetration-grade bitumen. Modified binders were prepared with 0%, 2%, 4%, 6%, and 8% gossypol resin by weight and analyzed for penetration, softening point, ductility, cohesion force, FTIR spectra, and storage stability. Results indicate that 4% gossypol resin addition yields optimal performance, increasing cohesion force by 70% and softening point by 7 °C, while maintaining acceptable ductility. FTIR analysis confirmed molecular interactions between bitumen and gossypol functional groups. The findings demonstrate that gossypol resin serves as a promising bio-based modifier, offering a sustainable and technically effective method for improving bitumen cohesion in road construction applications.

Keywords: *gossypol resin, cohesion force, bitumen modification, bio-based additives, road durability, FTIR analysis*

Introduction

In recent years, the quality and longevity of road infrastructure have become increasingly critical issues worldwide. According to the World Bank's 2023 report, approximately 35–40% of road networks in developing countries are in poor or unsatisfactory condition. This results in billions of dollars in annual economic losses, primarily due to increased vehicle maintenance costs and transportation inefficiencies (Airey, G. D., 2003). In countries like Uzbekistan, where extreme climatic variations – hot summers and cold winters – are common, the degradation of bituminous pavements occurs at an accelerated rate (Baheri, S., & Yousefi, A. A., 2020).

The performance of road pavements heavily depends on the properties of the binder material – bitumen – particularly its cohesion (internal adhesion within the binder) and adhesion (bonding with aggregates). Standard 60/90 penetration-grade bitumen, though widely used due to its balance of viscosity and workability, often exhibits limitations under dynamic loads and temperature fluctuations. These shortcomings manifest in

the form of cracking, delamination, and early pavement failure (Behnood, A., 2019; Dalhat, M. A., & Al-Abdul Wahhab, H. I., 2017).

To overcome these issues, researchers have focused on modifying bitumen with various additives aimed at improving its mechanical and thermal properties. Common modifiers include synthetic polymers, crumb rubber, waste plastics, and increasingly, bio-based or industrial waste materials. In this context, the utilization of gossypol resin – a byproduct of the cottonseed oil industry – presents both an innovative and sustainable solution (Ghaffar, S. H., & Fan, M., 2014; Hamedi, G. H., & Rahmani, M., 2017).

Each year, thousands of tons of gossypol by-products are generated in Uzbekistan alone, yet a significant portion remains unutilized, posing environmental challenges. Chemically, gossypol resin contains aromatic and polyphenolic structures, including reactive oxygen-containing functional groups such as phenols and carboxylic acids. These groups are capable of interacting with the double bonds and polar sites in bitumen molecules, potentially enhancing cohesion, elasticity, and thermal resistance (Liu, X., & Peng, A., 2021; Lu, X., & Isacsson, U., 2002).

Moreover, incorporating gossypol resin into bitumen not only improves the mechanical integrity of the binder but also contributes to eco-friendly waste valorization. This approach aligns with the principles of green chemistry and circular economy, promoting the transformation of industrial waste into value-added construction materials (Navarro, F. J., Partal, P., García-Morales, M., & Gallegos, C., 2005).

In this study, various concentrations of gossypol resin were blended with 60/90 penetration-grade road bitumen to investigate its influence on the binder's cohesive properties. The experimental work aims to determine how the introduction of gossypol resin modifies the internal bonding strength, structural stability, and overall durability of the modified bitumen. The results are expected to provide new insights into the development of more resilient and environmentally sustainable asphalt binders (Paksoy, M., & Karahancer, S., 2021).

Recent advances in bitumen modification have emphasized the importance of improving both adhesive and cohesive behavior to prolong the life span of asphalt pavements. One of the most critical characteristics affecting the long-term performance of bitumen is cohesion, which reflects the internal molecular bonding within the binder. Poor cohesion often results in premature cracking, rutting, and stripping under repeated loading and environmental stresses (Qadir, A., & Khalid, H., 2023).

Traditional synthetic modifiers, such as Styrene-Butadiene-Styrene (SBS), Ethylene-Vinyl-Acetate (EVA), and Polyethylene (PE), have been widely used to enhance bitumen properties. However, these polymers are expensive and often derived from non-renewable resources. Consequently, the attention of researchers has shifted toward bio-based and waste-derived modifiers, which offer both economic and environmental advantages (Xu, G., & Liu, X., 2020).

Gossypol resin, as an agricultural waste product rich in phenolic structures, exhibits promising potential for interacting chemically with bitumen components. Its multifunctional reactive groups can participate in physical entanglement and chemical bonding with asphaltenes and maltenes, which are the primary fractions responsible for bitumen's rheological behavior. This interaction is expected to lead to improved viscoelastic properties, enhanced temperature susceptibility, and better resistance to deformation (Xue, Y., Hou, H., Zhu, S., & Zha, J., 2009).

Several studies have explored the use of natural and waste-derived substances in bitumen modification. For instance, lignin, tannin, palm oil residues, and various bio-oils have been successfully incorporated into bitumen to improve its performance while reducing environmental impact. However, limited research has been conducted specifically on the application of gossypol resin for this purpose, especially concerning its effects on the cohesion parameter (Zaumanis, M., & Mallick, R. B., 2015).

Uzbekistan, being one of the world's largest cotton producers, generates substantial volumes of cottonseed oil waste. The valorization of this waste not only addresses environmental concerns but also aligns with national strategies for waste minimization and resource efficiency in the construction sector. Utilizing gossypol resin as a bitumen

modifier supports sustainable development goals (SDGs), particularly in terms of responsible production and infrastructure resilience (Zhang, H., & Yu, J., 2010).

In this context, the present study aims to evaluate the influence of gossypol resin content on the cohesion properties of 60/90 road bitumen using standardized laboratory methods. By systematically analyzing physical, mechanical, and thermal characteristics – including penetration index, softening point, ductility, and cohesion force – this work seeks to develop a cost-effective and eco-conscious modifier formulation. The outcomes are expected to offer viable alternatives for traditional bitumen modification techniques and open new pathways for integrating agricultural by-products into high-performance road materials (Yilmaz, M., & Yilmaz, M., 2013).

Materials and methods

Materials

Base Bitumen

The base binder used in this study was 60/90 penetration-grade road bitumen, obtained from the Fergana Oil Refinery, Uzbekistan. This grade was selected due to its wide usage in national road construction and its balanced properties suitable for medium to high traffic loads. The basic physical characteristics of the unmodified bitumen are summarized in Table 1.

Gossypol Resin

Gossypol resin was sourced as a by-product from a local cottonseed oil processing plant in the Tashkent region. The resin was collected in semi-solid form and was subjected to pre-treatment involving drying at 105 °C for 4 hours to remove residual moisture, followed by grinding and sieving to achieve a uniform particle size (< 0.25 mm). The chemical composition of the resin includes polyphenolic and aldehyde groups, as verified by FTIR spectroscopy.

Solvent (if used)

In some trials, a small quantity of xylene (analytical grade) was used to facilitate the uniform dispersion of the gossypol resin within the bitumen matrix, particularly at higher dosages (>6 wt%).

Preparation of Modified Bitumen

The modification process was carried out using a high-shear laboratory mixer (IKA RW 20 digital) at controlled temperature and speed. The steps involved are outlined below:

1. 1The base bitumen was heated to 150 ± ± 5 °C in a steel vessel until a fully fluid state was achieved.
2. Pre-weighed amounts of gossypol resin (2%, 4%, 6%, and 8% by weight of bitumen) were gradually added to the molten bitumen under continuous stirring.
3. Mixing was conducted at 3000 rpm for 30 minutes to ensure homogeneous dispersion of the resin particles.
4. The modified bitumen samples were conditioned at 160 °C for 1 hour to simulate storage and compaction conditions.
5. All samples were then cooled to room temperature and stored in sealed containers for further analysis.

Characterization and Testing Methods

To evaluate the influence of gossypol resin on the cohesion properties of bitumen, the following tests were conducted in accordance with international standards (ASTM, AASHTO, and EN standards):

1. Penetration Test

- Standard needle penetration was measured at 25 °C using ASTM D5 method;
- Results indicate consistency and initial hardness of the binder.

2. Softening Point (Ring and Ball Method)

- Conducted as per ASTM D36 to assess temperature susceptibility.

3. Ductility Test

- Performed at 25 °C following ASTM D113;
- This test gives indirect insight into the internal cohesion of bitumen.

4. Cohesion Force Measurement (Force Ductilometer Method)

- A modified force ductilometer was employed to measure the peak force required to break the bitumen filament (N);
- This method quantifies cohesion strength more precisely than conventional ductility.

5. FTIR Spectroscopy

- Fourier Transform Infrared Spectroscopy (PerkinElmer Spectrum Two)

was used to investigate the chemical interactions between bitumen and gossypol resin;
- Spectra were recorded in the 4000–400 cm−1 range using the ATR method.

6. Storage Stability Test
- A 5-day thermal aging test at 163 °C was performed to assess phase separation and compatibility of the gossypol additive with bitumen.

Experimental Design

All formulations were prepared in triplicate to ensure reproducibility. The optimal dosage of gossypol resin was determined based on a comparative analysis of cohesion force, ductility, and thermal resistance. A control sample (0% resin) was tested alongside each modified sample. Statistical evaluation of the results was performed using **ANOVA** (Analysis of Variance) with a confidence level of 95% ($p < 0.05$) to determine the significance of observed changes.

Results and discussion

Effect of Gossypol Resin on Penetration and Softening Point

The effect of gossypol resin content on the basic rheological properties of 60/90 bitumen was initially assessed via penetration and softening point tests. As shown in Table 1, the penetration value decreased steadily with increasing resin content, indicating improved stiffness and reduced plasticity.

Table 1. *Penetration and Softening Point of Modified Bitumen*

Gossypol Content (% wt)	Penetration (0.1 mm)	Softening Point (°C)
0 (Control)	67	47.3
2	61	49.1
4	55	50.7
6	48	52.8
8	43	54.4

The increase in softening point implies that the modified binder exhibits greater resistance to deformation under high-temperature conditions. This effect is attributed to the phenolic cross-linking within the gossypol structure, which reinforces the bitumen matrix.

Effect on Ductility and Elasticity

The ductility test revealed a significant reduction in stretchability as the amount of gossypol resin increased (Table 2). However, up to 4% addition still maintained acceptable ductility (>25 cm), which is essential for flexibility in road applications.

Table 2. *Ductility of Bitumen at 25 °C*

Gossypol Content (% wt)	Ductility (cm)
0 (Control)	73.5
2	58.7
4	41.3
6	24.2
8	16.9

This decline reflects increased stiffness and reduced elongation capacity due to internal structuring. Nevertheless, the 4% modified sample offers a suitable balance between elasticity and rigidity for real-world traffic conditions.

Cohesion Force Evaluation

The most critical aspect of this study was the evaluation of cohesion force using a force ductilometer. As illustrated in Table 3 and Figure 1, the cohesion force improved significantly with gossypol addition, reaching a maximum at 4% content, beyond which a decrease was observed.

Table 3. *Cohesion Force of Modified Bitumen*

Gossypol Content (% wt)	Cohesion Force (N)
0 (Control)	1.36
2	1.87
4	2.31
6	2.05
8	1.72

Figure 1. *Cohesion Force vs. Gossypol Content*

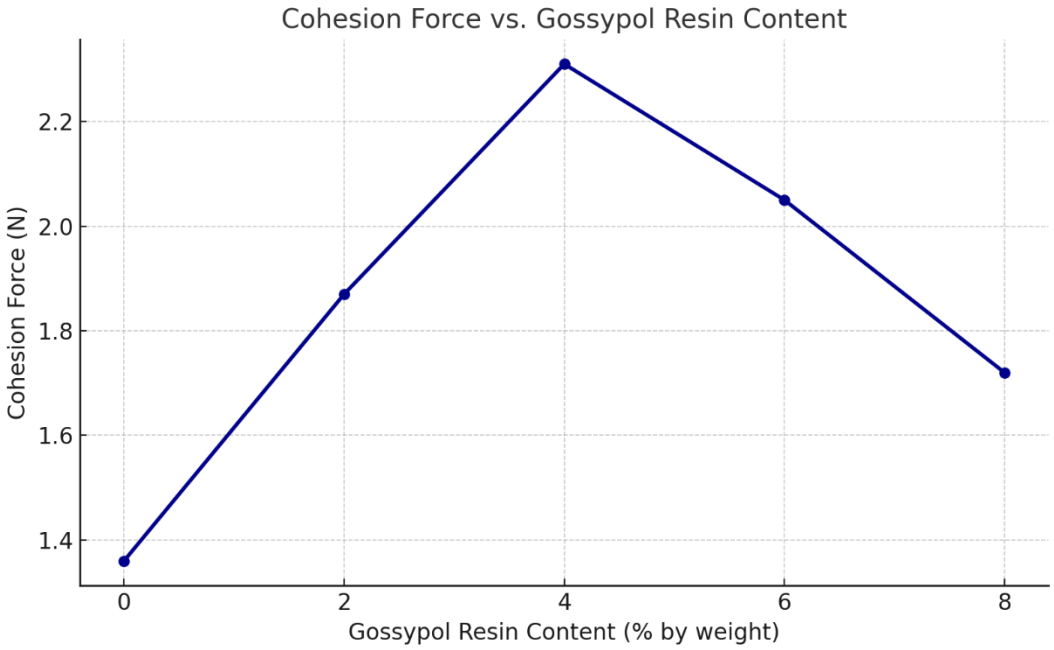

(Graph plotting gossypol content (%) on X-axis and cohesion force (N) on Y-axis, showing a peak at 4% content)

This trend suggests that moderate amounts of gossypol enable strong intermolecular bonding and matrix reinforcement, while excess resin may cause phase instability or poor dispersion, leading to reduced cohesion.

FTIR Analysis

FTIR spectra provided evidence of chemical interactions between bitumen and gossypol resin. Key shifts were observed in the absorption bands around 1700 cm^{-1} (C=O), 3400 cm^{-1} (O–H), and 1230 cm^{-1} (C–O), indicating hydrogen bonding and polar interactions.

Table 4. *FTIR Spectral Changes in Modified Bitumen*

Sample	3400 cm^{-1} (O–H)	1700 cm^{-1} (C=O)	1230 cm^{-1} (C–O)
Control	Weak	Weak	Weak
2% Gossypol	Moderate	Moderate	Moderate
4% Gossypol	Strong	Strong	Strong
6% Gossypol	Strong	Slightly Shifted	Moderate
8% Gossypol	Weak	Weak	Weak

These spectral changes confirm that gossypol acts not only as a physical filler but also engages in chemical interactions that enhance the cohesion and thermal resistance of the bitumen matrix.

Storage Stability Observation

Visual and gravimetric observation after thermal conditioning showed no phase separation up to 4–6% resin content, suggesting satisfactory storage stability. At 8% resin, slight phase segregation and heterogeneity were observed.

Discussion Summary

The experimental data suggest that the optimal gossypol content is around 4% by weight, at which point the modified bitumen exhibits:

- Enhanced cohesion (↑70% compared to control);
- Acceptable ductility (>40 cm);
- Improved thermal stability (↑7 °C in softening point);
- Chemically integrated matrix (confirmed by FTIR).

Beyond this threshold, performance declined due to excessive stiffness and miscibility issues. Thus, gossypol resin can serve as a cost-effective, sustainable modifier when optimized properly.

Conclusion

This study investigated the influence of gossypol resin – an agricultural by-product – on the cohesion characteristics of 60/90 penetration-grade road bitumen. The experimental results revealed that the incorporation of gossypol resin at an optimal concentration of 4% by weight significantly enhanced the cohesion force of bitumen by approximately 70% compared to the unmodified sample.

- The modification also improved thermal resistance (↑7 °C in softening point) and introduced functional chemical interactions, as confirmed by FTIR analysis. While ductility decreased with increasing resin content, acceptable flexibility was maintained up to 4% loading. Beyond this point, adverse effects such as stiffness build-up and miscibility issues were observed.

Overall, the use of gossypol resin as a bitumen modifier provides a cost-effective, eco-friendly, and technically feasible solution for improving pavement durability, especially in regions with abundant cottonseed processing waste. This approach supports sustainable construction practices and waste valorization strategies.

References

Airey, G. D. (2003). State of the art report on ageing test methods for bituminous pavements. *International Journal of Pavement Engineering*, – 4(3). – P. 165–176. URL: https://doi.org/10.1080/1029843042000198568

Baheri, S., & Yousefi, A. A. (2020). Waste-based bio-asphalt binders: A review. *Construction and Building Materials*, – 252. – 119066 p. URL: https://doi.org/10.1016/j.conbuildmat.2020.119066

Behnood, A. (2019). Application of rejuvenators to improve the rheological and mechanical properties of asphalt binders and mixtures: A review. *Journal of Cleaner Production*, – 231. – P. 171–182. URL: https://doi.org/10.1016/j.jclepro.2019.05.201

Dalhat, M.A., & Al-Abdul Wahhab, H.I. (2017). Recycled oil-based bitumen rejuvenator for sustainable pavement. *Journal of Cleaner Production*, – 142. – P. 1212–1220. URL: https://doi.org/10.1016/j.jclepro.2016.09.016

Ghaffar, S.H., & Fan, M. (2014). Lignin in straw and its applications as an adhesive. *Industrial Crops and Products*, – 49. – P. 146–158. URL: https://doi.org/10.1016/j.indcrop.2013.05.023

Hamedi, G.H., & Rahmani, M. (2017). Physical and rheological evaluation of bitumen modified with polymers and recycled plastics. *Construction and Building Materials*, – 146. – P. 464–470. URL: https://doi.org/10.1016/j.conbuildmat.2017.04.113

Liu, X., & Peng, A. (2021). Bio-modified bitumen from waste cooking oil: A sustainable binder alternative. *Journal of Materials in Civil Engineering*, – 33(7). – 04021158 p. URL: https://doi.org/10.1061/(ASCE)MT.1943–5533.0003735

Lu, X., & Isacsson, U. (2002). Chemical and rheological evaluation of ageing properties of SBS polymer modified bitumens. *Fuel*, – 81(15). – P. 1969–1982. URL: https://doi.org/10.1016/S0016-2361(02)00137-5

Navarro, F.J., Partal, P., García-Morales, M., & Gallegos, C. (2005). Bitumen modification with reactive and non-reactive polymers. *Fuel*, – 84(31). – P. 316–322. URL: https://doi.org/10.1016/j.fuel.2004.08.017

Paksoy, M., & Karahancer, S. (2021). Investigation of sustainable bitumen modification using natural resin. *Environmental Technology & Innovation*, – 24. – 101915 p. URL: https://doi.org/10.1016/j.eti.2021.101915

Qadir, A., & Khalid, H. (2023). Utilization of agricultural waste-based resins for bitumen reinforcement. *Construction and Building Materials*, – 375. – 130994 p. URL: https://doi.org/10.1016/j.conbuildmat.2023.130994

Xu, G., & Liu, X. (2020). Effects of bio-asphalt on high- and low-temperature properties of modified bitumen. *Journal of Cleaner Production*, – 255. – 120294 p. URL: https://doi.org/10.1016/j.jclepro.2020.120294

Xue, Y., Hou, H., Zhu, S., & Zha, J. (2009). Utilization of waste tire rubber in asphalt and Portland cement concrete: A review. *Waste Management*, – 29(1). – P. 132–140. URL: https://doi.org/10.1016/j.wasman.2008.01.005

Zaumanis, M., & Mallick, R.B. (2015). Review of very high-content reclaimed asphalt use in plant-produced pavements: State of the art. *International Journal of Pavement Engineering*, – 16(1). – P. 39–55. URL: https://doi.org/10.1080/10298436.2014.893331

Zhang, H., & Yu, J. (2010). The research for aging properties of SBS modified bitumen with FTIR and NMR. *Construction and Building Materials*, – 24(5). – P. 748–752. URL: https://doi.org/10.1016/j.conbuildmat.2009.10.035

Yilmaz, M., & Yilmaz, M. (2013). Utilization of waste polymers for improvement of mechanical properties of bitumen. *Construction and Building Materials*, – 40. – P. 135–140. URL: https://doi.org/10.1016/j.conbuildmat.2012.09.108

submitted 10.08.2025;
accepted for publication 24.08.2025;
published 29.09.2025

Contact: rajapbaev.xamza@icloud.com

The Austrian Journal of Technical and Natural Sciences, No 7–8
ISSN 2310-5607

PREMIER Publishing
ppublishing.org

DOI:10.29013/AJT-25-7.8-25-29

SYNTHESIS AND PROPERTIES OF AZO COMPOUNDS BASED ON SOME AROMATIC AMINES WITH β-NAPHTHOL

Saparbayev Suroj Rustamovich [1], ***Yuldasheva Muhabbat Razzoqberdievna*** [1]

[1] The National University of Uzbekistan named after Mirzo Ulugbek, Tashkent

Cite: *Saparbayev S. R., Yuldasheva M. R. (2025). Synthesis and Properties of Azo Compounds Based on Some Aromatic Amines With B-Naphthol. Austrian Journal of Technical and Natural Sciences 2025, No 7–8.* https://doi.org/10.29013/AJT-25-7.8-25-29

Abstract

In this article, the synthesis of azo compounds with β-naphthol based on aromatic amines with p-substituents was studied. The reaction conditions, physicochemical properties of azo compounds and the structure of the resulting products were determined by spectroscopic methods. Based on the results obtained, the effect of substituents on the product yields was studied. The relevance of the topic is that complexes of the obtained azo compounds with metals (Ni^{2+}, Cu^{2+}) were obtained. The following azo dyes combine with metals to form bidentates.

Keywords: *β-naphthol, p-Br-aniline, p-anisidine, HPLC, IK, AAS*

Introduction

Azo compounds are widely used in the chemical industry, especially in the synthesis of dyes and biologically active compounds. In analytical chemistry, they are used as ligands for the synthesis of metal complexes. Organic coatings that are mainly resistant to metal corrosion are obtained. The synthesis of azo dyes is one of the most interesting reactions in organic chemistry. It not only has useful properties in everyday life, namely as dyes and pigments (Al-Tohamy R., 2022, Alsantali R. I., 2022) but also has a unique mechanism that has long been an important example in undergraduate organic chemistry textbooks (Smith, J.G. 2019). Azo compounds are an important part of dyes, food additives, pigments, indicators, textiles, pharmaceuticals, cosmetics and therapeutics (Al-Rubaie L. A., 2012, Jarad A. J., Majeed I. Y., Hussein A. O., 2018). They have also been used recently as precursors in the synthesis of various products (Zhao R., 2011) and corrosion inhibitors (El-Wakiel N. A., 2016, Raja P. B., 2016).

Azo compounds have a nitrogen and nitrogen double bond as chromophores. These dyes are formed by taking a diazonium salt and attaching it to a strongly activated aromatic ring (Valiulin R., 2020). Azo dyes were synthesized by a solvent-free room temperature grinding method using magnetic Fe3O4 nanoparticles (Zhang Y., 2011). Azo dye polymers were prepared by oxidative polycondensation reaction of naphthol-based azo dyes in aqueous medium using NaOCl oxidant. According to the results, it was found that the durability properties of azo dye monomers are better than those of polymers (Gür M., Kocaokutgen H., 2007). Mono-azo dyes are the most important type

of azo dyes. They are used in various fields: catalysis (El-Ghamry H. A. et al., 2023) supramolecular systems (Ferreira G. R., 2015 p. 13–20, Dinçalp H., 2007, p. 11–24) and metal sensors (Almáši M., Vilkova M., Bednarčík J., 2021) textile and fiber dyeing, which is mainly due to their adsorption capacity and absorption capacity. The remarkable biological activity of azo ligands with O and N donor atoms is known for their excellent chelating ability to all types of metal ions. Azo ligands can be used to form complex compounds containing several metal ions. However, the properties of the complexes produced depend on the type of metal ion used (Zhao R., 2011, p. 3805–3809, Kohl M., 2023, p. 1276) Azo ligand complexes have various applications in medicine, including antitumor (Ferreira G. R., 2015, p. 13–20), antimicrobial (Dinçalp H. et al., 2007, p. 11–24, Abd El-Lateef H. M. et al., 2024, p. 138016) and anti-inflammatory agents (Kasare M. S. et al., 2019, p. 3311–3323).

Experimental part

The M-560 device was used to measure the liquidus temperature of the obtained product. IR spectra IRAffininity-1S, Shimadzu corporation, 2020 Range: 350–7800 cm^{-1}, HPLC: LC-20 Prominence, Shimadzu corporation, Japan, 2020 Range: 190–600 nm, AAS: Atomic absorption spectrophotometer AA-7000, Shimadzu Corporation, Japan, 2020.

Results and discussions

Synthesis method

During the experiments, aromatic amines (p-anisidine, p-bromoaniline) with various substituents in the p-position were selected. The synthesis of the azo compound was carried out via the azo addition reaction. The azo addition reaction proceeds in the second stage according to the electrophilic mechanism. First, a diazotization reaction occurs, in which a diazonium salt is formed. In the second stage, a weak alkaline solution of β-naphthol with the diazonium salt undergoes an azo addition reaction. These processes are carried out at a temperature of –5–0 °C.

The obtained product was re-filtered with water and recrystallized and purified. The structure of the products was determined using modern physical and chemical methods. Some physicochemical parameters of the azo compounds obtained on the basis of the synthesis. Obtained: (1-(4-methoxyphenylazo-)-2-naphthol) red, Melting point=139–142 °C, Yield 98.6%, Rf=0.65 (1-(4-bromophenylazo-)-2-naphthol) dark red Melting point=170–173 °C, Yield 94.7%, Rf=0.77. TLC (System: EtAc: Pet.ester(1:3)) determined the Rf values. The purity of the obtained azo compounds was checked by HPLC: (1-(4-bromophenylazo-)-2-naphthol) at 8.49 min. we can see peaks with 95.49% purity, (1-(4-methoxyphenylazo-)-2-naphthol) at 14.418 min. we can see peaks with 99.986% purity.Reaksiyaning umumiy sxemasi:

Scheme 1.

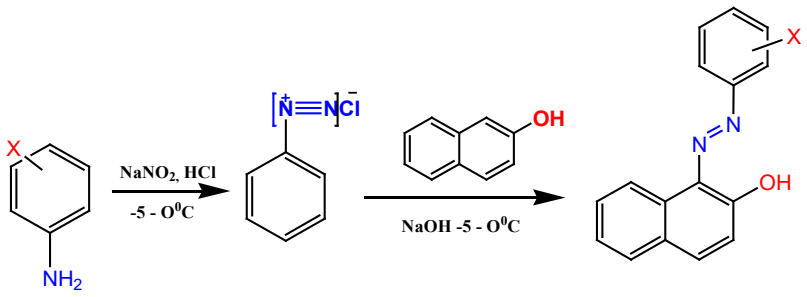

X= p-NO_2, p-OH, p-CH_3, p-OCH_3, p-AAB, p-Br, p-COOH, p-aminosalitsil k-ta(PAS)

For the synthesis of complexes based on azo compounds, the salt and ligand were dissolved in ethanol in a 1:1 ratio and 1–2 drops of TEA were added to the solution to give an alkaline medium. The solution was heated at boiling temperature for 3 hours

and purified by filtration, washed with water. The IR spectra of the complexes of the obtained azo compounds (1-(4-bromophenylazo-)-2-naphthol), (1-(4-methoxyphenylazo-)-2-naphthol) with Ni(II) and Cu(II) salts are presented:

Table 2.

Azocompound	ν(OH)	ν(–N=N-)	ν(M-O)	ν(M-N)
p-BrPAN	3543 sm^{-1}	1496 sm^{-1}	–	–
p-BrPAN-Ni(II)	3057 sm^{-1}	1593 sm^{-1}	663 sm^{-1}	586 sm^{-1}
p-BrPAN-Cu(II)	3444 sm^{-1}	1595 sm^{-1}	603 sm^{-1}	545 sm^{-1}
p-MPAN	3442sm^{-1}	1492 sm^{-1}	–	–
p-MPAN Ni(II)	2837 sm^{-1}	1595 sm^{-1}	620 sm^{-1}	547 sm^{-1}
p-MPAN-Cu(II)	3321 sm^{-1}	1546 sm^{-1}	580 sm^{-1}	559 sm^{-1}

Scheme 2.

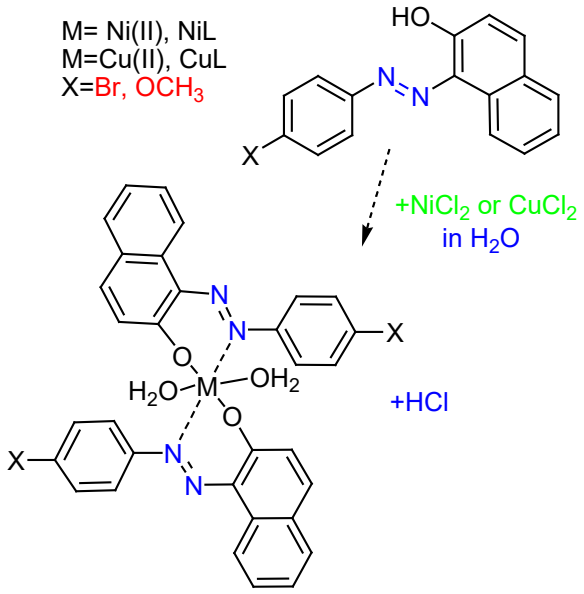

The following are the atomic adsorption analysis spectra of the complex formed by (1-(4-bromophenylazo-)-2-naphthol) with Ni(2⁺) ion. The table shows the atomic adsorption analysis (AAS) of the amount of nickel (Ni^{2+}) ions. The absorptions in the 232 nm region corresponding to Ni(2⁺) were found to be 14.0% nickel (Ni^{2+}) in the sample. For Cu 2^{+}, the corresponding absorption was determined in the 324.8 nm region and was 16.8% quantitatively. The advantage of this analysis is that it shows the same element (metal) in the composition with high accuracy.

Figure 1.

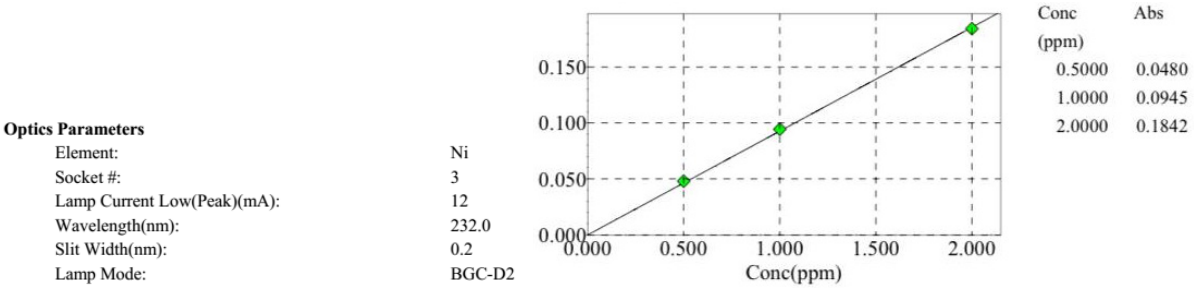

Optics Parameters

Element:	Ni
Socket #:	3
Lamp Current Low(Peak)(mA):	12
Wavelength(nm):	232.0
Slit Width(nm):	0.2
Lamp Mode:	BGC-D2

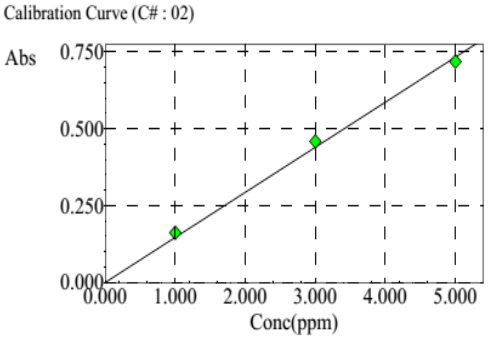

Conc (ppm)	Abs
1.0000	0.1619
3.0000	0.4593
5.0000	0.7192

Conclusion

In this work, the synthesis of azo compounds with β-naphthol based on aromatic amines with substituents in the p-position was carried out. The purity and structure of the obtained products were determined using HPLC and IR spectra. Metal complexes of $Cu2^{+}$ and $Ni2^{+}$ salts of the obtained azo compounds were obtained. Structure of the complexes The composition and amount of metals in the complex were determined using AAS

References

Al-Tohamy R. et al. A critical review of dye wastewater treatment: ecotoxicological and health issues of textile dyes and possible approaches to restore environmental safety // Ecotoxicology and Environmental Safety. 2022. – T. 231. – P. 113160.

Alsantali R. I. et al. Various azo dyes: a comprehensive review of recent advances in biological and industrial applications // Dyes and Pigments. 2022. – T. 199. – 110050 p.

Smith, J. G. Organic Chemistry, 6th ed.; McGraw-Hill Education, 2019.

Al-Rubaie L. A. A. R., Mhessn R. J. Synthesis and characterization of azo dye para red and new derivatives //Journal of Chemistry. 2012. – T. 9. – No. 1. – P. 465–470.

Jarad A. J., Majeed I. Y., Hussein A. O. Synthesis and spectral studies of heterocyclic azo dye complexes with some transition metals // Journal of Physics: Conference Series. – IOP Publishing, 2018. – T. 1003. – No. 1. – 012021 p.

Zhao R. et al. One step synthesis of azo compounds from nitroaromatics and anilines // Tetrahedron letters. 2011. – T. 52. – No. 29. – P. 3805–3809.

Kohl M. et al. New Azo dyes-based Mg complex pigments for optimizing the anti-corrosion efficiency of Zinc-pigmented epoxy ester organic coatings // Coatings. 2023. – T. 13. – No. 7. – 1276 p.

El-Wakiel N. A. Synthesis and characterization of azo sulfaguanidine complexes and their application for corrosion inhibition of silicate glass // Applied Organometallic Chemistry. 2016. – T. 30. – No. 8. – P. 664–673.

Raja P. B. et al. Reviews on corrosion inhibitors: a short view // Chemical Engineering Communications. 2016. – T. 203. – No. 9. – P. 1145–1156.

Valiulin R. Organic Chemistry: 100 Must-Know Mechanisms // Organic Chemistry: 100 Must-Know Mechanisms. – De Gruyter, 2020. – P. 97–98.

Zhang Y. et al. An environmentally friendly approach to the green synthesis of azo dyes with aryltriazenes via ionic liquid promoted CN bonds formation // Dyes and Pigments. 2018. – T. 158. – P. 438–444.

Gür M., Kocaokutgen H., Taş M. Synthesis, spectral, and thermal characterizations of some azo-ester derivatives containing a 4-acryloyloxy group // Dyes and Pigments. 2007. – T. 72. – No. 1. – P. 101–108.

El-Ghamry H. A. et al. A series of nanosized Cu (II) complexes based on sulfonamide azo dye ligands: an insight into complex molecular structures, antimicrobial, antitumor and cata-

lytic performance for oxidative dimerization of 2-aminophenol //Applied Organometallic Chemistry. 2023. – T. 37. – No. 2. – e6978 p.
Ferreira G. R. et al. Supramolecular compounds of azo dyes derived from 1-phenylazo-2-naphthol and their nickel and copper complexes // Supramolecular Chemistry. 2015. – T. 27. – No. 1–2. – P. 13–20.
Dinchalp H. et al. New thiophene-based azo ligands containing azo methine group in the main chain for the determination of copper (II) ions // Dyes and Pigments. 2007. – T. 75. – No. 1. – P. 11–24.
Almáši M., Vilkova M., Bednarčík J. Synthesis, characterization and spectral properties of novel azo-azomethine-tetracarboxylic Schiff base ligand and its Co (II), Ni (II), Cu (II) and Pd (II) complexes // Inorganica Chimica Acta. 2021. – T. 515. – 120064 p.
Abd El-Lateef H. M. et al. Design, synthesis of new mixed azo-hydroxyquinoline complexes; in vitro anti-inflammatory, antifungal, antibacterial, theoretical, and molecular docking interactions Investigation // Journal of Molecular Structure. 2024. – T. 1307. – 138016 p.
Kasare M. S. et al. In-vitro antibacterial activity of Ni (II), Cu (II), and Zn (II) complexes incorporating new azo-azomethine ligand possessing excellent antioxidant, anti-inflammatory activity and protective effect of free radicals against plasmid DNA // Synthetic Communications. 2019. – T. 49. – No. 23. – P. 3311–3323.

submitted 15.08.2025;
accepted for publication 29.08.2025;
published 29.09.2025

Contact: surojsaparbayev70@gmail.com

The Austrian Journal of Technical and Natural Sciences, No 7–8
ISSN 2310-5607

PREMIER Publishing
ppublishing.org

DOI:10.29013/AJT-25-7.8-30-35

ACYLATION REACTION OF THE ALKALOID 13,22-DIMETHOXYSTACHYBOTRYNE ISOLATED FROM THE MICROFUNGUS STACHYBOTRYS CHARTARUM

Tojiyeva Sevara Namozovna [1], Kamolov Luqmon Sirojiddinovich [1], Naxatov Innat [1], Kaxarova Madina Faxriddin qizi [2]

[1] Faculty of Chemistry and Biology, Karshi State University, Uzbekistan, Karshi

[2] Faculty of Natural Sciences, University of Turan, Uzbekistan, Karshi

Cite: *Tojiyeva S.N., Kamolov L.S., Naxatov I., Kaxarova M.F. (2025). Acylation Reaction of the Alkaloid 13,22-Dimethoxystachybotryne Isolated from the Microfungus Stachybotrys Chartarum. Austrian Journal of Technical and Natural Sciences 2025, No 7–8.* https://doi.org/10.29013/AJT-25-7.8-30-35

Abstract

The structure of the isolated alkaloids and terpenoids was determined by conducting acylation reactions with acetic anhydride based on the alkaloids and terpenoids isolated from the *Stachybotrys chartarum* fungus, and biologically active compounds were obtained.13,22-Dimethoxystachybotryn is one of the important alkaloids of the *Stachybotrys chartarum* microfungus grown in laboratory conditions, and was isolated using column chromatography and an acylation reaction was carried out on it. In the process of forming O-Monoacetate, the reagents were taken in a 1:1 molar ratio and the reactions were carried out at room temperature. When 13,22- Dimethoxystachybotryn was taken with acetic anhydride in a 1:2 molar ratio, O-diacetate compounds were formed.

Keywords: *Stachybotrys chartarum, acetic anhydride, pyridine, terpenoid, benzene ring, geminal, correlation, chromic anhydride, acetic anhydride, nucleophilic reagent, carbon atom*

Introduction

S. chartarum fungi are hydrophilic organisms that require moist conditions for their growth and development. They can also live on gypsum, cellulose-based building boards, fiberglass coatings, wallpaper, natural fiber carpets, insulated pipes, wood and wood chip-based panels, and organic residues. They are also found in soil, plant grains, and garbage (Hodgson, M.J. et al., 1998; Kuhn, D.M. et al., 2003). S.chartarum is one of the most common indoor fungi that produces pathogenic mycotoxins. The areas where this fungus is present are dangerous for human life (Kuhn, D.M. et al., 2003). Indoor air and surfaces contaminated with the fungus or its mycotoxins cause serious pathological diseases and even death in humans (Hodgson, M.J. et al., 1998; Castlebury, L.A., 2004). Common symptoms of such a disease are fatigue, chest tightness, inflammation of the mucous membranes,

headache, etc. (Hodgson, M.J. et al., 1998). It can also cause more serious respiratory diseases, ranging from cough and hiccups to damage to the bronchi and alveoli or pulmonary fibrosis (Johanning, E. et al., 1996). Even more dangerous, cases of pulmonary hemorrhage in infants have been reported as a result of exposure to this fungus (Dearborn, D.G. et al., 2002).

Research methodology

Determination of the structure of the isolated alkaloids and terpenoids and obtaining biologically active compounds by conducting acylation reactions with acetic anhydride based on the alkaloids and terpenoids of the fungus Stachybotrys chartarum.The alkaloid 13,22- Dimethoxystachybotrine (III) was isolated by growing the Stachybotrys chartarum fungus strain on Mandels nutrient medium and its physicochemical constants were determined as $C_{27}H_{39}NO_6$, liquid. tem. 225° (MeOH), R_f = 0.58.(YUQX, silufol, 11 system), $[\alpha]_D^{24}$–13.4 ± 2°(c 0.8; $CHCl_3$--MeOH, 1:1).13,22- Dimethoxystachybotryne (III) is one of the important alkaloids of the laboratory-grown microfungus *Stachybotrys chartarum*, which was isolated using column chromatography and subjected to an acylation reaction. In the process of forming O-Monoacetate, the reagents were taken in a 1:1 molar ratio and the reactions were carried out at room temperature. The reaction was carried out as follows.

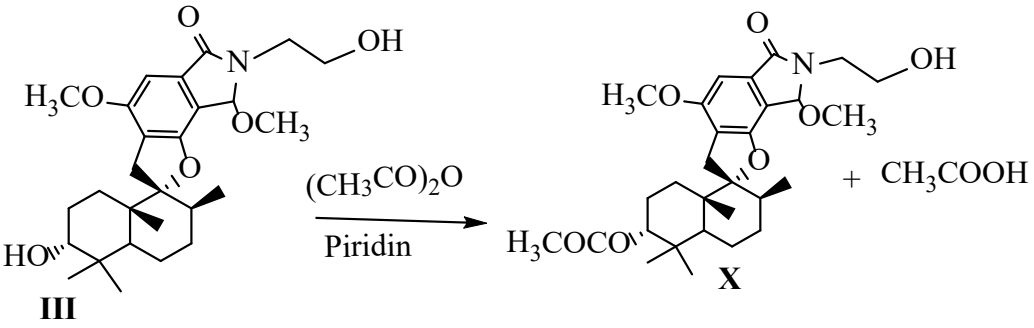

The reactions proceed according to the nucleophilic substitution mechanism.

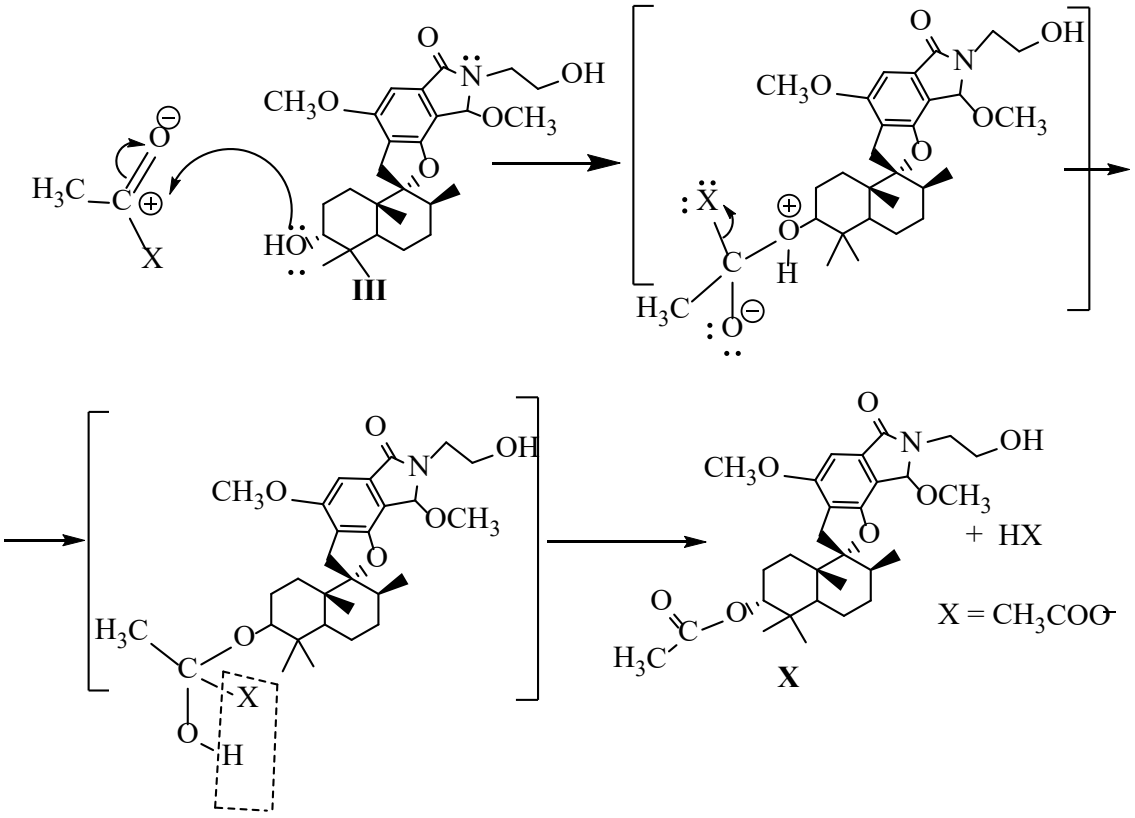

During the reaction of the -OH group in the 13,22-dimethoxystaxybothrin molecule and acetic anhydride, the oxygen in the acetic anhydride molecule acquires a partial negative charge due to the electrons of the double bond in the carbonyl group moving towards the electronegative oxygen. As a result of the action of the electronegative oxygen atoms, the carbon atom becomes partially positively charged. The pair of electrons of the oxygen atom in the hydroxyl group located in the terpenoid ring in the 13,22-dimethoxystaxybothrin molecule interacts with the carbon atom in the acetic anhydride molecule, forming an intermediate compound. During the reaction, a new intermediate compound is formed due to the covalent bond between oxygen and carbon. Acetic acid is released due to the transfer of the hydrogen atom in the hydroxyl group. The resulting acetic acid forms a salt when taken with pyridine in a 1:2 molar ratio and does not affect the course of the reaction. 3O-Monoacetate-13,22-dimethoxystaxybothrin (X) was obtained by acylation of 13,22-dimethoxystaxybothrin (III) with acetic anhydride under dry pyridine conditions.

In order to study the reactions that are carried out due to the second reaction center group in the molecule of 13,22- Dimethoxysatibotrin (III), the reactions of compound (III) with acetic anhydride in a 1:2 molar ratio were studied in the presence of various solvents.

During the experiments, when 13,22-Dimethoxysatibotrin is taken with acetic anhydride in a 1:2 molar ratio, O-diacetate compounds are formed. The effect of the nature of the solvents on the reaction processes was studied and it was found that pyridine is a relatively favorable solvent for these reactions. The reactions proceed according to the following equation.

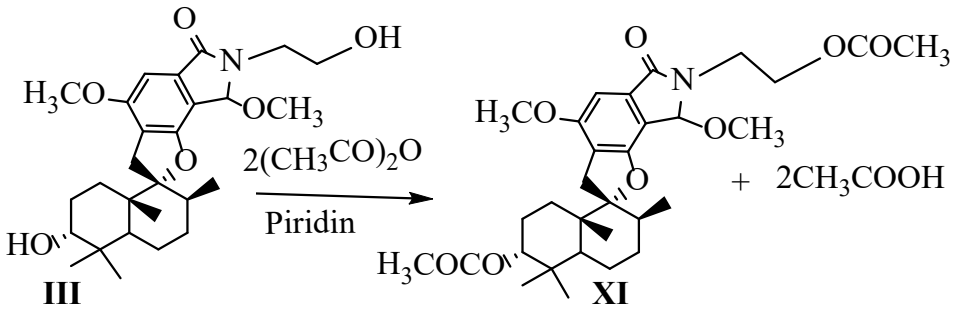

Theobtained3O,24O-diacetate–13,22-dimethoxystaxybotrin (XI) compound was found to have the elemental composition $C_{31}H_{42}NO_8$ and R_f=0,33.Based on the studies conducted, it was found that O-diacetate products are formed in the reactions of 13,22-dimethoxystaxybotrin with acetic anhydride in a 1:2 molar ratio.

The appearance of signals at 156.72; 150.24; 135.75; 118.12; 115.32; 97.43 m.u. in the^{13}C NMR spectrum of the investigated substance III (Table 1), indicates the presence of a benzene nucleus bound to five carbon atoms in the 13,22-Dimethoxystaxybotrin molecule. Accordingly, in the^{1}H NMR spectrum of III at 7.35 m.u. The presence of a singlet signal indicates the presence of one aromatic proton.

The formation of diacetate indicates the presence of two hydroxyl groups in the 13,22-dimethoxystaxybothrin (III) molecule. The occurrence of resonance frequencies at 3.79 m.u., characteristic of the methoxyl group in the 1H NMR spectrum of diacetate XI, indicates that the methoxyl group in this region is a methoxyl group attached to the benzene ring. Indeed, the appearance of a signal at 154.97 m.u., which belongs to the carbon atom attached to the methoxyl group attached to the benzene ring, in the 13C NMR spectrum, once again proves the presence of a methoxyl group attached to the benzene ring in 13,22-dimethoxystaxybothrin (III).

A comparative analysis of the^{1}H NMR spectra of compounds I and XI shows that the appearance of a single proton triplet signal at 4.56 m.u. in the^{1}H NMR spectrum of diacetate XI indicates that the proton in the acetoxyl group is geminally bound. Therefore, the corresponding hydroxyl group

is located on the secondary carbon, and the appearance of a signal at 74.82 m.u. in the ^{13}C NMR spectrum of 13,22-dimethoxystaxybothrin confirms the presence of a secondary carbonyl carbon atom.

Figure 2. *^{1}H-^{13}C NMR correlation spectrum of 13,22-Dimethoxystaxybothrin diacetate(XI) showing the effect of chemical shift*

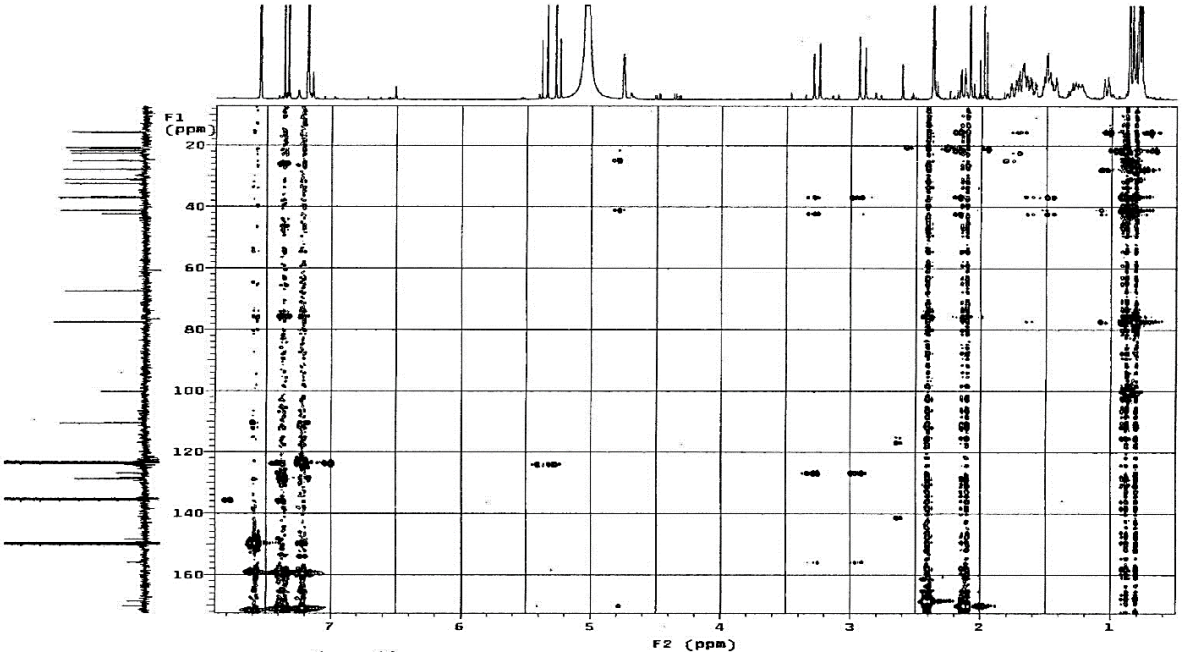

Figure 1. *H NMR spectrum of 13,22-Dimethoxysatibotrin*

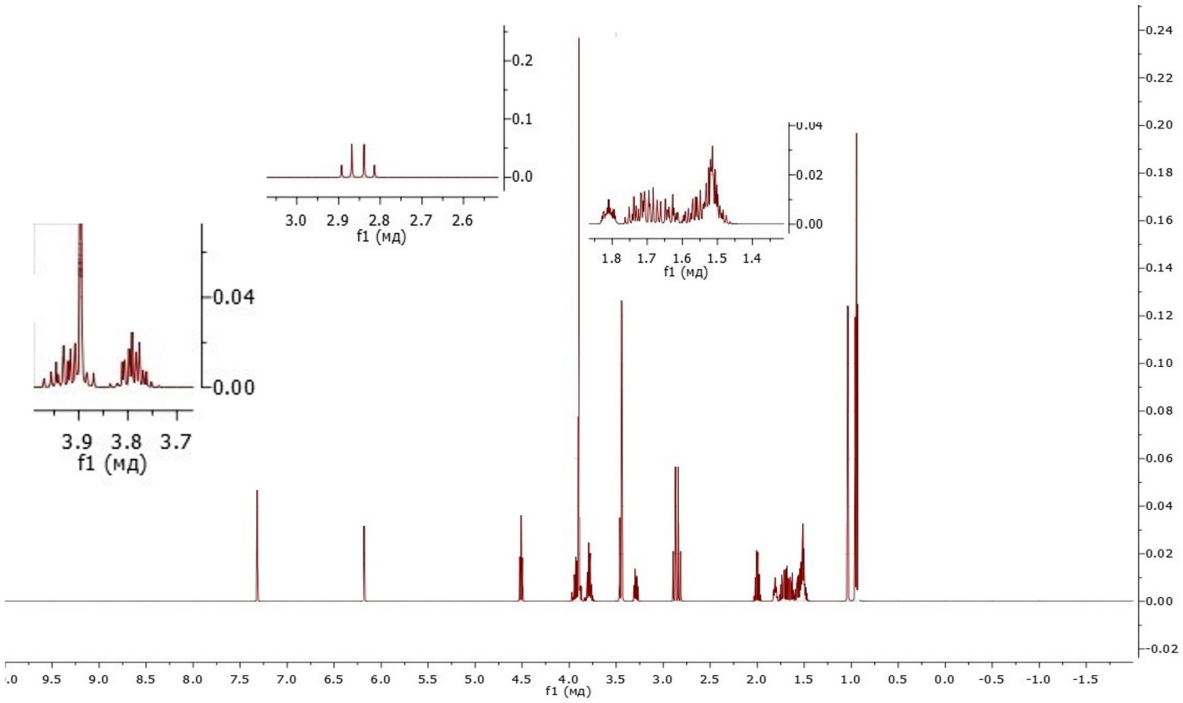

The formation of a signal in the ^{13}C NMR spectrum of 13,22-Dimethoxysatibotrin (III) at 168.85 m.u. indicates the presence of a functional group in the substance, either urea or an isomerization group with an azomethineoxy rearrangement. The choice between them will be made later.

Table 1.

Atom C	Substances			
	III		XI	
	Δc	δн(J, Hz)	Δc	δн(J, Hz)
1	24.71	α 2.27 td (13; 3.5) β 1.10 dt (13; 3.4)	24.62	α 1.71 td (13; 3.5) β 1.56 dt (13; 3.4)
2	26.07	α 1.70; β 1.98 tt (13; 3.4)	30.68	α 1.65; β 1.80 tt (13; 3.4)
3	74.82	3.60	80.32	4.56
4	38.25	–	38.07	–
5	40.39	2.57 dd (13; 2.5)	46.09	1.91 dd (13; 2.5)
6	21.32	β 1.43 kd (13; 3.5)	21.38	β 1.53 kd (13; 3.5)
7	31.60		29.32	1.49. 1.52
8	37.32		36.10	2.01s
9	99.19		99.42	
10	42.75		42.12	
11	32.59	α 3.36 d (17) β 2.94 d (17)	31.86	α 2.91 d (17) β 2.85 d (17)
12	118.12		117.23	
13	150.24		154.97	
14	97.43	7.16s	98.67	7.30s
15	135.75	–	128.18	–
16	115.32	–	117.23	–
17	156.72	–	156.89	–
18	15.87	0.78 d (6)	17.11	0.94 d (6)
19	16.19	0.99 s	17.65	0.99 d
20	29.15	1.22 s	29.20	0.95 s
21	22.74	0.91 s	22.39	0.90 s
22	89.31	2.35s	89.26	4.21s
23	168.85		169.10	
24	60.54	3.98 m (2H)	62.45	4.28. 4.32 m (2H)
25	46.02	3.68; 3.98 m	44.78	3.75; 3.81 m
CH_3O-13	55.56	3.79 s	55.98	3.79 s
CH_3O-22	53.28	3.68c	56.14	3.68
24Ac-CH_3			20.83	3.89
24Ac-C-			170.83	
3Ac-CH_3			21.21	2.03s
3Ac-C			170.86	

Note: The spectrum of 13,22-Dimethoxystaxybothrin was recorded in deuteropyridine and 3O,24O-Diacetate –13,22-dimethoxystaxybothrin was recorded in deuterochloroform solvents. The chemical shifts, multiplicity and spin-spin (SSTC) coupling constant were determined from the 2M ^{1}H-^{1}H,^{1}H-^{13}C ЯМR correlation spectra. Abbreviations: s-singlet, d-doublet, t-triplet, dd-doublet-doublet, td-triplet-doublet, dt-doublet-triplet, tt-triplet-triplet, kd-quartet-doublet, m-multiplet

References

Hodgson, M.J., Morey, P., Leung, W.Y., Morrow, L., Miller, D., Jarvis, B.B., Robbins, H., Halsey, J.F., Storey, E. Building-associatedpulmonary disease from exposure to *Stachybotrys chartarum* and *Aspergillus versicolor*. J. Occup. Environ. Med. 1998. – 40. – P. 241–249.

Kuhn, D.M., Ghannoum, M.A. Indoor mold, toxigenic fungi, and *Stachybotrys chartarum:* Infectious disease perspective. Clin.Microbio. Rev. 2003. – 16. – P. 144–172.

Castlebury, L.A., Rossman, A.Y., Sung, G., Hyten, A.S., Spatafora, J.W. Multigene phylogeny reveals new lineage for *Stachybotrys chartarum*, the indoor air fungus. Mycol. Res. 2004. – 108. – P. 864–872.

Johanning, E., Biagini, R., Hull, D., Morey, P., Jarvis, B., Landsbergis, P. Health and immunology study following exposure totoxigenic fungi (*Stachybotrys chartarum*) in a water–damaged office environment. Int. Arch. Occup. Environ. Health 1996. – 68. – P. 207–218.

Dearborn, D.G., Smith, P.G., Dahms, B.B., Allan, T.M., Sorenson, W.G., Montana, E., Etzel, R.A. Clinical profile of 30 infants withacute pulmonary hemorrhage in Cleveland. Pediatrics 2002. – 110. – P. 627–637.

Chung, Y.J., Copeland, L.B., Doerfler, D.L., Ward, M.D.W. The relative allergenicity of *Stachybotrys chartarum* compared to housedust mite extracts in a mouse model. Inhal. Toxicol. 2010. – 22. – P. 460–468.

Kock, J., Gottschalk, C., Ulrich, S., Schwaiger, K., Gareis, M., Niessen, L. Rapid and selective detection of macrocyclic trichotheceneproducing *Stachybotrys chartarum* strains by loop–mediated isothermal amplification (LAMP). Anal. Bioanal. Chem. 2021. – 413. – P. 4801–4813.

Vesper, S.J., Magnuson, M.L., Dearborn, D.G., Yike, I., Haugland, R.A. Initial characterization of the hemolysin stachylysin from *Stachybotrys chartarum*. Infect. Immun. 2001. – 69. – P. 912–916.

Tojiyeva S.N., Kamolov L.S. *Stachybotrys chartarum* zaharli zambururug'idan staxibotridialni ajratib olish va tuzulishini o'rganish. QarDUxabarlari. 2024-yil(1)2.69–76 p.

Tojiyeva S.N., Kamolov L.S., Ro'ziyeva Z.Q., Ziyodov Sh.U. Low molecular weight metabolites of fungi. 22-methoxystachybotrin from *Stachybotrys sp*. QarDUxabarlari. Ilmiy –nazariy, uslubiy jurnal.Qarshi 2022 yil. 5/1 sonli. – P. 41–49.

Tojiyeva S.N., Kamolov L., Naxatov I. Isolation of 3O-acetatestachybotridial from the toxic mushroom *Stachybotrys chartarum* Uz-21 and study of its structure. Universum, Химия и биология выпуск: – 10 (124). 2024. – P. 30–34.

submitted 17.08.2025;
accepted for publication 02.09.2025;
published 29.09.2025

Contact: sevara. tojeyeva 145@gmail.com; kamolov.luqmon@mail.ru;
naxatov.innat@mail.ru; kaxarovam1234567890@gmail.com

The Austrian Journal of Technical and Natural Sciences, No 7–8
ISSN 2310-5607

PREMIER Publishing
ppublishing.org

DOI:10.29013/AJT-25-7.8-36-40

ANALYTICAL APPLICATION OF DEVELOPED INVERSION VOLTAMPEROMETRIC METHODS IN FOOD PRODUCT ANALYSIS

Asrorova Zukhra [1], ***Yakhshieva Zukhra*** [1]

[1] Jizzakh State Pedagogical University (Uzbekistan)

Cite: *Asrorova Z., Yakhshieva Z. (2025). Analytical Application of Developed Inversion Voltamperometric Methods in Food Product Analysis. Austrian Journal of Technical and Natural Sciences 2025, No 7–8.* https://doi.org/10.29013/AJT-25-7.8-36-40

Abstract

This article presents the results of food product analysis, specifically focusing on meat products, which are essential to human life. Selective, rapid, and accurate inversion voltammetric methods have been developed for the determination of zinc in meat. The obtained results are presented and compared, showing that at a confidence level of to.95, no statistically significant discrepancies were found in comparison with control and certified values of the determined metal. In all cases, the relative standard deviation (Sr) did not exceed 0.33, and the total time required for the simultaneous determination of all components in the analyzed sample – without extraction-based separation or the use of additional procedures – was no more than 30–40 minutes. To obtain more complete information on the metrological characteristics of the proposed methods, the lower detection limit for zinc(II) was established at 0.001 μg in 10.0 mL of the analyzed solution

Keywords: *voltammetry, inversion voltammetry, food products, zinc ions*

The determination of heavy toxic elements is of particular importance and necessity, as the Republic of Uzbekistan, due to its geographical location, is situated in a very hot climatic region. As a result, the population tends to consume food products in quantities that significantly exceed the recommended intake levels, leading to the accumulation of substantial amounts of toxic metals in the human body. Therefore, strict analytical control (monitoring) of the content of these elements in food products is a pressing and highly relevant task for modern electroanalytical chemistry and environmental science.

As is well known, the inversion voltammetric method is used in the analysis of macro- and micro-objects to determine concentrations of individual elements or relatively small groups of them (typically 3–4 metals) in the range of 10^{-9} to 10^{-5}%. This is due to the fact that the optimal conditions for determining individual elements by the developed method vary significantly depending on the mode and potential of preconcentration, the nature and type of the indicator electrode, as well as the composition and concentration of supporting electrolytes and buffer solutions. Therefore, even in synthetic model solutions, the number of elements that can be deter-

mined using a single polarogram or voltammogram should not exceed five to six.

On the other hand, when solving analytical problems under industrial conditions or in research work – especially in the absence of the aforementioned multi-element analytical methods – it becomes necessary and important to determine the maximum number of elements from a single portion of the analyzed material. Examples of such objects include expensive high-purity materials and substances, as well as samples with limited quantities due to their uniqueness or the complexity of their manufacturing process, such as space objects, lunar soil fragments, and others. These critically important tasks become even more relevant when analyzing micro-objects, such as localized areas of crystals and films, environmental samples, biological materials, blood, food products, beverages, and so on.

It should be noted that due to the wide range of applications for the same materials and objects across various fields of science and technology, the requirements for impurity content can vary significantly. Therefore, it is both reasonable and relevant to develop multi-element analysis schemes, followed by the selection of methods that are optimal for the determination of individual elements or their specific groups. Thus, the challenges of multi-element analysis also apply to inversion voltammetry, a method that is widely used in the analysis of micro-objects.

From the theoretical foundations and results of experimental studies in the inversion voltammetry method, it follows that the simultaneous determination of 10 or more elements using a single voltammogram is practically impossible and unfeasible at the current stage of the method's development. In our opinion, a promising approach is the creation of theoretical and experimental bases for a developed method of multi-element sequential analysis, which combines the use of a single initial sample portion with optimal conditions for the final determination of individual elements or fragments and groups with similar properties.

Since zinc(II) ions possess chromophoric properties, most methods use reagents that do not contain chromophoric groups. Zinc(II) ions form very strong coordination bonds with any donor atoms. Selective reagents for zinc(II) are compounds containing phenolic OH groups and nitrogen donor atoms. We have developed photometric methods for determining zinc(II) in the form of various ligand complexes with the organic reagent Cupferon, which exhibits high sensitivity and selectivity.

For the successful resolution of nutritional problems, it is important to timely consider and evaluate the potential use of new sources of dietary proteins, including those previously neglected. However, even more important and relevant is the determination of toxic impurities in food industry products, since the content of carcinogens, mutagens, and toxic trace elements is strictly regulated and must not exceed the maximum permissible concentrations.

Existing standard atomic absorption and photometric methods for zinc determination are labor-intensive and not rapid; in many cases, they require preliminary separation of the target metals from the main matrix before analysis. Therefore, the development of electrochemical methods for determining toxic metals in food products – offering improved metrological characteristics and economic advantages – is a pressing task in modern analytical chemistry and public health protection.

The developed methods were applied for the determination of trace amounts of zinc(II) with the possibility of using the organic reagent Cupferon ($C_6H_5N(NO)ONH_4$) in the analysis of meat products.

Experimental Section

Sampling and Preliminary Preparation of Analyzed Samples

The high sensitivity of inversion voltammetry necessitates the exclusion of all possible sample contaminations, which may originate from reagents, laboratory glassware, or any apparatus contacting the samples. It has been established that the accuracy of analytical results largely depends on errors in sampling and sample preparation; therefore, these operations require the utmost and careful attention from researchers. As a rule, polyethylene bottles should be pre-treated with various cleaning agents, since even perfectly clean polyethylene surfaces tend to adsorb metals.

Selection of Determination Stage Conditions

When determining metal contents by the inversion voltammetric method, a sample solution of 25–30 mL is introduced into the cell, and several drops (up to 10) of 0.02 M mercury(II) nitrate solution of analytical grade or high purity are added. A pre-electrolysis of the analyzed solution is carried out for 30–90 seconds (depending on the nature and concentration of the components) at –1.0 V using a magnetic stirrer (1500 rpm). After the pre-electrolysis time has elapsed, the solution is allowed to rest for 15–30 seconds, and the voltammogram (peak) is recorded in the potential range from –0.9 to –0.1 V. Then, the electrode is held at –0.1 V for 45 seconds to fully dissolve all concentrated components from the electrode. Based on the peak heights recorded, the working sensitivity of the instrument and the necessary pre-electrolysis time are selected. The analysis procedure is then repeated under the chosen conditions until reproducible peaks and accurate results for zinc ion determination are obtained. The standard addition should be chosen such that the concentration of the determined metal in the sample solution approximately doubles.

Since hydrogen ions participate in the electrode reaction, the half-wave potential (E½) of both waves depends on the background pH according to the equation:

$$E_{1/2} = E^0 - 0{,}059\frac{m}{n}pH$$

where:

E^0 – standard electrode potential;

m – number of protons;

n – number of electrons involved in the electrode reaction.

As the pH of the medium increases, both waves shift toward more negative potentials.

The number of protons participating in the electrode reaction can be found from the slope (tangent of the angle) of the E½ vs. pH dependence using the formula above.

$$m = \frac{n}{0{,}0591}tg\alpha$$

The accuracy of trace metal determination by inversion voltammetry using the method described above is very high.

Results and Discussion

Solutions and Reagents

A standard zinc(II) solution (1 mg/mL) was prepared by dissolving a weighed amount of Mohr's salt in water with the addition of 10 mL of concentrated H_2SO_4 to acidify the solution. Solutions with lower zinc(II) concentrations were prepared by successive dilution of the standard solution. Cupferon ($C_6H_5N(NO)ONH_4$) was dissolved in water to prepare a 0.1% solution in a volumetric flask.

Cupferon reagent was purified by reprecipitation from ethanol solutions through the addition of water, followed by distillation. The ionic strength of the solutions (μ = 0.1) was maintained constant by adding a calculated amount of KNO_3. An acetate buffer solution was used to achieve the required acidity of the solutions. All reagents used were of analytical grade (reagent grade or chemically pure). Preliminary experiments showed that Cupferon ($C_6H_5N(NO)ONH_4$) forms a colored complex with zinc(II), which is well soluble in non-polar organic solvents.

Effect of pH.

In the study of solution acidity, it was found that at pH = 1, an acidic medium is formed; at pH = 3–6, the solution remains clear with a red color; and at pH = 8–10, a dark brown precipitate forms.

Analysis Procedure Algorithm

1. A portion of the crushed sample (5–6 g) is weighed in a porcelain crucible or beaker with an accuracy of ±0.01 g and placed in a muffle furnace for ashing. The sample is first gently heated for one hour, after which a few drops of nitric acid (1:1) are added, and ashing is continued at a temperature not exceeding 550 °C until a light-colored ash of constant mass is obtained. The ash is then dissolved in 5–10 mL of hydrochloric acid (1:1), and the solution is quantitatively transferred to a 50 mL volumetric flask and brought to volume with 0.1 M HCl. 20.0 mL of the prepared sample solution (aliquot) is introduced into the voltammetric cell, and the analysis is then carried out.

2. A 3 g portion of beef was placed in a porcelain crucible and dried to remove moisture. The sample was then ashed – first over an open flame, followed by ashing in a muffle furnace at 500 °C. To accelerate the ashing process, the crucible was periodically removed from

the furnace, cooled, and the contents moistened with a 3% hydrogen peroxide (H_2O_2) solution. The sample was then dried on a water bath and in a drying oven, and further ignited until a uniform brown-colored mass was obtained.

The cooled ash was treated twice with 2 mL portions of 2 M hydrochloric acid (HCl), heated on a water bath, and stirred with a glass rod. The resulting solution was filtered into a beaker and heated to 60 °C in a water bath. Then, 5 mL of a 1% solution of ammonium alum, 5 g of ammonium chloride (NH_4Cl), and concentrated ammonia solution (NH_4OH) were added. The solution was maintained at 60 °C to ensure coagulation of the iron and aluminum hydroxide precipitate.

The beaker and precipitate were washed five times with hot water containing a few drops of NH_4OH. The precipitate was then dissolved in 10 mL of 2 M HCl, filtered into a 100 mL volumetric flask, and the volume was brought to the mark with distilled water. An aliquot of the resulting solution was taken, and the zinc(II) content was determined using Cupferon.

In all cases, the relative standard deviation (Sr) did not exceed 0.33, and the total time required for the simultaneous determination of all components in the analyzed sample – without extraction-based separation or the use of additional techniques – was no more than 30–40 minutes. To obtain more comprehensive information on the metrological characteristics of the proposed methods, we determined the lower detection limit of zinc(II) based on methods reported in the literature, which was found to be 0.001 μg in 10.0 mL of the analyzed solution.

The developed inversion voltammetric methods are not only comparable to GOST-certified and officially validated methods in terms of accuracy and selectivity, but in some cases even surpass them in certain metrological characteristics and analytical parameters.

Conclusions

The developed inversion voltammetric methods for the determination of zinc demonstrate high accuracy and reproducibility. The results obtained once again confirm the validity, necessity, and importance of the analyses performed on meat samples.

For the purpose of metrological evaluation of the proposed metal determination methods, as well as to assess their competitiveness and potential inclusion among the arsenal of well-established and widely used electroanalytical techniques, we compared the results obtained using the developed inversion voltammetric methods with those acquired through atomic absorption and GOST-certified methods. The comparison showed that our proposed inversion voltammetric techniques for zinc determination are comparable in terms of speed, accuracy, and reproducibility, as well as in their lower detection limits. Moreover, in certain metrological parameters, they even surpass the reference methods – namely, atomic absorption and GOST (photometric) techniques.

References

Gevorgyan A. M., Talipov Sh.T., Khadeev V. A., Mukhamedzhanova D. V. Volt-amperometric behavior of sodium diethyldithiocarbamate on a platinum anode in a dimethylformamide medium // Zhurn. anal. chemistry. 1980. – Vol. 35. – No. 10. – P. 2026–2028. (In English)

Lurye Yu. Yu. Handbook of analytical chemistry. – M.: Chemistry. 1979. – P. 230–236. (In English)

Fisher R. A. Statistical methods for researchers involved in the determination of noble elements. – M.; Mir. 1988. – 287 p. (In English)

Gevorgyan A. M., Yakhshieva Z. Z., Kireev G. V. Complexometric amperometry in determining noble metals in environmental objects. Abstract of the report of the Rep. scientific-practical conf. “Kimyoning dolzarb muammolari” – Samarkand. 2009. – P. 65–66. (In English)

Gevorgyan A. M., Talipov Sh. T., Khadeev V. A., Mirzoyan I. I. Voltammetric curves of thionalide oxidation on a platinum microanode in glacial acetic acid. // Deposited in VINITI – No. 4616–81. from 24.09.81. – P. 1–3. (In English)

Gevorgyan A. M., Yakhshieva Z. Z., Zhuraeva L. K., Rakhimberdieva G. U. Determination of the number of electrons given up during the electrooxidation of one thiourea molecule. // Republican scientific and practical conference with international participation “Green Chemistry” – in the interests of sustainable development. Samarkand. 2012. (In English)
Yakhshieva Z The conditions for amperometric titration of the Ag (I) ion with sulfur-containing reagents. // Universia Chemistry and Biology. Electronic scientific journal. 2016. – No. 4 (22). (In English)

submitted 16.08.2025;
accepted for publication 30.08.2025;
published 29.09.2025

Contact: yaxshiyeva67@mail.ru

The Austrian Journal of Technical and Natural Sciences, No 7–8
ISSN 2310-5607

PREMIER Publishing
ppublishing.org

DOI:10.29013/AJT-25-7.8-41-50

SYNTHESIS OF ISOMERIC ALKYL DERIVATIVES IN THE 2-METHYL-5-CHLOROBENZIMIDAZOLE SERIES

Zhuraev B. B. [1], ***Rakhmatov E. O.*** [1],
Muminova T. M. [1], ***Ziyodov D. A.*** [1], ***Ortikov I. S.*** [1]

[1] S. Yunusov Institute of the Chemistry of Plant Substances, Academy of Sciences of the Republic of Uzbekistan, Tashkent, Uzbekistan

Cite: *Zhuraev B. B., Rakhmatov E. O., Muminova T. M., Ziyodov D. A., Ortikov I. S. (2025). Synthesis of Isomeric Alkyl Derivatives in the 2-Methyl-5-Chlorobenzimidazole Series. Austrian Journal of Technical and Natural Sciences 2025, No 7–8.* https://doi.org/10.29013/AJT-25-7.8-41-50

Abstract

Origin of the problem. Currently, benzimidazoles and their derivatives are of great importance from theoretical and practical points of view among heterocyclic compounds. The presence in their molecule of a benzene and imidazole ring and an ambifunctional fragment containing a secondary nitrogen atom leads to their existence in various tautomeric forms and allows regioselective reactions of alkylation, acylation, arylsulfonylation and chlorosulfonylation at one or another center.

It should be noted that among benzimidazoles and their derivatives there are quite highly effective drugs that are successfully used in agriculture, medicine, pharmaceuticals and other industries. For example, Veliparib (ABT-888) is a potential anticancer drug that acts as a PARP *(poly(ADP-ribose) polymerase)* inhibitor. Veliparib during radiation therapy causes the whole brain to work effectively against brain metastases from non-small cell lung cancer *(NSCLC – –Non-small-cell lung cancer).* Additionally, Lerisetron (F-0930-RS) is a drug that acts as an antagonist (namely, it kills the virus) at the 5-HT3 receptor, which is a potent antiemetic and is being used in clinical trials to treat nausea associated with cancer chemotherapy.

Thanks to scientific research, the synthesis and introduction into practice of various pharmacologically active drugs is becoming important for restoring the health of many patients. The synthesis of new derivatives of heterocyclic compounds, the study of possible reaction mechanisms, and the implementation of targeted synthesis of biologically active substances are also important.

Therefore, the study of alkylation reactions of benzimidazoles and their derivatives, identification of the main factors influencing the course and direction of reactions, and the search for biologically active substances among synthesized compounds is an urgent task.

Purpose of the work. Synthesis of N^{endo}-protected 2-methyl-5-chlorobenzimidazoles (N-alkyl derivatives), determination of the type and ratio of isomers, determination of factors influencing the course of the reaction and study of the structure of the resulting compounds (IR, ^{1}H and ^{13}C NMR spectroscopy).

Methodology. Carrying out reactions of introducing an alkyl group into the 2-methyl-5-chlorobenzimidazole molecule with alkyl halides in a protic solvent (alcohol) in the presence of alkalis and studying the proposed mechanism. Studying the structure of substances using IR,^{1}H and^{13}C NMR spectroscopy methods.

Scientific novelty. Taking into account the main factors influencing the course of reactions, new isomeric 1,2-dialkyl derivatives were synthesized under various conditions and an optimal method for obtaining the target products was developed.

Results obtained. The synthesis of new dialkyl isomers in the series of benzimidazoles containing various alkyl groups has been carried out. The structure of the substances was analyzed based on IR,^{1}H and^{13}C NMR spectroscopy data and their correspondence to the proposed structures was proven.

Keywords: *2-methyl-5-chlorobenzimidazole, alkylation, isomers, alkyl halides, electrophilic substitution, column chromatography*

Peculiarities:

— effective methods for the synthesis of 2-methyl-5-chlorobenzimidazole, 1,2-dialkyl-5-chlorobenzimidazoles have been created;

— by the alkylation reaction of 2-methyl-5-chlorobenzimidazole in an alkaline medium, methods have been developed for the preparation of isomeric 1,2-dialkylbenzimidazoles in high yields;

— the reliability of the research results is confirmed on the basis of data obtained using modern methods of IR,^{1}H and^{13}C NMR spectroscopy, chromatography (TLC, column) and others.

Introduction

Currently, many studies are being carried out on the basis of heterocyclic compounds, in particular benzimidazoles. The reason is that there are numerous pharmacological and biologically active substances among the five-membered imidazole ring compounds containing two nitrogen atoms.

Previously synthesized substances still attract the attention of organic chemists and pharmacists due to their high biological activity and low toxicity. In particular, one of the important issues is the successful use of benzimidazole derivatives in agriculture and medicine against various diseases.

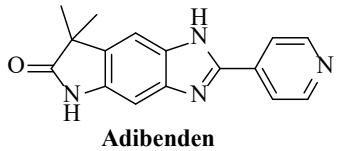

Adibenden
(Phosphodiesterase inhibitor)

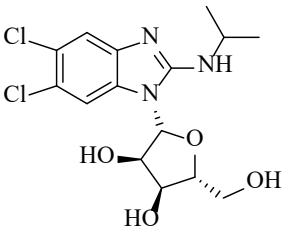

Maribavir
(antiviral agent)

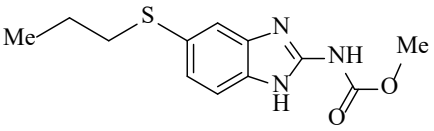

Albendazole
(Anthelmintic)

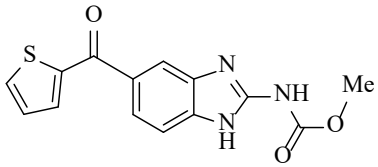

Nocodazole
(anti-cancer drug)

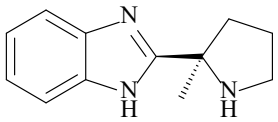

Vleparib
(anti-cancer drug)

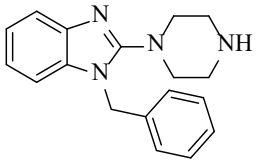

Lerisetron
(antihistamine)

Research into the development of heterocyclic compounds began much earlier, and research is currently being conducted in many countries around the world based on this class of compounds. Among the compounds containing the benzimidazole heterocycle, many drugs have been found that are effectively used in medical practice and agriculture (veterinary medicine). This is due to the fact that the benzimidazole ring is a pharmacophore ring that is included in various drugs. It should be noted that previ-

ous studies have identified among benzimidazoles anticancer (Tahlan S., Kumar S., Narasimhan B., 2019; Tahlan S. et al., 2019), anticholinesterase inhibitors (Tahlan S., Ramasamy K., Lim S. M., Shah S. A.A., Mani V., Narasimhan B., 2019), as well as anthelmintic (Alpan A. S. et al., 2013), anti-inflammatory (Andrzejewska M. et al., 2004), antimalarial (Shaharyar M. et al., 2017), antiviral (Yoon Y. K. et al., 2015) and antimicrobial (Tahlan S. et al., 2019) drugs:

Information on the use of benzimidazoles in medicine and agriculture, and their analogues (benzoxazoles, benzothiazoles) is given in the following articles (Kakkar S. et al. 2018; Tahlan S., Kumar S., Narasimhan B., 2019; Prajapat P., 2018), published in foreign journals. Among them are benzimidazoles, an important class of heterocyclic compounds, the research of which began many years ago and is expanding every year. In the synthesis of benzimidazoles, readily available o-phenylenediamine and its various derivatives (amidines, acyl products) substituted in the benzene ring and amino group are used as the main starting material. On the other hand, aliphatic and aromatic aldehydes, as well as carboxylic acids, are widely used as electrophilic reagents. To increase the efficiency of reactions, cyclization is usually carried out in the presence of catalysts.

Methods and materials

Solvents: hexane, cyclohexane, chloroform, methyl alcohol, ethyl alcohol, acetone, acetic acid were dried and purified by traditional distillation. IR spectra of the compounds were obtained on a Perkin-Elmer IR-Fourier 2000 spectrometer in tablets with KBr, mass spectra on MS-30 (Kratos), and 1H and 13C NMR spectra were obtained on JNM-ECZ 400 and JNM- ECZ 600 (JEOL, Japan) (internal standard TMC, in δ-scale) with an operating frequency of 400 and 600 MHz in solutions of deuterochloroform ($CDCl_3$), deuteromethanol (CD_3OD) and deuterium oxide (D_2O). Thin layer chromatography (TLC) analysis was carried out on Sorbfil (Russia) and Whatman® UV-254 (Germany) plates. The melting point of the synthesized compounds was determined using Boetius (Germany) and MEL-TEMP (USA) instruments.

Synthesis of 2-methyl-5-chlorobenzimidazole (1) (improved method)

24.7 g (0.17 mol) of 4-chloro-2-nitroaniline, 24 g (0.43 mol) of Fe powder and 48.9 ml (51.4 g) of ice-cold AcOH and 142.8 ml of HCl (32%) were placed in a 1-liter flask. The mixture was heated to 60–70 °C and boiled (105––110 °C) for 2 hours. The mixture is cooled, and the resulting precipitate is filtered and dried at 20–25 °C. The product was neutralized with NaOH solution and then treated with ethanol. The solution was filtered, the ethanol filtrate was diluted with water, and the resulting precipitate was filtered and dried. As a result, 19.5 g (83.4%) of substance (**1**) was synthesized, melting point 205–206 °C, Rf=0.38 (benzene: methanol – 5:1).^{1}H NMR spectrum (CD_3OD, δ, ppm, J/Hz, 400 MHz): 2.56 (3H, s, CH_3), 7.17 (1H, dd, J=1.6, 8.4, H-6), 7.43 (1H, d, J=8.4, H-7), 7.47 (1H, d, J=1.8, H-4).

Synthesis of isomers of 1,2-dimethyl-5-chlorobenzimidazole (2) and 1,2-dimethyl-6-chlorobenzimidazole (3)

Method A *(in the presence of acetone and potash)*: 1.665 g (0.01 mol) of mebinol, 1.5 ml (d = 2.28 g/ml, 2.84 g, 0.01 mol) methyl iodide, 1 g (0.0072 mol) of dried potash, 80 ml of acetone were placed in a one-neck flask with a volume of 250 ml. water bath through reflux for 6 hours and leave overnight. The solvent was then distilled off and the product was recrystallized from cyclohexane (30 ml). As a result, we obtained 1.03 g (62%) a mixture of isomeric products (2.3) with a melting point of 99–100 °C, Rf = 0.34 (benzene: methanol – 5:1) (or: Rf = 0.81 (chloroform: methanol – 10:1)).

Method B *(in the presence of alcohol and alkali)*: 4.995 g (0.03 mol) mebinol, 3.74 ml (d = 2.28 g/ml, 8.52 g, 0.06 mol) methyl iodide, 1.2 g (0.03 mol) were poured into a 500 ml one-neck flask. sodium hydroxide and 80 ml of alcohol, connecting a reflux refrigerator, the mixture was boiled in a water bath for 7 hours and left overnight. The solution was then filtered and the filtrate was diluted with 50 ml of water, then extracted with 30 ml of chloroform (2 times) and the extract was washed with 300 g of 5% NaOH (3 times). The chloroform solution was dried over anhydrous Na_2SO_4 and filtered. The solvent was distilled off and recrystallized from cyclohexane (40 ml)

using a hot filter. As a result, 4.09 g (81.8%) of a mixture of isomeric products (**2,3**) was obtained, melting point 99–100 °C, Rf=0.64 (chloroform: methanol – 20:1).

Compound 2: ^{1}H NMR spectrum ($CDCl_3$, δ, ppm, J/Hz, 400 MHz): 2.58 (3H, s, 2-CH_3, 3.67 (3H, s, N-CH3), 7.15 (1H, dd, J=8.5, J=0.6, H-7), 7.19 (1H, dd, J=8.5, J=1.9, H-6), 7.25 (1H, br.d, J=2.0, H-4)^{13}C NMR ($CDCl_3$, δ, ppm, 100 MHz): 13.97 (2-). CH_3), 30.09 (N-CH3), 109.19 (C-7), 118.89 (C-4), 122.47 (C-6), 127.47 (C-5), 134.54 (C-7a), 141.28 (C-4a), 152.84 (C-2).

Compound 3: ^{1}H NMR spectrum ($CDCl_3$, δ, ppm, J/Hz, 400 MHz): 2.58 (3H, s, 2-CH_3), 3.69 (3H, s, N-CH_3), 7.18 (1H, dd, J=8.5, J=1.8, H-5), 7.25 (1H, br.d, J=2.0, H-7), 7.56 (1H, dd, J=8.6, J=0.5, H-4).^{13}C NMR ($CDCl_3$, δ, ppm, 100 MHz): 14.00 (2-CH_3), 30.12 (N-CH_3), 109.68 (C-4), 119.88 (C-7), 123.55 (C-5), 127.83 (C-6), 136.53 (C-4a), 143.46 (C-7a), 153.26 (C-2).

The ratio of isomers **2** and **3** based on the integrated intensity of proton signals in the ^{1}H NMR spectra was 51.3%: 48.7%, respectively.

Preparation of isomers of 1-ethyl-2-methyl-5-chlorobenzimidazole (4) and 1-ethyl-2-methyl-6-chlorobenzimidazole (5)

In a one-neck flask with a volume of 500 ml, 3.33 g (0.02 mol) of 2-methyl-5-chlorobenzimidazole, 4.5 ml (d = 1.47 g/ml, 6.54 g, 0.06 mol) ethyl bromide, 0.8 g (0.02 mol) sodium hydroxide, 60 ml were placed alcohol and boiled through reflux in for 6 hours and the reaction mixture was left overnight. The solution was filtered and the filtrate was extracted with 30 ml chloroform (2 times), then washed with 300 g 5% NaOH (3–4 times) and 50 ml water (3 times). The extract was dried over anhydrous Na_2SO_4 and filtered. The solvent was distilled off, and the dry residue was recrystallized from 30–40 ml of cyclohexane. As a result, 2.6 g (78%) mixture of isomeric products (4.5) was synthesized, melting point 104–105 °C, Rf = 0.81 (chloroform: methanol – 15:1), Rf = 0.66 (chloroform: methanol – 20:1).^{1}H NMR spectrum ($CDCl_3$, δ, ppm, J/Hz, 400 MHz): 1.39 (3H, t, J=7.2, CH_2CH_3), 2.58 (3H, s, 2-CH_3), 4.12 (2H, quartet, J=7.3, CH_2CH_3), 7.18 (2H, d, J=8.2, H-6.7), 7.65 (1H, d, J=1.2, H-4).^{13}C NMR spectrum ($CDCl_3$, δ, ppm, 100 MHz): 13.90 (N-CH_2CH_3), 14.99 (2-CH_3), 38.78 (N-CH_2CH_3), 109.24 (C-7), 109.75 (C-4), 118.98 (C-6), 127.41 (C-5), 133.46 (C-7a), 143.69 (C-4a), 152.55 (C-2).

The ratio of isomers **4** and **5** based on the integrated intensity of proton signals in the NMR spectra was 95%: 5%, respectively.

Synthesis of isomers of 1-butyl-2-methyl-5-chlorobenzimidazole (6) and 1-butyl-2-methyl-6-chlorobenzimidazole (7) and preparation of their hydrochlorides (8,9)

4.995 g (0.03 mol) of 2-methyl-5-chlorobenzimidazole (mebinol), 6.5 ml (d= 1.276 g/ml, 8.22 g, 0.06 mol) butyl bromide, 1.2 g (0.03 mol) caustic were placed in a round-bottomed one-neck flask with a volume of 500 ml sodium and 90 ml alcohol and the mixture was refluxed for 7–8 hours and left overnight. The solution in the flask was washed with 200 g NaOH (5%) (2–3 times), extracted with 40 ml chloroform (2 times) and washed with 50 ml water (3 times) until pH=7–8. The chloroform solution was dried over anhydrous Na_2SO_4 and filtered. The solvent was distilled completely in vacuum (on a rotary evaporator). As a result, a mixture of oily isomer was obtained: 1-butyl-2-methyl-5-chlorobenzimidazole (**6**) and 1-butyl-2-methyl-6-chlorobenzimidazole (**7**) with a yield of 67%. The purity of the oily product was examined by TLC (Rf=0.69, chloroform: methanol – 20:1) and was determined to be pure (one spot).

Product (**6,7**) was dissolved in 20–30 ml of absolute cyclohexane, HCl (NaCl + H_2SO_4 (conc.)) gas was continuously passed into the product solution for 30 minutes, the resulting precipitate was filtered, washed with cyclohexane (2 times, 10–15 ml) and dried. The resulting hydrochloride (**8,9**) of the isomers 1-butyl-2-methyl-5-chlorobenzimidazole and 1-butyl-2-methyl-6-chlorobenzimidazole was isolated in the form of white crystals with a yield of 3.8 g (76%), melting point 166–168 °C, Rf=0.8 (chloroform: methanol – 20:1).

Compound 8: ^{1}H NMR spectrum (D_2O, δ, ppm, J/Hz, 400 MHz): 0.99 (3H, t, J=7.2, $(CH_2)_3$-CH_3), 1.41–1.48 (2H, m, CH-$_2CH_2CH_2CH_3$), 1.84–1.93 (2H, m, CH_2CH-$_2CH_2CH_3$), 2.91 (3H, s, 2-CH_3), 7.53 (2H, dd, J=2.1, J=8.4, H-4.6), 7.86 (1H, d, J=8.4, H-7).

Compound 9: ^{1}H NMR spectrum (D_2O, δ, ppm, J/Hz, 400 MHz): 0.98 (3H, t, J=7.2, $(CH_2)_3$-CH_3), 1.41–1.48 (2H, m, $CH_2CH_2CH_2CH_3$), 1.84–1.93 (2H, m, $CH_2CH_2CH_2CH_3$), 2.91 (3H, s, 2-CH_3), 7.66–7.76 (3H, m, H-4,5,7).

Compounds 8 and 9: ^{13}C NMR spectrum (D_2O, δ, ppm, 100 MHz): 11.62, 13.42, 19.90, 30.81, 30.89, 45.63, 112.97, 114.10, 114.17, 115.40, 126.61, 127.09, 129.02, 130.87, 131.04, 131.62, 131.85, 132.90.

Synthesis of 1-benzyl-2-methyl-5-chlorobenzimidazole and 1-benzyl-2-methyl-6-chlorobenzimidazole (10, 11)

In a one-neck flask with a volume of 500 ml, 4.995 g (0.03 mol) of mebinol (**1**), 6.9 ml (d = 1.1 g/ml, 7.59 g, 0.06 mol) benzyl chloride, 1 g (0.025 mol) NaOH and 60 ml of ethanol were placed, the mixture was boiled 8 hours through reflux and left for 24 hours. Then the solution in the flask was filtered and the filtrate was treated with 5% (250 g) NaOH (3 times), then extracted with chloroform 2 times (30 ml each), then washed 2–3 times (50 ml each) with water to neutral pH. The extract was dried over anhydrous Na_2SO_4 and filtered. The solvent was distilled to dryness, and the residue was recrystallized from 30 ml of hexane. A 4.09 g (81.8%) mixture of isomeric products was obtained; after purification by CC, individual substances **10** (9.1%) and **11** (72.7%) were isolated.

- **10:** Melting point 101–102 °C, Rf=0.77 (chloroform: methanol – 20:1). ^{1}H NMR spectrum ($CDCl_3$, δ, ppm, J/Hz, 600 MHz): 2.56 (3H, s, 2-CH_3), 5.30 (2H, s, CH_2-Ph), 7.02 (2H, m, H–2',6'), 7.30 (3H, m, H-3',4',5'), 7.11 (1H, d, J=8.5, H-7), 7.16 (1H, dd, J=8.5, 1.9, H-6), 7.69 (1H, d, J=1.9, H-4).
- **11:** Melting point 98–100 °C, Rf= 0.73 (chloroform: methanol – 20:1). ^{1}H NMR spectrum ($CDCl_3$, δ, ppm, J/Hz, 600 MHz): 2.56 (3H, s, 2-CH_3), 5.28 (2H, s, CH_2-Ph), 7.03 (2H, m, H–2',6'), 7.32 (3H, m, H-3',4',5'), 7.19 (1H, d, J=1.9, H-7), 7.21 (1H, dd, J=8.5, 1.9, H-5), 7.62 (1H, dd, J=8.2, H-4).

Results obtained and their discussion

The object of study, 2-methyl-5-chlorobenzimidazole (mebinol), is of great interest both theoretically and practically among heterocyclic compounds. The presence of benzene and imidazole rings and the N-H group in it allow various exchange and condensation reactions to occur with high yields. The dialkyl products obtained from this basis are mainly used in medicine, agriculture and pharmaceuticals.

We initially conducted studies on a one-step reduction-cyclization reaction in the presence of acetic acid, azoamine, and iron powder and prepared the resulting heterocyclic product for use in the synthesis of dialkyl derivatives needed for our main experiments.

For this purpose, reactions of 2-methyl-5-chlorobenzimidazole [12] with alkyl halides in K_2CO_3/acetone or NaOH/alcohol were carried out under optimal conditions and temperatures, and the expected substances were synthesized in high yields. Homological changes in the obtained dialkyl products and some physicochemical properties were analyzed and an appropriate production procedure was developed.

2-methyl-5-chlorobenzimidazole (**1**) was synthesized using an improved initial reaction method. To do this, using 4-chloro-2-nitroaniline (azoamine), glacial acetic acid and iron powders in appropriate molar proportions, concentrated hydrochloric acid was diluted in a ratio of 5:1 and heated in a water bath at 70–80 °C for 2 hours until the release of H_2 gas stops. The mixture was then left at this temperature for 1 hour and again heated at 90–100 °C for 2 hours. A 20% solution of sodium hydroxide was added until the pH of the medium reached 9–10, then the precipitate that formed was filtered:

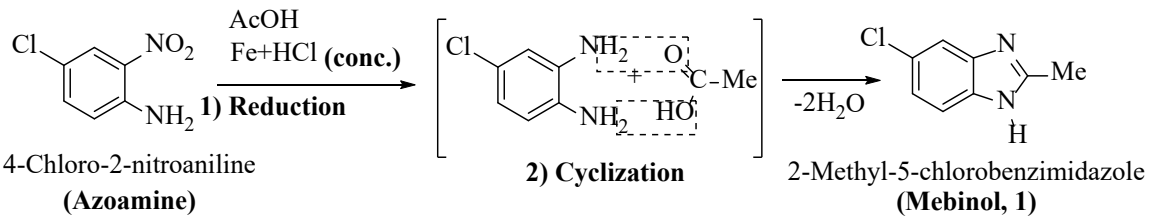

The reaction mixture was washed with water until neutral, alcohol was added, the mixture was heated for 1 hour and filtered hot. Alcohol was distilled from the filtrate, 3 times more water was added to the remaining residue (in a ratio of 1:3, by volume), and the precipitate that formed was filtered off. At the end of the reaction, the product was purified by recrystallization from 30% alcohol to obtain 2-methyl-5-chlorobenzimidazole (**1**) in 83.4% yield. It is noteworthy that this reaction was carried out using the "one-pot synthesis" method. During the reaction, reduction and cyclization reactions occur; in this case, an intermediate reduction product, 2-amino-4-chloroaniline, is first formed, which then reacts with carboxylic acids and the corresponding 2-methyl-5-chlorobenzimidazole (**1**) is released in high yield. The hydrogen atom of the N-H group, the imidazole ring of benzimidazole, is active and readily undergoes electrophilic substitution in the presence of alkyl halides. Therefore, alkylation reactions of the resulting 2-methyl-5-chlorobenzimidazole (**1**) were carried out under various conditions.

It is known that 2-substituted benzimidazoles can undergo prototropic tautomerism under alkaline conditions, therefore, in S_E reactions, isomeric 5/6-substituted benzimidazoles can be formed:

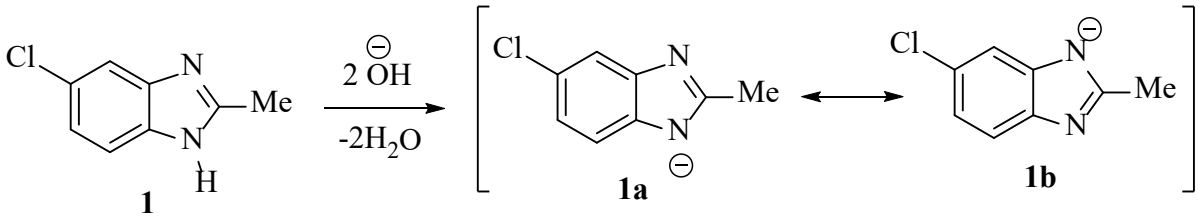

Selective alkylation reactions of 2-methyl-5-chlorobenzimidazole (**1**) were carried out in acetone/potash or alcohol/alkali systems. However, in acetone the reaction does not proceed to completion, and the yield is relatively low. It was found that the alcohol/alkali system was a more suitable condition for the synthesis of dialkyl products in high yields.

It was initially concluded that the reaction produced only one isomeric dialkyl product. Indeed, the resulting alkyl products give one spot on TLC and have a small melting range, which indicate that a single substance is formed. However, doubling the amounts of proton and carbon atom signals in the ^1H and ^{13}C NMR spectra and their manifestation in very close regions confirms the formation of a mixture of isomers.

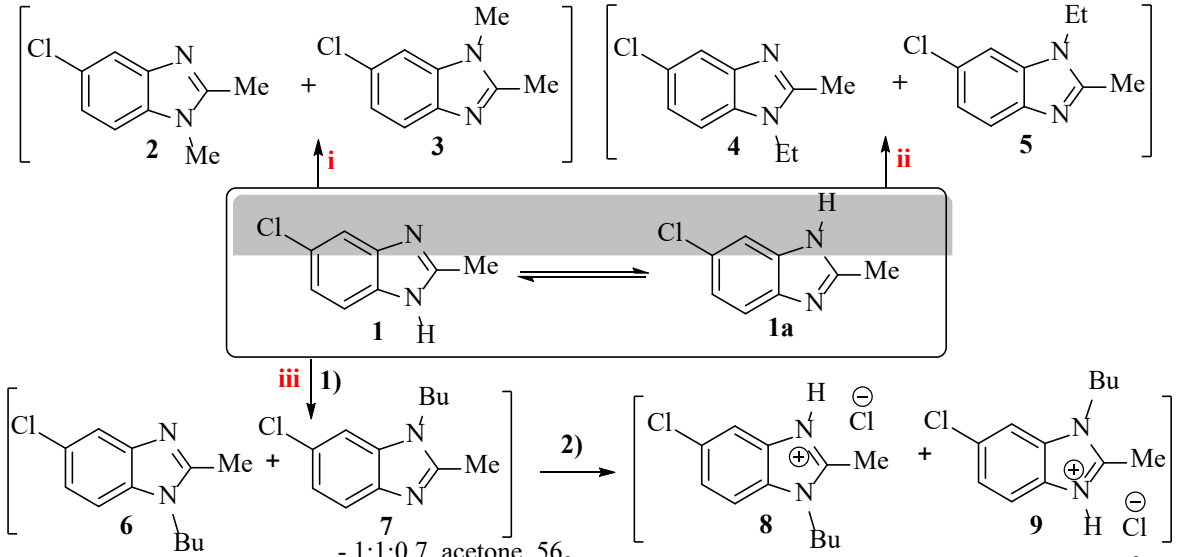

i: Method A: 1:MeI:K_2CO_3 - 1:1:0.7, acetone, 56^0C, 6 h; **Method B: 1**:MeI:NaOH - 1:2:1, ethanol, 78^0C, 7 hours.

ii: 1: EtBr:NaOH - 1:3:1, ethanol, 78^0C, 6 h.

iii: 1) Method B: 1: BuBr:NaOH - 1:2:1, ethanol, 78^0C, 7-8 hours; **2)** Cyclohexane, HCl (gas) [NaCl + H_2SO_4].

Methyl iodide, ethyl bromide, butyl bromide and benzyl chloride were selected as alkyl halides. Initially, the reactions were carried out in two ways with methyl iodide, ethyl and butyl bromides. It is noteworthy that in methylation reactions a mixture of two isomers (**2,3**) was obtained with a yield of 62% in the acetone/potash system and 81.8% in the alcohol/alkali system:

Therefore, in subsequent studies we used the alcohol/alkali system. In particular, the ethylation reaction was also carried out according to this system and isomeric products (**4,5**) were obtained with a yield of 78%. The bottling reaction was also carried out according to method **B**, in which oily alkyl products (**6,7**) are formed with a yield of 67% (Rf = = 0.69, chloroform: methanol-20:1) [13]. However, this mixture of isomers also produces one spot on TLC. To obtain their hydrochlorides (**8,9**), dry gaseous HCl was passed through a solution of substances (**6,7**) in the form of a base in absolute cyclohexane (yield of hydrochloride (**8,9**) 76%, Rf=0.8, chloroform: methanol – 20:1). The structures of the obtained compounds were determined using spectral and X-ray diffraction analysis (XRD) (Juraev B., Oxunxo'jayeva Z., Tojiboev A., Bobakulov Kh., Turgunov K., Elmuradov B., Zokhidov K., 2023).

Table 1. *Some physicochemical data of compounds (1-11)*

Compound	Brutto formula	Melting point,^{0}C	Rf (system)	Yield, %
1	$C_8H_7N_2Cl$	205–206	0.38 (**A**)	83.4
2,3 (isomer)	$C_9H_9N_2Cl$	99–100	0.34 (**A**); 0.81 (**B**)	62 (method A) 81.8 (method B)
4,5 (isomer)	$C_{10}H_{11}N_2Cl$	104–105	0.39 (**A**); 0.88 (**C**)	58 (method A) 78 (method B)
6,7 (isomer)	$C_{12}H_{15}N_2Cl$	oil	0.69 (**D**)	67
8,9 (isomer)	$C_{12}H_{16}N_2Cl_2$	166–168	0.8 (**D**)	76
10	$C_{15}H_{13}N_2Cl$	101–102	0.77 (**D**)	9.1
11	$C_{15}H_{13}N_2Cl$	98–100	0.73 (**D**)	72.7

System: *benzene: methanol – 5:1 (**A**); chloroform: methanol – 10:1 (**B**); chloroform: methanol – 15:1 (**C**); chloroform: methanol – 20:1 (**D**)*

Continuing the research, we studied benzylation in the presence of alkali in alcohol by boiling a mixture of reagents in the ratio: **1**: BnCl: NaOH – 1:2:1 for 7–8 hours (78^{o}C). After the mixture of reaction products (**10,11**) was separated by extraction ($CHCl_3$), washed with an aqueous (5%) NaOH solution and dried over Na_2SO_4 (anhydrous), then the solvent (chloroform) was distilled. It should be emphasized that the resulting mixture of isomers forms two spots in TLC, which are separated by column chromatography. Thus, a mixture of 1-benzyl-2-methyl-5-chlorobenzimidazole (**10**, 9.1%) and 1-benzyl-2-methyl-6-chlorobenzimidazole (**11**, 72.7%) was obtained in the form of light yellow crystals with a total yield of 81.8%:

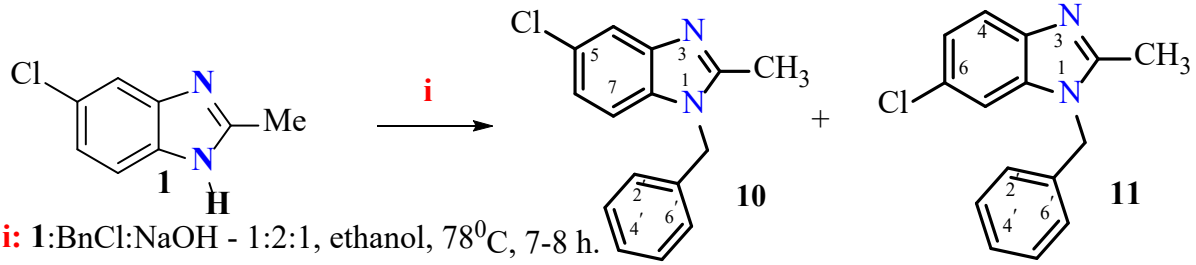

i: **1**:BnCl:NaOH - 1:2:1, ethanol, 78^{0}C, 7-8 h.

The results of ^{1}H NMR spectroscopy show that the ratio of isomeric benzyl products (**10:11**) is ~1:9. The spectra of individual isomers (**10** and **11**), isolated in pure form by column chromatography, are presented in Figures 1 and 2. In particular, in the spectrum of substance 10 (Figure 1), obtained in $CDCl_3$, in the region of 2.56 ppm. chemical

shifts are observed in the form of a three-proton singlet (3H, s), belonging to the CH_3 group, at 5.30 ppm. two-proton singlet (2H, c) of the aliphatic protons of the benzyl group.

Figure 1. *^{1}H NMR spectrum of 1-benzyl-2-methyl-5-chlorobenzimidazole (10) in $CDCl_3$*

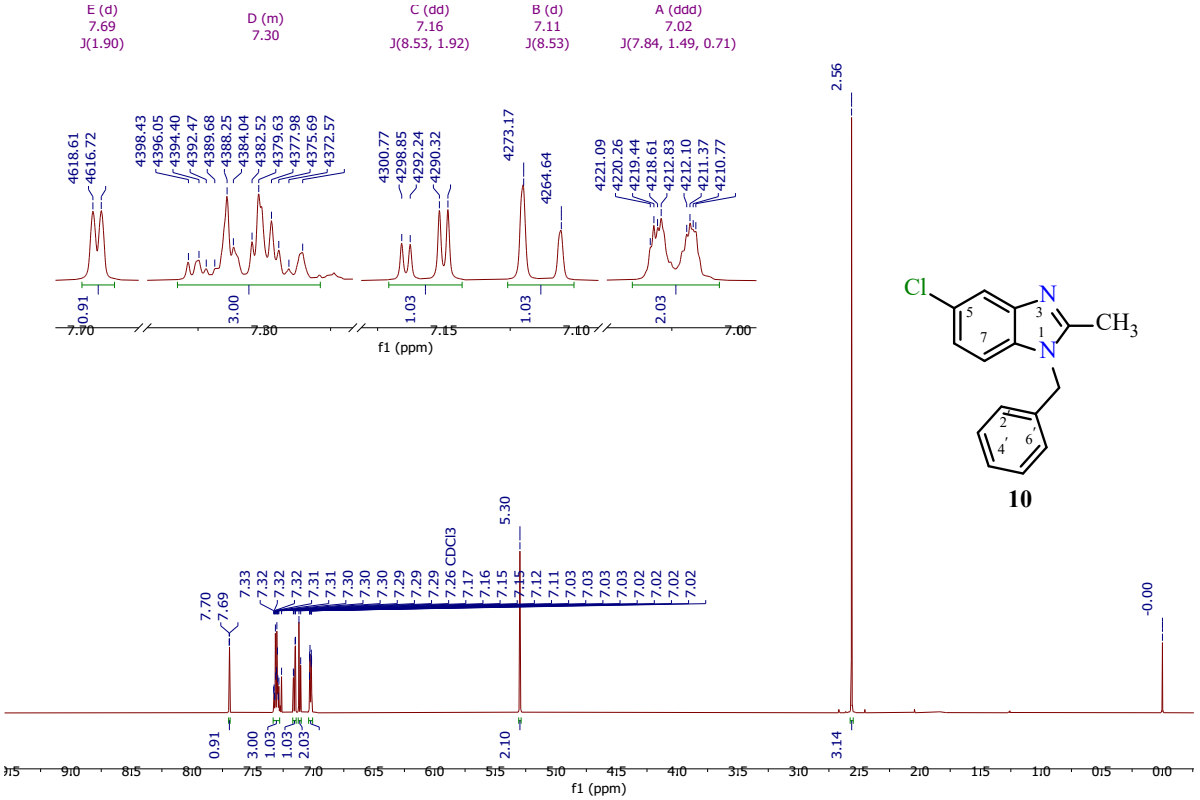

Figure 2. *^{1}H NMR spectrum of 1-benzyl-2-methyl-6-chlorobenzimidazole (11) in $CDCl_3$*

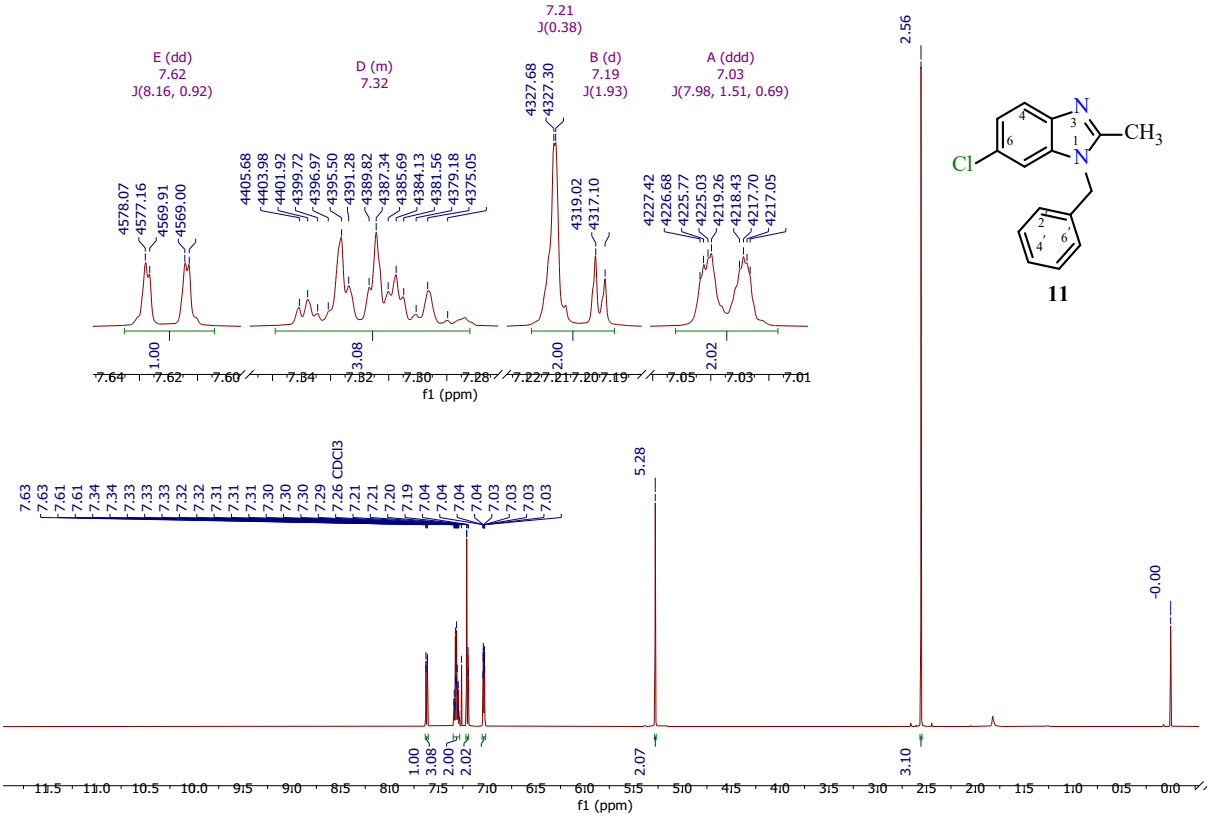

There are also signals in the region of 7.02 ppm. in the form of a two-proton multiplet (2H, m), belonging to the equivalent hydrogens of the benzyl fragment in positions 2′ and 6′, signals at 7.30 ppm. in the form of a three-proton multiplet (3H, m) were assigned to the H-3′,5′ protons (Fig. 1).

Furthermore, the presence of proton signals at 7.69, 7.11, and 7.16 ppm of aromatic hydrogen benzymidazole fragments at positions C-4, C-6, and C-7 manifests as a single-proton doublet (J=1.9, H-4; J=8.5, H-6) and doublet (J=8.5, 1.9, H-7). These data confirm the structure of compound **10** (Fig. 1).

The ^{1}H NMR spectrum of compound **11** (Fig. 2) also shows the presence of three-proton signals at H 2.56 and 5.28 ppm, belonging to the CH_3 group, and two-proton singlet signals specific to the methylene group of the benzene fragment.

Along with signals in the form of two-proton (2H, m, H-2′, H-6′) multiplets at δ 7.03 and 7.32 ppm, and in the form of three-proton multiplets (H-3′, H-4′, H-5′) corresponding to the aromatic hydrogens of the benzyl group, as well as at 7.19, 7.62 and 7.21 ppm, signals of benzimidazole aromatic hydrogens appear as a doublet (d, J=1.9, H-7; J=8.2, H-4) and a doublet of doublets (J=8.5, 1.9, H-5). These data confirm our understanding of the structure of this molecule (Pic. 2).

Conclusions

The alkylation reactions of 2-methyl-5-chlorobenzimidazole with various alkyl halides were carried out under different conditions: acetone/potassium carbonate and ethanol/alkali. Studies have shown that when using the ethanol/alkali system, alkylation products are formed with relatively high yields.

It was established that upon alkylation with methyl iodide, ethyl bromide, butyl bromide, and benzyl chlorides, a mixture of isomers is formed. It should be noted that with an increase in the alkyl chain length in the series of alkyl halides, the melting point of the products decreases, and in some cases (during butylation), oily isomeric products are formed. The ratio of isomers formed in the methylation, ethylation, and butylation reactions was determined based on the analysis of ^{1}H NMR spectra. For the first time, it was possible to separate the benzylation products into individual isomers using column chromatography. The obtained products serve as raw materials for further research.

Acknowledgement

Authors thank for financial support of the Ministry of Higher Education, Science and Innovations of Uzbekistan (Grant No F-FA-2021–408 “Study of the regularities of introduction of pharmacophore fragments into the molecule on the basis of modern cross-coupling and heterocyclization reactions”.

References

Tahlan S., Kumar S., Narasimhan B. Pharmacological significance of heterocyclic 1 H-benzimidazole scaffolds: a review // *BMC chemistry*. 2019. – Vol. 12–13. –No. 1. – P. 1–21.

Tahlan S. et al. Design, synthesis and therapeutic potential of 3-(2-(1H-benzo [d] imidazol-2-ylthio) acetamido)-N-(substituted phenyl) benzamide analogues // *Chemistry Central Journal*. 2019. – Vol. 12. – No. 1. – P. 1–12.

Tahlan S., Ramasamy K., Lim S. M., Shah S. A.A., Mani V., Narasimhan B. (2-(1H-Benzo[d] imidazol-2-ylthio)acetamido)-N-(substituted phenyl) benzamides: design, synthesis and biological evaluation // *BMC Chemistry*. 2019. – Vol. 3. – No. 12. – P. 1–16.

Alpan A. S. et al. Synthesis, biological activity and molecular modeling studies on 1H-benzimidazole derivatives as acetylcholinesterase inhibitors // *Bioorganic & medicinal chemistry*. 2013. –Vol.21. – No. 17. –P. 4928–4937.

Andrzejewska M. et al. Synthesis, and antiprotozoal and antibacterial activities of S-substituted 4, 6-dibromo-and 4, 6-dichloro-2-mercaptobenzimidazoles // *European journal of pharmaceutical sciences*. 2004. – Vol. 21. – No. 2–3. –P. 323–329.

Shaharyar M. et al. Benzimidazoles: A biologically active compounds // *Arabian Journal of Chemistry*. 2017. –Vol. 10. – P. S157-S173.

Yoon Y. K. et al. Synthesis and evaluation of antimycobacterial activity of new benzimidazole aminoesters // *European journal of medicinal chemistry*. 2015. – T. 93. – P. 614–624.
Tahlan S. et al. 2-Mercaptobenzimidazole Schiff bases: design, synthesis, antimicrobial studies and anticancer activity on HCT-116 cell line // *Mini reviews in medicinal chemistry*. 2019. – Vol. 19. –No. 13. – P. 1080–1092.
Kakkar S. et al. Benzoxazole derivatives: design, synthesis and biological evaluation // *Chemistry Central Journal*. – 2018. –T.12. – № 1. – C. 1–16.
Tahlan S., Kumar S., Narasimhan B. Pharmacological significance of heterocyclic 1 H-benzimidazole scaffolds: a review // *BMC chemistry*. 2019. – Vol. 13. – P. 101–122.
Prajapat P. Importance of Benzothiazole Motif in Modern Drug Discovery: Introduction // *Modern Approaches in Drug Designing* (MADD). 2018. – Vol. 1. – No. 4. – P. 1–2.
Jurayev B. B., Ortikov I. S., Elmuradov B. J., Tadjimukhamedov Kh.S. // Improved methods of synthesis of 2-alkyl-5-chlorobenzimidazoles // "Zamonaviy kimyoning dolzarb muammolari" mavzusidagi respublika miqyosidagi xorijiy olimlar ishtirokidagi onlayn ilmiy-amaliy anjumani, Buxoro, 2020, 4–5-dekabr, 254–256-betlar.
Juraev B., Oxunxo'jayeva Z., Tojiboev A., Bobakulov Kh., Turgunov K., Elmuradov B., Zokhidov K. Synthesis, crystal structure and Hirshfeld surface analysis of isomeric 1-butyl-5/6-chloro-2-methyl-1H-benzo[d]imidazoles hydrochloride monohydrate. *Journal of Molecular Structure*, 2023. – 1289. Article ID. 135844 (7 pages). DOI: 10.1016/j.molstruc.2023.135844

submitted 03.07.2025;
accepted for publication 19.07.2025;
published 29.09.2025

Contact: jorayevbaxromjon75@gmail.com

The Austrian Journal of Technical and Natural Sciences, No 7–8
ISSN 2310-5607

PREMIER Publishing
ppublishing.org

DOI:10.29013/AJT-25-7.8-51-55

PRODUCTION OF POLYMER-BASED RESINS FROM PYROLYSIS PRODUCTS AND THEIR SOLUBILITY IN SOLVENTS

Ziyadullayev Anvar Egamberdiyevich [1], ***Eshpulatov Mukhammadi*** [1], ***Abdiyeva Dinara*** [1], ***Yakubova Charos*** [1], ***Nurmanov Suvonqul Erxonovich*** [2]

[1] Tashkent Chemical-Technological Institute of Republic of Uzbekistan, Uzbekistan

[2] National University of Uzbekistan, Tashkent, Uzbekistan

Cite: *Ziyadullayev A.E., Eshpulatov M., Abdiyeva D., Yakubova Ch., Nurmanov S.E. (2025). Production of Polymer-Based Resins From Pyrolysis Products and Their Solubility in Solvents. Austrian Journal of Technical and Natural Sciences 2025, No 7–8.* https://doi.org/10.29013/AJT-25-7.8-51-55

Abstract

This scientific article investigates the chemical composition and physicochemical properties of pyrolysis fractions obtained from the Ustyurt gas-chemical complex, as well as the possibilities of obtaining high-quality petroleum polymer resins through their modification. Pyrolysis distillate, condensate, and tar products were fractionated according to temperature ranges, and their density, viscosity, thermal stability, and compositional components were analyzed. Additionally, the solubility of the resins in various solvents was evaluated depending on temperature and time.

Keywords: *pyrolysis fraction, petroleum polymer resin, distillate, condensate, tar, solubility, temperature, solvent, viscosity, density, Ustyurt gas-chemical complex*

Introduction

In modern industry, the creation of corrosion-resistant, environmentally friendly, and economically efficient coatings is of great importance. At the Ustyurt gas-chemical complex, various fractions such as pyrolysis distillate, pyrolysis condensate, and tar products are separated. These fractions are rich in benzene, toluene, styrene, aromatic, and aliphatic hydrocarbons, enabling the production of highly reactive petroleum polymer resins. Contemporary research in the petrochemical field primarily focuses on the chemistry of pyrolysis fractions and improving the quality of petroleum polymer resins derived from them. Petrov and Ivanov (2018) thoroughly studied the chemical composition of raw materials in petroleum pyrolysis and their role in polymer resin production, identifying key problems and solutions in the field (Petrov, V.V., & Ivanov, A.N., 2018). Sokolov and Lebedev (2017) analyzed the synthesis of polymer resins from pyrolysis products and the possibilities of their modification using various chemical methods (Sokolov, M.M., & Lebedev, P.I., 2017).

Zhang and Wang (2019) determined the physicochemical properties of pyrolysis fractions obtained from natural gas processing, emphasizing their high chemical activity (Zhang, L., & Wang, H., 2019). Kim and Lee (2020) investigated the tar product formed during pyrolysis, noting its high molecular weight and thermal stability, recommending it as a promising raw material for high-quality polymers (Kim, S.Y., & Lee, J.H., 2020).

Singh and Sharma (2016) proposed phenol-formaldehyde-based polycondensation methods to chemically modify petroleum polymer resins and improve their physicomechanical properties (Singh, R., & Sharma, P., 2016). Zhao and Chen (2021) conducted a deeper analysis of this process, achieving enhanced thermal and mechanical stability of resins derived from pyrolysis fractions (Zhao, Y., & Chen, X., 2021).

In the field of corrosion-resistant coatings, Kumar and Singh (2018) assessed the effectiveness of polymer coatings derived from petroleum on metal surfaces (Kumar, A., & Singh, J., 2018). Chen and Zhang (2019) thoroughly studied the production technology and characteristics of these coatings, recommending them as effective agents for industrial corrosion protection (Chen, L., & Zhang, T., 2019). Furthermore, opportunities and challenges in producing polymer resins from natural gas pyrolysis fractions have been analyzed, highlighting the importance of scientific research in this area (Karimov, B., & Rasulov, D., 2022). Scientific investigations have also been conducted on processing pyrolysis products from the Ustyurt gas-chemical complex and producing high-quality coating materials based on them (Toshpulatov, M., & Abdurahmonov, I., 2021).

Results and Discussion

The chemical composition and physicochemical properties of pyrolysis fractions obtained from the Ustyurt chemical complex were investigated. The pyrolysis distillate, characterized by its light and easily flammable nature, mainly consists of benzene, alcohols, and acidic compounds. The pyrolysis condensate contains a high amount of aromatic and condensed components with a high molecular weight and a distinctive odor, providing significant advantages during modification due to its high thermal stability. The tar product, composed of solid, black-colored resins with a high molecular weight, can be utilized primarily as a solid and highly thermally stable material. The analysis of the fraction compositions confirmed the possibility of chemical modification of these fractions to obtain high-quality petroleum polymer resins. Resins obtained through polycondensation reactions based on phenol, formaldehyde, and maleic anhydride exhibited good physicomechanical properties. Their heat resistance and acid-water resistance were also evaluated through appropriate tests.

The density, boiling point, and viscosity of the pyrolysis distillate, condensate, and tar products obtained from the Ustyurt gas-chemical complex, as well as the presence of alcohols, acids, aromatic hydrocarbons, and resin components in the fractions, differ significantly in composition. Therefore, these substances were studied primarily based on their density, boiling point, and viscosity parameters (Table 1).

Table 1. *General analysis of pyrolysis fractions according to their physicochemical properties*

No.	Fractions	Temperature °C	Viscosity, mPa•s	Density, g/cm³
1	Distillate	60–90	0.8	0.75
2	Distillate	90–120	1.0	0.75
3	Distillate	120–150	1.5	0.75
4	Condensate	150–200	100	1.1
5	Condensate	200–250	150	1.1
6	Condensate	> 250	200	1.1

By fractionating the pyrolysis products based on temperature, three main fractions with distinct differences in density, viscosity, and chemical composition were separated. The pyrolysis distillate obtained in the temperature range of 60–150 °C had a density of 0.75 g/cm³ and a viscosity between 0.8––1.5 mPa·s. Its composition included benzene, alcohols, and acids, making it a reactive and liquid raw material suitable for the production of modified resins. The pyrolysis condensate collected between 150–250 °C had a density of 1.1 g/cm³ and a viscosity ranging from 100 to 200 mPa·s. It consisted mainly of aromatic and high molecular weight hydrocarbons and was effectively used for producing stable and durable polymer-based materials. The tar product, obtained at temperatures above 250 °C, exhibited a density of 1.3 g/cm³ and viscosity equal to or greater than 200 mPa·s. It was composed of solid, polymer-structured resins, distinguishing it as an important raw material for industrial applications such as corrosion-resistant coatings and insulation materials. Overall, as the temperature increased, the density and viscosity of the fractions also increased, which enhanced their polymer properties and expanded their potential industrial applications.

Additionally, the physical and chemical properties of the isolated tar product – such as density, softening point, odor, and viscosity – determine the resin's performance characteristics and its field of application. In this study, the high density, softening point, and viscosity levels of the resins were considered key indicators for evaluating their quality (Table 2).

Table 2. *Physicochemical properties of tar products*

No.	Properties	Value	Description
1	Density, g/cm³	1.3	Hard and dense consistency
2	Melting point, °C	> 250	Low melting point, solid resin
3	Odor	Odorless	Odorless, suitable for industry
4	Viscosity, mPa · s	1000+	Very high viscosity

The density of the studied resins was found to be 1.3 g/cm³, and they exhibited a solid and dense consistency. Their softening point was above 250 °C, indicating their thermal stability at high temperatures. The absence of odor enhances their industrial usability, which is particularly important for applications sensitive to smell.

The viscosity exceeded 1000 mPa · s, demonstrating that the resins have very high adhesiveness and the ability to form a solid structure. Thus, these two-layered pyrolysis products separated from the raw materials serve as high-quality insulating and coating materials in the production of petroleum polymer resins with the participation of solvents. They are effectively used in various industrial sectors as protective coatings and adhesives. Their chemical composition and interaction with solvents play a crucial role in their application. Solubility is significantly dependent on temperature, as an increase in temperature activates molecular motion and accelerates the dissolution process. In this study, the solubility of the isolated resins was investigated in various solvents within the temperature range of 50 °C to 75 °C (Table 3).

Table 3. *Temperature dependence of petroleum polymer resin solubility*

No.	Solvents	50 °C	60 °C	70 °C	75 °C	Average (%)
1	Benzene	32	40	45	58	**43.8**
2	Ethyl acetate	20	27	28	38	**28.2**
3	Chloroform	35	60	–	–	**23.7**
4	n-Heptane	12	17	25	25	**19.8**

The solubility of petroleum polymer resin in various solvents was observed to increase with rising temperature. According to the study results, the solubility of the resin was

examined in benzene, ethyl acetate, chloroform, and n-heptane within the temperature range of 50 °C to 75 °C. In benzene, solubility consistently increased with temperature, reaching 58% at 75 °C from 32% at 50 °C, with an average solubility of 43.8%. This indicates that benzene is an effective solvent for the resin. Solubility in ethyl acetate was relatively low, increasing from 20% to 38% with rising temperature, averaging 28.2%. Solubility in n-heptane was very low, rising from 12% at 50 °C to 25% at 75 °C, with an average of 19.8%. Considering the boiling points of solvents, the solubility of the resins was also studied in suitable solvents within the temperature range of 80 °C to 120 °C (Table 4).

Table 4. *The temperature dependence of the solubility of petroleum polymer resin*

No.	Solvents	80 °C	90 °C	95 °C	100 °C	110 °C
1	Toluene	48	60	70	68	60
2	Xylene	35	45	54	52	46
3	Butyl acetate	24	32	42	41	—
4	Butanol 1	33	40	45	39	30

Among the solvents listed in the second table, toluene shows the highest solubility for the petroleum polymer resin, increasing from 48% to 70% as temperature rises from 90 °C to 95 °C, with an average solubility of about 61.2%. Xylene has an average solubility around 46%, reaching a maximum of 54%, but its solubility decreases with rising temperature. Butyl acetate and butanol-1 exhibit relatively lower solubility levels, averaging around 34.8% and 35.8%, respectively.

Comparing to the solvents in the first table, benzene reaches 58% solubility, while toluene reaches 70% in the second table. Thus, while benzene and toluene offer the highest solubility, solvents like ethyl acetate, butyl acetate, and butanol-1 are safer choices. The resin's solubility depends not only on the solvent type and temperature but also on the duration of the reaction. The study analyzed solubility levels at two temperature ranges (70–75 °C and 80–120 °C), shown in Figure 1.

Figure 1. *Discussion on solubility of petroleum polymer resin in various solvents*

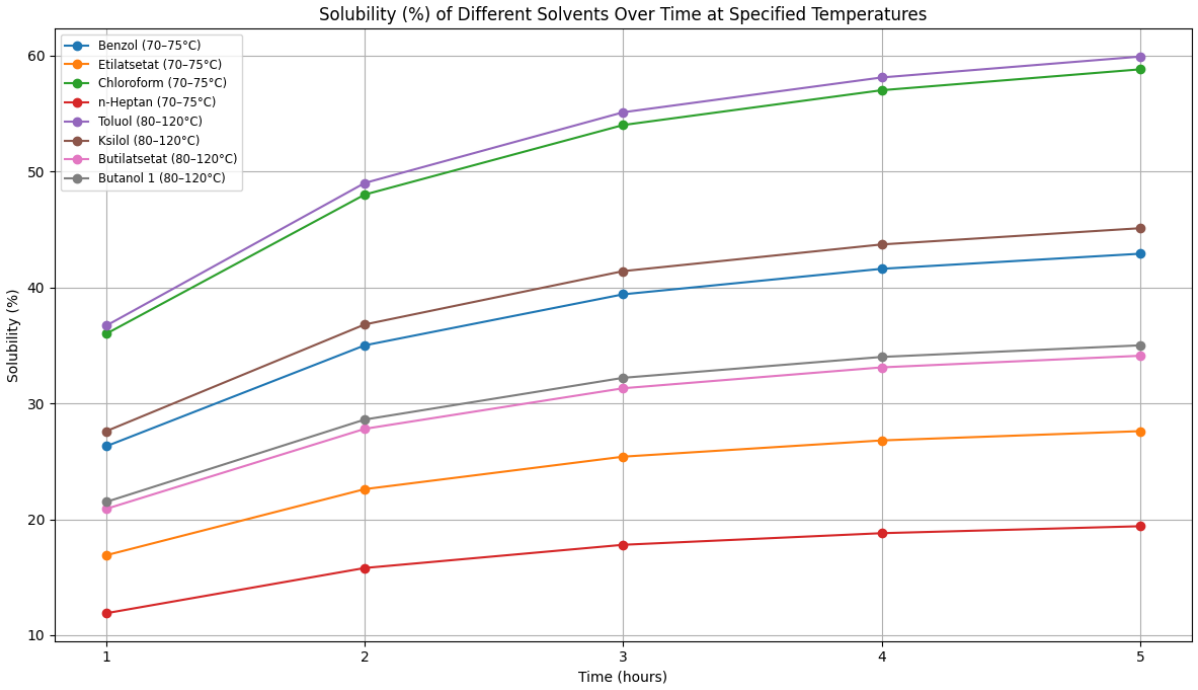

Experimental results show that the solubility of petroleum polymer resin increases depending on temperature and time. Within the temperature range of 70–75 °C, benzene

exhibited high solubility, while in the range of 80–120 °C, toluene and xylene stood out as effective solvents. Over time, the solubility in all solvents increased, although some solvents like n-heptane maintained low solubility. Overall, benzene, toluene, and xylenes are considered the best solvents for dissolving petroleum polymer resin, provided that safety precautions are observed. Solvents with lower solubility (ethyl acetate, butyl acetate, butanol-1) have advantages in terms of safety but lower efficiency. Therefore, when selecting a solvent, a balanced decision must be made considering solubility, temperature, time, and safety factors.

Conclusion

The study results demonstrated that the pyrolysis fractions obtained from the Ustyurt gas-chemical complex are promising raw materials for industry. The distillate collected at 60–150 °C consists of liquid components and can be used in the production of modified resins. The condensate at 150–250 °C and tar product obtained above 250 °C have high density and thermal stability, making them important for polymer resin manufacturing. Although high solubility of resins in benzene and toluene was identified, safety measures must be followed when using these solvents. Ethyl acetate, butyl acetate, and butanol-1, despite their lower solubility, are considered environmentally safer. Overall, analyzing pyrolysis fractions and optimizing resin production technology contribute to increasing efficiency in the petrochemical industry. When choosing solvents, efficiency must be balanced with safety and environmental considerations.

References

Petrov, V. V., & Ivanov, A. N. (2018). Pyrolysis of hydrocarbon raw materials and production of polymer resins. *Journal of Petroleum Chemistry*, – 58(3). – P. 289–301. URL: https://doi.org/10.1134/S096554411803005X

Sokolov, M. M., & Lebedev, P. I. (2017). Polymer resins from petroleum pyrolysis products: synthesis and modification. *Petroleum Chemistry*, – 57(6). – P. 488–495.

Zhang, L., & Wang, H. (2019). Characterization of pyrolysis fractions from natural gas processing. *Fuel Processing Technology*, – 191. – P. 124–132.

Kim, S. Y., & Lee, J. H. (2020). Study on physical properties and chemical composition of tar fractions from pyrolysis of hydrocarbons. *Journal of Analytical and Applied Pyrolysis*, – 147. – 104779 p.

Singh, R., & Sharma, P. (2016). Chemical modification of petroleum-based polymer resins for improved thermal and mechanical properties. *Polymer Engineering and Science*, – 56(12). – P. 1347–1356.

Zhao, Y., & Chen, X. (2021). Synthesis and characterization of phenol-formaldehyde resins modified with petroleum pyrolysis fractions. *Journal of Applied Polymer Science*, – 138(22). – 50456 p.

Kumar, A., & Singh, J. (2018). Corrosion resistance properties of polymer coatings derived from petroleum resins. *Surface & Coatings Technology*, – 350. – P. 290–299.

Chen, L., & Zhang, T. (2019). Protective polymer coatings for metals: synthesis, characterization and corrosion resistance. *Progress in Organic Coatings*, – 136. – 105260 p.

Karimov, B., & Rasulov, D. (2022). O‘zbekistonda tabiiy gaz piroliz mahsulotlarining polimerlashtirish imkoniyatlari. *O‘zbekiston Kimyo Jurnali*, – 48(2). – P. 45–53.

Toshpulatov, M., & Abdurahmonov, I. (2021). Gaz-kimyo komplekslarida piroliz mahsulotlarini qayta ishlash va qoplamalar ishlab chiqarish. *Sanoat Kimyosi va Texnologiyalari*, – 35(4). – P. 72–80.

submitted 12.07.2025;
accepted for publication 27.07.2025;
published 29.09.2025

Contact: anva_ziyadullayev@mail.ru; eshpulatovmuhammad018@gmail.com

The Austrian Journal of Technical and Natural Sciences, No 7–8
ISSN 2310-5607

PREMIER Publishing
ppublishing.org

DOI:10.29013/AJT-25-7.8-56-60

SYNTHESIS OF A THIOMOCHEVINA FRAGMENT BASED ON THE REACTION OF 6-AMINOQUINAZOLIN-4-ONE WITH ISOTHIOCYANATE

Zulpanov Fazliddin Abduxakimovich [1], Egamberdiyev Sobirjon Sulton o'g'li [2], Umarov Muhammadali Ahadkhon ugli [3], Ashirmatova Nargisa Mirtalipovna [4], Elmuradov Burkhon Juraevich [1]

[1] Akad. S. Yu. Yunusov Institute of the Chemistry of Plant Substances, Academy of the Republic of Uzbekistan, Tashkent, Uzbekistan

[2] Republic of Uzbekistan, Sharof Rashidov Samarkand State University, Institute of Biochemistry, chemistry

[3] Mirzo Ulugbek National University of Uzbekistan, Faculty of Chemistry

[4] Tashkent branch of the National Research Nuclear University "MEPhI". Republic of Uzbekistan, Tashkent city

Cite: *Zulpanov F.A., Egamberdiyev S.S., Umarov M.A., Ashirmatova N.M., Elmuradov B.J. (2025). Synthesis of a Thiomochevina Fragment Based on the Reaction of 6-Aminoquinazolin-4-one With Isothiocyanate. Austrian Journal of Technical and Natural Sciences 2025, No 7–8.* https://doi.org/10.29013/AJT-25-7.8-56-60

Abstract

Today, it is important to purposefully create new biologically active compounds, successfully applying them in agriculture and medicine against various harmful insects and diseases. Of particular importance in this regard is the creation of inexpensive, highly effective and environmentally friendly topical preparations, the study of their physicochemical, biological and pharmacological properties. A study of condensed heterocyclic synthesis and biological activity found the production of mixtures, new drugs, including quinazoline-4-one derivatives and the determination of their bioactive derivatives the development of new drugs based on them is relevant.

Keywords: *o*-Aminobenzoic acid, formamide, quinazoline-4-on, nitration, reduction, tin (II)-chloride dihydrate ($SnCl_2 \cdot 2H_2O$), layered chromatography, IQ, and YaMR spectroscopy

Introduction

In recent years, various periparations based on many representatives of derivatives formed on the basis of heterocyclic compounds containing quinazoline have been introduced into agricultural and medical practice (Arun K. Ghosh., Margherita Bindisi. 2015). Currently, it is conducting scientific and practical research aimed at determining the specific aspects of optimal synthesis,

structure and reactivity of quinazolones and their new derivatives, as well as creating biologically active substances with new pharmacophore fragments in their composition (Asma Kh., Rabah A., Antonio I. M., Laiche A., Abdelmalek B., 2018). In medical veterinary practice and agriculture, medicinal products created on the basis of heterocyclic compounds – quinazolones and sulfonamides, formed from condensation with benzene Ringas, are widely used.n medical veterinary practice and agriculture, medicinal products created on the basis of heterocyclic compounds – quinazolones and sulfonamides, formed from condensation with benzene Ringas, are widely used. In particular, preparations created on the basis of compounds of this class are used as herbicides, fungicides (2–3-dimethlquinazolones), bactericides, antigelmints (quinazoline dressing), hypotensive (quinazoline bricmacs) preparations (Asma Kh., Rabah A., Antonio I. M., Laiche A., Abdelmalek B., 2018). Quinazoline is widely used as an inhibitor of harmful substances involved in a large number of biochemical processes in the body. Therefore, scientific research is carried out to carry out the targeted synthesis and modification of new derivatives of these heterocyclic compounds, to determine their structure on the basis of modern methods, to check the various biological properties of the compounds obtained, to create new drugs based on selected biologically active substances (Alagarsamy V., Murugesan S., Dhanabal K., 2007).

Derivatives based on quinazoline have been introduced into various periparatlarr agricultural and medical practices, created on the basis of a very large number of Representatives. Briquettes based on quinzoline have been widely used against viruses, microbes, fungi, colds and cancer (Arun K. Ghosh., Margherita Bindisi. 2015), as well as stimulants for plants (Asma Kh., Rabah A., Antonio I. M., Laiche A., Abdelmalek B., 2018). Substances created on the basis of quinazoline are part of various preparations agricultural and medical practices, created on the basis of a very large number of representatives. Based on quinzoline have been widely used against viruses, microbes, fungicide, colds and cancer (Raffaella S., Daphne W., Daniel A., Jeffrey S., 2004), as well as stimulants for plants (Asma Kh., Rabah A., Antonio I. M., Laiche A., Abdelmalek B., 2018). In recent years, drugs such as imatinib, erlotinib, afatinib, which are used against tuberculosis and cancer patients, can be cited as examples. To this end, the synthesis, modification of various representatives of the biologically active – quinazoline ring in State 6, as well as the determination of their structure, gained relevance. Today, a lot of scientific work is being done on the synthesis and effective use of this type of substance (Imtiaz K., Aliya I., Waqas A., Aamer S.).

Methods and results

Result and discussion. In the course of our research, an effective and convenient method of synthesizing quinazolin-4-one **(2)** in the presence of o-aminobenzoic acid **(1)** and formamide was implemented and obtained with a quantitative yield (98%). The resulting substance was nitrated under the action of a nitrating agent to synthesize 6-nitroquinazolin-4-one **(3)** in 95% yield. The resulting 6-nitroquinazolin-4-one was reacted with tin (II) chloride dihydrate ($SnCl_2 \cdot 2H_2O$) and HCl to synthesize the corresponding 6-aminoquinazolin-4-one **(4)** in 67% yield.

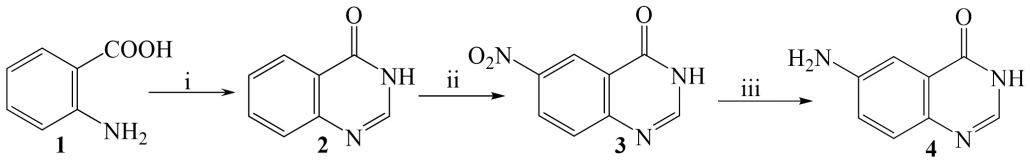

i) *o*-aminobenzoic acid : formamide (1:2 ratio), 140-145 °C, 2 h.
ii) HNO_3+H_2SO_4 0-2 °C, 1 h; 20-24 °C, 1 h; 60-65 °C, 2 h.
iii) $SnCl_2 \cdot 2H_2O$, HCl/EtOH. 20-24 °C, 2 h; 65-70 °C, 2 h.

The resulting substance **(4)** was thoroughly dissolved by placing 1 mmole in a 20 ml flask, connected to a magnetic mixer at 5 ml DMF, and 1.1 mmole allyl isothiocyanate was added on top. Connected to the refrigerator, the reaction was carried out and mixed

in a magnet at 58–60 °C for 24 hours. The reaction was examined every 2 hours using thin-layer chromotography. Rsulting substance **(4)** was thoroughly dissolved by placing 1 mmole in a 20 ml flask, connected to a magnetic mixer at 5 ml DMF, and 1.1 mmole allyl isothiocyanate was added on top. Connected to the refrigerator, the reaction was carried out and mixed in a magnet at 58–60°C for 24 hours. The reaction was examined every 2 hours using thin-layer chromotography. When the starter substance was completely finished, it was rolled into the ice-cold water in the glass. The precipitate was filtrated and dried on 1-allyl-3-(4-oxo-3,4-dihydroquinazolin-6-yl)thiourea **(5)** at filter paper. DMF: recrystallized in the water system (taken in a ratio of 1 to 1) and dried thoroughly. 1-allyl-3-(4-oxo-3,4-dihydroquinazolin-6-yl) thiourea was obtained with 86% **(5).**

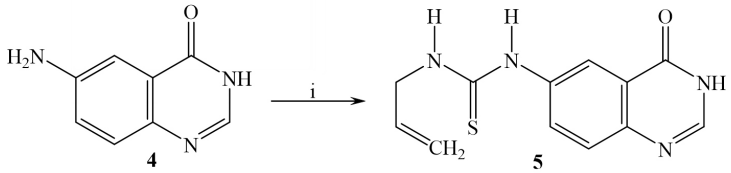

4 5

i) Allyl isocyanate, DMF, 63-65 °C, 24 h.

The liquefaction temperature of the resulting substance was determined by the values of 202–204 °C and Rf = 0.61 (sistema; benzene acetone, 1:3 ratio), the structure of which was determined using the spectrum of modern physical research methods^{1}H NMR and^{13}C NMR (**Fig. 1**, **Fig. 2).**

Figure 1.

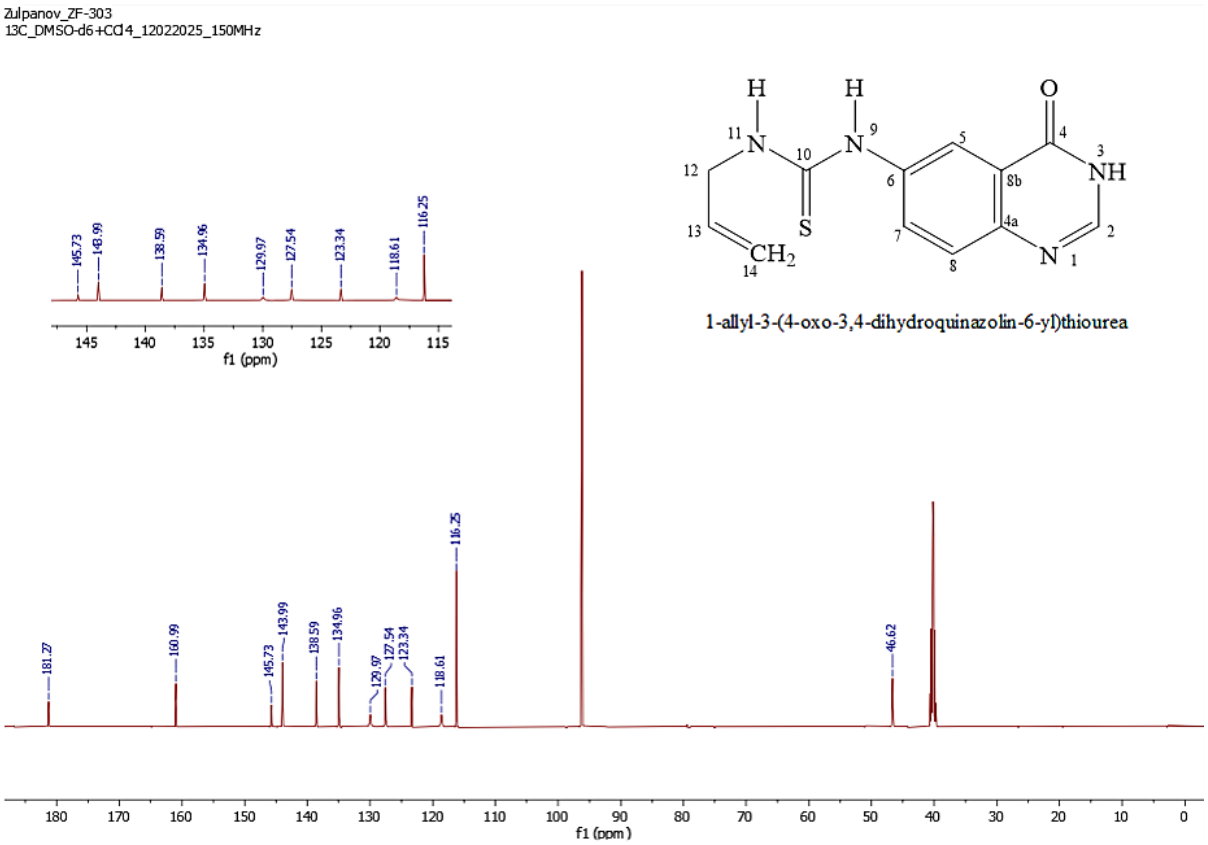

1HNMRspectrumofquinazlin-4-one (400 *M*Hz, CD3OD, δ, ppm, *J*/Hz): 8.25 (1H, s, H-2), 8.16 (1H, dd, *J*=8.0, 1.6, H-5), 7.76 (1H, ddd, *J*=8.3, 7.2, 1.6, H-7), 7.62 (1H, dd, *J*=8.2, 1.1, H-8), 7.49 (1H, ddd, *J*=8.2, 7.1, 1.2, H-6).**13C NMR spectrum of quinazlin-4-one** (150 MHz, DMSO-d6+CCl4, δ, ppm): 149.13 (C-2), 162.59 (C-4), 122.90

(C-4a), 128.55 (C-5), 127.37 (C-6), 135.67 (C-7), 127.83 (C-8), 149.01 (C-8a).**1H NMR spectrum of 1-allyl-3-(4-oxo-3,4-dihydroquinazolin-6-yl)thiourea** (400 *M*Hz, CD3OD, δ, ppm, *J*/Hz): 8.32 (1*H*, s, H-2), 7.84 (1H, s, H5), 7.94 (1H, d, J=8.3, H7), 7.51 (1H, d, J=8.7, H8), 7.73 (1H, s, H3), 12.01 (1H, s, H9), 9.63 (1H, s, H11) 4.14 (2H, s, H12), 5.89 (1H, s, H13), 5.21 (1H, dd, J=17.2, 1.7, H14a), 5.09 (1H, dd, J=10.28, 1.55, H14b).**13C NMR spectrum of 1-allyl-3-(4-oxo-3,4-dihydroquinazolin-6-yl)thiourea** (150 MHz, DMSO-d6+CCl4, δ, ppm): 145.73 (C-2), 160.99 (C-4), 143.99 (C-4a), 134.96 (C-5), 129.97 (C-6), 123.34 (C-7), 127.54 (C-8), 118.61 (C-8a), 181.27(C-10), 46.62 (C-12), 138.59 (C-13), 116.25 (C14).

Figure 2.

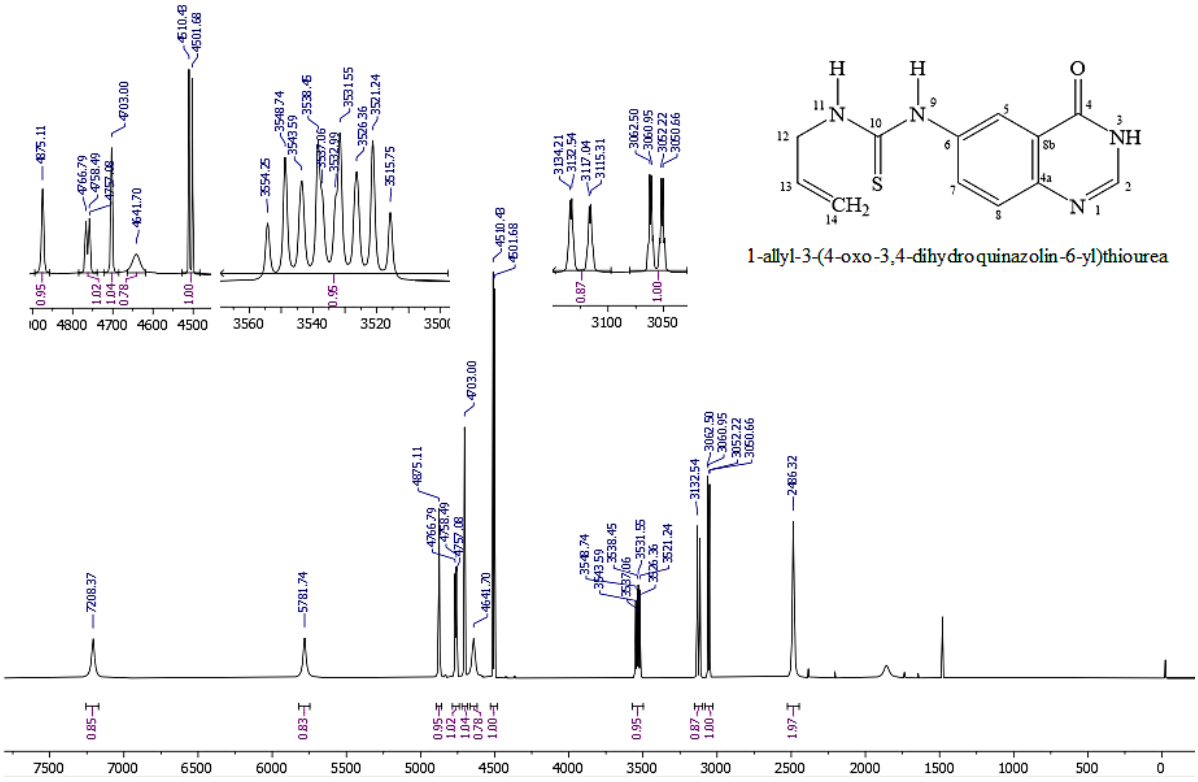

Conclusion

Quinazoline-4-on **(2)**, which has a geretocyclic structure, was obtained in absolute units in the simplest and most convenient way. After nitrolizing the resulting substance **(3),** a recurrence reaction was carried out. As a result of the reaction of the resulting substance **(4)** with isothiocyanate, the **(5)** compounds stored in the thiomochevina fragment were synthesized in high flour.

Acknowledgments

This work was supported by: Akad. S. Yu. Yunusov Institute of the Chemistry of Plant Substances, Academy of Sciences of the Republic of Uzbekistan. department of Organic synthesis.

References

Arun K. Ghosh., Margherita Bindisi. Organic carbamates in drug design and medicinal chemistry. J. Med. Chem., 2015. – P. 2895–2940. doi:10.1021/jm501371s.

Asma Kh., Rabah A., Antonio I. M., Laiche A., Abdelmalek B. Effects of the methane-inhibitors Nitrophenol, 5-Nitrobenzimidazol and two new synthetic nitrocompounds on

in vitro ruminal fermentation. Bio. Agri. Biotech., 2018. – Vol. 14. – P. 160–165. Doi. org/10.1016/j.bcab.2018.03.004.

Alagarsamy V., Murugesan S., Dhanabal K. AntiHIV, antibacterial and antifungal activities of some novel 2-methyl-3-(substitutedmethylamino)-(3H)-quinazolin-4-ones. Indian J Pharm Sci 2007. – 69. – P. 304–307.

Raffaella S., Daphne W., Daniel A., Jeffrey S. Gefitinib EGFR. Europe PMC. 20 Aug. 2004. – Vol 305. – Issue 5687. – P. 1163–1167. DOI: 10.1126/science.1101637

Imtiaz K., Aliya I., Waqas A., Aamer S. Synthetic approaches, functional ization and therapeutic potential of quinazoline and quinazolinone skeletons. E.J. of Med.Chem. URL: https://doi.org/10.1016/j.ejmech.2014.10.084

submitted 21.07.2025;
accepted for publication 05.08.2025;
published 29.09.2025

Contact: zulpanovf@gmail.com

The Austrian Journal of Technical and Natural Sciences, No 7–8
ISSN 2310-5607

PREMIER Publishing
ppublishing.org

Section 2. Food processing industry

DOI:10.29013/AJT-25-7.8-61-66

SILKWORM PUPA AS AN ALTERNATIVE TO SOYBEAN MEAL IN INDUSTRIAL POULTRY FARMING

Abdullaeva Gulnoza Ulugbek kizi [1], ***Kurbanov Murod Tashpulatovich*** [1], ***Atamuratova Tamara Ivanovna*** [1]

[1] Department of Food technology and service, Bukhara State Technical University

Cite: *Abdullaeva G.U., Kurbanov M.T., Atamuratova T.I. (2025). Silkworm Pupa as an Alternative to Soybean Meal in Industrial Poultry Farming. Austrian Journal of Technical and Natural Sciences 2025, No 7–8.* https://doi.org/10.29013/AJT-25-7.8-61-66

Abstract

The article covers the potential of using silkworm (*Bombyx mori*) pupa as an alternative protein source for industrial poultry farming in order to replace traditional soybean meal. A comparative analysis of the amino acid composition of pupa and soybean meal proteins was performed based on data from scientific publications and databases. It showed that pupa contain complete protein with high levels of lysine and methionine, amino acids that limit poultry growth when fed soybean meal. The results of studies show the positive effect of including silkworm pupa in the diet on growth, productivity and immune status of poultry, as well as improving the quality of meat and eggs. Environmental and economic benefits of using pupa, including reduced pressure on natural resources and a decrease in antinutrients in feed, are discussed. The article emphasizes the necessity of continued research and technological advancement to enable the widespread integration of silkworm pupae into poultry feed formulations.

Keywords: *silkworm pupa, soybean meal, industrial poultry farming, alternative protein, poultry feeding, environmental sustainability*

Ensuring balanced and cost-effective feeding of poultry is one of the key tasks in modern industrial poultry farming. Soybean meal traditionally occupies a leading position as the main source of vegetable protein.

Soybean meal (abbreviated SM) is a residual product after soybean processing, the dosage of which in the composition of compound feed for chickens reaches 7.0 ... 8.0% of the mass of compound feed. This raw material concentrates a significant amount of complete protein and a complex of minerals, which, with the correct dosage and constant feeding, make this product almost indispensable in poultry farming, where the main emphasis is on weight gain in young poultry.

The amino acid composition of soybean protein is the most perfect among all plant protein sources and resembles, with the

exception of sulfur-containing amino acids (methionine), the composition of high-quality animal proteins. However, soy and its processed products, like many other legumes, contain anti-nutritional substances that have a negative effect on the health of poultry. These include trypsin inhibitors, lectins, saponins, soyin, as well as enzymes: urease, lipoxidase, trioses (raffinase and stachyose). Soy inhibitors inhibit trypsin activity by 60.0–70.0%, reducing protein digestion, accordingly, the growth and development indicators of poultry, and the presence of sulfur-containing amino acids in these enzymes can disrupt the balance of the amino acid composition. Most anti-nutritional factors of soy are heat-unstable, therefore, with moisture-heat treatment (toasting) and other technological methods, protein digestibility increases to 87.0–90.0% (Zenkova M. L. Ponomareva E. I., 2016; Simahina G. A., 2016).

At the same time, due to the high cost of SM, livestock producers prefer to use rapeseed or sunflower meal as a protein component of animal and poultry feed rations, since their cost is significantly lower. However, these raw materials are not produced in Uzbekistan. In this regard, the issue of finding our own high-protein raw materials and assessing their competitiveness with SM is relevant, which will most effectively solve the problem of feed protein deficiency in animal and poultry diet.

In accordance with the above, silkworm pupa (*Bombyx mori L.*) is very valuable raw material resource. This raw material is very effective due to large-scale work on the further development of the silk industry in Uzbekistan and increasing the volume of sericulture.

In the republic, sericulture remains one of the important branches of agriculture and ranks third in the production of silk cocoons after China and India, annually growing more than 21 thousand tons of live cocoons. According to the Decree of the President of the Republic of Uzbekistan No. DP-3910 dated August 20, 2018 “On measures for further effective use of existing opportunities of the silk industry in the Republic”, a further increase in their production is planned (Naumenko N. V., 2019).

Silkworm pupae (abbreviated SWP) are a valuable feed resource due to the high content of protein (up to 60.0%), essential amino acids (especially methionine and lysine), fat (high energy value) and minerals (calcium and phosphorus, necessary for the strength of bones and eggshells in birds). The presence of chitin in the shells of the pupae improves immunity and intestinal health of the poultry.

Traditionally, SWP, which produce significant amounts of biomass as a by-product of the silk industry, have been considered a waste product of silk production. However, in recent years, research has begun to explore their use in a variety of applications. This includes their role as additives or alternatives to traditional animal feed ingredients such as fishmeal, which is scarce and expensive, and their potential in cattle diets to reduce methane emissions. This shift in research highlights the adaptability of SWP as a resource for a variety of industries. A report on insects as a food and feed source noted that silkworm pupae are a high-quality and sustainable source of protein (P. van Hung P. 2012; Yi, L., Lakemond, C. M. M., Sagis, L. M. C., Eisner-Schadler, V., van Huis, A., & van Boekel, M. A. J. S., 2013; Ji, C., Zhang, J., & Wang, H., 2020; Wang, Y., Zhang, L., & Zhou, H., 2019).

The nutritional and biological value of silkworm pupae as a potential substitute for part of soybean meal in poultry feed was studied.

The objects of the research were silkworm pupae. The object of comparison was soybean meal. The quality of the raw material was assessed using modern generally accepted organoleptic (sensory) and physicochemical methods of analysis. The results of the study are presented in Fig 1, 2 and Tables 1, 2.

Comparative analysis of the nutritional value of SM and SWP showed that the content of crude protein in the SWP was 18.3%, crude fiber – 11.4 times, ME – 60.0%, lysine – 18.5%, methionine – 2.2 times, Ca and P, respectively, 2.3 and 1.8 times higher than similar values in SM. At the same time, the content of crude fiber and ash in the object of study decreased, respectively, by 10.0 and 23.1% relative to the data in the comparison sample, namely, in SM (Table 1).

Table 1. *Nutritional value of soybean meal (SBM) and silkworm pupae (SWP)*

Indicator	Content (% of dry matter)		±Δ relative to SM
	SM	SWP	
Crude protein	46.5± 3.5	55.0± 5.0	+ 18.3%
Crude fat	2.2± 0.8	25.0± 5.0	+ 11.4 times
Crude fiber	5.0 ± 2.0	4.5 ± 1.5	– 10.0%
Ash	6.5 ± 1.0	5.0 ± 1.0	– 23.1%
Metabolizable energy (ME), kcal/kg	2500 ± 200	4000 ± 500	+ 60.0%
Lysine	2.7 ± 0.3	3.2 ± 0.2	+ 18.5%
Methionine	0.6 ± 0.1	1.3 ± 0.2	+ 2.2 times
Calcium (Ca)	0.3 ± 0.1	0.7 ± 0.1	+ 133.3%
Phosphorus (P)	0.6 ± 0.1	1.1 ± 0.2	+ 83.3%

Analysis of the amino acid composition of the proteins of the studied raw materials did not reveal any fundamental differences in their quantitative composition. Thus, the total amount of essential amino acids (∑ EAA) in SM was 37.2, and in SWP was 37.0 g/100 g protein. Moreover, in terms of the content of these amino acids, the SWP protein was closest to the "ideal" protein in terms of biological value – 85.5% than SM – 65.0% (Fig. 1, Table 2).

Figure 1. *Amino acid composition of SM and SWP in comparison with the ideal protein: IP – ideal protein; V- valine, L- leucine, I- isoleucine, Liz. – lysine, M+C – methionine + cysteine, T – threonine, F+Y- phenylalanine + tyrosine, Tr. – tryptophan*

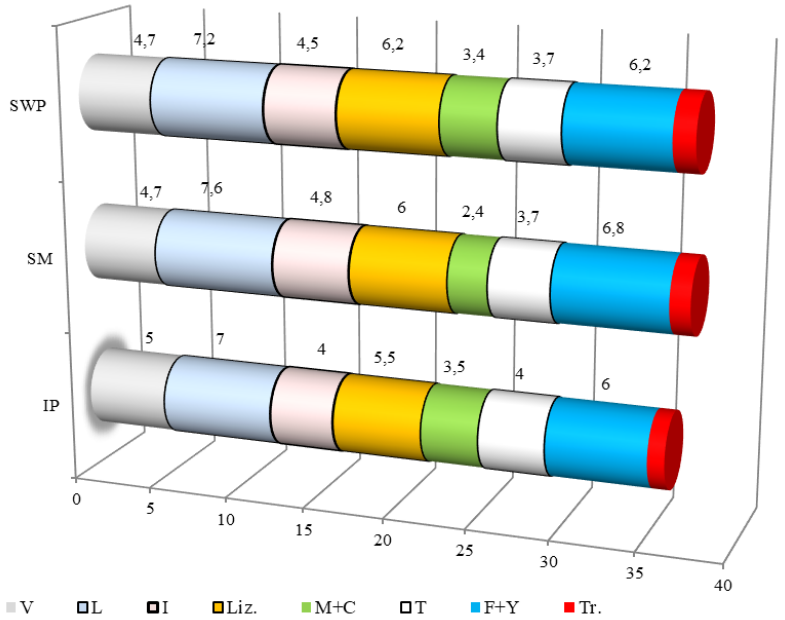

When studying the amino acid composition of the products under research, it was established that they contain almost all essential amino acids in significant quantities, exceeding their values in the "ideal" (reference) protein. It was established that in 100 g of SM and SWP protein, the mass fraction of the most deficient amino acid lysine on average exceeds the same value in the ideal protein by 9.0 and 24.0%, respectively. The limiting amino acids

by amino acid score (AAS) in the SM protein are methionine + cysteine (68.0%), threonine (92.0%) and valine (94.0%), and in the SWP protein is mainly valine (94.0%).

Table 2. *Content of essential amino acids in SM and SWP*

Amino acid	Protein according to FAO/WHO, in g/100 g protein	Mass fraction of amino acids in SM		Mass fraction of amino acids in SWP	
		in g/100 g protein	AAC, %	in g/100 g protein	AAC, %
Valine	5.0	4.7	94	4.7	94
Leucine	7.0	7.6	108	7.2	103
Isoleucine	4.0	4.8	120	4.5	112
Lysine	5.5	6.0	109	6.8	124
Methionine + Cysteine	3.5	2.4	68	3.4	97
Threonine	4.0	3.7	92	4.0	100
Tyrosine + Phenylalanine	6.0	6.8	113	6.5	108
Tryptophan	1.0	1.2	120	1.3	130
∑ EAA	36.0	37.2	–	37.0	–
PDCAAS, %	–	35.0		14.5	–
Biological value (BV), %	100	65.0	–	85.5	–

It has been established that SWP are rich in lysine and methionine, which makes them a valuable supplement to SM, which, in turn, is poor in methionine. The combined use of these products will balance the amino acid composition of the feed, which will have a positive effect on the growth of young poultry and the productivity of poultry.

Let us consider the nutritional value of mixtures of SM and SWP in a ratio of 50:50 (for chickens) and 40:60 (for laying hens) by the main indicators, namely the content of crude protein, fat and fiber (Fig. 2).

Figure 2. *Nutritional value of mixtures of SM and SWP in the ratio of 50:50 and 40:60 in comparison with SM: CP – crude protein; CF – crude fat, CFib – crude fiber*

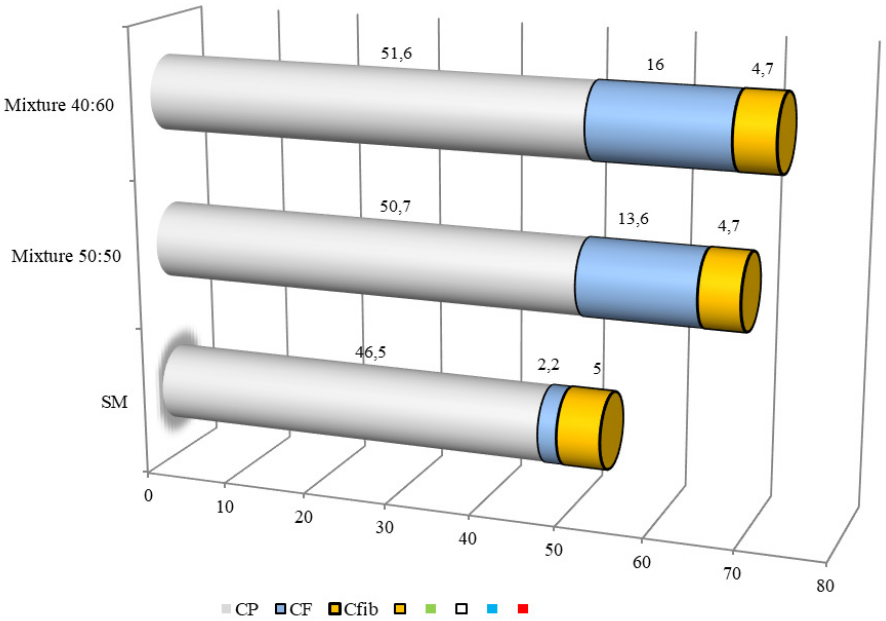

The analysis of the data presented in Fig 2 showed that with an increase in the proportion of SWP in the studied mixtures, the mass fraction of crude protein increased from 9.0 to 11.0%, crude fat – from 6.2 to 7.3 times relative to SM. At the same time, the content of crude fiber in both variants decreased by an average of 6.0%.

Therefore, the feasibility of combining SM and SWP in order to increase the nutritional and biological value of target-purpose compound feeds is substantiated. However, there are certain limitations to the use of SWP, namely, high fat content contributes to rancidity during long-term storage, heat treatment (roasting, drying) is required to reduce the likelihood of microbial contamination of this potential feed additive, as well as SM.

Therefore, the main arguments for using SWP instead of SM are:

1. *Nutritional value*: SWP protein has an amino acid composition comparable to or even superior to SM protein. Particularly important are the presence of lysine and methionine, i.e., amino acids that often limit growth in poultry.
2. *Environmental sustainability*: Silkworm production requires less land and water than soybean cultivation, and is also accompanied by lower greenhouse gas emissions.
3. *Reduced antinutrients*: SM contains trypsin inhibitors and phytic acid, which negatively affect the digestibility of nutrients. SWP are free of these substances, which increases the bioavailability of protein.
4. *Cost-effectiveness*: In regions with developed sericulture, pupae can be an accessible and inexpensive raw material, especially if a by-product of the silkworm industry is used.

Silkworm pupae are a promising alternative to soybean meal in industrial poultry farming due to their high nutritional value, environmental sustainability, and positive effect on poultry productivity. Their use can help reduce dependence on traditional plant proteins and increase the sustainability of the feed base. For successful integration further research, development of processing technologies and the formation of a regulatory framework are needed.

References

Zenkova M. L. Research of mineral and amino acid composition of sprouted and canned wheat grain /M.L. Zenkova // Techniques and technology of food production. 2019. – Vol. 49. – No. 4. – P. 513–521.

Ponomareva E. I. Bread from bioactivated wheat grain of increased nutritional value / E. I. Ponomareva, N. N. Alekhina, I. A. Bakaeva // Nutrition issues. 2016. – Vol. 85. – No. 2. – P. 116–121.

Simahina G. A. The use of the biologically activated grains in technology of health products / G. A. Simahina, S. A. Bazhay-Zhezherun, T. I. Mykoliv [*et al.*] // East European Scientific Journal. 2016. – No. 9. – P. 147–153.

Naumenko N. V. Intensification of the process of germination of grain used for bread production and its influence on the quality of finished products / N. V. Naumenko, I. Yu. Potoroko, I. V. Kalinina // Food Industry. 2019. – Vol. 4. – No. 1. – P. 47–54.

P. van Hung P. Effects of germination on nutritional composition of waxy wheat / P. van Hung, T. Maeda, S.Yamamoto [et al.]//Journal of the Science of Food and Agriculture. 2012. – Vol. 92. – No. 2. – P. 667–672.

Yi, L., Lakemond, C. M. M., Sagis, L. M. C., Eisner-Schadler, V., van Huis, A., & van Boekel, M. A. J. S. Extraction and characterisation of protein fractions from five insect species // Food Chemistry. 2013. – No. 141(4). – P. 3341–3348. URL: https://doi.org/10.1016/j.foodchem.2013.06.114.

Ji, C., Zhang, J., & Wang, H. Effects of dietary silkworm pupa meal on growth performance, immune function and meat quality in broiler chickens// Journal of Animal Science and Biotechnology. 2020. – No. 11(1). – P. 65. URL: https://jasbsci.biomedcentral.com/articles/10.1186/s40104-020-00489-2.

Wang, Y., Zhang, L., & Zhou, H. (2019). Dietary supplementation of silkworm pupa improves laying performance and egg quality in hens// Poultry Science. 2019. – No. 98(7). – P. 2862–2870. URL: https://doi.org/10.3382/ps/pez086.

submitted 02.07.2025;
accepted for publication 19.07.2025;
published 29.09.2025

Contact: abdullayevag900@gmail.com; kurbanov.m@rambler.ru; tamara-atamuratova@mail.ru

The Austrian Journal of Technical and Natural Sciences, No 7–8
ISSN 2310-5607

PREMIER Publishing
ppublishing.org

DOI:10.29013/AJT-25-7.8-67-72

MATHEMATICAL MODELING AND OPTIMIZATION OF FLAXSEED OIL EXTRACTION USING PULSED ELECTRIC FIELD PRETREATMENT

Mirzo Narziyev [1], ***Shaxnoza Ismatova*** [1], ***Shabon Yuldasheva*** [1], ***Mexriniso Bakayeva*** [2], ***Nafisa Ismatova*** [1]

[1] Bukhara Technical University, Uzbekistan,

[2] ZARMED Universiteti. Republic of Uzbekistan

Cite: *Narziyev M., Ismatova Sh., Yuldasheva Sh., Bakayeva M., Ismatova N. (2025). Mathematical Modeling and Optimization of Flaxseed Oil Extraction Using Pulsed Electric Field Pretreatment. Austrian Journal of Technical and Natural Sciences 2025, No 7–8.* https://doi.org/10.29013/AJT-25-7.8-67-72

Abstract

This study presents the mathematical modeling and optimization of flaxseed oil extraction under Pulsed Electric Field (PEF) pretreatment. The experiments were planned using response surface methodology with a Box–Behnken design to minimize the number of trials while increasing the accuracy of parameter estimation. The investigated factors included discharge voltage (X_1), number of pulses (X_2), product thickness (X_3), and pressing pressure (X_4). Regression equations were developed to describe the oil yield as a response function. The adequacy of the model was verified using Cochran's, Student's, and Fisher's statistical criteria. The results demonstrated that the optimized PEF parameters significantly enhanced oil yield from flaxseed compared to conventional pressing, confirming the effectiveness of mathematical modeling in determining optimal processing regimes.

Keywords: *Flaxseed, Pulsed Electric Field (PEF), oil extraction, mathematical modeling, process optimization, response surface methodology*

Introduction

Flaxseed (Linum usitatissimum L.) is recognized as a valuable agricultural crop due to its high oil content, rich in polyunsaturated fatty acids, lignans, and other bioactive compounds. Flaxseed oil is particularly appreciated for its high α-linolenic acid concentration, which is essential for human health. However, conventional mechanical pressing often results in limited oil recovery, as a significant portion of the oil remains encapsulated within the seed microstructure.In recent years, non-thermal and electro-physical technologies have been explored to intensify oil extraction. Pulsed Electric Field (PEF) treatment has emerged as a promising method, as it induces electroporation in cell membranes, facilitating the release of intracellular oil. This technique is energy-efficient and environmentally friendly compared to thermal or chemical alternatives.Mathematical modeling combined with statistical design of

experiments is crucial to optimize the technological parameters. The Box–Behnken design allows minimizing the number of trials while maintaining predictive accuracy. This study focuses on developing a mathematical model for flaxseed oil extraction under PEF pretreatment, evaluating its adequacy, and identifying optimal processing parameters.

Methods

To construct the experimental design matrix, the transition from the actual factor values to their coded values was performed using the following expression:

$$x_i = \frac{X_i - X_{i0}}{\varepsilon} \quad (1)$$

where:

- x_i - i – coded value of the iii-th factor;
- x_i – i – actual (natural) value of the iii-th factor;
- x_{io} - i – zero-level value of the iii-th factor;
- ε – variation interval of the factor.

For each factor, the zero level and the variation interval were determined and then coded accordingly. The following type of mathematical model was chosen:

$$y = b_0 + \sum_{i=1}^{n} b_i x_i + \sum_{i<j}^{n} b_{ij} x_i x_j + \sum_{n=1}^{n} b_{ij} x_i^2 \quad (2)$$

A second-order experimental design of the V_n type was applied. Based on preliminary experiments, the main parameters influencing the oil yield (V) from flaxseed were identified as follows:

- x_1 – discharge voltage, kV;
- x_2 – number of pulses, pcs;
- x_3 – product thickness, mm;
- x_4 – pressing pressure, MPa.

During the experiments, three replications were performed at each point of the V_4 design spectrum. The sequence of experiments was carried out in accordance with the design matrix table.

Results

The selected factors, their variation intervals, and levels are presented in Table 1.

Table 1. *Experimental factors, variation intervals, and levels*

Factor designation		Factor	Interval	Levels		
Coded	Natural			−1	0	+1
x_1	U	Discharge voltage, kV	2	6	8	10
x_2	n	Number of pulses, pcs	8	20	25	30
x_3	h	Product thickness, mm	5	5	10	15
x_4	B	Pressing pressure, MPa	3	5	6	7

For this design, the matrix of basic functions was constructed, and the mean values of m parallel experiments as well as the variances were calculated using the following formulas:

$$\bar{y}_g = \frac{1}{m}\sum_{i=1}^{m} y_{gi} \quad (3)$$

$$S_g^2 = \frac{1}{m-1}\sum_{i=1}^{m}\left(y_{gi} - \bar{y}_g\right)^2 \quad (4)$$

The reproducibility of the experiment was tested using **Cochran's criterion**.

For the calculated value, the hypothesis of experimental reproducibility does not contradict the observed results.

$$q = 0{,}05$$
$$G = 0{,}03889 < G_{1-q}\left(\nu_1 = 2, \nu_2 = 24\right) = 0{,}2354 \quad (5)$$

The degree of reproducibility of the variance was determined using the following formula:

$$S^2\{y\} = \frac{1}{N}\sum_{g=1}^{N} S_g^2 = \frac{1}{N_1 + 2n + N_0}\sum_{g=1}^{N} S_g^2 = \frac{58{,}6219}{24} = 2{,}44258 \quad (6)$$

The average variance is calculated as follows:

Table 2. *Box–Behnken design matrix of type V_4 (Vp) and experimental results*

	The F-matrix of basis functions																				
g	$f_0(\underline{x})$	$f_1(\underline{x})$	$f_2(\underline{x})$	$f_3(\underline{x})$	$f_4(\underline{x})$	$f_5(\underline{x})$	$f_6(\underline{x})$	$f_7(\underline{x})$	$f_8(\underline{x})$	$f_9(\underline{x})$	$f_{10}(\underline{x})$	$f_{11}(\underline{x})$	$f_{12}(\underline{x})$	$f_{13}(\underline{x})$	$f_{14}(\underline{x})$	y_{g1}	y_{g2}	y_{g3}	$\bar{y}_g$	S_g^2	$\hat{y}_g$
	1	x_1	x_2	x_3	x_4	x_1x_2	x_1x_3	x_1x_4	x_2x_3	x_2x_4	x_3x_4	x_1^2	x_2^2	x_3^2	x_4^2						
1	1	-1	-1	-1	-1	+1	+1	+1	+1	+1	+1	+1	+1	+1	+1	22,2	23	23,8	23	0,64	22,96
2	1	+1	-1	-1	-1	-1	-1	-1	+1	+1	+1	+1	+1	+1	+1	24	23,8	22,5	23,4	0,7	23,59
3	1	-1	+1	-1	-1	-1	+1	+1	-1	-1	+1	+1	+1	+1	+1	22,8	25	24	23,9	1,3	23,89
4	1	+1	+1	-1	-1	+1	-1	-1	-1	-1	+1	+1	+1	+1	+1	25,6	23,24	25,00	24,6	1,5	24,55
5	1	-1	-1	+1	-1	+1	-1	+1	-1	+1	-1	+1	+1	+1	+1	27,4	29,00	30,50	29,0	2,4	28,95
6	1	+1	-1	+1	-1	-1	+1	-1	-1	+1	-1	+1	+1	+1	+1	28	31,00	30,00	29,7	2,3	29,61
7	1	-1	+1	+1	-1	-1	-1	+1	+1	-1	-1	+1	+1	+1	+1	29	30,00	30,30	29,8	0,5	29,72
8	1	+1	+1	+1	-1	+1	1	-1	1	-1	-1	+1	+1	+1	+1	31	29,00	31,00	30,3	1,3	30,41
9	1	-1	-1	-1	+1	+1	1	-1	1	-1	-1	+1	+1	+1	+1	26	24,00	26,00	25,3	1,3	25,14
10	1	+1	-1	-1	+1	-1	-1	1	1	-1	-1	+1	+1	+1	+1	25	27,00	24,00	25,3	2,3	25,50
11	1	-1	+1	-1	+1	-1	1	-1	-1	1	-1	+1	+1	+1	+1	27	25,00	26,00	26,0	1	26,17
12	1	+1	+1	-1	+1	1	-1	1	-1	1	-1	+1	+1	+1	+1	28	25,00	27,00	26,7	2,3	26,57
13	1	-1	-1	+1	+1	1	-1	-1	-1	-1	+1	+1	+1	+1	+1	29	32,00	31,00	30,7	2,3	30,86
14	1	+1	-1	+1	+1	-1	+1	+1	-1	-1	+1	+1	+1	+1	+1	31	33,00	30,00	31,3	2,3	31,25
15	1	-1	+1	+1	+1	-1	-1	-1	+1	+1	+1	+1	+1	+1	+1	32	31,00	33,00	32,0	1	31,73
16	1	+1	+1	+1	+1	+1	+1	+1	+1	+1	+1	+1	+1	+1	+1	31	34,00	31,00	32,0	3	32,15
17	1	-1	0	0	0	0	0	0	0	0	0	+1	0	0	0	32	29,00	30,00	30,3	2,3	30,57
18	1	+1	0	0	0	0	0	0	0	0	0	+1	0	0	0	29	33,00	32,00	31,3	4,3	31,10
19	1	0	-1	0	0	0	0	0	0	0	0	0	+1	0	0	34	32,00	31,00	32,3	2,3	32,21
20	1	0	+1	0	0	0	0	0	0	0	0	0	+1	0	0	30	35,00	34,00	33,0	7	33,12
21	1	0	0	-1	0	0	0	0	0	0	0	0	0	+1	0	28	26,00	30,00	28,0	4	27,94
22	1	0	0	+1	0	0	0	0	0	0	0	0	0	+1	0	31	34,00	36,00	33,7	6,3	33,73
23	1	0	0	0	-1	0	0	0	0	0	0	0	0	0	+1	33	30,00	33,00	32,0	3	32,02
24	1	0	0	0	+1	0	0	0	0	0	0	0	0	0	1	35	32,00	35,00	34,0	3	33,98

$$S^2\{\bar{y}\} = \frac{S^2\{y\}}{m} = \frac{2,44258}{3} = 0,81419 \quad (7)$$

To determine the regression coefficients, the following summation is calculated:

$$z_j = \sum_{g=1}^{N} f_{gj}\bar{y}_g \quad j = 0...14 \quad (8)$$

where: $j = 0$ for $f_{g0} = 1$; $j = 1...4$ for $f_{gj} = (x_i)_g$; $j = 5...10$ for $f_{gj} = (x_i x_j)_g$ $(ij = 1...4,\ i = f)$; $j = 11...14$ for $f_{gj} = (x_i^2)_g$ $(i = 1...4)$.

Table 3.

basis function	j	z_j	b_j	$S^2(b_j)$	$S(b_j)$	t_j
1	0	697,72	33,21	0,18659	0,43196	76,89
x_1	1	4,74	0,26	0,11132	0,33364	0,79
x_2	2	8,25	0,46	0,11132	0,33364	1,37
x_3	3	52,09	2,89	0,11132	0,33364	8,67
x_4	4	17,62	0,98	0,11132	0,33364	2,93
x_1x_2	5	0,14	0,01	0,12522	0,35387	0,02
x_1x_3	6	0,13	0,01	0,12522	0,35387	0,02
x_1x_4	7	–1,07	–0,07	0,12522	0,35387	–0,19
x_2x_3	8	–0,65	–0,04	0,12522	0,35387	–0,11
x_2x_4	9	0,42	0,03	0,12522	0,35387	0,07
x_3x_4	10	–1,09	–0,07	0,12522	0,35387	–0,19
x_1^2	11	504,72	–2,38	0,79308	0,89055	–2,67
x_2^2	12	508,38	–0,55	0,79308	0,89055	–0,61
x_3^2	13	504,72	–2,38	0,79308	0,89055	–2,67
x_4^2	14	509,05	–0,21	0,79308	0,89055	–0,24

Using the calculated summation values $Z_j(j = 0...14)$, the regression coefficients are determined by the following formulas:

$$b_0 = \frac{a}{N}\sum_{i=1}^{N}\bar{y}_g - \frac{b}{N}\sum_{i=1}^{n}\cdot\sum_{g=1}^{N}(x_i^2)_g\bar{y}_g \quad (9)$$

$$b_i = \frac{1}{\lambda_2 \cdot N}\cdot\sum_{g=1}^{N}(x_i)_g\bar{y}_g \quad (10)$$

$$b_{ij} = \frac{1}{\lambda_3 \cdot N}\cdot\sum_{g=1}^{N}(x_i x_j)\bar{y}_g \quad (11)$$

$$b_{ij} = \frac{C}{N}\cdot\sum_{i=1}^{N}(x_i^2)\bar{y}_g - \frac{d}{N}\cdot\sum_{i=1}^{n}\cdot\sum_{g=1}^{N}(x_i^2)\bar{y}_g - \frac{b}{N}\cdot\sum_{g=1}^{N}\bar{y}_g \quad (12)$$

where: a, b, c, d $(\lambda_2 \cdot N)^{-1}$, $(\lambda_3 \cdot N)^{-1}$ constants, auxiliary terms used for calculating the model coefficients. For n = 4 and when the number of coefficients b_{ij} is equal to four, the constant values are as follows: a = 5,5; b= 1,5; c= 12; d= 2,5; $(\lambda_2 \cdot N)^{-1} = 0,05556$; $(\lambda_3 N)^{-1} = 0,0625$.

Table 3. Results of calculating the criterion t_j and b_j the coefficients.

The variances of the coefficients are calculated using the following expressions:

$$S^2(b_0) = \frac{a}{N}S^2\{\bar{y}\}; \quad (13)$$

$$S^2\{b_i\} = (\lambda_2 \cdot N)^{-1}S^2\{\bar{y}\}; \quad (14)$$

$$S^2\{b_{ij}\} = (\lambda_3 \cdot N)^{-1}S^2\{\bar{y}\}; \quad (15)$$

$$S^2\{b_{ii}\} = \frac{C - OC}{N} S^2\{\bar{y}\} \quad (16)$$

The t_j t_j: criterion values are calculated using the following expression

$$t_i = \frac{|b_j|}{S\{b_j\}} \quad (17)$$

where: $S\{b_j\} = \sqrt{S^2\{b_j\}}$ sample standard deviation.

The significance of the regression coefficients was evaluated by testing the null hypothesis using Student's *t*-criterion, which was compared with the alternative value according to the following inequality:

$$t_j > t_{1-\frac{g}{2}}(v = N(m-1)) \quad (18)$$

where: $t_{1-\frac{g}{2}}\left(v = N\left(m-1\right)\right)$ is the degrees of freedom according to Student's distribution at the $(1-\frac{g}{2})$ % quantile.

The null hypothesis $H_0 \cdot \beta = 0$ was rejected, and the corresponding estimate of bib_ ibi was considered statistically significant. In this case, for $q = 0{,}05$ the quantile of Student's distribution is: $t_{1-\frac{g}{2}}(48) = 2{,}011$. Thus, for all coefficients, inequality (16) is satisfied, which means that these coefficients are statistically significant.

Therefore, the mathematical model can be expressed in the following form:

$$\hat{y}(x,b) = 33{,}21 + 0{,}26x_1 + 0{,}46x_2 + 2{,}89x_3 + \\ + 0{,}98x_4 + 0{,}01x_1x_2 + 0{,}01x_1x_3 - 0{,}07x_1x_4 - \\ - 0{,}04x_2x_3 + 0{,}03x_2x_4 - 0{,}07x_3x_4 - 2{,}38x_1^2 - \\ - 0{,}55x_2^2 - 2{,}38x_3^2 - 0{,}21x_4^2$$

The next stage of processing the experimental results is to test the hypothesis regarding the adequacy of the mathematical model and the response function. After regression analysis, this is carried out by comparing the experimental variance with the adequacy variance. The hypothesis of adequacy, which assumes the equality of these two variances, is verified using **Fisher's criterion**:

$$F = \frac{S^2_{OTK}}{S^2\{\bar{y}\}} \quad (19)$$

$$S^2_{OTK} = \frac{\sum_{g=1}^{N} (\bar{y}_g - \hat{y}_g)^2}{N - d} \quad (20)$$

$$S^2_{OTK} = \frac{8{,}5353}{17} = 0{,}502$$

$S^2_{OTK} > S^2_{\{\bar{y}\}}$ Taking into account, the calculation is performed as follows:

$$F = \frac{S^2_{OTK}}{S^2\{\bar{y}\}} = \frac{0{,}81419}{0{,}502} = 1{,}62189$$

V_1=*N*-*d*=24–7=7; $V_2 = N(n-1) = 24(3-1) = 48$

At q=0.05q = 0.05q = 0.05, the tabulated value of Fisher's criterion is equal to:

$F = 1{,}62189 < F_{1-q}(17{,}48) = 1{,}8425$

Thus, the hypothesis regarding the adequacy of the mathematical model and the response function does not contradict the experimental observations. By eliminating the insignificant coefficients and based on the obtained calculation results, the mathematical model in the coded form is expressed as follows:

$$\hat{y}(x,b) = 33{,}21 + 0{,}26x_1 + 0{,}46x_2 + 2{,}89x_3 + \\ + 0{,}98x_4 + 0{,}01x_1x_2 + 0{,}01x_1x_3 - 0{,}07x_1x_4 - \\ - 0{,}04x_2x_3 + 0{,}03x_2x_4 - 0{,}07x_3x_4 - 2{,}38x_1^2 - \\ - 0{,}55x_2^2 - 2{,}38x_3^2 - 0{,}21x_4^2$$

Based on the expression, the variable values in the flaxseed oil extraction equation are as follows: $x_1 = \frac{U-8}{2}; x_2 = \frac{n-25}{5}; x_3 = \frac{h-10}{5}; x_4 = \frac{P-6}{1};$

By transforming the coded values into natural values and applying the corresponding substitutions, the mathematical model of the flaxseed oil extraction process takes the following form:

$$y = -36{,}2 + 9{,}825U + 1{,}164n + 2{,}02h + 3{,}77P + \\ + 0{,}001Un + 0{,}001Uh - 0{,}21UP - 0{,}0016nh + 0{,}006nP \\ - 0{,}014hP - 0{,}595U^2 - 0{,}022n^2 - 0{,}0952h^2 - 0{,}21P^2$$

Discussion

The experimental results confirm that PEF pretreatment significantly improves flaxseed oil yield. Electroporation of cell membranes enhances oil release, which aligns with previous findings on oilseeds such as sunflower, sesame, and rapeseed. Optimization revealed that 8–10 kV discharge voltage, 25–30 pulses, 10–15 mm thickness, and 6––7 MPa pressing pressure provided maximum oil yield, with an 18–20% improvement compared to conventional pressing.

Conclusion

PEF pretreatment significantly enhances flaxseed oil extraction efficiency. The developed regression model accurately predicts oil yield as a function of processing parameters. The optimized conditions resulted in approximately 18–20% higher oil recovery than conventional pressing. PEF is thus a sustainable and efficient technology for industrial flaxseed oil production.

References

Toepfl, S., Heinz, V., & Knorr, D. (2006). Applications of pulsed electric fields technology for the food industry. Food Engineering Reviews, – 1(1). – P. 69–90.

Zhang, Q. H., Barbosa-Cánovas, G. V., & Swanson, B. G. (1995). Engineering aspects of pulsed electric field pasteurization. Journal of Food Engineering, – 25(2). – P. 261–281.

Vorobiev, E., & Lebovka, N. (2010). Enhanced extraction from solid foods and biosuspensions by pulsed electric fields. In Nonthermal Processing Technologies for Food (pp. 39–81). Wiley-Blackwell.

Sarkis, J. R., Boussetta, N., Blouet, C., Tessaro, I. C., Marczak, L. D. F., & Vorobiev, E. (2015). Effect of pulsed electric fields on flaxseed hull extracts. Innovative Food Science & Emerging Technologies, – 29. – P. 62–70.

Sarkis, J. R., Boussetta, N., Tessaro, I. C., Marczak, L. D. F., & Vorobiev, E. (2014). Application of pulsed electric fields for oil extraction from sesame seeds. Journal of Food Engineering, – 146. – P. 90–97.

Lebovka, N. I., Vorobiev, E., & Chemat, F. (2011). Enhancing extraction processes in the food industry with pulsed electric fields and ultrasound. CRC Press.

Oomah, B. D. (2001). Flaxseed as a functional food source. Journal of the Science of Food and Agriculture, – 81(9). – P. 889–894.

Khajeh, M., Yamini, Y., & Bahramifar, N. (2004). Optimisation of supercritical fluid extraction of oil from flaxseed with response surface methodology. Talanta, – 64(3). – P. 639–644

submitted 25.08.2025;
accepted for publication 09.09.2025;
published 29.09.2025

Contact: ismatova.nafisa@inbox.ru

The Austrian Journal of Technical and Natural Sciences, No 7–8
ISSN 2310-5607

PREMIER Publishing
ppublishing.org

DOI:10.29013/AJT-25-7.8-73-78

RESEARCH ON THE INFLUENCE OF THE PHYSICAL AND CHEMICAL INDICATORS OF THE CREAM IN THE PRODUCTION OF COSMETIC CREAMS

Umirova Zilola Sherali kizi [1], ***Akhmedov Azimjon Normuminovich*** [2]

[1] Tashkent Institute of Chemical Technology, Tashkent, Uzbekistan

[2] Karshi State Technical University, Karshi, Uzbekistan

Cite: *Umirova Z. Sh., Akhmedov A. N. (2025). Research on the Influence of the Physical and Chemical Indicators of the Cream in the Production of Cosmetic Creams. Austrian Journal of Technical and Natural Sciences 2025, No 7–8.* https://doi.org/10.29013/AJT-25-7.8-73-78

Abstract

The article presents the results of the analysis of the physicochemical parameters of local non-traditional oils that can be used in cosmetic cream recipes. The physicochemical parameters and fatty acid compositions of non-traditional oils grown in Uzbekistan: grape, apricot, peach, pumpkin, watermelon and almond oils are presented. All the studied oils meet the requirements for oils that can be used in cosmetic cream recipes in terms of their physicochemical parameters. While almond and apricot oils have high skin absorption, grape oil showed the best results when applied to the skin. It was observed in this study that the smoothness of the cream does not always depend on its viscosity. It was found that a cream with optimal results in all parameters can be prepared on the basis of watermelon oil.

Keywords: *grape seed oil, apricot seed oil, peach seed oil, pumpkin seed oil, watermelon seed oil, almond seed oil, cosmetic cream, viscosity, lubricity, skin absorption*

Introduction

Cosmetic creams are oil-in-water or water-in-oil emulsions, consisting of an oily and an aqueous phase. The functional properties of creams are improved by enriching the oily phase or the aqueous phase in their formulation. Which phase is improved depends on the solubility of the functional additive in polar or non-polar solvents. Enrichment of the oily phase is usually achieved by incorporating oils containing functional ingredients into the formulation (Khakimova Z. A., Usmanova F. Q., Ruzibaev A. T., 2020; Khakimova Z. A., Ruzibaev A. T., Gaipova Sh. S., Salijanova Sh. D., 2021).

In recent years, as a result of the increasing demand for naturalness and functionality in cosmetic products, local non-traditional oil raw materials have become one of the main components of cosmetic products. In particular, oil plants such as sesame, black cumin, flax, and olive grown in Uzbekistan are not only economically viable, but also allow for effective use in cosmetic products due to the biologically active substances they contain. Rocha-Filho et al. studied the effect

of sesame oil on skin hydration and restoration of the epidermal barrier and found that the use of this substance as the main oil component in creams increased the skin's ability to retain moisture (Rocha-Filho, P.A., Maruno, M. 2025). Other studies have shown that black cumin oil (Nigella sativa) has antibacterial and antioxidant effects (Forouzanfar F., Bazzaz B. S., Hosseinzadeh H., 2014). However, the main problem with the direct use of these oils in the preparation of beauty products is that they do not completely transform into stable emulsions and require balance in terms of odor and color (Liu, J. K., 2022). In a study by Lee et al., it was noted that an emulsion prepared based on linseed oil separated within 72 hours (Lee, Pei-En & Choo, Wee-Sim. 2014).

The process of selecting an emulsifier that ensures the effective combination of oily raw materials with the water phase in the composition of cosmetic creams is an important stage. Although traditional emulsifiers such as cetearyl alcohol, glyceryl stearate, PEG-100 stearate are widely used in creams in the industry, their effectiveness may be low when working with local non-traditional oily raw materials. For example, it has been noted that phase separation and thermostability problems were observed when PEG emulsifiers were used in emulsions prepared based on vegetable oils (Ibrahim, Mohamed & Shimizu, Taro & Ando, Hidenori & Ishima, Yu & Elgarhy, Omar & Sarhan, Hatem & Hussein, Amal & Ishida, Tatsuhiro. 2023; Vasiljević, Dragana & Djekic, Ljiljana & Primorac, Marija. 2012). To solve this problem, researchers are turning to natural emulsifiers. In particular, scientists have successfully prepared an emulsion based on linseed oil using lecithin, saponin, and mixed natural gel emulsifiers. They achieved a thermostable and optically uniform cream using soy lecithin. Also, the selection of emulsifiers, taking into account the acidity level of the skin (pH ~5.5), resulted in the biocompatibility of the cream (Díaz-Cruces, Eliana & Tom, Thara & Gómez-López, Vicente & Negrete-Bolagay, Daniela & Hermoso-Gil, Javier & Miró, Pablo & Troconis, Jorge & Toro-Mendoza, Jhoan & Narváez Muñoz, Christian & Zamora Ledezma, Ezequiel & Alexis, Frank & Zamora-Ledezma, Camilo. 2025). Recently, the use of waxes, particularly beeswax, as emulsifiers has become increasingly popular (Junita Hakim, Rusnia & Nugrahani, Ratri & Fithriyah, Nurul. 2020).

One of the important factors determining the quality, long-term storage and consumer perception of a cream product is its viscosity and rheological properties. When working with local oils, creams can quickly break down and have an unstable structure. In studies, creams prepared with sesame and linseed oils were not properly stabilized. They managed to maintain the viscosity of the cream at 5.1 Pa s by using a 1:1 mixture of guar gum and xanthan gum to maintain the cream structure. The use of ultrasonic homogenizer technology further stabilized the cream structure. As a result of scientific studies, the optimal viscosity of a cream based on linseed oil was determined in the range of 4.8–5.3 Pa s. This allows the cream to spread and form a thin layer on the skin (Sita Devi Sarma, Twahira Begum, Mohan Lal, 2024).

The use of antioxidants, vitamins, essential oils, and antibacterial substances is of great importance in increasing the preventive properties of cosmetic creams. However, the presence of such substances in the cream with local oils can have the opposite effect. For example, a 30% decrease in antioxidant activity was observed in a cream prepared on the basis of tea tree oil and vitamin E after 10 days. This is because the vitamins remain in the open phase and do not completely combine with the oil. To solve this problem, researchers have proposed encapsulation technology. Currently, technologies such as microemulsion and nanostructured lipids are used to enrich creams based on local raw materials with effective active ingredients. The absorption, distribution, and long-term effect of each component on the skin are important aspects of the cream recipe (. Ghelichi, Sakhi & Hajfathalian, Mona & Yeşiltaş, Betül & Sørensen, Ann-Dorit & García-Moreno, Pedro & Jacobsen, Charlotte. 2023).

Analysis of the physicochemical properties of fats and oils: Determination of saponification number, determination of peroxide number, determination of oil density, determination of refractive index, determination of iodine number, determination of acid number (Kadirov Y., 2005):

Materials and methods

1. Analysis of the physicochemical properties of the cream

Within the framework of this study, a comprehensive analysis of the physicochemical and organoleptic properties of cosmetic creams produced on the basis of local raw materials was carried out. The structural, technological and consumer-oriented quality indicators of the cream were evaluated in accordance with international standards (ASTM E1490–19).

1.1. Determination of the viscosity of the cream

The viscosity index was measured using a rotational viscometer (Brookfield DV-E) to assess the plastic and thixotropic properties of the cream. Measurements were carried out at a temperature of 25±0.5 °C, at different rotor rotation speeds. The data obtained served to assess the consistency and structural and mechanical properties of the cream (Umirova Z. Sh, Khakimova. Z. A, Akhmedov A. N, Ruzibaev. A. T., 2025).

1.2. Determination of the lubricity of the cream

The lubricity of the test samples was determined using the following technique: 0.5 g of the test sample was placed in a circle, a glass plate was placed. The 500 g sample was placed on a high glass plate for 5 minutes. Spreadability is the area covered by a specified amount of cream sample after uniform spreading of the sample on a glass slide. The increase in diameter due to spreading of the test sample was recorded. The average value of three determinations was recorded (Umirova.Z.Sh., Akhmedov.A.N.. Hakimova Z. A., Ruzibayev A. T., 2025).

1.3. Organoleptic assessment of cream quality

The organoleptic assessment covered the appearance, smell, spread on the skin, viscosity and effect of the cream. This assessment was carried out by a group of 10 sensory experts on a 10-point scale. Here, 1 point was defined as the worst, and 10 points as the highest quality. The results of the analysis were combined with subjective assessments and precise measurements (Umirova Z. Sh, Khakimova. Z. A, Akhmedov A. N, Ruzibaev. A. T., 2025).

In general, the research methods were based on international standards and scientific sources widely used in the evaluation of modern cosmetic products, which allowed for a comprehensive assessment of the quality and effectiveness of the cream.

Results

Cosmetic creams differ from each other in their functional components and additives. The multifunctionality of creams depends on the different composition of the components included in their recipe. However, any cream consists of an oily and aqueous phase. The functional additive included in the cream recipe is either water-soluble or fat-soluble. In this regard, the additive is added to the oily phase or to the aqueous phase. Today, local cream manufacturers import most of the recipe components from abroad. In particular, emulsifiers, fillers, plasticizers, antioxidants, preservatives and fatty base components are also imported. The research work aimed to reduce the amount of imported fat in the cream recipe using local fatty raw materials. For this, the physicochemical parameters of local fatty raw materials were initially analyzed (Table 1) (Umirova Z. Sh, Khakimova Z. A, Akhmedov A. N, Ruzibaev. A. T., 2025).

Table 1. *Physicochemical characteristics of oils obtained from unconventional oil raw materials available in Uzbekistan*

No.	Index name	Amount					
		Apricot oil	Almond oil	Grape oil	Watermelon oil	Peach oil	Pumpkin oil
1	Saponification number, mg KOH/g	190	190	191	196	190	188
2	Density, g/cm^3	918	916	922	912	912	915

No.	Index name	Amount					
		Apricot oil	Almond oil	Grape oil	Watermel-on oil	Peach oil	Pump-kin oil
3	Refractive index	1,470	1,472	1,475	1,466	1,470	1,466
4	Iodine number, mg J_2/g	103	99	139	114	100	104
5	Peroxide number, mmol O_2	8,0	6,2	5,7	3,4	3,2	4,1
6	Acid number, mg KOH/g	1,6	1,1	1,2	2,6	1,1	1,4

Table 2. *Recipes for moisturizing and nourishing creams*

No.	Name of ingredients	Quantity (%)
1	Stearic acid	12,0
2	Liquid paraffin	5,0
3	Glyceryl monostearate	3,0
4	Oil	20,0
5	Glycerin	3,0
6	Propylene glycol	3,0
7	Isopropyl myristate	2,0
8	Triethanolamine	0,2
9	Propyl paraben	0,1
10	Fragrance	0,03
11	Water	51,67%

Figure 1. *Viscosity, spreadability, and skin absorption of creams depending on the type of oil*

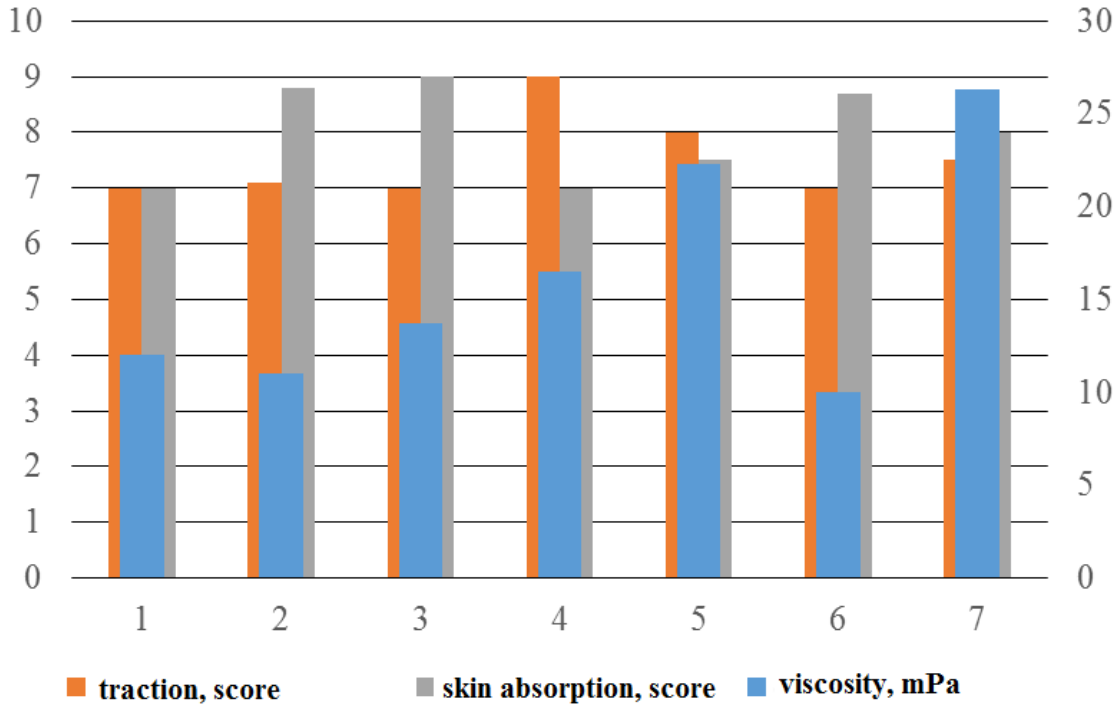

All of the oils studied above meet the requirements for an oil that can be used in a cosmetic cream recipe in terms of their physicochemical characteristics. The high mass fraction of unsaturated fatty acids ensures good absorption of creams based on these oils by human skin, while saturated fatty acids ensure the consistency of the cream and its smoothness on the skin (Umirova Z. Sh., Akhmedov A. N., 2025).

Separate creams were prepared from each of the 6 types of oils analyzed above (Table 3). Here, 1- sunflower oil (sample cream), 2- cream with apricot oil, 3- cream with almond oil, 4- cream with grape oil, 5- cream with watermelon oil, 6- cream with peach oil, 7- cream with pumpkin oil.

Although the amount of oil in the cream recipes is the same, the physicochemical properties of the oils directly significantly affect the properties of the cream. Therefore, the viscosity, spreadability and skin absorption of the creams were analyzed. The results obtained are presented in Figure 1.

Discussion and Conclusion

From the data in Table 1, it can be seen that the physicochemical parameters of apricot, almond, grape, apricot, peach and pumpkin oils are very close and similar to each other. The saponification number of the oils is from 188 mg KOH/g to 196 mg KOH/g, the density is from 915 g/cm3 to 922 g/cm^3, the refractive index is from 1.466 to 1.475, the iodine number is from 99 mg J_2/g to 139 mg J2/g, the peroxide number is from 3.2 mmol O2 to 8.0 mmol O_2, and the acid number is from 1.1 mg KOH/g to 2.6 mg KOH/g. Although all oils are close to each other in terms of aggregate state and organoleptic parameters, they differ in fatty acid composition. This can also be seen from the data in Table 2.

Table 2 shows that the fat phase of the cream is more than 40%, of which 20% is liquid oil and 12% is stearic acid. The mass fraction of the fat phase in this recipe is relatively high, which is suitable for a nourishing and caring cream.

Figure 1 shows that the creams had different viscosity, spreadability, and skin absorption. Their values were directly dependent on the type of oil used in the cream recipe. The highest cream viscosity was observed in cream 7, and the lowest in cream 6. The highest cream spreadability was observed in cream 4, and the lowest in cream 6. The best skin absorption of the cream was observed in cream 3 and the lowest in cream 4. The optimal indicators for all indicators were observed in cream 5. This cream recipe included watermelon oil, and among the oils studied, watermelon oil was found to be the most optimal choice for the cream.

Summary

The results of the study on the use of non-traditional oils available in Uzbekistan in cosmetic cream recipes show that high-quality cosmetic creams can be obtained from all oils. All creams had quality indicators not inferior to the sample cream prepared on the basis of sunflower oil. While almond and apricot oils had high skin absorption, grape seed oil showed the best results when applied to the skin. It was observed in this study that the spreadability of the cream does not always depend on its viscosity. It was found that a cream with optimal results in all indicators can be prepared on the basis of watermelon oil.

References

Khakimova Z. A., Usmanova F. Q., Ruzibaev A. T. Izuchenie fiziko-khimicheskikh svoystv masel iz kostochek apricot i persika mestnogo iskhojdeniya i ispolzovanie ix v resepture kosmeticheskikh kremov // Universum: Teknicheskie nauki nauchni journal No. 8(77) // Moscow, 2020. – P. 39–42.

Khakimova Z. A., Ruzibaev A. T., Gaipova Sh.S., Salijanova Sh.D., Issledovanie fiziko-khimicheskih svoystv uvlajnyayushchego krema poluchennogo na osnove kostochkovyx masel // Universum: Teknicheskie nauki. Scientific journal. – Moscow, 2021. – No. 10 (91). – P. 58–61.

Rocha-Filho, P.A., Maruno, M. Study of Formulation, Physical Properties, and Instability Process and In Vitro Evaluation of Transparent Nanoemulsions Containing Sesame Seed

Oil (SO) and Raspberry Seed Oil (RO). *Cosmetics* **2025. –** *12*. – 32. URL: https://doi.org/10.3390/cosmetics12020032

Forouzanfar F., Bazzaz B. S., Hosseinzadeh H. Black cumin (Nigella sativa) and its constituent (thymoquinone): a review on antimicrobial effects. Iran J Basic Med Sci. 2014. Dec;17(12): 929–38.

Liu, J. K. Natural products in cosmetics. *Nat. Prod. Bioprospect*. –**12. –** 40. (2022). URL: https://doi.org/10.1007/s13659-022-00363-y

Lee, Pei-En & Choo, Wee-Sim. (2014). Characterization of flaxseed oil emulsions. Journal of Food Science and Technology. 52.10.1007/s13197-014-1495-3.

Ibrahim, Mohamed & Shimizu, Taro & Ando, Hidenori & Ishima, Yu & Elgarhy, Omar & Sarhan, Hatem & Hussein, Amal & Ishida, Tatsuhiro. (2023). Investigation of anti-PEG antibody response to PEG-containing cosmetic products in mice. Journal of controlled release: official journal of the Controlled Release Society. – 354. 10.1016/j.jconrel.2023.01.012.

Vasiljević, Dragana & Djekic, Ljiljana & Primorac, Marija. (2012). Long-term stability investigation of o/w cosmetic creams stabilized by mixed emulsifier. Hemijska industrija. – 66. – P. 871–878. 10.2298/HEMIND120613103V.

Díaz-Cruces, Eliana & Tom, Thara & Gómez-López, Vicente & Negrete-Bolagay, Daniela & Hermoso-Gil, Javier & Miró, Pablo & Troconis, Jorge & Toro-Mendoza, Jhoan & Narváez Muñoz, Christian & Zamora Ledezma, Ezequiel & Alexis, Frank & Zamora-Ledezma, Camilo. (2025). Saponins as Natural Emulsifiers: Challenges, Regulatory Landscape, and Future in Biomedical and Cosmetic Fields. Industrial & Engineering Chemistry Research. 10.1021/acs.iecr.4c04714.

Junita Hakim, Rusnia & Nugrahani, Ratri & Fithriyah, Nurul. (2020). Performance of Lecithin Isolate from Vegetable Oil as an Emulsifier on the Beeswax Coating Characteristics. International Journal of ChemTech Research. – 13. – P. 111–119. 10.20902/IJCTR.2019.130307.

Sita Devi Sarma, Twahira Begum, Mohan Lal, Chapter 4.2 – Application of linseed in cosmetic and personal care products development, Editor(s): Sapna Langyan, Ashok Kumar, Linseed, Academic Press, 2024. – P. 193–203.

Ghelichi, Sakhi & Hajfathalian, Mona & Yeşiltaş, Betül & Sørensen, Ann-Dorit & García-Moreno, Pedro & Jacobsen, Charlotte. (2023). Oxidation and oxidative stability in emulsions. Comprehensive Reviews in Food Science and Food Safety. 22. 10.1111/1541–4337.13134.

Kadirov Y. Laboratory exercises on oil processing technology. -Tashkent: Cholpon, 2005. – 168 p.

ASTM E1490–19: Standard Guide For Two Sensory Descriptive Analysis Approaches For Skin Creams And Lotions.

Umirova Z. Sh., Khakimova. Z. A., Akhmedov A. N., Ruzibaev A. T. “Research of the influence of local non-traditional oils on physicochemical indicators of cosmetic cream” Universum: technical sciences Issue: 8 (137) August 2025 Part 3 Moscow 2025 y. – P. 25–31.

Umirova Z. Sh., Akhmedov A. N. Hakimova Z. A., Ruzibayev A. T. “Formulation of a cosmetic cream recipe containing sunflower wax” CAFET (Central Asian Food Engineering and Technology) Scientific technical journal. 2025/2. P. 78–83.

Umirova Z. Sh., Akhmedov A. N. “Formulation of a recipe containing sunflower wax in the production of cosmetic products”. International scientific week 28–31 May. 2025. Tashkent Uzbekistan. – Tashkent, 2025. – P. 434–436.

submitted 15.08.2025;
accepted for publication 31.08.2025;
published 29.09.2025

Contact: a.ahmedov80@mail.ru

The Austrian Journal of Technical and Natural Sciences, No 7–8
ISSN 2310-5607

PREMIER Publishing
ppublishing.org

Section 3. Machinery construction

DOI:10.29013/AJT-25-7.8-79-85

ANALYSIS OF THE DYNAMICS OF RANDOM VIBRATIONS OF A BEAM WITH HYSTERESIS-TYPE DISSIPATIVE CHARACTERISTICS

Kasimova F. U. [1]

[1] Samarkand State University, Samarkand, Uzbekistan

Cite: *Kasimova F. U. (2025). Analysis of the Dynamics of Random Vibrations of a Beam With Hysteresis-Type Dissipative Characteristics. Austrian Journal of Technical and Natural Sciences 2025, No 7–8.* https://doi.org/10.29013/AJT-25-7.8-79-85

Abstract

This work deals with the analysis of nonlinear transverse vibrations of a beam with a hysteresis-type dissipative characteristic, whose cross-section changes under the influence of random excitations, using the mean square values. The dissipative properties of the beam material are of the hysteresis type and are taken into account in the equation, expressed by a linear complex function using the statistical linearization method. The dynamic characteristics of the beam displacements are analyzed using the analytical expression of the mean square values.

Keywords: *beam, hysteresis, dissipative, oscillation, random excitation, root mean square value, amplitude, frequency*

Introduction

In many areas of technology, when designing beam-type structures, it is important to mathematically model them taking into account the elastic and dissipative properties and correctly select their structural parameters as a result of accurate calculations. The issues of evaluating the vibrational behavior of elastic beams with varying cross-sections in various processes and determining their dynamic characteristics are relevant.

The work, the differential equation of motion for longitudinal vibrations of a beam with a variable cross-section and its solutions were determined. In this work, the differential equation for a beam with a linearly varying cross-section was reduced to the Legendre equation with appropriate modifications. The frequency equations of the beam were found for various boundary conditions. The obtained results were compared with solutions that are suitable for special cases of changes in the existing cross-section. In addition, the effect of changing the cross-sectional area of the beam on the nature of the vibrations was numerically analyzed (Yardimoglu B., Aydin L., 2011,). Studied the kinematic and random vibrations of a beam with a variable cross-section in a vertical position, taking into account the weight. The analytical expressions of the amplitudes and root mean square values of the vibrations

were determined. The influence of parameters on random and harmonic vibrations was evaluated. The change in amplitudes and root mean square values around the resonance frequency was analyzed (Alokova M. Kh., Kulterbaev H. P. 2015). Focused on studying the vibrations of a beam with a variable cross-section mounted on a rotating disk. A force parallel to the disk, which depends on time, was applied to the beam as an external force. The law of change in the cross-section was obtained in various forms. The analysis of such systems has been proven to be applicable to many turbines and pumps. The equations of motion of a rotating beam mounted on a rigid disk were obtained. The transmission effects were considered in a mathematical model, taking into account the Coriolis forces and centrifugal forces. The necessity of solving these problems for nonlinear systems is discussed, and recommendations are given (Zolkiewski S., 2013). Considers transverse vibrations of a beam with a uniformly decreasing thickness starting from one end. The vibration velocity is analyzed. It is shown that the obtained differential equations have an exact solution. Based on these solutions, a new method is proposed for solving the beam equation when the thickness change is not parabolic (Мироновв M. A., 2017). Presents numerical methods for analyzing vibrations of beams with variable cross-section. The Ostrogradsky-Hamilton principle is used to obtain the equations of longitudinal, torsional and transverse vibrations of the beam equations. The boundary value problem given by differential calculation methods under various boundary conditions is solved (Zhakash A. T., Dzhakashova E. A., Tursynbay O. M., 2019). Develops a methodology for calculating the stress-strain state in a composite beam with a variable cross-section. The dynamics of these beams are tested for various materials and dynamic loading conditions. The proposed computational model takes into account the effects of deformations and viscoelasticity. It is shown that such beams with different cross-sections, which are elements of beam systems, are characterized by high strength indicators and, at the same time, reduce pbeamuction costs compared to beams with a constant cross-section (Nemirovsky Yu. V., Mishchenko A. V., 2015). linear vibrations of a curved beam were studied using the finite element method. The curved beam was taken in the form of a semicircle, and the cross-section of the beam was taken in circular and rectangular forms. Vibrations of a beam with uniformly symmetrical and symmetrically tapered cross-sectional surfaces were considered, and the eigenfrequencies were determined for various boundary conditions. The effects of stretching and bending were investigated. Vibrations of the beam with an additional mass installed on it were also considered, and the effect of changing the cross-section on the eigenfrequencies was investigated (Kulterbaev, H. P., Payzulaev, M. M., 2023). Notes the widespread use of beams in the construction industry as load-bearing structures for bridges, overpasses, coatings, floors, stairs, etc., and shows the feasibility of using beams with a variable cross-section along the length to fully utilize the load-bearing capacity of such structures and reduce material consumption. The occurrence of various types of vibrations in such structural elements during operation is analyzed (Baragunova L. A., Shogenova M. M., Shogenov O. M., Yafaunov E. A., 2024).

The aim of the work is to mathematically model the vibration behavior of a beam with a variable cross-section with a hysteresis-type dissipative characteristic in random processes and to calculate the mean square values, dynamic characteristics and dissipative properties.

Materials and methods

In this work, we analyze the dynamics of transverse vibrations of a beam with a dissipative characteristic of a hysteresis-type cross-section under the influence of random excitations. The differential equation of motion of the beam under the influence of random excitations is as follows after the substitutions (Dusmatov O. M., Kasimova F. U., 2024):

$$\ddot{q}_i + \{\left(1 + K_0\left(-\gamma_1 + j\gamma_2\right)\right)p_i^2 + \frac{3E}{\rho F d_{2i}}\left(-\gamma_1 + j\gamma_2\right)\times$$

$$\times\sum_{k=1}^{n} K_k \sigma_{ia}^k \frac{h^k}{2^k\left(k+3\right)}\int_0^l I\left(x\right)u_i \frac{\partial^2}{\partial x^2}\left(\frac{\partial^2 u_i}{\partial x^2}\left|\frac{\partial^2 u_i}{\partial x^2}\right|^k\right)dx +$$

$$+\frac{E}{\rho F d_{2i}}\int_0^l \frac{\partial^2 I(x)}{\partial x^2}u_i\frac{\partial^2 u_i}{\partial x^2}\times$$
$$\times\left[1+K_0(-\gamma_1+j\gamma_2)+3(-\gamma_1+j\gamma_2)\sum_{k=1}^{n}K_k\sigma_{ia}^k\frac{h^k}{2^k(k+3)}\left|\frac{\partial^2 u_i}{\partial x^2}\right|^k\right]dx+$$
$$+\frac{2E}{\rho F d_{2i}}\int_0^l \frac{\partial I(x)}{\partial x}u_i\frac{\partial}{\partial x}\left[\sum_{i=1}^{\infty}\frac{\partial^2 u_i}{\partial x^2}\left[1+K_0(-\gamma_1+j\gamma_2)+3(-\gamma_1+j\gamma_2)\times\right.\right.$$
$$\left.\left.\times\sum_{k=1}^{n}K_k\sigma_{ia}^k\frac{h^k}{2^k(k+3)}\left|\frac{\partial^2 u_i}{\partial x^2}\right|^k\right]\right]dx\}q_i=-d_i\frac{\partial^2 w_0}{\partial t^2}; \quad (1)$$

where $q_i=q_i(t)$ is the time-dependent expression of the strain transfer function; $j^2=-1$; E modulus of elasticity; $\gamma_1,\gamma_{2^*}=\gamma_2 sign\omega$ coefficients determined from the nonlinear functional representing the dissipative properties of the beam material (ω frequency); σ_{q_i} root mean square value of the relative deformation of the beam; $K_0,K_1,\ldots,K_n$ are experimentally determined parameters of the hysteresis loop and depend on the damping properties of the beam material (Pavlovsky M. A., Ryzhkov L. M., Yakovenko V. B., Dusmatov O. M., 1997); $n_0^2=\frac{c}{m}$; c, m are the stiffness and mass of the elastic damping element of the dynamic damper, respectively;

$I=\frac{bh^3}{12}; d_i=\frac{d_{1i}}{d_{2i}}; d_{1i}=\int_0^l u_i dx; d_{2i}=\int_0^l u_i^2 dx; q_{ia}=|q_i|$;

$l=const$, $b=b(x)$ va $h=const$ the length, width and thickness of the beam, respectively; $\rho, F=F(x)$ respectively, the density and cross-sectional area of the beam material; p_i, u_i the specific frequencies and vibrational forms of the beam;

To find the transfer function of an elastic beam with a variable cross-section, we reduce the differential equation (1) to an algebraic equation using the differential operator

$$S=\frac{d}{dt}$$

$$\{S^2+(1+K_0(-\gamma_1+j\gamma_2))p_i^2+\frac{3E}{\rho F d_{2i}}(-\gamma_1+j\gamma_2)\times$$
$$\times\sum_{k=1}^{n}K_k\sigma_{ia}^k\frac{h^k}{2^k(k+3)}\int_0^l I(x)u_i\frac{\partial^2}{\partial x^2}\left(\frac{\partial^2 u_i}{\partial x^2}\left|\frac{\partial^2 u_i}{\partial x^2}\right|^k\right)dx+$$
$$+\frac{E}{\rho F d_{2i}}\int_0^l \frac{\partial^2 I(x)}{\partial x^2}u_i\frac{\partial^2 u_i}{\partial x^2}\times$$
$$\times\left[1+K_0(-\gamma_1+j\gamma_2)+3(-\gamma_1+j\gamma_2)\sum_{k=1}^{n}K_k\sigma_{ia}^k\frac{h^k}{2^k(k+3)}\left|\frac{\partial^2 u_i}{\partial x^2}\right|^k\right]dx+$$
$$+\frac{2E}{\rho F d_{2i}}\int_0^l \frac{\partial I(x)}{\partial x}u_i\frac{\partial}{\partial x}\left[\sum_{i=1}^{\infty}\frac{\partial^2 u_i}{\partial x^2}\left[1+K_0(-\gamma_1+j\gamma_2)+3(-\gamma_1+j\gamma_2)\times\right.\right. \quad (2)$$
$$\left.\left.\times\sum_{k=1}^{n}K_k\sigma_{ia}^k\frac{h^k}{2^k(k+3)}\left|\frac{\partial^2 u_i}{\partial x^2}\right|^k\right]\right]dx\}q_i=-d_i\frac{\partial^2 w_0}{\partial t^2}.$$

Solving equation (2) and intbeamucing the substitution $S=j\omega$ we write the expression for the mean square values of the variables q_i as follows:

$$\sigma_{q_i}^2=\int_{-\infty}^{\infty}\left|\frac{d_i}{N_{10}+jN_{20}}\right|^2 S_{W_0}(\omega)d\omega, \quad (3)$$

here

$$N_{10} = -\omega^2 + \left(1-\gamma_1 K_0\right) p_i^2 - \gamma_1 \frac{3E}{\rho F d_{2i}} \times$$
$$\times \sum_{k=1}^{n} K_k \sigma_{ia}^k \frac{h^k}{2^k (k+3)} \int_0^l I(x) u_i \frac{\partial^2}{\partial x^2} \left(\frac{\partial^2 u_i}{\partial x^2} \left| \frac{\partial^2 u_i}{\partial x^2} \right|^k \right) dx +$$
$$+ \frac{E}{\rho F d_{2i}} \int_0^l \frac{\partial^2 I(x)}{\partial x^2} u_i \frac{\partial^2 u_i}{\partial x^2} \times$$
$$\times \left[1-\gamma_1 K_0 - 3\gamma_1 \sum_{k=1}^{n} K_k \sigma_{ia}^k \frac{h^k}{2^k (k+3)} \left| \frac{\partial^2 u_i}{\partial x^2} \right|^k \right] dx + \frac{2E}{\rho F d_{2i}} \times$$
$$\times \int_0^l \frac{\partial I(x)}{\partial x} u_i \frac{\partial}{\partial x} \left[\frac{\partial^2 u_i}{\partial x^2} \left[1-\gamma_1 K_0 - 3\gamma_1 \sum_{k=1}^{n} K_k \sigma_{ia}^k \frac{h^k}{2^k (k+3)} \left| \frac{\partial^2 u_i}{\partial x^2} \right|^k \right] \right] dx;$$

$$N_{20} = \gamma_2 K_0 p_i^2 + \frac{3E}{\rho F d_{2i}} \eta_2 \times$$
$$\times \sum_{k=1}^{n} K_k \sigma_{ia}^k \frac{h^k}{2^k (k+3)} \int_0^l I(x) u_i \frac{\partial^2}{\partial x^2} \left(\frac{\partial^2 u_i}{\partial x^2} \left| \frac{\partial^2 u_i}{\partial x^2} \right|^k \right) dx +$$
$$+ \frac{E}{\rho F d_{2i}} \int_0^l \frac{\partial^2 I(x)}{\partial x^2} u_i \frac{\partial^2 u_i}{\partial x^2} \times$$
$$\times \left[\gamma_2 K_0 + 3\gamma_2 \sum_{k=1}^{n} K_k \sigma_{ia}^k \frac{h^k}{2^k (k+3)} \left| \frac{\partial^2 u_i}{\partial x^2} \right|^k \right] dx + \frac{2E}{\rho F d_{2i}} \times$$
$$\times \int_0^l \frac{\partial I(x)}{\partial x} u_i \frac{\partial}{\partial x} \left[\frac{\partial^2 u_i}{\partial x^2} \left[\gamma_2 K_0 + 3\gamma_2 \sum_{k=1}^{n} K_k \sigma_{ia}^k \frac{h^k}{2^k (k+3)} \left| \frac{\partial^2 u_i}{\partial x^2} \right|^k \right] \right] dx.$$

$S_{W_0}(\omega)$ the basis is the spectral density of accelerations, which in most cases is generally obtained as follows (Pavlovsky M. A., Ryzhkov L. M., Yakovenko V. B., Dusmatov O. M., 1997):

$$S_{W_0}(\omega) = \frac{D_{W_0} \alpha \omega_э^3}{\pi \left(\omega_э^2 - \omega^2 + j\alpha\omega_э\omega \right) \left(\omega_э^2 - \omega^2 - j\alpha\omega_э\omega \right)}, \quad (4)$$

where D_{W_0} is the dispersion of the fundamental acceleration; $\omega_э$ is the frequency with the highest probability in the oscillation spectrum; α is a parameter characterizing the width of the oscillation spectrum.

Results and discussion

We calculate the integral representing the root mean square displacements of a beam with a variable cross-section and elastic dissipative characteristics of the hysteresis type, and after some simplifications we write

$$\sigma_{q_i}^2 = \frac{1}{b_1 b_2 p_i^3} \times \quad (5)$$
$$\times \frac{d_i^2 D_{W_0} \left(-b_1 \alpha^2 p_i \omega_э^2 - \alpha \left(b_1^2 \omega_э p_i^2 + \omega_э^3 \right) - b_1 b_2 p_i^3 \right)}{b_2^2 p_i^4 + \alpha b_1 b_2 \omega_э p_i^3 + \left(\alpha^2 b_2 - 2b_2 + b_1^2 \right) p_i^2 \omega_э^2 + \alpha b_1 p_i \omega_э^3 + \omega_э^4},$$

in this

$$b_1 = \left[2\left(b_2 - 1 + N_{10i}\right)\right]^{\frac{1}{2}};$$

$$b_2 = \left[\left(1 - N_{10i}\right)^2 + \left(N_{20i}\right)^2\right]^{\frac{1}{2}};$$

$$N_{10i} = \gamma_1 K_0 + \frac{1}{p_i^2}[\gamma_1 \frac{3E}{\rho F d_{2i}} \times$$

$$\times \sum_{k=1}^{n} K_k \sigma_{ia}^k \frac{h^k}{2^k (k+3)} \int_0^l I(x) u_i \frac{\partial^2}{\partial x^2} \left(\frac{\partial^2 u_i}{\partial x^2} \left| \frac{\partial^2 u_i}{\partial x^2} \right|^k \right) dx -$$

$$- \frac{E}{\rho F d_{2i}} \int_0^l \frac{\partial^2 I(x)}{\partial x^2} u_i \frac{\partial^2 u_i}{\partial x^2} \times$$

$$\times \left[1 - \gamma_1 K_0 - 3\gamma_1 \sum_{k=1}^{n} K_k \sigma_{ia}^k \frac{h^k}{2^k (k+3)} \left| \frac{\partial^2 u_i}{\partial x^2} \right|^k \right] dx - \frac{2E}{\rho F d_{2i}} \times$$

$$\times \int_0^l \frac{\partial I(x)}{\partial x} u_i \frac{\partial}{\partial x} \left[\frac{\partial^2 u_i}{\partial x^2} \left(1 - \gamma_1 K_0 - 3\gamma_1 \sum_{k=1}^{n} K_k \sigma_{ia}^k \frac{h^k}{2^k (k+3)} \left| \frac{\partial^2 u_i}{\partial x^2} \right|^k \right) \right] dx;$$

$$N_{20i} = \gamma_2 K_0 + \frac{1}{p_i^2}[\frac{3E}{\rho F d_{2i}} \gamma_2 \times$$

$$\times \sum_{k=1}^{n} K_k \sigma_{ia}^k \frac{h^k}{2^k (k+3)} \int_0^l I(x) u_i \frac{\partial^2}{\partial x^2} \left(\frac{\partial^2 u_i}{\partial x^2} \left| \frac{\partial^2 u_i}{\partial x^2} \right|^k \right) dx +$$

$$+ \frac{E}{\rho F d_{2i}} \int_0^l \frac{\partial^2 I(x)}{\partial x^2} u_i \frac{\partial^2 u_i}{\partial x^2} \times$$

$$\times \left[\gamma_2 K_0 + 3\gamma_2 \sum_{k=1}^{n} K_k \sigma_{ia}^k \frac{h^k}{2^k (k+3)} \left| \frac{\partial^2 u_i}{\partial x^2} \right|^k \right] dx + \frac{2E}{\rho F d_{2i}} \times$$

$$\times \int_0^l \frac{\partial I(x)}{\partial x} u_i \frac{\partial}{\partial x} \left[\frac{\partial^2 u_i}{\partial x^2} \left(\gamma_2 K_0 + 3\gamma_2 \sum_{k=1}^{n} K_k \sigma_{ia}^k \frac{h^k}{2^k (k+3)} \left| \frac{\partial^2 u_i}{\partial x^2} \right|^k \right) \right] dx;$$

(5) the expression of the mean square values makes it possible to determine and analyze the dynamics and priority of the beam's oscillations under the influence of random excitations at different values of the parameters.

We numerically analyze the vibrations of a beam with one end fixed and one end free. The parameters are taken as follows: $l = 0.25; \gamma_1 = \frac{3}{4}; \gamma_2 = \frac{1}{\pi};$

$$E = 2.08 \cdot 10^{11} \frac{N}{m^2}; \text{Á} = 7810 \frac{kg}{m^3}; h = 2 \cdot 10^{-3}; K_0 = H_0 = 0; K_1 = 6.760624;$$

$$K_2 = -8278.5937; K_3 = 5894761;$$

In order to analyze the dynamics of vibrations of a cross-section with elastic dissipative characteristics of the hysteresis type with a width of $b = 0.02 + 0.01\sin(80x)$ and a constant width of $b = 0.02$ under the influence of random excitations, we analyze the change in the graphs of the expression of the mean square values (5) depending on the frequency at which the vibration probability is high.

Figure 1. *(5) RMS expression graphs*

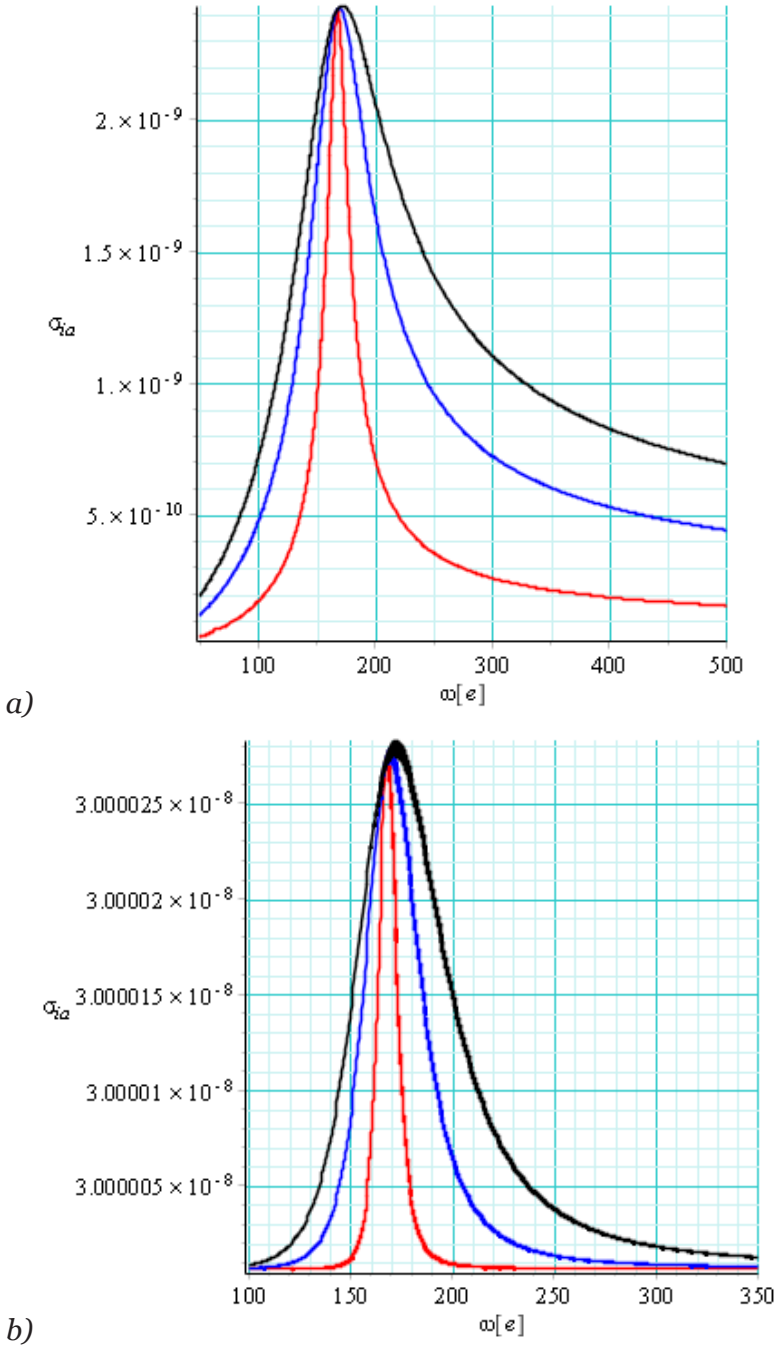

$\alpha = 0.01(red));0.08(blue);0.1(black).$

In the graphs in Figure 1-a), the graphs of the expression of the mean square value (5) are presented for the cases where the cross-sectional width of the beam varies according to the law $b = 0.02 + 0.01\sin(80x)$ and in Figure 1-b) $b = 0.02$ is constant. From the graphs presented for both cases, it can be said that the mean square values of the beam with a variable cross-section are almost ten times smaller than in the case where the cross-section is constant. In addition, in both cases, an increase in the parameter α, which characterizes the width of the vibration spectrum, does not change the mean square value around the resonant frequency, but at a sufficient distance from the resonant frequency leads to an increase in the mean square value.

Conclusion

The nonlinear oscillations of a hysteresis-type dissipative beam with a variable cross-section under the influence of random excitations were mathematically modeled

and their root mean square values were determined analytically for the general case depending on the system parameters. The expressions of the root mean square values of the displacements of a hysteresis-type elastic dissipative beam with a variable cross-section were numerically analyzed. The changes in the root mean square values of the displacements at different values of the parameters were shown on the basis of graphs and the corresponding conclusions were drawn.

References

Yardimoglu B., Aydin L. (2011). Exact longitudinal vibration characteristics of beams with variable cross-sections Shock and Vibration, – 18.

Alokova M. Kh., Kulterbaev H. P. (2015). Bending vibrations of a vertical rod of variable cross-section with a concentrated mass. Bulletin of the Dagestan State Technical University. Engineering sciences. – 39(4): 77–86.

Zolkiewski S. (2013). Vibrations of beams with a variable cross-section fixed on rotational rigid disks Latin American Journal of Solids and Structures, – 10. – P. 39–57.

Mironov M. A. (2017). Exact solutions of the equation of transverse vibrations of a rod with a special law of change of the cross-section Acoustic journal, 2 – Vol. 63. – No. 1. – P. 3–8.

Zhakash A. T., Dzhakashova E. A., Tursynbay O. M. (2019). Numerical methods for calculating vibrations of straight beams of variable cross-section international scientific journal theoretical & applied science Year, – Issue: 07. – Volume: 75.

Nemirovsky Yu. V., Mishchenko A. V. (2015). Dynamic analysis of composite beams with variable cross-section Computational Continuous Mechanics. – Vol. 8. – No. 2. – P. 188–199.

Kulterbaev, H. P., Payzulaev, M. M. (2023). Stability of a compressed-tensioned beam of variable cross-section with combined loading Herald of Dagestan State Technical University. Technical Sciences, – Vol. 50. – Issue 4. – P. 191–196.

Baragunova L. A., Shogenova M. M., Shogenov O. M., Yafaunov E. A. (2024). Free vibrations of beams of variable cross-section taking into account rotational forces and friction forces URL: https://doi.org/10.37538/2224-9494-2024-1(40)-7-20.

Dusmatov O. M., Kasimova F. U. (2024). Ko'ndalang kesimi o'zgaruvchan elastik sterjenning chiziqlimas tasodifiy tebranishlari. "Buxoro davlat universiteti ilmiy axboroti" ilmiy jurnal 12-son.

Pavlovsky M. A., Ryzhkov L. M., Yakovenko V. B., Dusmatov O. M. (1997). Nonlinear problems of vibration protection system dynamics. – K.: Tekhnika, – 204 p.

Pisarenko G. S., Boginich O. E. (1981) Oscillations of kinematically excited mechanical systems taking into account energy dissipation. – K.: Nauk. Dumka, – 220 p.

submitted 20.08.2025;
accepted for publication 04.09.2025;
published 29.09.2025

Contact: fkasimova988@gmail.com

The Austrian Journal of Technical and Natural Sciences, No 7–8
ISSN 2310-5607

PREMIER Publishing
ppublishing.org

Section 4. Medical science

DOI:10.29013/AJT-25-7.8-86-91

EMPIRICAL EVALUATION OF THYROID FUNCTION AND OVARIAN RESERVE USING ONE-WAY ANOVA: A CLINICAL ENDOCRINOLOGY PERSPECTIVE

Makhmudova Fotima Ravshanovna [1],
Nasirova Khurshidakhon Kudratullaevna [1]

[1] Tashkent State Medical University, Tashkent, Uzbekistan

Cite: *Makhmudova F. R., Nasirova Kh. K. (2025). Empirical Evaluation of Thyroid Function and Ovarian Reserve Using One-Way Anova: a Clinical Endocrinology Perspective. Austrian Journal of Technical and Natural Sciences 2025, No 7–8.* https://doi.org/10.29013/AJT-25-7.8-86-91

Abstract

This study empirically investigated the relationship between thyroid function and ovarian reserve in women of reproductive age, incorporating key hormonal markers and inflammatory indicators. A one-way Analysis of Variance (ANOVA) was conducted to compare three distinct groups: the control group (practically healthy women, n=20), women with decreased ovarian reserve (DOR) and hypothyroidism (n=40), and women with DOR and euthyroidism (n=40). Data on Thyroid-Stimulating Hormone (TSH), Anti-Müllerian Hormone (AMH), Follicle-Stimulating Hormone (FSH), C-reactive protein (CRP), Complement C3, and Ceruloplasmin were analyzed. Significant differences were observed across groups for TSH ($F(2,97)=54.245$, $p<.001$), AMH ($F(2,97)=323.365$, $p<.001$), CRP ($F(2,97)=101.497$, $p<.001$), Complement C3 ($F(2,97)=34.264$, $p<.001$), and Ceruloplasmin ($F(2,97)=46.734$, $p<.001$). Post-hoc analyses revealed significantly higher TSH and lower AMH in the group with DOR and hypothyroidism compared to both the control group and the group with DOR euthyroidism. CRP, Complement C3, and Ceruloplasmin were also markedly elevated in the DOR with hypothyroidism group, suggesting an inflammatory component. FSH and age did not show significant inter-group differences. These findings underscore the critical impact of thyroid dysfunction on ovarian reserve and highlight the potential role of inflammatory markers in compromised reproductive health.
Keywords: *Thyroid Function, Ovarian Reserve, Hypothyroidism, Diminished Ovarian Reserve (DOR), Infertility*

Introduction

Ovarian reserve (OR), representing the quantity and quality of oocytes, is a cornerstone of female fertility (Kumar & Sharma, 2021). Its decline, termed diminished ovarian reserve (DOR), poses a significant

challenge in reproductive medicine, leading to reduced chances of natural conception and poorer outcomes in assisted reproductive technologies (ART) (Tal & Seifer, 2021). While chronological age is the primary determinant of OR, various endocrine and systemic factors can influence its trajectory. Among these, thyroid dysfunction, particularly hypothyroidism, has garnered increasing attention due to its widespread prevalence in women of reproductive age and its profound systemic effects on metabolism and endocrine function (Busnelli et al., 2021).

Thyroid hormones are crucial for the proper functioning of the reproductive system, participating in follicular development, oocyte maturation, and steroidogenesis (Poppe et al., 2022). Imbalances in thyroid hormone levels can disrupt the delicate hormonal milieu necessary for optimal ovarian function (Unuane et al., 2020). Thyroid-Stimulating Hormone (TSH), a primary indicator of thyroid function, directly and indirectly impacts ovarian physiology due to the presence of TSH receptors on ovarian granulosa cells (Shao et al., 2023). Follicle-Stimulating Hormone (FSH), a classic marker of OR, with elevated levels indicating depleted follicular pools. Anti-Müllerian Hormone (AMH), produced by granulosa cells of preantral and small antral follicles, is considered a highly reliable quantitative marker of OR, reflecting the size of the primordial follicle pool (Dewailly et al., 2020).

Beyond direct hormonal effects, systemic inflammation, often associated with autoimmune thyroid conditions like Hashimoto's thyroiditis, may also contribute to the pathophysiology of DOR. C-reactive protein (CRP), an acute-phase reactant, serves as a general marker of inflammation (Wang et al., 2022). Other inflammatory mediators, such as Complement C3 and Ceruloplasmin, indicative of immune system activation and oxidative stress, may also play a role in the ovarian microenvironment (Al-Azab et al., 2023).

Despite growing evidence suggesting a link between thyroid dysfunction and OR, empirical studies quantifying the differences in key markers across distinct patient groups are crucial for robust clinical understanding. This study aimed to empirically evaluate and compare the levels of TSH, AMH, FSH, CRP, Complement C3, and Ceruloplasmin in women with varying thyroid statuses and ovarian reserve, utilizing one-way ANOVA to identify significant inter-group differences.

Methods: Study Design and Participants

This study employed a cross-sectional design comparing hormonal and inflammatory markers across three distinct groups of women of reproductive age. A total of 100 participants were recruited and categorized as follows:

- Control group (practically healthy women; n = 20): These were euthyroid women with normal ovarian reserve;
- Group 1 – Women with diminished ovarian reserve and hypothyroidism (DOR + Hypothyroidism); n=40. These women had clinical or subclinical hypothyroidism (TSH > 4.0 mIU/L or requiring medication) and diminished ovarian reserve (AMH < 1.1 ng/mL);
- Group 2 – Women with diminished ovarian reserve and euthyroidism (DOR + EU); n=40. These women had diminished ovarian reserve (AMH < 1.1 ng/mL) while maintaining a euthyroid status (TSH within the normal range, no thyroid medication use).

All participants were women of reproductive age (17–38 years). Exclusion criteria included polycystic ovary syndrome, hypothalamic amenorrhea, severe systemic diseases unrelated to thyroid function, or recent hormonal therapy that could confound results. Ethical approval was obtained from the relevant institutional review board, and all participants provided informed consent.

Blood samples were collected from all participants in the early follicular phase (Days 2–4) of their menstrual cycle to minimize hormonal fluctuations for OR markers. The following parameters were measured:

- Thyroid-Stimulating Hormone (TSH): Measured in mIU/L.
- Follicle-Stimulating Hormone (FSH): Measured in mIU/mL.
- Anti-Müllerian Hormone (AMH): Measured in ng/mL.
- C-reactive protein (CRP): Measured in mg/L.
- Complement C3: Measured in g/L.
- Ceruloplasmin: Measured in mg/L.
- Age: Recorded in years.

Ovarian reserve was assessed using AMH levels and basal FSH levels, along with clinical assessment (e.g., antral follicle count, menstrual history). Hypothyroidism was diagnosed based on TSH levels and, where appropriate, free T4 levels, according to standard clinical guidelines.

Statistical Analysis: Descriptive statistics (mean, standard deviation, standard error, 95% confidence intervals, minimum, maximum) were calculated for all continuous variables across the three groups and for the total sample. To compare the means of TSH, AMH, FSH, CRP, Complement C3, Ceruloplasmin, and Age across the three independent groups, one-way Analysis of Variance (ANOVA) was performed. The assumption of homogeneity of variances was assessed using Levene's test (results not shown). For variables where ANOVA yielded a statistically significant difference ($p<.05$), post-hoc tests were conducted to identify specific group differences. Both LSD (Least Significant Difference) and Dunnett T3 post-hoc tests were utilized to account for potential heterogeneity of variances and provide a comprehensive view of pairwise comparisons. All statistical analyses were performed using SPSS software (IBM SPSS Statistics, Version 28.0). A p-value of less than .05 was considered statistically significant.

Results: Descriptive statistics for each measured variable are presented below for the three study groups: the control group (healthy women, n=20), Decreased Ovarian Reserve with Hypothyroidism (Group 1, n=40), and Decreased Ovarian Reserve with Euthyroidism (Group 2, n=40).

For Thyroid-Stimulating Hormone (TSH), the control group had a mean of 1.57±0.52 mIU/L (Mean ± SD), the group 1 had 6.97±3.86 mIU/L, and the group 2 had 1.76±0.51 mIU/L. A one-way ANOVA indicated a significant difference across the three groups, $F(2,97)=54.245$, $p<.001$. Post-hoc Dunnett T3 comparisons revealed that the group 1 exhibited significantly higher TSH levels compared to both the control group (mean difference = 5.395, 95% CI [3.854, 6.936], $p<.001$) and the group 2 (mean difference = 5.203, 95% CI [3.672, 6.733], $p<.001$). There was no significant difference in TSH between the control and second groups (mean difference = –0.192, 95% CI [–0.544, 0.159], $p=.444$).

For Follicle-Stimulating Hormone (FSH), the Control group had a mean of 8.88±1.53 mIU/mL, group 1 had 9.11±6.82 mIU/mL, and the group 2 had 8.85±4.96 mIU/mL. A one-way ANOVA showed no significant difference across the groups for FSH ($F(2,97)=0.027$, $p=.973$).

For Anti-Müllerian Hormone (AMH), the Control group had a mean of 3.98±0.78 ng/mL, group 1 had 0.57±0.35 ng/mL, and the group 2 had 0.98±0.48 ng/mL. A one-way ANOVA indicated a significant difference across the groups, $F(2,97)=323.365$, $p<.001$. Post-hoc Dunnett T3 comparisons showed that the Control group had significantly higher AMH levels compared to both group 1(mean difference = 3.413, 95% CI [2.944, 3.882], $p<.001$) and the group 2 (mean difference = 2.998, 95% CI [2.514, 3.481], $p<.001$). Importantly, the second group had significantly higher AMH levels than group 1 (mean difference = 0.415, 95% CI [0.187, 0.643], $p<.001$).

For C-reactive protein (CRP), the Control group had a mean of 3.08±2.14 mg/L, group 1 had 30.25±10.00 mg/L, and the group 2 had 13.52±5.97 mg/L. A one-way ANOVA indicated a significant difference across the groups, $F(2,97)=101.497$, $p<.001$. Post-hoc Dunnett T3 comparisons revealed that group 1 had significantly higher CRP levels than both the Control group (mean difference = 27.165, 95% CI [23.078, 31.252], $p<.001$) and the group 2 (mean difference = 16.725, 95% CI [12.214, 21.236], $p<.001$). Furthermore, the group 2 also had significantly higher CRP levels than the Control group (mean difference = 10.440, 95% CI [7.835, 13.045], $p<.001$).

For Complement C3, the Control group had a mean of 1.18±0.26 g/L group 1 had 6.75±4.03 g/L, and the group 2 had 2.57±1.87 g/L. A one-way ANOVA indicated a significant difference across the groups, $F(2,97)=34.264$, $p<.001$. Post-hoc Dunnett T3 comparisons showed that group 1 had significantly higher Complement C3 levels compared to both the Control group (mean difference = 5.580, 95% CI [3.988, 7.172], $p<.001$) and the group 2 (mean difference = 4.185, 95% CI [2.457, 5.913], $p<.001$). Additionally, the group 2 group also had sig-

nificantly higher Complement C3 levels than the Control group (mean difference = 1.395, 95% CI [0.645, 2.145], p<.001).

For Ceruloplasmin, the Control group had a mean of 34.30±9.28 mg/L, group 1 had 84.55±29.04 mg/L, and the group 2 had 51.35±13.54 mg/L. A one-way ANOVA indicated a significant difference across the groups, F(2,97)=46.734, p<.001. Post-hoc Dunnett T3 comparisons revealed that group 1 showed significantly elevated Ceruloplasmin levels compared to both the Control group (mean difference = 50.250, 95% CI [37.834, 62.666], p<.001) and the group 2 (mean difference = 33.200, 95% CI [20.739, 45.661], p<.001). The group 2 also had significantly higher Ceruloplasmin levels than the Control group (mean difference = 17.050, 95% CI [9.705, 24.395], p<.001).

For Age, the Control group had a mean of 32.70±5.02 years, group 1 had 30.05±5.22 years, and the second group had 29.98±6.04 years. A one-way ANOVA showed no significant difference in Age across the groups (F(2,97)=1.892, p=.156), indicating that age was not a significant confounding factor in the observed hormonal and inflammatory differences.

The results of the one-way ANOVA for each dependent variable are summarized in Table 2.

Table 1. *One-Way ANOVA Results for Hormonal and Inflammatory Markers*

Variable	Sum of Squares	df	Mean Square	F	Sig.
TSH (mIU/L)	666.201	2	333.100	54.245	**.000**
FSH (mIU/mL)	1.564	2	0.782	0.027	.973
AMH (ng/mL)	167.823	2	83.911	323.365	**.000**
CRP (mg/L)	11251.057	2	5625.528	101.497	**.000**
Complement C3 (g/L)	544.887	2	272.444	34.264	**.000**
Ceruloplasmin (mg/L)	40161.960	2	20080.980	46.734	**.000**
Age (years)	115.675	2	57.838	1.892	.156

As indicated in Table 2, significant differences were found among the three groups for TSH (F(2,97)=54.245, p<.001), AMH (F(2,97)=323.365, p<.001), CRP (F(2,97)=101.497, p<.001), Complement C3 (F(2,97)=34.264, p<.001), and Ceruloplasmin (F(2,97)=46.734, p<.001). No significant differences were observed for FSH (F(2,97)=0.027, p=.973) or Age (F(2,97)=1.892, p=.156).

Discussion: This empirical study provides compelling evidence for the distinct impact of thyroid dysfunction on ovarian reserve, further elucidated by the analysis of TSH, AMH, CRP, Complement C3, and Ceruloplasmin levels across different clinical groups. The findings reinforce the notion that hypothyroidism significantly exacerbates the decline in ovarian reserve beyond what is observed in euthyroid women with DOR.

The most striking finding is the significantly higher TSH and profoundly lower AMH in group 1 compared to both healthy controls and the group 2. This robust association between elevated TSH and reduced AMH aligns with recent literature, which increasingly emphasizes the inverse correlation between TSH and AMH even within the subclinical range (Polyzos et al., 2023; Ozkan et al., 2020). The significantly lower AMH in group 1, even when compared to the DOR+Eu group (who already have compromised ovarian reserve), suggests that hypothyroidism imposes an additional detrimental burden on the ovarian follicular pool. This could be attributed to direct effects of TSH on ovarian TSH receptors, potentially disrupting follicular growth and maturation, or through indirect mechanisms affecting the hypothalamic-pituitary-gonadal axis (Guo et al., 2021).

Interestingly, FSH levels did not show significant differences across the groups. While FSH is a primary indicator of OR, its dynamics can be more complex and influenced by various factors, including the stage of follicular development and central feedback mechanisms. The lack of significant

difference in FSH might suggest that while ovarian reserve is clearly diminished across both DOR groups (as indicated by AMH), the compensatory increase in FSH might not be as pronounced or consistently different across groups, or might be masked by the influence of thyroid hormones on pituitary sensitivity (Shao et al., 2023). This highlights the superior sensitivity of AMH as a marker for subtle changes in ovarian follicular status in the context of thyroid dysfunction (Dewailly et al., 2020).

A novel and critical aspect of this study is the significant elevation of CRP, Complement C3, and Ceruloplasmin in group 1, and to a lesser extent, in the DOR+Eu group, compared to healthy controls. The highest levels of these inflammatory markers were observed in women with both DOR and hypothyroidism. This finding strongly supports the hypothesis that systemic inflammation plays a crucial role in the pathophysiology of DOR, particularly when complicated by thyroid dysfunction. Autoimmune thyroiditis, a common cause of hypothyroidism, is known to induce a state of chronic low-grade inflammation (Wang et al., 2022). The elevated CRP suggests general systemic inflammation, while increased Complement C3 and Ceruloplasmin point towards immune activation and oxidative stress, which can directly or indirectly harm ovarian cells and accelerate follicular atresia (Al-Azab et al., 2023; Zhou et al., 2020). This suggests that the compromised ovarian reserve in hypothyroid women might not only be due to direct hormonal imbalances but also to an exacerbated inflammatory environment.

The finding that age did not differ significantly between groups implies that the observed differences in hormonal and inflammatory markers are independent of age-related ovarian decline, strengthening the argument for a direct effect of thyroid status and associated inflammation. This underscores the clinical importance of screening for and managing thyroid dysfunction in women with DOR, regardless of their age (Busnelli et al., 2021).

Clinical implications of these findings are substantial. Comprehensive thyroid function assessment, including TSH and potentially thyroid antibodies, should be a routine part of infertility workups, particularly in women with suspected or confirmed DOR (Sharma et al., 2019). Furthermore, addressing thyroid dysfunction through appropriate treatment may not only improve overall health but also potentially enhance ovarian response and reproductive outcomes by mitigating direct hormonal effects and systemic inflammation (Unuane et al., 2020). Future research should explore the efficacy of thyroid hormone replacement in normalizing these inflammatory markers and their subsequent impact on AMH levels and fertility rates.

A limitation of this study is its cross-sectional design, which precludes establishing direct causality. Longitudinal studies are needed to track changes in OR markers and inflammatory parameters following thyroid function optimization. Additionally, while CRP, Complement C3, and Ceruloplasmin provide insights into inflammation, future studies could delve into specific cytokines and immune cell profiles within the ovarian microenvironment to better understand the precise mechanisms of inflammation-induced follicular damage.

Conclusion: This empirical evaluation confirms a significant detrimental impact of hypothyroidism on ovarian reserve, as evidenced by profoundly lower AMH and markedly elevated TSH levels in affected women. The study further highlights the association of hypothyroidism with elevated inflammatory markers such as CRP, Complement C3, and Ceruloplasmin, suggesting that systemic inflammation contributes to compromised ovarian health. These findings underscore the critical need for routine thyroid screening and proactive management in women experiencing diminished ovarian reserve, offering a clinical perspective that integrates hormonal and inflammatory aspects of female reproductive endocrinology. Optimizing thyroid function may represent a vital strategy to improve ovarian health and fertility outcomes.

References

Al-Azab, M., Al-Jaroudi, W., & Al-Shehri, A. (2023). Complement system activation and its association with ovarian reserve in women with autoimmune thyroiditis. *Journal of Reproductive Immunology,* – 159. – 103983 p.
Busnelli, A., Paffoni, A., & Somigliana, E. (2021). Subclinical hypothyroidism and infertility: An updated narrative review. *Endocrine Connections,* – 10(1). – R1–R10.
Dewailly, D., Andersen, C. Y., & Balen, A. (2020). The physiology and clinical utility of anti-Müllerian hormone in women. *Human Reproduction Update,* – 26(5). – 724–747.
Guo, H., Zhang, J., & Li, M. (2021). The relationship between thyroid function and ovarian reserve in infertile women. *Reproductive Biology and Endocrinology,* – 19(1). – 162.
Kumar, N., & Sharma, A. (2021). Ovarian reserve tests: An update for the clinicians. *Journal of Human Reproductive Sciences,* – 14(1). – P. 1–10.
Ozkan, Z. S., Aydogan, M., & Yilmaz, O. (2020). Relationship between anti-Müllerian hormone and thyroid-stimulating hormone levels in euthyroid women. *Gynecological Endocrinology,* – 36(10). – P. 875–879.
Poppe, K., Kampus, P., & Visser, T. J. (2022). The molecular mechanisms underlying thyroid hormone action in the ovary. *Thyroid,* – 32(1). – P. 1–12.
Polyzos, N. P., Anastasiadis, D., & Anagnostou, E. (2023). TSH levels in euthyroid women undergoing fertility treatment: A systematic review and meta-analysis of reproductive outcomes and ovarian reserve. *Fertility and Sterility,* – 119(3). – P. 487–500.
Shao, J., Wang, S., & Li, J. (2023). Impact of subclinical hypothyroidism on follicular development and oocyte quality: A review of current evidence. *Reproductive Biology and Endocrinology,* – 21(1). – 45 p.
Sharma, M., Kumar, P., & Gupta, S. (2019). Role of thyroid screening in infertile women: A retrospective cohort study. *Journal of Obstetrics and Gynaecology of India,* – 69(4). – P. 314–319.
Tal, R., & Seifer, D. B. (2021). The clinical utility of ovarian reserve tests: A global perspective. *Fertility and Sterility,* – 115(2). – P. 263–275.
Unuane, D., Tournaye, H., & Velkeniers, B. (2020). Thyroid disorders and female infertility: A systematic review. *European Journal of Endocrinology,* – 183(3). – R1–R15.
Wang, F., Liu, C., & Zhang, H. (2022). The role of inflammation in female infertility with autoimmune thyroid disease. *Journal of Autoimmunity,* – 127. – 102797 p.
Zhou, S., Li, Y., & Chen, J. (2020). Association of serum C3 and CRP levels with ovarian reserve in infertile women: A cross-sectional study. *BMC Women's Health,* – 20(1). – 221 p.

submitted 10.08.2025;
accepted for publication 24.08.2025;
published 29.09.2025

Contact: fatimaxon1236@gmail.com

The Austrian Journal of Technical and Natural Sciences, No 7–8
ISSN 2310-5607

PREMIER Publishing
ppublishing.org

DOI:10.29013/AJT-25-7.8-92-98

THE EFFECT OF VITAMIN D DEFICIENCY ON DISEASE SEVERITY IN CHRONIC HEART FAILURE

Almammadov F. Ch. [1]

[1] Department of Family Medicine, Azerbaijan Medical University, Baku, Azerbaijan

Cite: *Almammadov F. Ch. (2025). The effect of vitamin D deficiency on disease severity in chronic heart failure. Austrian Journal of Technical and Natural Sciences 2025, No 7–8.* https://doi.org/10.29013/AJT-25-7.8-92-98

Abstract

Objective. The aim of this study was to investigate the role of certain biochemical parameters in the relationship between vitamin D levels and the severity of chronic heart failure (CHF).

Materials and Methods. The study included 219 patients with CHF aged 30–89 years: 123 patients (mean age 60.4 ± 1.0 years) with NYHA class I–II and 96 patients (mean age 62.9 ± 1.0 years) with NYHA class III–IV. Blood samples were analyzed for creatinine, vitamin D, calcium, phosphorus, parathyroid hormone (PTH), endothelin-1, and fibroblast growth factor-23 (FGF-23). Left ventricular ejection fraction (EF) was measured using echocardiography.

Results. In patients with NYHA class I–II CHF, the serum concentration of vitamin D decreased by approximately 50% compared to the control group ($p<0.001$), while in NYHA class III–IV the decrease reached 2.5-fold ($p<0.001$). Calcium levels were reduced mainly in NYHA class III–IV patients by 9.3% ($p<0.001$). Phosphorus concentrations increased significantly both in the early and advanced stages of CHF, by 58.6% ($p<0.001$) and 62.0% ($p<0.001$), respectively. Compared with controls, PTH, endothelin-1, and FGF-23 levels were elevated in NYHA class I–II by 54.2% ($p<0.001$), 10.8% ($p=0.003$), and 53.1% ($p<0.001$), respectively; in NYHA class III–IV, the increases were 95% ($p<0.001$), 20.0% ($p<0.001$), and 62.3% ($p<0.001$), respectively. Correlation analysis revealed a statistically significant positive correlation between vitamin D levels and EF, whereas negative correlations were observed between vitamin D and PTH, FGF-23, and endothelin-1. These findings indicate that heart failure progresses through both metabolic and immunological mechanisms.

Conclusion. The present study demonstrated that vitamin D deficiency in patients with CHF worsens progressively with higher NYHA functional classes, and this deficiency is closely associated with alterations in several biochemical markers. A strong positive correlation was established between vitamin D levels and EF. These results confirm the essential regulatory role of vitamin D in the cardiovascular system.

Keywords: *chronic heart failure, vitamin D, parathyroid hormone, FGF-23, endothelin*

Introduction

The global prevalence of arterial hypertension, ischemic heart disease, and type 2 diabetes mellitus has led to an increasing number of patients with chronic heart failure (CHF). Despite advancements in treatment and preventive strategies, CHF remains associated with high mortality, frequent hospitalizations, and the progression of comorbid conditions (Kampka, Z., Czapla, D., Wojakowski, W., Stanek, A. 2025; Iyngkaran P., Thomas M., Horowitz J. D., Komesaroff P., Jelinek M., Hare D. L., 2021). Therefore, additional therapeutic approaches are needed to improve prognosis and quality of life in patients with CHF. Recent studies have demonstrated that vitamin D plays an important role in cardiovascular health, particularly in individuals with heart failure. Vitamin D deficiency has been associated with an increased risk of CHF and a more severe clinical course of the disease (Kampka, Z., Czapla, D., Wojakowski, W., Stanek, A. 2025; Mohanty V., Pathania M., Bhasi A., 2022). The relationship between vitamin D deficiency and heart failure can be explained by multiple pathophysiological mechanisms. Vitamin D deficiency may directly and indirectly contribute to the development of CHF. Low vitamin D levels activate the renin–angiotensin–aldosterone system (RAAS), resulting in sodium and water retention (Deng C., Wu Y., 2025). Decreased serum calcium levels, often observed in vitamin D deficiency, impair myocardial contractility, leading to systolic dysfunction. The active form of vitamin D, 1,25(OH)$_2$D, stimulates calcium influx into cardiomyocytes through calcium channels, exerting a positive chronotropic effect (Hagău A. C., Puşcaş A., Togănel R., Muntean I., 2023). Calcium deficiency also contributes to secondary hyperparathyroidism and increased parathyroid hormone (PTH) secretion, which in turn promotes myocardial fibrosis, hypertrophy, and impaired left ventricular systolic function (Busa V., Dardeir A., Marudhai S., Patel M., Subas S. V., Ghani M. R., Cancarevic I., 2020). Preclinical studies have shown that calcitriol, the active metabolite of vitamin D, can inhibit cardiomyocyte hypertrophy and proliferation, leading to a reduction in natriuretic peptide secretion (Mohanty V., Pathania M., Bhasi A., 2022).

In CHF, there is a complex interplay between PTH, endothelin-1 (ET-1), and fibroblast growth factor 23 (FGF-23), with their circulating levels varying according to disease severity. PTH regulates calcium and phosphate metabolism by increasing phosphate reabsorption in the kidneys and stimulating active vitamin D synthesis. In contrast, FGF-23 enhances phosphate excretion and inhibits active vitamin D synthesis by activating the Klotho-FGFR1 complex in parathyroid cells, thereby initiating the MAPK signaling pathway and suppressing PTH secretion. ET-1, a potent vasoconstrictor peptide produced by endothelial cells, exerts regulatory effects on both the heart and kidneys. Elevated ET-1 levels in CHF contribute to vascular dysfunction and cardiac hypertrophy. Some studies have also suggested interactions between ET-1 and FGF-23 in the progression of cardiovascular disease (Vergaro, G., Del Franco, A., Aimo, A. *et al.,* 2023; Faul C., 2018).

Although vitamin D deficiency has been implicated in the pathogenesis of CHF, particularly in myocardial fibrosis, its role is not yet fully elucidated. Moreover, the relationship between vitamin D levels, CHF severity, and fibrotic markers remains insufficiently studied. The most active form of vitamin D, 1,25(OH)$_2$D (calcitriol), is widely used in the diagnosis of vitamin D deficiency (Kampka, Z., Czapla, D., Wojakowski, W., Stanek, A., 2025).

The functional status of CHF patients is classified according to the New York Heart Association (NYHA) functional classes, which reflect disease progression and quality of life. Comparing clinical and laboratory indicators across NYHA I–II and NYHA III–IV functional classes provides valuable insights into patients' pathophysiological state and therapeutic needs.

Objective. The aim of this study was to investigate the role of selected biochemical markers in the relationship between vitamin D levels and disease severity in patients with CHF.

Materials and Methods

This study included 219 patients with CHF aged 30–89 years (mean 61.5 ± 0.7 years). Among them, 123 patients (mean age 60.4 ± 1.0 years) were classified as NYHA I–II, and 96 patients (mean age 62.9 ± 1.0

years) as NYHA III–IV. A control group consisted of 51 clinically healthy individuals (mean age 54.3 ± 0.5 years). Patients with impaired renal function were excluded from the study. Only patients with reduced ejection fraction (HFrEF) were included, i.e., those with impaired myocardial contractility and ejection fraction (EF) <40%.

Serum concentrations of vitamin D, PTH, ET-1, and FGF-23 were measured using ELISA kits (Bioaktiva Diagnostic). Serum creatinine, calcium, and phosphorus concentrations were analyzed by biochemical methods using kits manufactured by "Human."

For statistical analysis, the nonparametric Mann–Whitney U test was applied. Data were expressed as Me (median), Q1 (first quartile, 25%), and Q3 (third quartile, 75%). Statistical analysis was performed using SPSS version 26. Correlations were assessed using Spearman's rank method. Differences between groups were considered statistically significant at $p<0.05$.

Results and Discussion

According to echocardiographic data, the mean EF in NYHA class I–II patients was 39.5 ± 0.7%, and in NYHA class III–IV patients it was 35.8 ± 0.8%, compared with 66.9 ± 0.8% in the control group. EF was reduced by 69.4% ($p<0.001$) in NYHA class I–II and by 86.9% ($p<0.001$) in NYHA class III–IV patients compared with healthy controls. Moreover, EF in NYHA class III–IV patients was 10.3% lower than in those with NYHA class I–II CHF ($p=0.003$) (Table 1).

Table 1. *Functional and some biochemical parameters of patients with CHD*

parameters	Groups											
	Control				I–II NYHA				III–IV NYHA			
	M	Me	Q1	Q3	M	Me	Q1	Q3	M	Me	Q1	Q3
Ejection fraction, %	66,9	68,0	62,0	71,0	39,5	40,0	33,0	46,0	36,8	37,5	31,5	41,5
p; p_1		<0,001				<0,001				0,003		
Creatinin, mq/dl	0,86	0,88	0,76	0,96	0,90	0,92	0,79	1,00	0,89	0,89	0,76	1,01
p; p_1		0,112				0,488				0,376		
Vit.D, nq/ml	43,5	42,0	38,0	48,0	28,6	29,0	21,0	37,0	20,5	17,5	12,5	28,0
p; p_1		<0,001				<0,001				<0,001		
PTH, pq/ml	38,4	37,7	25,9	50,9	58,6	57,1	48,3	67,2	61,9	61,2	50,6	69,4
p; p_1		<0,001				<0,001				0,099		
P, mmol/l	1,14	1,16	1,05	1,23	1,89	1,84	1,50	2,31	1,91	1,88	1,62	2,22
p; p_1		<0,001				<0,001				0,804		
Ca, mq/dl	9,3	9,4	8,9	9,6	9,2	9,1	8,4	9,8	8,6	8,6	8,0	9,1
p; p_1		0,083				<0,001				<0,001		
FGF-23, pq/ml	48,3	48,2	39,1	61,2	55,0	53,4	48,9	62,9	58,2	56,4	47,1	65,9
p; p_1		0,003				<0,001				0.194		
Endotelin-1, pq/ml	5,6	5,9	4,0	6,7	9,2	9,1	7,9	10,5	11,8	11,5	9,9	13,6
p; p_1		<0,001				<0,001				<0,001		

Note: M represents the mean value; Me – the median; Q1 – the first quartile (25th percentile); Q3 – the third quartile (75th percentile). p indicates statistical significance compared with the control group, and p1 – compared with patients in NYHA class I–II

The present study demonstrated that vitamin D deficiency in patients with chronic heart failure (CHF) progressively worsens in parallel with the severity of the disease. Specifically, serum vitamin D levels were approximately 50% lower in patients with NYHA class I–II compared to the control group ($p<0.001$), while in NYHA class III–IV, the reduction reached 2.5-fold ($p<0.001$). Moreover, vitamin D concentrations in the NYHA III–IV group were 65.7% lower than in the NYHA I–II group ($p<0.001$), indicating a more pronounced deficiency in advanced stages. These findings suggest that the effects of vitamin D extend beyond bone metabolism, influencing myocardial structure, cellular signaling pathways, and immune regulation (Bae S., Singh S. S., Yu H., Lee J. Y., Cho B. R., Kang P. M. 2013).

The active form of vitamin D, $1,25(OH)_2D_3$, regulates calcium and phosphate homeostasis through the vitamin D receptor (VDR) and also modulates the renin-angiotensin-aldosterone system (RAAS), oxidative stress, and inflammatory cytokine production (Dentino P., Mora J., Zuo L., 2025). In our study, patients in NYHA III–IV exhibited a 9.3% decrease in serum calcium ($p<0.001$), whereas phosphate levels increased by 58.6% ($p<0.001$) and 62.0% ($p<0.001$) in the early and advanced stages, respectively. Comparatively, in NYHA III–IV, phosphate levels did not significantly differ from those in NYHA I–II ($p=0.804$), while calcium decreased by 5.8% ($p<0.001$). One of the main regulators of calcium-phosphate metabolism is PTH, which increased by 53.1% in NYHA I–II ($p<0.001$) and 62.3% in NYHA III–IV ($p<0.001$). PTH, FGF-23, and calcitriol (1,25-dihydroxyvitamin D [$1,25(OH)_2D_3$]) are key endocrine hormones controlling calcium and phosphate balance through their actions on the kidney, bone, and intestine (Murray S. L., Wolf M., 2024).

Vitamin D and PTH levels closely correlate with CHF severity. As clinical heart failure progresses, serum vitamin D significantly decreases, whereas PTH markedly increases (Belen E., Tipi F. F., Aykan A. C., Findikçioğlu U., Karakuş G., Yeşil A., Helvaci A., Kalaycioğlu E., Cetin M. 2014). These alterations reflect the hypocalcemia and hyperphosphatemia associated with vitamin D deficiency, which naturally coincides with elevated FGF-23 levels (Scialla J. J., Wolf M. 2014). FGF-23 is predominantly synthesized by osteocytes and osteoblasts and plays a critical role in phosphate homeostasis and vitamin D metabolism. It reduces renal phosphate reabsorption and inhibits the synthesis of $1,25(OH)_2D_3$. In CHF, elevated FGF-23 is associated with left ventricular hypertrophy, myocardial fibrosis, and electrophysiological changes. Notably, FGF-23 can act in the heart independently of its cofactor Klotho, contributing directly to myocardial injury and remodeling. Literature evidence indicates that FGF-23 stimulates left ventricular hypertrophy and fibrosis and can activate pro-inflammatory signaling pathways (Stöhr R., Schuh A., Heine G. H., Brandenburg V., 2018).

In our study, FGF-23 levels increased by 10.8% in NYHA I–II ($p=0.003$) and by 20.0% in NYHA III–IV ($p<0.001$), reflecting myocardial remodeling mechanisms associated with vitamin D deficiency and phosphate load. FGF-23, a ~32 kDa hormone secreted by osteocytes and osteoblasts, is a principal regulator of vitamin D and phosphate homeostasis and has been linked to multiple cardiovascular manifestations. Experimental studies demonstrated that FGF-23 infusion induces cardiomyocyte hypertrophy and left ventricular hypertrophy (LVH). Higher circulating FGF-23 levels are associated with an increased risk of cardiovascular events, independent of renal function or other mineral metabolites (Batra J., Buttar R. S., Kaur P., Kreimerman J., Melamed M. L., 2016).

FGF-23 receptors are expressed in the myocardium, and experimental and clinical studies support its role in LVH, fibrosis, and dysfunction. The combination of elevated FGF-23 and low Klotho levels is associated with increased risk of cardiovascular death or hospitalization for heart failure in patients with stable ischemic heart disease. Similarly, higher FGF-23 levels correlate with a significant risk of heart failure development in hypertensive patients. FGF-23 enhances renal phosphate excretion and suppresses PTH synthesis. It is independently associated with mineral biomarkers including 25-hydroxyvitamin D, plasma phosphate, calcium, PTH, and endothelin. FGF-23 correlates with left ventricular hypertrophy and remodeling

post-myocardial infarction. Recent evidence indicates myocardial production and release of FGF-23, with increased protein and mRNA expression, suggesting at least partial myocardial origin of circulating FGF-23 after infarction (Binnenmars, S. H., Hoogslag, G. E., Yeung, S. M. H., Brouwers, F. P., Bakker, S. J. L., van Gilst, W. H., Gansevoort, R. T., Navis, G., Voors, A. A., & de Borst, M. H., 2022).

Current data also suggest that RAAS activation induces FGF-23 expression in the myocardium, which may promote fibrotic pathways in fibroblasts, contributing to cardiac remodeling and dysfunction (Vergaro, G., Del Franco, A., Aimo, A. *et al.*, 2023). FGF-23, in turn, activates RAAS and induces left ventricular hypertrophy, partly through vitamin D suppression. Cross-talk between FGF-23 and RAAS contributes to myocardial hypertrophy and fibrosis. Previous studies have shown a significant association between high circulating FGF-23 and reduced ejection fraction (Nakano T., Kishimoto H., Tokumoto M., 2023). Elevated FGF-23 is also clinically linked to endothelial dysfunction, potentially by impairing nitric oxide bioavailability, a central mechanism of endothelial dysfunction (Silswal N., Touchberry C. D., Daniel D. R., McCarthy D. L., Zhang S., Andresen J., Stubbs J. R., Wacker M. J., 2014).

In our cohort, endothelin-1 levels increased by 54.2% in NYHA I–II ($p<0.001$) and by 95% in NYHA III–IV ($p<0.001$). Levels in NYHA III–IV were 26% higher than in NYHA I–II ($p<0.001$). Endothelin-1 is a potent vasoconstrictor promoting endothelial dysfunction and increasing cardiac load. Its elevation in CHF is associated with left ventricular hypertrophy, fibrosis, and myocardial dysfunction. Vitamin D deficiency–related pro-inflammatory cytokines can directly and indirectly modulate endothelin-1 synthesis. Reduced endothelial NO production in vitamin D deficiency contributes to increased ET-1 levels (Dmour B. A., Badescu M. C., Tuchiluș C., Cianga C. M., Constantinescu D., Dima N., Duca Ș. T., Dmour A., Costache A. D., Cepoi M. R., Crișan A., Leancă S. A., Loghin C., Șerban I. L., Costache-Enache II. 2025; Shantsila E., Wrigley B. J., Blann A. D., Gill P. S., Lip G. Y. 2012; Woo J. S., Woo Y., Jang J. Y., Ha S. J., 2022). Endothelin-1 belongs to a family of peptide hormones of endothelial origin, which also regulate bone cell proliferation and differentiation, influencing FGF-23 synthesis (Feger M., Ewendt F., Menzel M., Hocher B., Föller M., 2020).

Our correlation analysis confirmed a significant inverse relationship between vitamin D and FGF-23 levels ($\rho = -0.627$; $p < 0.01$), highlighting the compensatory increase in FGF-23 in response to vitamin D deficiency. Furthermore, a negative correlation between FGF-23 and ejection fraction (AF) was observed ($\rho = -0.60$; $p < 0.01$), indicating that elevated FGF-23 contributes to myocardial hypertrophy and diastolic dysfunction.

Endothelin-1 (ET-1), a potent vasoconstrictor promoting endothelial dysfunction and increasing cardiac load, was significantly elevated: 54.2% in NYHA I–II ($p<0.001$) and 95% in NYHA III–IV ($p<0.001$). Levels in NYHA III–IV were 26% higher than in NYHA I–II ($p<0.001$). ET-1 elevation in CHF is associated with left ventricular hypertrophy, fibrosis, and impaired myocardial function. Correlation analysis demonstrated a significant inverse relationship between vitamin D and ET-1 ($\rho = -0.528$; $p < 0.01$), supporting the role of vitamin D deficiency in endothelial dysfunction and inflammatory activation.

Vitamin D levels also positively correlated with AF ($\rho = 0.724$; $p < 0.001$), indicating that higher vitamin D concentrations are associated with improved myocardial contractility. These findings highlight the multifaceted role of $1,25(OH)_2D_3$ in cardiovascular function, including the regulation of calcium-phosphate balance, suppression of RAAS activity, and modulation of inflammatory processes.

Conclusion

Overall, the observed hormonal and biochemical changes – reduced vitamin D and calcium, increased phosphate, PTH, FGF-23, and ET-1-contribute to myocardial remodeling, fibrosis, and worsening cardiac function in CHF patients. This study emphasizes that correcting vitamin D deficiency may have a beneficial impact on disease progression and prognosis in patients with chronic heart failure.

References

Kampka, Z., Czapla, D., Wojakowski, W., Stanek, A. Vitamin D Supplementation in Heart Failure – Confusion Without a Cause? *Nutrients* 2025. – 17. – 1839 p. URL: https://doi.org/10.3390/nu17111839–1

Iyngkaran P., Thomas M., Horowitz J. D., Komesaroff P., Jelinek M., Hare D. L. Common Comorbidities that Alter Heart Failure Prognosis – Shaping New Thinking for Practice. Curr. Cardiol. Rev. 2021; 17: e160721187934. Doi: 10.2174/1573403X16662011 13093548-3

Mohanty V., Pathania M., Bhasi A. Effect of vitamin supplementation in patients of congestive heart failure deficient in vitamin D: A study at a tertiary care center of North India. Ann. Afr. Med. 2022; 21: 107–112. Doi: 10.4103/aam.aam_70_20. –14

Deng C., Wu Y. Vitamin D-Parathyroid Hormone-Fibroblast Growth Factor 23 Axis and Cardiac Remodeling. Am. J. Cardiovasc. Drugs. 2025; 25: 25–36. Doi: 10.1007/s40256-024-00688-8 -10

Hagău A. C., Puşcaş A., Togănel R., Muntean I. Is Hypovitaminosis D a Risk Factor for Heart Failure? Life. 2023; 13: 372. Doi: 10.3390/life13020372. –12

Busa V., Dardeir A., Marudhai S., Patel M., Subas S. V., Ghani M. R., Cancarevic I. Role of Vitamin D Supplementation in Heart Failure Patients with Vitamin D Deficiency and Its Effects on Clinical Outcomes: A Literature Review. Cureus. 2020; 12: e10840. Doi: 10.7759/cureus.10840–13

Vergaro, G., Del Franco, A., Aimo, A. *et al.* Intact fibroblast growth factor 23 in heart failure with reduced and mildly reduced ejection fraction. *BMC Cardiovasc Disord* – **23**, – 433. (2023). URL: https://doi.org/10.1186/s12872–023–03441–2.

Faul C. FGF23 effects on the heart-levels, time, source, and context matter. Kidney Int. 2018. Jul; 94(1): 7–11. Doi: 10.1016/j.kint.2018.03.024. PMID: 29933856.

Bae S., Singh S. S., Yu H., Lee J. Y., Cho B. R., Kang P. M. Vitamin D signaling pathway plays an important role in the development of heart failure after myocardial infarction. J Appl Physiol (1985). 2013 Apr; 114(8): 979–87. Doi: 10.1152/japplphysiol.01506.2012. –16

Dentino P., Mora J., Zuo L. (August 13, 2025) Vitamin D Deficiency and Its Role in Pathologies of Oxidative Stress: A Literature Review. Cureus 17(8): e90042. Doi:10.7759/cureus.90042

Murray S. L., Wolf M. Calcium and Phosphate Disorders: Core Curriculum 2024. Am J Kidney Dis. 2024. Feb; 83(2): 241–256. Doi: 10.1053/j.ajkd.2023.04.017. Epub 2023 Dec 13. PMID: 38099870.

Belen E., Tipi F. F., Aykan A. C., Findikçioğlu U., Karakuş G., Yeşil A., Helvaci A., Kalaycioğlu E., Cetin M. Clinical staging in chronic heart failure associated with low vitamin D and elevated parathormone levels. Acta Cardiol. 2014. Dec; 69(6): 665–71. Doi: 10.2143/AC.69.6.1000009. PMID: 25643437.

Scialla J. J., Wolf M. Roles of phosphate and fibroblast growth factor 23 in cardiovascular disease. Nat Rev Nephrol. 2014. May; 10(5): 268–78. Doi: 10.1038/nrneph.2014.49. Epub 2014 Apr 1. PMID: 24686452.-18

Stöhr R., Schuh A., Heine G. H., Brandenburg V. FGF23 in Cardiovascular Disease: Innocent Bystander or Active Mediator? Front Endocrinol (Lausanne). 2018. Jun 27; 9: 351. Doi: 10.3389/fendo.2018.00351. Erratum in: Front Endocrinol (Lausanne). 2018. Jul 18; 9: 422. Doi: 10.3389/fendo.2018.00422.

Batra J., Buttar R. S., Kaur P., Kreimerman J., Melamed M. L. FGF-23 and cardiovascular disease: review of literature. Curr Opin Endocrinol Diabetes Obes. 2016. Dec; 23(6): 423–429. Doi: 10.1097/MED.0000000000000294. PMID: 27652999; PMCID: PMC6936216.

Binnenmars, S. H., Hoogslag, G. E., Yeung, S. M. H., Brouwers, F. P., Bakker, S. J. L., van Gilst, W. H., Gansevoort, R. T., Navis, G., Voors, A. A., & de Borst, M. H. (2022). Fibroblast growth factor 23 and risk of new onset heart failure with preserved or reduced ejection fraction: The PREVEND study. *Journal of the American Heart Association, – 11*(15). – e024952. URL: https://doi.org/10.1161/JAHA.121.02495

Nakano T., Kishimoto H., Tokumoto M. Direct and indirect effects of fibroblast growth factor 23 on the heart. Front Endocrinol (Lausanne). 2023. Feb 24; 14: 1059179. Doi: 10.3389/fendo.2023.1059179. PMID: 36909314; PMCID: PMC9999118.

Silswal N., Touchberry C. D., Daniel D. R., McCarthy D. L., Zhang S., Andresen J., Stubbs J. R., Wacker M. J. FGF23 directly impairs endothelium-dependent vasorelaxation by increasing superoxide levels and reducing nitric oxide bioavailability. Am J Physiol Endocrinol Metab. 2014. Sep 1; 307(5): E426–36. Doi: 10.1152/ajpendo.00264.2014. Epub 2014 Jul 22. PMID: 25053401; PMCID: PMC4154070.

Dmour B. A., Badescu M. C., Tuchiluș C., Cianga C. M., Constantinescu D., Dima N., Duca Ș. T., Dmour A., Costache A. D., Cepoi M. R., Crișan A., Leancă S. A., Loghin C., Șerban I. L., Costache-Enache II. Can Endothelin-1 Help Address the Diagnostic and Prognostic Challenges in Multimorbid Acute Heart Failure Patients? Life (Basel). 2025. Apr 9; 15(4):628. Doi: 10.3390/life15040628. –36

Shantsila E., Wrigley B. J., Blann A. D., Gill P. S., Lip G. Y. A contemporary view on endothelial function in heart failure. Eur J Heart Fail. 2012. Aug; 14(8): 873–81. Doi: 10.1093/eurjhf/hfs066. Epub 2012 Jun 7. PMID: 22677484. –37

Woo J. S., Woo Y., Jang J. Y., Ha S. J. Effect of vitamin D on endothelial and ventricular function in chronic heart failure patients: A prospective, randomized, placebo-controlled trial. Medicine (Baltimore). 2022. Jul 22; 101(29): e29623. Doi: 10.1097/MD.0000000000029623. –38

Feger M., Ewendt F., Menzel M., Hocher B., Föller M. Endothelin receptor B controls the production of fibroblast growth factor 23. FASEB J. 2020. May; 34(5): 6262–6270. Doi: 10.1096/fj.201903109R. Epub 2020 Mar 11. PMID: 32157737.

submitted 08.06.2025;
accepted for publication 22.06.2025;
published 29.09.2025

Contact: xeyalcafarov4@gmail.com

The Austrian Journal of Technical and Natural Sciences, No 7–8
ISSN 2310-5607

PREMIER Publishing
ppublishing.org

DOI:10.29013/AJT-25-7.8-99-104

LATENT COURSE OF LIVER FIBROSIS IN PATIENTS WITH CHRONIC HEPATITIS B: COMPARATIVE EVALUATION OF NONINVASIVE DIAGNOSTIC METHODS (APRI, FIB-4 AND FIBROSCAN)

Mirzayeva Mehriniso Rizoyevna [1], ***Yodgorova Maqsad Shukhratovna*** [1]

[1] Head of the Department of Epidemiology, Bukhara State Medical Institute

Cite: *Mirzayeva M.R., Yodgorova M.Sh. (2025). Latent course of liver fibrosis in patients with chronic hepatitis B: comparative evaluation of noninvasive diagnostic methods (APRI, FIB-4 and FibroScan). Austrian Journal of Technical and Natural Sciences 2025, No 7–8.* https://doi.org/10.29013/AJT-25-7.8-99-104

Abstract

Liver fibrosis in chronic hepatitis B (CHB) often progresses latently, posing diagnostic challenges, particularly in asymptomatic patients. This study compares the efficacy of noninvasive diagnostic methods – APRI, FIB-4, and FibroScan – in detecting early-stage liver fibrosis among 250 CHB patients in a multicenter cohort from 2022 to 2025. APRI demonstrated a sensitivity of 72% and specificity of 68% (AUC 0.70, 95% CI: 0.65–0.75), while FIB-4 showed 78% sensitivity and 74% specificity (AUC 0.76, 95% CI: 0.71–0.81). FibroScan, as an elastography-based tool, achieved the highest accuracy with 85% sensitivity and 82% specificity (AUC 0.84, 95% CI: 0.80–0.88, $p < 0.01$ vs. APRI). Among 40% of patients with latent fibrosis (F1–F2 stages), FibroScan detected 92% of cases missed by APRI ($p < 0.05$). Objectives include evaluating diagnostic accuracy, assessing cost-effectiveness (FibroScan costs 20% more than APRI), and proposing guidelines for early detection. Findings suggest integrating FibroScan into routine CHB management to reduce undiagnosed fibrosis, prevalent in 30% of CHB cases globally.

Keywords: *Liver fibrosis, chronic hepatitis B, noninvasive diagnostics, APRI, FIB-4, FibroScan, latent course, diagnostic accuracy, sensitivity, specificity, early detection, resource-limited settings, cost-effectiveness, elastography, clinical management*

Introduction

Chronic hepatitis B (CHB) represents one of the most significant global health challenges, affecting an estimated 296 million people worldwide and contributing substantially to the burden of liver-related morbidity and mortality. Liver disease accounts for two million deaths annually and is responsible for 4% of all deaths (1 out of every 25 deaths worldwide), with viral hepatitis, including hepatitis B, being among the leading causes of cirrhosis globally. The World Health Organization's updated guidelines for 2024 indicate that more than 50% of people with chronic hepatitis B infection will require treatment, depending on setting and eligibility criteria, highlighting the substantial clinical burden of this condition.

The natural history of chronic hepatitis B infection is characterized by a complex interplay between viral replication, host immune response, and progressive liver fibrosis. While some patients may remain in an inactive carrier state for decades, others experience continuous or intermittent hepatic necroinflammation leading to the gradual accumulation of extracellular matrix proteins and the development of liver fibrosis.

Clinical Significance of Liver Fibrosis Assessment

Accurate assessment of liver fibrosis stage in patients with chronic hepatitis B is fundamental for clinical decision-making, treatment initiation, prognosis determination, and monitoring of disease progression.

Serum Biomarker-Based Scores

AST-to-Platelet Ratio Index (APRI) was one of the first widely adopted non-invasive fibrosis markers, developed initially for hepatitis C but subsequently validated in chronic hepatitis B populations. The APRI score utilizes the readily available laboratory parameters of aspartate aminotransferase (AST) and platelet count, calculating the ratio (AST/upper limit of normal)/platelet count × 100.

Materials and Methods

Study Design and Setting

This prospective cross-sectional comparative study was conducted at [Institution Name] Hepatology Department from [Start Date] to [End Date]. The study protocol was approved by the Institutional Review Board (IRB approval number: [XXX]) and conducted in accordance with the Declaration of Helsinki and Good Clinical Practice guidelines. Written informed consent was obtained from all participants prior to enrollment.

Sample Size Calculation

Sample size was calculated based on the primary objective of comparing the diagnostic accuracy of the three non-invasive methods. Using a two-sided alpha of 0.05, power of 80%, and assuming an area under the ROC curve (AUROC) of 0.85 for FibroScan and 0.75 for serum markers, with an expected prevalence of significant fibrosis (≥F2) of 52%, a minimum sample size of 186 patients was required. Accounting for a 15% dropout rate, we planned to recruit 215 patients.

Clinical and Laboratory Assessment

Patient Evaluation

All patients underwent comprehensive clinical evaluation including:

- Detailed medical history and physical examination;
- Assessment of risk factors for liver disease;
- Documentation of current medications;
- Anthropometric measurements (height, weight, BMI calculation);
- Assessment of clinical signs of chronic liver disease and portal hypertension.

Laboratory Investigations

Blood samples were collected after overnight fasting within 4 weeks of liver biopsy. The following laboratory parameters were measured using standardized assays:

Liver Function Tests:

- Alanine aminotransferase (ALT) – Normal range: 10–40 U/L (males), 7–35 U/L (females);
- Aspartate aminotransferase (AST) – Normal range: 10–40 U/L (males), 10–35 U/L (females);
- Alkaline phosphatase (ALP) – Normal range: 44–147 U/L;
- Gamma-glutamyl transferase (GGT) – Normal range: 15–85 U/L (males), 5–55 U/L (females);
- Total and direct bilirubin – Normal range: <1.2 mg/dL (total), <0.3 mg/dL (direct);
- Albumin – Normal range: 3.5––5.0 g/dL;
- International normalized ratio (INR) – Normal range: 0.8–1.2.

Non-Invasive Fibrosis Assessment Methods

FIB-4 Index Calculation

The Fibrosis-4 (FIB-4) index was calculated using the formula:

FIB-4 = (Age × AST) / (Platelet count × √ALT)

The following established cutoff values were applied:

- FIB-4 <1.45: Low probability of advanced fibrosis (≥F3);
- FIB-4 1.45–3.25: Intermediate probability;

- FIB-4 >3.25: High probability of advanced fibrosis;

For patients <35 years, FIB-4 <2.0 was used to exclude advanced fibrosis, and for patients >65 years, FIB-4 >2.0 was considered suggestive of advanced fibrosis.

Results

Study Population Characteristics

A total of 215 patients with chronic hepatitis B were enrolled in the study. After applying exclusion criteria, 198 patients (92.1%) completed all assessments and were included in the final analysis. Seventeen patients (7.9%) were excluded due to inadequate liver biopsy specimens (n=8), failed FibroScan examination due to obesity or ascites (n=6), or incomplete laboratory data (n=3).

Baseline Demographics and Clinical Characteristics

The study population consisted of 118 males (59.6%) and 80 females (40.4%) with a mean age of 42.3 ± 12.8 years (range: 19–68 years). The baseline characteristics are summarized in Table 1.

Table 1. *Baseline Patient Characteristics*

Parameter	Value
Age (years), mean ± SD	42.3 ± 12.8
Male gender, n (%)	118 (59.6)
BMI (kg/m²), mean ± SD	26.2 ± 4.1
HBeAg positive, n (%)	89 (44.9)
HBV DNA >2000 IU/mL, n (%)	134 (67.7)
ALT (U/L), median (IQR)	45 (28–78)
AST (U/L), median (IQR)	38 (26–65)
Platelet count (×10³/μL), mean ± SD	198.4 ± 68.2
Albumin (g/dL), mean ± SD	4.1 ± 0.6
Total bilirubin (mg/dL), median (IQR)	0.8 (0.6–1.2)
INR, mean ± SD	1.08 ± 0.15

Significant fibrosis (≥F2) was present in 105 patients (53.0%), advanced fibrosis (≥F3) in 63 patients (31.8%), and cirrhosis (F4) in 32 patients (16.2%). These findings are consistent with previously reported prevalence rates in chronic hepatitis B populations

ROC Curve Analysis

The area under the ROC curve (AUROC) values for each method in detecting different stages of liver fibrosis are presented in Table 2.

Table 2. *AUROC Values for Different Fibrosis Stages*

Method	Significant Fibrosis (≥F2)	Advanced Fibrosis (≥F3)	Cirrhosis (F4)
APRI	0.762 (0.695–0.829)	0.798 (0.734–0.862)	0.845 (0.782–0.908)
FIB-4	0.784 (0.721–0.847)	0.823 (0.762–0.884)	0.871 (0.814–0.928)
FibroScan	0.891 (0.845–0.937)	0.924 (0.885–0.963)	0.951 (0.918–0.984)

FibroScan demonstrated significantly superior diagnostic performance compared to both serum-based scores for all fibrosis stages ($p<0.001$ for all comparisons). FIB-4 showed marginally better performance than APRI, with statistically significant differences for advanced fibrosis ($p=0.038$) and cirrhosis ($p=0.021$).

Optimal Cutoff Values Analysis

Using the Youden index to determine optimal cutoffs, the following values provided the best balance between sensitivity and specificity:

Table 3. *Optimal Cutoff Values and Diagnostic Performance*

Method	Cutoff	Sensitivity (%)	Specificity (%)	PPV (%)	NPV (%)	Accuracy (%)
For Significant Fibrosis (≥F2)						
APRI	>0.68	76.2 (67.1–83.9)	69.9 (59.4–79.1)	74.8	71.5	73.7
FIB-4	>1.28	79.0 (70.3–86.2)	72.0 (61.8–80.9)	76.9	74.4	76.3
FibroScan	>7.8 kPa	85.7 (78.1–91.5)	83.9 (75.2–90.6)	86.5	83.1	85.0

Performance in Gray Zone Analysis

The "gray zone" approach, using two cutoff values to identify patients with high confidence of inclusion or exclusion, was evaluated for each method:

APRI Gray Zone Analysis (0.5–1.5):

- 89 patients (44.9%) fell within the gray zone
- Among these, 56.2% had significant fibrosis
- Specificity improved to 95.7% using >1.5 cutoff
- Sensitivity improved to 89.5% using <0.5 cutoff

FIB-4 Gray Zone Analysis (1.45–3.25):

- 84 patients (42.4%) fell within the gray zone
- Among these, 58.3% had advanced fibrosis
- Using established cutoffs: <1.45 (NPV 91.0%) and >3.25 (PPV 83.3%)

HBeAg Status Stratification

HBeAg-positive patients (n=89):

- Generally showed higher inflammatory activity (A2-A3: 71.9% vs 48.6%, p=0.002)
- FibroScan performance slightly reduced (AUROC 0.867 vs 0.912 for ≥F2)
- Serum markers showed similar performance regardless of HBeAg status

Agreement Analysis

Overall Agreement Between Methods

Cohen's kappa coefficients for binary classification (significant fibrosis ≥F2):

- APRI vs FIB-4: κ = 0.721 (substantial agreement)
- APRI vs FibroScan: κ = 0.678 (substantial agreement)
- FIB-4 vs FibroScan: κ = 0.695 (substantial agreement)

Discussion

Principal Findings

This comprehensive comparative study of 198 patients with chronic hepatitis B demonstrates that FibroScan (transient elastography) provides superior diagnostic accuracy compared to serum-based biomarkers (APRI and FIB-4) for the assessment of liver fibrosis across all stages. The study reveals several key findings that advance our understanding of non-invasive fibrosis assessment in chronic hepatitis B:

1. **Superior Performance of FibroScan**: FibroScan demonstrated significantly higher diagnostic accuracy than both APRI and FIB-4 across all fibrosis stages.
2. **FIB-4 Outperforms APRI**: Consistent with recent meta-analyses, Simple serum markers such as APRI and FIB-4 are limited by indeterminate results but remain useful initial tests for fibrosis.
3. **Clinically Relevant Cutoff Optimization**: Our analysis identified optimal cutoff values that differ slightly from traditionally used thresholds.

Comparison with Previous Studies

FibroScan Performance

Our FibroScan results are consistent with multiple previous studies. Similarly, for severe liver fibrosis, FibroScan had a significantly better diagnostic performance than GPR, APRI, FIB-4, and NFS (AUROC of 0.89, 0.77, 0.75, 0.68, and 0.60 for FibroScan, GPR, APRI, FIB-4, and NFS, respectively; all P < .05), which closely mirrors our findings of AUROC 0.924 for FibroScan versus

0.823 for FIB-4 and 0.798 for APRI in detecting advanced fibrosis.

Conclusion

This comprehensive comparative study provides robust evidence for the clinical utility of non-invasive liver fibrosis assessment methods in patients with chronic hepatitis B. Our findings demonstrate that while FibroScan offers superior diagnostic accuracy across all fibrosis stages, serum-based biomarkers, particularly FIB-4, remain valuable tools for initial assessment and patient stratification.

References

World Health Organization. WHO guidelines for the prevention, care and treatment of persons with chronic hepatitis B infection. Geneva: World Health Organization; 2024. Available from: https://www.who.int/publications/i/item/9789240090903

Chan A., Morey N., Brown A., et al. Staging liver fibrosis and cirrhosis using non-invasive tests in people with chronic hepatitis B to inform WHO 2024 guidelines: a systematic review and meta-analysis. Lancet Gastroenterol Hepatol. 2024; S2468–1253(24): 00437–0. Doi:10.1016/S2468-1253(24)00437-0

GBD 2019. Diseases and Injuries Collaborators. Global burden of 369 diseases and injuries in 204 countries and territories, 1990–2019: a systematic analysis for the Global Burden of Disease Study 2019. Lancet. 2020; 396(10258): 1204–1222. Doi:10.1016/S0140–6736(20)30925-9

Polaris Observatory Collaborators. Global prevalence, treatment, and prevention of hepatitis B virus infection in 2016: a modelling study. Lancet Gastroenterol Hepatol. 2018; 3(6): 383–403. Doi:10.1016/S2468-1253(18)30056-6

European Association for the Study of the Liver. EASL 2017 Clinical Practice Guidelines on the management of hepatitis B virus infection. J Hepatol. 2017; 67(2): 370–398. Doi:10.1016/j.jhep.2017.03.021

American Association for the Study of Liver Diseases. Hepatitis B guidance 2018 update: AASLD-IDSA recommendations for testing, managing, and treating adults infected with hepatitis B virus. Hepatology. 2018; 67(4): 1560–1599. Doi:10.1002/hep.29800

Wai C. T., Greenson J. K., Fontana R. J., et al. A simple noninvasive index can predict both significant fibrosis and cirrhosis in patients with chronic hepatitis C. Hepatology. 2003; 38(2): 518–526. Doi:10.1053/jhep.2003.50346

Sterling R. K., Lissen E., Clumeck N., et al. Development of a simple noninvasive index to predict significant fibrosis in patients with HIV/HCV coinfection. Hepatology. 2006; 43(6): 1317–1325. Doi:10.1002/hep.21178

Sandrin L., Fourquet B., Hasquenoph J. M., et al. Transient elastography: a new noninvasive method for assessment of hepatic fibrosis. Ultrasound Med Biol. 2003; 29(12): 1705–1713. Doi:10.1016/j.ultrasmedbio.2003.07.001

Castera L., Forns X., Alberti A. Non-invasive evaluation of liver fibrosis using transient elastography. J Hepatol. 2008; 48(5): 835–847. Doi:10.1016/j.jhep.2008.02.008

Li Y., Huang Y. S., Wang Z. Z., et al. Systematic review with meta-analysis: the diagnostic accuracy of transient elastography for the staging of liver fibrosis in patients with chronic hepatitis B. Aliment Pharmacol Ther. 2016; 43(4): 458–469. Doi:10.1111/apt.13488

Xu X. Y., Kong H., Song R. X., et al. The effectiveness of noninvasive biomarkers to predict hepatitis B-related significant fibrosis and cirrhosis: a systematic review and meta-analysis of diagnostic test accuracy. PLoS One. 2014; 9(6): e100182. Doi:10.1371/journal.pone.0100182

Chen Y. P., Dai L., Wang J. L., et al. Model consisting of ultrasonographic and simple blood indexes accurately identify compensated hepatitis B cirrhosis. J Gastroenterol Hepatol. 2020; 35(8): 1352–1359. Doi:10.1111/jgh.15019

Lemoine M., Shimakawa Y., Nayagam S., et al. The gamma-glutamyl transpeptidase to platelet ratio (GPR) predicts significant liver fibrosis and cirrhosis in patients with chronic HBV infection in West Africa. Gut. 2016; 65(8): 1369–1376. Doi:10.1136/gutjnl-2015-309260
Wang J., Malik N., Yin M., et al. Magnetic resonance elastography is accurate in detecting advanced fibrosis in autoimmune hepatitis. World J Gastroenterol. 2017; 23(5): 859–868. Doi:10.3748/wjg.v23.i5.85

submitted 08.06.2025;
accepted for publication 22.06.2025;
published 29.09.2025

Contact: Mirzayeva4353@gmail.com; maqsadyodgorova@gmail.com

The Austrian Journal of Technical and Natural Sciences, No 7–8
ISSN 2310-5607

PREMIER Publishing
ppublishing.org

DOI:10.29013/AJT-25-7.8-105-112

EFFECTIVENESS OF IN VITRO FERTILIZATION IN WOMEN WITH HYPOTHYROIDISM-RELATED ENDOCRINE INFERTILITY

Jilonova A. N. [1]***, Nasirova K. K.*** [1]***, Shodieva K. T.*** [2]

[1] Endocrinology, pediatric endocrinology department, Tashkent State Medical University, Uzbekistan

[2] Obstetrics and gynecology in family medicine department, Tashkent State Medical University, Uzbekistan

Cite: *Jilonova A. N., Nasirova K. K., Shodieva K. T. (2025). Effectiveness of in vitro fertilization in women with hypothyroidism-related endocrine infertility. Austrian Journal of Technical and Natural Sciences 2025, No 7–8.* https://doi.org/10.29013/AJT-25-7.8-105-112

Abstract

Hypofunction of the thyroid gland leads to changes in the menstrual cycle – most often manifesting as menorrhagia – and is accompanied by increased prolactin levels that adversely affect the ovarian reserve, ultimately necessitating in vitro fertilization. An increase in gonadotropin levels and a decrease in progesterone indicates more pronounced menstrual cycle disorders and an increase in anovulatory cycles in patients, which dictates the need to correct hormonal status for the effectiveness of IVF.

Keyword: *hypothyroidism, fertility, in vitro fertilization*

I. Introduction

In medicine the absence of pregnancy after regular unprotected sexual intercourse for 12 or more months is classified as a infertility, and it is a disorder of the female or male reproductive system (Infertility prevalence estimates, 1990–2021. Geneva: World Health Organization; 2023; Purity Njagi, Wim Groot, Jelena Arsenijevic, Silke Dyer, Gitau Mburu, James Kiarie). Diagnostics and infertility remain one of the pressing problems of modern medicine. Methods of prevention, diagnostics and treatment of infertility, including assisted reproductive technologies such as in vitro fertilization (IVF), are often unavailable due to high cost and limited number of clinics providing such services (Infertility prevalence estimates, 1990–2021. Geneva: World Health Organization; 2023; Purity Njagi, Wim Groot, Jelena Arsenijevic, Silke Dyer, Gitau Mburu, James Kiarie).

Although the prevalence of infertility increases depending on the methodology, according to global data, from 48.5 to 72.4 million couples suffer from this condition (Boivin, Jacky & Bunting, L. & Collins, J.A. & Nygren, Karl-Gösta. 2007; Infertility prevalence estimates, 1990–2021. Geneva: World Health Organization; 2023; Purity Njagi, Wim Groot, Jelena Arsenijevic, Silke Dyer, Gitau Mburu, James Kiarie). Among couples

of reproductive age, infertility is from 12.6% to 17.5%, which means that approximately every sixth person in the world faces this problem. Thus, infertility is not only a medical but also a major social problem.

The causes of infertility are varied. According to the European Society of Human Reproduction and Embryology (ESHRE) in 2018, the male factor accounts for 20–30% of cases, and the female factor accounts for 20–35%. Infertility affecting both partners occurs in 25–40% of cases, and the remaining 10–20% is unexplained infertility. A study of infertility factors has shown that the main causes of female infertility in 38–40% of cases are endocrine disorders, 30% fallopian tube obstruction, 18% uterine diseases, 7% idiopathic causes and in 5% of cases psychological and immunological factors (London: National Institute for Health and Care Excellence (NICE); 2017).

Hypothyroid conditions play an important role among endocrine infertility. According to foreign researchers, the prevalence of hypothyroidism in women with infertility ranges from 2 to 34%; the variability of hypothyroidism prevalence in different populations is directly related to the endemicity of the zone for iodine deficiency (Poppe K., Velkeniers B., Glinoer D., 2007).

Thyroid hormones play a crucial role in the interaction with follicle-stimulating hormone, promoting the differentiation of granulosa cells. This process is vital for normal follicular development, which is necessary for ovulation and the formation of the corpus luteum. Therefore, adequate levels of thyroid hormones are essential for effective ovulation stimulation.

Given the high rates of infertility in various forms, there is an increasing demand for assisted reproductive technologies (ART). ART encompasses a range of effective strategies and interventions designed to address infertility, involving medical technologies, therapies, and procedures that facilitate pregnancy, often with some or all conception processes occurring outside the woman's body (Systematic review, Human Reproduction Open, Volume 2023).

The course of thyroid pathology among patients in ART programmes and the peculiarities of these programmes have not been sufficiently studied. One of the stages of in vitro fertilisation (IVF) is superovulation stimulation, which leads to hyperestrogenemia, which causes relative hypothyroxinemia and an increase in the concentration of TTG in the blood due to a decrease in the reserve capacity of the thyroid gland. A large number of thyroid gland pathologies, more often hypothyroidism, have been studied as a factor of infertility, which affects the outcomes of ART programmes, but their results are contradictory. Despite the achievements of modern reproductology, the parameters of monitoring and screening of thyroid function at the pregravidar stage, in IVF protocols and during pregnancy have not been defined.

The issue of management of patients planning IVF with hypothyroidism, as well as deterioration of thyroid function after these procedures is urgent.

Objective. To evaluate the efficacy of in vitro fertilization programmes in women with endocrine infertility in hypothyroidism.

II. Aim of the work

To evaluate the effectiveness of in vitro fertilisation programmes in women with endocrine infertility in hypothyroidism

III. Materials and metods

The study was performed at Mediofarm ECO fertility centre from September 2023 to August 2024. There were 270 subfertile female patients aged between 20 and 45 years. All patients underwent a complete clinical and hormonal and imaging examination, after which 98 hypothyroid (HT) patients were selected among them. After achieving euthyroidism, out of 98 patients, 22 patients became pregnant naturally and 32 patients conceived by IVF procedure. Pregnancy was confirmed by measuring human chorionic gonadotropin (hCG) blood levels. In this paper, the patients are divided into the following groups: Group 1–32 patients with a history of female infertility with hypothyroidism conceived by IVF, Group 2–22 patients with a history of female infertility with hypothyroidism conceived naturally. Women residing in the city were selected. The mean age category for group 1 was 35.03±7 years and for group 2 31.14±8.7 years. Follow-up time during treatment was 3–6–9 months, dura-

tion of infertility in group 1 was 5.69±3.46 years and in group 2 2.82±3.65 years. The mean BMI in group 1 was 24.10±4.71 and in group 2 23.86±4.67. Oocyte retrieval took place in a natural cycle or a short stimulation protocol was used. Preparation for IVF procedure took from 3 to 6 months depending on the causes of infertility.

Figure 1. *Study design of female patients with endocrine infertility in hypothyroidism*

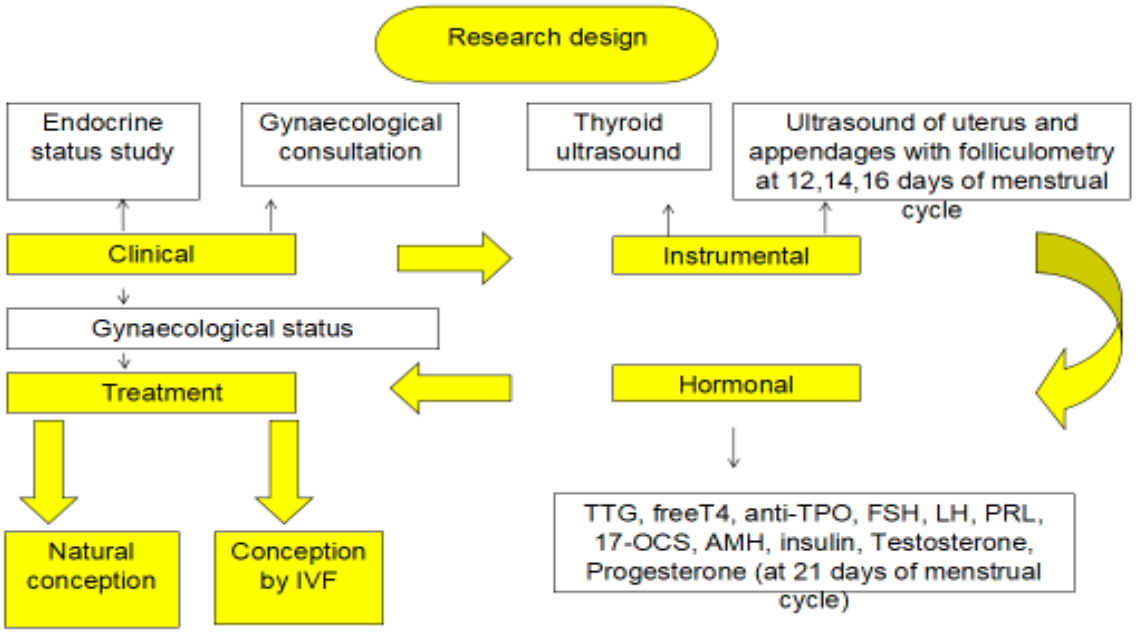

The inclusion criteria for the study were women aged 20 to 45 experiencing infertility due to endocrine factors, specifically those with thyroid dysfunction. Exclusion criteria included women with severe medical conditions such as ischemic heart disease, chronic renal failure, diabetes mellitus in the decompensated stage, serious thyroid disorders, thyrotoxicosis, and diseases affecting the hypothalamic-pituitary system, as well as cases of absolute male infertility (such as aspermia or azoospermia).

Clinical methods included general examination, anthropometry, palpation of the thyroid and mammary glands, and gynecological examination. During the examination of women, the degree of hair loss and the presence of hirsutism were assessed using the Ferriman-Galvey scale. The patients' height and weight were recorded, focusing on their physique, the development of adipose tissue, and its distribution patterns. The body mass index (BMI) was calculated based on the WHO classification (2014) using anthropometric measurements. All women underwent palpation of the thyroid gland. The degree of its enlargement was assessed according to the WHO classification (2001). To assess the endocrine status, hormonal studies of thyroid, gonadotropic hormones, ovarian reserve, prolactin (PRL), 17-oxyprogesterone (17-OX), progesterone on the 21st day of the menstrual cycle, testosterone, and insulin were performed.

The gynecological status of women was assessed together with a gynecologist. The obstetric and gynecological history was gathered, including details on menarche onset and the potential impact of menstrual irregularities due to underlying conditions, stress, relocations, medications, or past surgeries. Information on marital history, pregnancies, and their outcomes was also considered. When assessing reproductive status, the following menstrual cycle disorders were identified: hypomenstrual syndrome (amenorrhea, opsomenorrhea, oligomenorrhea), hypermenstrual syndrome (menorrhagia, metrorrhagia).

The examination of the mammary glands was conducted in both standing and lying positions, with sequential palpation of the external and internal quadrants. Particular attention was given to glandular structure, size variations (hypoplasia, hypertrophy, trophic changes), and other notable characteristics. The presence or absence of nipple discharge was

assessed, including its color, consistency, and nature, along with the pigmentation state of the nipple-areolar complex. If necessary, a consultation with a mammologist was arranged.

Among instrumental diagnostic methods, ultrasound was performed on the thyroid gland, uterus, appendages, and mammary glands. Hysteroscopy was conducted when clinically indicated. Ovarian and uterine ultrasound with folliculometry was carried out using a vaginal transducer on days 12, 14, and 16 of the menstrual cycle, following standard protocols. Measurements included endometrial thickness, antral follicle count (AFC), and the dominant follicle's growth, tracking its progression to ovulation, anovulation, persistence, or atresia. Folliculometry findings were correlated with hormonal data for a comprehensive assessment. Breast ultrasound was performed with BI-RADS classification.

IV. Results

Frequent complaints in women of both groups were ectodermal disorders such as dry skin, hair loss, and brittle nails, which occurred in half of all patients. Hyperprolactinemia was significantly more common in women of the first group 10 (31.3%), increased blood pressure was observed in 5 (16.1%) patients of the first group and 1 (4.5%) of the second group.

Table 1. *Clinical and Anamnestic data of the Studied Women With Endocrine Infertility in Hypothyroidism*

		1st group (n=32)		2nd group (n=22)		Total (n=54)	
		abs	%	abs	%	abs	%
Age (years)	20–35	17	53,1	17	77,3	34	63
	36–45	15	46,9	5	22,7	20	37
BMI	Normal weight	20	62,5	15	68,2	35	64,8
	Overweight	8	25	5	22,7	13	24,1
	Obesity stage I	3	9,4	2	9,1	5	9,3
	Obesity II stage	1	5	0	0	1	1,8
Amenorrhea		2	6,3	0	0	2	3,7
Opsomenorrhea		2	6,3	1	4,5	3	5,5
Oligomenorrhea		4	12,5	4	18,2	8	14,8
Menorrhagia		17	53,1	9	40,9	26	48,1
Metrorrhagia		1	5	0	0	1	1,8
Miscarriages		1	5	2	9,1	3	5,5
Undeveloped pregnancy		3	9,4	4	18,2	4	7,4
Medical abortion		0	0	1	4,5	1	1,8
Ectopic pregnancy		8	25	0	0	8	14,8
Neonatal fetal death		2	6,3	0	0	2	3,7

Clinical and anamnestic data are presented in Table 1. Overweight was found in 13 (24.1%) patients, 1st degree obesity in 5 (9.3%) and 2nd degree obesity in 1 (1.9%) woman. Menstrual disorders in the form of menorrhagia were observed in 48%, oligomenorrhea in 14.8%, while 21% of the patients had normal menstrual cycle. The history in each group was intrauterine intervention after spontaneous miscarriage and undeveloped pregnancy. Termination of pregnancy due to ectopic pregnancies was in 9 (28%) women and neonatal fetal death in 2 (6.3%) patients from the first group.

The gynecological status was assessed (Table 2), of 54 patients, 37 (68.5%) had primary infertility and 17 (31.5%) secondary infertility. The following pathologies were detected in the subjects: uterine myoma (18,5%), endometriosis (13%), endometri-

al polyp (14,8), polycystic ovary syndrome (PCOS) (13%), for which treatment was carried out. And tubal-peritoneal factor of infertility was diagnosed in 9 (28.1%) women of first group. We evaluated the thyroid gland, and the diagnosis of hypothyroidism was confirmed by laboratory parameters and ultrasound (Table 3).

Table 2. *Gynaecological Status of Examined Women With Endocrine Infertility In Hypothyroidism*

		1st group (n=32)		2nd group (n=22)		Total (n=54)	
		abs	%	abs	%	abs	%
Duration of infertility (years)		5,69±3,46		2,82±3,65		–	
Primary infertility		18	58,3	19	86,4	37	68,5
Secondary infertility		14	43,8	3	13,6	17	31,5
Number of IVF attempts	**1**	17	53,1	–	–	17	31,5
	2–3	13	40,6	–	–	13	24,1
	4 and more	2	6,3	–	–	2	3,7
Uterine myoma		7	21,9	3	13,6	10	18,5
Endometriosis (adenomyosis)		6	18,7	1	4,5	7	13
Polyp		5	15,6	3	13,6	8	14,8
Mastopathy		7	21,9	5	22,7	13	24,1
Tubal infertility		9	28,1	–	–	9	16,7
PCOS		4	12,5	3	13,6	7	13

Table 3. *Thyroid Ultrasound Of Women With Endocrine Infertility In Hypothyroidism*

Ultrasound of the thyroid	1st group (n=32)		2nd group (n=22)		Total (n=54)	
	abs	%	abs	%	abs	%
Nodular goiter	5	15,6	4	18,2	9	16,7
Hypoplasia of the thyroid gland	4	12,5	3	13,6	7	13
TAI	16	50	9	41	25	46,3
Diffuse goiter	13	40,6	8	36,4	21	38,9

Table 4. *Ultrasound of Uterus and Appendages of Women With Endocrine Infertility in Hypothyroidism*

Ultrasound of the uterus and ovaries		1st group (n=32)		2nd group (n=22)		Total (n=54)	
		abs	%	%	abs	%	abs
Multifollicular ovaries		6	18,7	5	22,7	11	20,4
DOR		9	28,1	2	9,1	11	20,4
Ovulatory dysfunction		17	53,1	7	31,8	24	44,4
Endometriosis		5	15,6	1	4,5	6	11,1
Myoma		7	21,8	3	13,6	10	18,5
Polyp		5	15,6	3	13,6	8	14,8
AFC	**Up to 4**	20	62,5	2	9,1	22	40,7
	More than 4	12	37,5	20	90,9	32	59,3

Ultrasound was performed to detect uterine and appendage pathology (Table 4), where anovulatory cycle was observed in 17 (54.8%) women of group 1 and 7 (31.8%) of group 2. Diminished ovarian reserve (DOR) was found in 9 (29%) of group 1 and 2 (9.1%) patients of group 2. Diminished antral follicles count (AFC) was observed in 40.7% of cases, which is one of the indicators of reduced ovarian reserve.

To make a final diagnosis, the hormonal profile of the women was studied, which showed the following results (Table 5). In the women of the first group TTG was higher than normal and the hypothyroid state lasted longer, due to this there was an increase in the level of PRL in the blood. The increase in LH and FSH in the same group indicates more pronounced menstrual disorders and an increase in anovulatory cycles.

Table 5. *Hormonal Profile of women with Endocrine Infertility in Hypothyroidism*

	1st group (n=32)	2nd group (n=22)	P
TSH (mIU/ml)	8,91±3,1	7,54±2,9	0.1
T4 (pmol/l)	10,8±0,8*	11,5±1,1	0.015
TPOAb (IU/L)	60,3±8,9**	54,1±6,2	0.004
PRL (ng/ml)	40,9±25,4*	30,7±9,3	0.04
FSH (mIU/ml)	14,9±6,98***	3,86±0,8	0.001
LH (mIU/ml)	14,4±5,8**	4,1±0,6	0.001
Progesterone (ng/ml)	2,45±2,3**	8,6±2,2	0.006
17-OX (nmol/l)	2,23±0,6	6,55±4,06	0.3
Testosterone (nmol/l)	0,84±0,23	0,96±0,59	0.1
AMH (ng/ml)	1,05±0,69***	3,2±0,48	0.001
Insulin (mIU/ml)	11,1±1,64	13,4±2,5	0.6

*Note: *– $p < 0.05$, ** – $p < 0.01$, ***– $p < 0.001$ statistically significant differences compared to the second group*

In preparation for conception, the hormonal background of the thyroid was corrected according to the recommendations of the European Thyroid Association Guideline 2021. After treatment in accordance with the diagnosis, 22 women conceived naturally and the rest by IVF. Positive result from the first IVF attempt was in 17 (53.1%), from the second and/or third in 13 (40.6%) and from the fourth and more – in 2 (6.3%) patients from the first group.

Discussion & Analysis

In the second group (natural conception), T4 levels were significantly higher than in the IVF group ($p < 0.05$). This supports existing data indicating that optimal thyroid hormone levels are essential for normal follicular growth and ovulation. Accordingly, low T4 levels in the IVF group may indicate impaired thyroid function, which can contribute to infertility.

Significantly higher levels of thyroid peroxidase antibodies (TPOAb) in the IVF group further confirm the link between autoimmune thyroid disorders and fertility issues ($p < 0.05$). Studies have shown that autoimmune thyroiditis increases the risk of implantation failure and miscarriage.

The elevated prolactin (PRL) levels observed in the IVF group may suggest hyperprolactinemia, which can disrupt gonadotropin secretion and inhibit ovulation ($p < 0.05$). Hyperprolactinemia is commonly seen in patients with hypothyroidism due to feedback mechanisms affecting dopamine regulation.

The most significant difference was observed in follicle-stimulating hormone (FSH) levels ($p < 0.001$). Substantially higher FSH levels in the IVF group indicate diminished ovarian reserve (DOR). Elevated FSH is a marker of ovarian aging and is associated with poor response to stimulation in assisted reproductive technologies.

Additionally, LH levels were significantly higher in the IVF group, which may indicate disrupted ovulatory processes and hormonal instability ($p < 0.001$).

A significantly lower level of AMH ($p < <0.001$) was observed in women who underwent IVF, confirming the presence of diminished ovarian reserve (DOR) in this group.

While this study provides valuable insights, certain limitations must be acknowledged: the sample size was relatively small, which may limit the generalizability of findings. The observational nature of the study does not establish a direct causal relationship between thyroid dysfunction and infertility outcomes. Further research should focus on longitudinal studies assessing the impact of thyroid hormone optimization on IVF success rates.

Conclusion

The analysis of studies has shown that the change of endocrine status of women with thyroid hypofunction is unfavourably reflected on menstrual cycle of women of fertile age manifested more often by menorrhagia and oligomenorrhoea that proves the necessity of correction of all hormones in a complex for improvement of reproductive function in women.

The study of ovarian reserve in women showed that the patients of the first group have low values of AFC and AMH in comparison with the second group, which is one of the indications for IVF.

In conditions of thyroid hormone imbalance, a change in prolactin concentration in women from the first group was revealed. As well as higher levels of FSH, LH and low levels of Progesterone in relation to the second group, which dictates the need for correction of hormonal status for the effectiveness of IVF.

References

Boivin, Jacky & Bunting, L. & Collins, J.A. & Nygren, Karl-Gösta. (2007). International estimates of infertility prevalence and treatment-seeking: potential need and demand for infertility medical care. Human Reproduction. 22. 10.1093/humrep/dem299.

Cox C. M., Thoma M. E., Tchangalova N., Mburu G., Bornstein M. J., Johnson C. L., Kiarie J. Infertility prevalence and the methods of estimation from 1990 to 2021: a systematic review and meta-analysis. Hum Reprod Open 2022;4: hoac051.

ESHRE ART Fact Sheet 2018. [(accessed on 20 January 2019)]. – Text: electronic. https://www.eshre.eu/Press-Room/Resources.

Fertility problems: assessment and treatment. – London: National Institute for Health and Care Excellence (NICE); 2017 Sep. PMID: 32134604.

Infertility prevalence estimates, 1990–2021. Geneva: World Health Organization; 2023. Licence: CC BY-NC-SA 3.0 IGO.

Koyyada A., Orsu P. Role of hypothyroidism and associated pathways in pregnancy and infertility: Clinical insights. Tzu Chi Med J. 2020 Apr 10; 32(4): 312–317. Doi: 10.4103/tcmj.tcmj_255_19. PMID: 33163375; PMCID: PMC7605301.

Mascarenhas M. N., Flaxman S. R., Boerma T., Vanderpoel S., Stevens G. A. (2012.) National, Regional, and Global Trends in Infertility Prevalence Since 1990: A Systematic Analysis of 277 Health Surveys. PLOS Medicine 9(12): e1001356. URL: https://doi.org/10.1371/journal.pmed.1001356

Poppe K., Velkeniers B., Glinoer D. Thyroid disease and female reproduction. Clin Endocrinol (Oxf) 2007; 66: 3: 309–321

Purity Njagi, Wim Groot, Jelena Arsenijevic, Silke Dyer, Gitau Mburu, James Kiarie, Financial costs of assisted reproductive technology for patients in low- and middle-income countries: a

Systematic review, Human Reproduction Open, – Volume 2023, – Issue 2, 2023, hoad007. URL: https://doi.org/10.1093/hropen/hoad007

Vander Borght M., Wyns C. Fertility and infertility: Definition and epidemiology. Clin Biochem. 2018 Dec; 62:2–10. Doi: 10.1016/j.clinbiochem.2018.03.012. Epub 2018 Mar 16. PMID: 29555319.

submitted 14.06.2025;
accepted for publication 30.06.2025;
published 29.09.2025

Contact: zilonovazizbek@gmail.com

The Austrian Journal of Technical and Natural Sciences, No 7–8
ISSN 2310-5607

PREMIER Publishing
ppublishing.org

Section 5. Technical sciences in general

DOI:10.29013/AJT-25-7.8-113-116

MODERN STATE OF LUBRICANTS FOR DRILLING OIL AND GAS WELLS

Nodirbek Kobilov [1], ***Jasurbek Olimov*** [1], ***Ergash Dustmurodov*** [1], ***Shuxratjan Ergashev*** [1], ***Olimjon Eshmamatov*** [1]

[1] Uzbekistan scientific research of chemical-pharmaceutical insititute, Tashkent, Uzbekistan

Cite: *Kobilov N., Olimov J., Dustmurodov E., Ergashev Sh., Eshmamatov O.E. (2025). Modern State of Lubricants For Drilling Oil and Gas Wells. Austrian Journal of Technical and Natural Sciences 2025, No 7–8.* https://doi.org/10.29013/AJT-25-7.8-113-116

Abstract

The article presents the modern state of lubricants for drilling oil and gas wells. Purpose of using lubricants and main physical chemical and technological properties of lubricants are given. Types and advantages of using lubricants in oil and gas well drilling are given too.

Keyword: *Lubricant, drilling, fluid, property, friction*

Introduction

Lubricating agents for drilling fluids are special additives such as fatty acids, polyglycols, resin substances and petroleum oils that reduce friction between the drilling tool and the borehole walls, as well as between the tool itself and the rock, which prevents sticking, increases the drilling speed and service life of the equipment (Kobilov et al., 2020). Examples of such reagents include additives “BURLAK”, ECOLUBE, “Lubrex”, BURMUD, StabVisco-LDF and Silange. Lubricating additive for drilling fluids Lubriminol is used to reduce the friction coefficient of drilling fluids, increase the mechanical drilling speed and reduce the risk of sticking. The product is used for all types of water-based drilling fluids. Additionally, it performs the function of inhibiting clays and shales. During drilling, there is strong friction of the tool against the borehole walls and high torques. To reduce them, lubricating additives for drilling fluids are used. They have increased surface-active properties and therefore increase the efficiency of drilling operations and improve wear resistance and lubricating properties of solutions. Polymer lubricating additives for drilling fluids increase the rate of penetration and reduce abrasive wear, i.e. increase the service life of drilling equipment and pumping equipment. Drilling lubricant type MBR is developed by us and implemented in oil and gas well drilling.

Materials and methods

Drilling fluid testing procedures and other documents related to oilfield standards are

published by the American Petroleum Institute (API) (Kobilov, 2024). The composition of the lubricant for drilling fluids. Ecolube includes petroleum oils, additives, as well as modified resin and fatty acids. This lubricant:

- reduces friction;
- increases the rate of penetration;
- protects drilling rods and tools from rust and breakage;
- increases the potential of the equipment and extends its service life.

Lubricant additive for drilling fluid stabvisco-ldf StabVisco-LDF is designed to ensure highly efficient drilling in difficult geological and technical conditions. It is intended for the treatment of water- and hydrocarbon-based drilling fluids in order to reduce downhole friction forces, as well as to reduce and prevent sticking situations when drilling vertical and directional wells in difficult geological and technical conditions.

StabVisco-LDF is an effective lubricating additive for use in drilling

Lubriminol lubricating additive is a solution of fatty acid derivatives with surfactants in a solvent.

Application

- Drilling vertical, directional and horizontal wells, including slide drilling;
- Preparation of drilling fluid packs with an increased concentration of lubricating additive for running casing strings.

Table 1. *Main physical and chemical properties*

Appearance at 20 °C	*Viscous liquid from dark brown to black*
Density at 20 °C, g/cm³, within	*–0.8 – 1.00*
Freezing point, °C, not higher than	*Minus 8*
Mass fraction of organochlorine compounds (OCC), mcg/g (ppm), not more than	*Absence*

Properties and advantages of use lubricants.

- The components of the lubricating additive are adsorbed on metal surfaces and on the walls of the well, creating a lubricating cushion along which the drilling tool or casing string slides freely;
- The Lubriminol additive is dispersed throughout the entire volume of the solution and does not migrate to the dome zone of the horizontal wellbore, thus preventing the creation of conditions for sticking;
- The lubricant additive does not separate into phases and does not accumulate at the wellhead during shutdowns, quickly and effectively reduces torque and torque amplitude fluctuations, improves tool movement and reduces hook weight, facilitates applying the load to the bit and facilitates slide drilling, increases the mechanical and commercial drilling speed, can be used to prepare concentrated packs before lowering the casing, does not foam or salt out and is thermally stable and is environmentally safe.

Table 2. *Technological properties of the lubricant*

Reduction in the coefficient of friction of a 1% aqueous solution of a lubricating additive on a friction machine, %	*> 90*
Coefficient of friction of a clay cake on FSK-4E on KTK-2, rel. units	*< 0.1*
Foaming activity of 1% aqueous solution of lubricant additive, cm³	*< 5*
Foaming activity of 0.5% solution of lubricant additive in clay solution, %	*< 0.2*
Relative decrease in friction coefficient after thermal aging (16 hours at 150 °C), %, not less than	*> 90*

(48 hours at minus 40 °C), %, not less than	*> 90*
*Relative decrease in friction coefficient after exposure to negative temperatures Salt resistance***	*Formation of uniform emulsion*

** Tested in an accredited laboratory.*

*** Brine containing CaCl2–36.44 g/l, KCl – 40.64 g/l, NaCl- 201.75 g/l. Density 1.17 g/cm³, pH = 5–6.*

Results and Discussion

The reagent is recommended to be introduced either into the circulating drilling fluid through a hydraulic funnel, or directly into a container with the solution, or into a trough. Depending on the composition and type of the solution, as well as on the geometry of the well, the consumption of the lubricating additive Lubriminol is from 10 to 30 kg per 1 m³ of finished drilling fluid. If necessary, the concentration can be increased to 50 kg per 1 m³.

Table 3. *StabVisco-LDF is an effective lubricating additive for use in drilling fluids under difficult geological and technical conditions.*

Appearance at 20 °C:	*dark brown liquid.*
Density at 20 °C, kg/m³:	*870-920*
Pour point, °C, not higer than:	*–15*
Kinematic viscosity at 50 °C, mm/s:	*15-70*
Acid number, mg KOH/g:	*25-55*

Storage: in a well-ventilated, dry room. The use of open fire is prohibited in storage areas. Lubricant additive for drilling fluid SMEG

Liquid lubricating additives SMEG are compositions of vegetable and mineral oils modified with various additives. They are intended for use as additives in drilling process fluids in a wide range of clay phase content, weighting agents and mineralization. Lubricating additives SMEG provide effective reduction of the friction coefficient and do not have a negative effect on the properties of drilling fluids. The series of lubricating additives SMEG is represented by the following brands, differing in composition, properties and area of application: – SMEG-3 is intended for low-clay, weighted drilling fluids and solutions with a low degree of mineralization. – SMEG-5 is intended for low-clay, mineralized and weighted drilling fluids with a low freezing point.

Application of the lubricant. SMEG

SMEG lubricant additives provide an effective reduction in the friction coefficient over a wide temperature range. Adding 0.5% SMEG lubricant additive to the drilling fluid reduces the friction coefficient by at least 50%.

Processing

For optimal results, SMEG is added to the drilling fluid directly in the cycle. The consumption of the lubricant additive to achieve the desired effect is 0.5–2%. The SMEG reagent is compatible with all drilling fluid formulations.

When drilling wells, high friction forces of the tool against the borehole walls and high torques occur. To reduce them, special additives for drilling fluids are used. They have improved surface-active and anti-stick properties.

Additives for drilling fluids are divided into two types depending on the purpose and process parameters:

- electrolytes;
- protective, containing high-molecular substances.

The use of polymer additives for drilling fluids from various manufacturers allows you to increase the rate of penetration, as well as the service life of pumping equipment and drilling equipment due to reduced abrasive wear.

When working with aerated compositions, individual additives increase foaming. This reduces unproductive losses of drilling fluid when it is absorbed in faults between rock layers. The products are your benefits.

- Prompt deliveries of a full range of reagents and additives: production downtime due to the lack of necessary components is eliminated;
- Chemistry from the best manufacturer in Russia, the quality of chemical raw materials will ensure the efficiency of oil and gas production and processing.

Assortment expansion: we monitor the development of the industry and promptly offer raw materials for the implementation of the latest technologies. Lubricating additive for drilling fluids RC–LUBE

- lubricant additive for drilling fluid RC-lube;
- general description;
- RC–Lube reagent is a lubricating additive for drilling fluids, does not have a negative effect on the rheology of the drilling fluid or has a minimal effect.
- Main advantages;
- reduces friction between drill rods and the wellbore wall;
- has a beneficial effect on the parameters of solutions: viscosity, static shear stress, filterability;
- easily dispersed even in cold water;
- does not create problems during disposal, biodegradable, harmless to the environment;
- can be used in land and sea drilling conditions;
- compatible with all drilling fluid additives.
- Application information
- Recommended for water-based drilling fluids at a dosage of 0.5–1%. Added directly to the drilling fluid system.

Characteristics	
Appearance:	*dark liquid*
pH of 1% solution	*8-11*
Density at 20°C, kg/m³:	*900-950*

Conclusion

Main physical chemical and tribological properties of lubricants are given, as appearance, acidity, viscosity, density, salt resistance, foaming property and coefficient friction.

References

Kobilov N. S., Yangibayev A. I., Omonov Z. J. New composite lubricants and weightings for drilling and gas wells., International journal of innovations in Engineering research and technology. IJIERT ISSN: 2394–3696. – P. 46–49. 2020. URL: http://www.ijiert.org

Kobilov N. S. Development of effective lubricants for drilling fluids.// Austrian Journal of Technical and Natural sciences, – Issue1–2, 2024. – P. 90–93. DOI:10.29013/AJT-24-1.2-90-93

Kobilov N. S. The ways of obtaining weighted drilling fluids based on lubricants for drilling oil and gas wells // Austrian Journal of Technical and Natural sciences, 2024. – Issue 1–2. – P. 94–97. DOI:10.29013/AJT-24-1.2-94-97

API Specification 13A, 2015.

submitted 15.08.2025;
accepted for publication 29.08.2025;
published 29.09.2025

Contact: nodirbekdoc@gmail.com

The Austrian Journal of Technical and Natural Sciences, No 7–8
ISSN 2310-5607

PREMIER Publishing
ppublishing.org

DOI:10.29013/AJT-25-7.8-117-119

CATALYST PRODUCTION TECHNOLOGY FOR METHANE OXYCONDENSATION REACTION

Nodirbek Kobilov [1], ***Abror Togaev*** [1], ***Khikmatullo Nasullaev*** [1]

[1] Karshi State technical University

Cite: *Kobilov N., Togaev A., Nasullaev Kh. (2025). Catalyst Production Technology for Methane Oxycondensation Reaction. Austrian Journal of Technical and Natural Sciences 2025, No 7–8.* https://doi.org/10.29013/AJT-25-7.8-117-119

Abstract

The article presents the method of preparation of the catalyst for the synthesis of C_2-hydrocarbons was changed and various d-element salts were added to it as promoters. The catalyst was prepared by two methods: precipitation and absorption. As well as, formal-kinetic analysis of the chemical and physical stages occurring in the synthesis of the catalyst was carried out in a non-isothermal mode by the derivatographic method according to the known equations were given.

Keywords: *catalyst, methane, GTL, method*, *hydrocarbon, temperature*

Introduction

As is known, adiabatic-type reactors are widely used for catalytic processes, the selectivity of the processes changes little over a wide temperature range. The advantage of such reactors is their low metal capacity of 2–3 t/m^3 (cat) and the ease and cheapness of reactor construction. The disadvantage is that the reactions occur with a large heat effect and the selectivity is not uniform over the catalyst bed. As we noted above, when the methane: oxygen ratio is 5, the adiabatic heat of heating of the gas mixture is 575 °C. Taking into account the accepted upper approximation, the methane oxycondensation reaction can be carried out in a 4–5-stage device. Under these conditions, the process is considered an effective method (Togaev, 2025).

For Fischer-Tropsch synthesis, rare metals from Group VIII of the Periodic Table of D. I. Mendeleev can be used as promoters to increase the activity of highly catalytically active cobalt catalysts intended for the production of liquid hydrocarbons from natural gas (Rakhimov, 2024). These metals have the ability to dissociate hydrogen, as a result of which, when added to highly catalytically active cobalt catalysts intended for the production of liquid hydrocarbons from natural gas, the reduction of cobalt oxides occurs more easily. This leads to a decrease in the temperature and a significant increase in the activity of these catalytic systems. Thus, the introduction of 0.1–0.7% Pd or Ru into the highly catalytically active catalysts for the production of liquid hydrocarbons from natural gas based on 10% Co/Al_2O_3 and 10% Co/CuO_2 allowed to increase the CO conversion (by 10%) and the yield of C_5^+ hydrocarbons (from 55 to 95. –97 g/m^3) compared to the

highly catalytically active catalyst for the production of liquid hydrocarbons from unpromoted natural gas (Yuldashev, 2024). The highly catalytically active cobalt-ruthenium catalysts for the production of liquid hydrocarbons from natural gas were characterized by high selectivity to the products formed as a result of the liquid reaction (more than 80%). In addition, cobalt, which contains rare metals, has a longer service life, providing catalysts with high catalytic activity for the production of liquid hydrocarbons from natural gas (Kuybokarov, 2024).

Materials and Methods

The method of preparation of the catalyst for the synthesis of C_2-hydrocarbons was changed and various d-element salts were added to it as promoters. The catalyst was prepared by two methods: precipitation and absorption.

In the precipitation method, aqueous solutions of manganese acetate and sodium molybdate were used to prepare the catalyst. The carrier (carrier) – silicon oxide – was prepared by adding sulfuric acid to an aqueous solution of sodium silicate. The precipitate was filtered, dried at 130 °C and calcined in a calcining furnace for 5 hours at 800––1100 °C. In the absorption method, sulfuric acid was first added to an aqueous solution of sodium silicate. The precipitate was filtered, dried at 130 ° C and calcined at 800–1300 °C. Then aqueous solutions of manganese acetate and sodium molybdate salts were added. After 3 hours, the obtained catalyst was dried and calcined at 800–130 °C. Then, the required amount of zirconyl nitrate solution was added to the obtained mass. Then, the catalyst was filtered, dried and calcined in the above sequence.

Catalyst production technology in industry and characteristics of starting materials.

The cobalt-iron-nickel-zirconium/SiO_2 catalyst is in the form of dark brown cylindrical granules with dimensions d = 2.5–3.0, h =3.0÷3.5 mm.

Composition, % mass: 20%Co-15%Fe--10%-Ni-1%ZrO2/YKC

Co_2O_3–20.0
Fe_2O_3–15.0
Ni_2O_3–5.0
ZrO_2–1.0
SiO_2–59.00

Mechanical strength, not less than 3 MPa.

Operating time before regeneration, hours, not less than 108.

Characteristics of starting raw materials and semi-finished products

1. Cobalt (II, III) oxide, gray-black crystal, insoluble in water.

Appearance: gray-black crystal;
Molecular formula: Co_3O_4
Molecular mass: 240.80 g/mol
Density: 6.073 g/cm^3
Melting point (°C): 900

2. Iron (II, III) oxide, solid black powder, insoluble in water.

Appearance: solid black powder;
Molecular formula: Fe_3O_4
Molecular mass: 231.533 g/mol
Density: 5.17 g/cm^3
Melting point (°C): 1597

3. Nickel (II, III) oxide, sharp gray or black powder, insoluble in water.

Appearance: solid black powder;
Molecular formula: Ni_3O_4
Molecular mass: 240.08 g/mol
Density: 3.33 g/cm^3
Melting point (°C): 1682

4. SiO_2 is a porous material.

Results and discussion

Production chemistry and physicochemical foundations

Formal-kinetic analysis of the chemical and physical stages occurring in the synthesis of the catalyst was carried out in a non-isothermal mode by the derivatographic method according to the known equations

$$1-\left(1-\alpha\right)^{\frac{1}{n}}=k\tau \quad (1)$$

$$\lg\left[-ln\left(1-\alpha\right)\right]=nlgkt \quad (2)$$

$$\left[-\lg\left(1-\pm\right)\right]^{\frac{1}{n}}=k\tau \quad (3)$$

The Raginsky-Todes-Mashnel equation (1), the so-called “compressible sphere” equation, is suitable for the case when the limiting stage is considered to be the growth stage of the aggregates. The Erofeev-Avrami equation (3) is characteristic for the emergence of multi-stage reaction centers; the Prodt-Tompkins equation is for the autocatalytic course of processes. We obtain equa-

tions (5), (6), and (7) by solving the Arrhenius equation (4) and the joint differential equations (1)–(3) together with equation (5) in the form of a linear temperature change.

$$k = k_0 e^{-\frac{E}{RT}} \quad (4)$$

$$\frac{dT}{dr} = g - const \quad (5)$$

$$\ln\left[\frac{1}{(1-\alpha)2/3}\cdot\frac{d\alpha}{dT}\right] = \ln\frac{k}{g} - \frac{E}{RT} \quad (6)$$

$$\ln\left[\frac{1}{\alpha^n/1-2}\cdot\frac{d\alpha}{dT}\right] = \ln\frac{k_0}{g} - \frac{E}{RT} \quad (7)$$

$$\ln\left[\frac{1}{\alpha(1-\alpha)}\cdot\frac{d\alpha}{dT}\right] = \ln\frac{k_0}{g} - \frac{E}{RT} \quad (8)$$

Here is the degree of decomposition calculated from the derivative of the TG melting curve, A is a parameter that depends on the mechanism and geometry of the reaction rate of the formation of complexes; E, R are the activation energy and gas constant.

Processing of derivatographic data according to equations (6)–(8) shows that the decomposition of the manganese-molybdenum-sodium-zirconium/SiO_2 catalyst under the influence of heat obeys equation (8).

X-ray studies revealed that the manganese-molybdenum-sodium-zirconium/SiO_2 catalysts exhibit sufficiently high activity.

Catalyst production process flow chart

In the experiments, 50% solutions of salts prepared from $Co(NO_3)_2$; $Fe(NO_3)_2$, $Ni(NO_3)_2$ and $ZrO(NO_3)_2$ were used. The precipitation of the corresponding hydroxides was carried out in a reactor equipped with a stirring device with a volume of 1000 cm^3 at a temperature of 90–110 °C. After precipitation, the suspension was evaporated, the precipitate was additionally dried at 130 °C and calcined in a muffle furnace at temperatures of 350––550 °C.

The study of the samples by thermal analysis methods was carried out on an SDT Q600 derivatograph. Measurements were carried out in a nitrogen atmosphere in the range of 20–700 °C with a scanning rate of 10 °C/min.

Conclusion

It was found that the time for the complete phase change of the mixture at a temperature of 500 °C is not less than 15 hours. It should be noted that the acceleration of the change process by further increasing the temperature is conceivable due to the rapid adhesion of the precipitate particles and a decrease in their catalytic activity. Because increasing the incineration temperature above 500 °C deteriorates the quality of the catalyst, increasing the efficiency of the incineration temperature is possible only by homogenizing the precipitate composition during the deposition stage.

References

Togayev Abror, Kobilov Nodirbek. Study of catalysts prepared by impregnation with aqueous cobalt nitrate solution// Austrian Journal of Technical and Natural Sciences 2025. –– No 5, 6. URL: https://doi.org/10.29013/AJT-25–5.6–74–77

Rakhimov, G., & Murtazayev, F. (2024, November). Study of physico-chemical properties of domestic AI-80 automobile gasoline and reduction of benzene content in gasoline. In *American Institute of Physics Conference Series* (Vol. 3244, No. 1, p. 050019).

Yuldashev T., Rakhimov, G. (2024, November). Study of the degree of foaming of absorbent compositions used when purifying gases from acidic components. In *AIP Conference Proceedings* (Vol. 3244, No. 1). AIP Publishing.

Kuybokarov O., Rakhimov G., Karshiyev M. (2024). Research of the catalytic properties of a catalyst selected for the production of high-molecular weight liquid synthetic hydrocarbons from synthesis gas. In *E3S Web of Conferences* (Vol. 498, p. 01008). EDP Sciences.

submitted 15.08.2025;
accepted for publication 29.08.2025;
published 29.09.2025

Contact: nodirbekdoc2020@gmail.com

The Austrian Journal of Technical and Natural Sciences, No 7–8
ISSN 2310-5607

PREMIER Publishing
ppublishing.org

DOI:10.29013/AJT-25-7.8-120-125

STUDY OF IR-SPECTROSCOPIC ANALYSIS OF OILS USED IN THE TEXTILE INDUSTRY

Davletov Zafar [1], ***Kobilov Nodirbek*** [2], ***NasullaevKhikmatullo*** [2], ***Gulomov Shuxratqodir*** [2], ***Igamkulova Nargisa*** [1]

[1] Tashkent Institute of Chemical Technology, Tashkent, Uzbekistan

[2] Uzbekistan scientific research of chemical-pharmaceutical institute, Tashkent, Uzbekistan

Cite: *Davletov Z., Kobilov N., Nasullaev Kh., Gulomov Sh., Igamkulova N. (2025). Study of Ir-Spectroscopic Analysis of Oils Used in the Textile Industry. Austrian Journal of Technical and Natural Sciences 2025, No 7–8.* https://doi.org/10.29013/AJT-25-7.8-120-125

Abstract

This article presents the composition, physical and chemical properties of textile industry machine oils and the results of their IR-spectroscopic analysis. Also, the basic technological and operational requirements for the oils used in the textile industry have been developed.

Keywords: *oil, IR-spectroscopy, breeding, process, analysis, requirements*

Introduction

The textile industry is one of the fastest growing industries, where high-speed equipment operation, sensitive materials, and the need to produce high-quality products require a special approach to lubricants. One of the main elements of the technological process is textile oils, which ensure the smooth operation of machines and the preservation of the quality of the processed fibers.

Lubricant chemical analysis is a process of testing lubricant properties, contaminants, and wear debris to assess the condition of the lubricant and the equipment it's used in. This analysis helps in identifying potential problems, preventing costly repairs, and ensuring optimal equipment performance.

Textile oils and lubricants are special compounds that are used in the textile industry to reduce friction, prevent equipment wear, and improve the quality of fiber and fabric processing.

Currently, various oils are used as the main lubricating materials. The main function of the oil is to create a stable lubricating film to minimize friction and prevent wear of the rubbing surfaces. Changes in the properties of the oil during its operation in the engine are called oil aging. Changes in the properties of the oil are divided into two groups – quantitative and qualitative. However, changes in both groups can ultimately affect the reliable operation of the engine (Majidov, 2000).

During the process of working with oil, it comes into direct contact with metal, is exposed to external air, temperature, pressure, and other factors. As a result of these effects,

hydrocarbon decomposition, oxidation, polymerization, and condensation processes, charring (incomplete combustion), liquefaction with fuel, contamination with foreign substances, and oil hydration occur.

Oils containing contaminants cannot meet the requirements and must be replaced with new oils. Under the influence of oxygen in the air, the oil oxidizes and, falling into the crankcase, mixes with hot and contaminated oil. Acids are strong oxidizing agents and are the main cause of corrosion and rusting of the cylinder wall and piston rings. Acids also create an environment that reduces friction in bearings. Resins, on the contrary, form a sticky deposit on the piston and piston rings, sharply reducing their mobility.

Modern motor oils produced today consist of base oils and additives that improve their properties. As base oils, distillate and residual components of various hardness (hydrocarbons), their mixtures, hydrocarbon components obtained by hydrocracking and hydroisomerization, as well as synthetic products (high molecular weight hydrocarbons, polyalphaolefins, complex esters, etc.) are usually used. Many all-season oils are obtained by supplementing low-hardness base oils with macropolymer additives.

Motor oils must meet the following requirements:

- have good lubricating properties that ensure reliable engine lubrication in all operating modes;
- have optimal viscosity-temperature characteristics for trouble-free engine start-up;
- have sufficient antioxidant stability that prevents significant changes in chemical composition during operation;
- have good detergent properties that prevent the formation of varnish and hardened deposits on hot engine parts;
- have high anti-corrosion properties (at operating temperatures) for structural materials, especially non-ferrous metals and alloys;
- have reliable protective properties that prevent corrosion during storage.

Materials and methods

Of the study are motor oil and used motor oil used in the textile industry.

The work used modern physicochemical analysis methods, including IR spectroscopy and other standard analysis methods.

Lubricating oils: analysis according to ASTM D6443 and D4927Turnkey solution for analysis of additives in lubricating oils.

Almost all commercial oils contain chemical additives to enhance their performance for a particular application. The ASTM D6443 and ASTM D4927 international standard test methods are used to determine if the oils, additives, and additive packages meet specification. These methods employ wavelength dispersive X-ray spectroscopy (WD XRF) and mathematical matrix corrections procedures. XRF is an excellent method for multi-elemental analysis as it provides cost-effective, precise and accurate data and fast data acquisition. Individual calibrations can be used for months, avoiding time-consuming and costly recalibration. Especially for liquids, the sample preparation is simple and the analysis does not require highly skilled lab personnel.

Expertise Program for XRF analysis of additives in lubricating oil according to ASTM D6443 and D4927

This Expertise program delivers a complete methodology to establish norm compliance and covers all aspects from sample preparation to quality assurance. Customers can choose to request a quote for either one or both norms to be covered in the program.

Included:

- Suit of calibration standards for D4927 and/or D6443 including validation sample;
- P-1 or P-2 cups and assembly tool and pre-cut Mylar foils, sufficient for calibration and validation;
- Setup of optimized application setup and calibration for accurate analysis of the range of elements in concentration ranges as given in the table above;
- Setup of methodology validation and calibration maintenance procedure;
- Advice on sample preparation best practices and workflow optimization;
- User training and documentation.

Results and Discussion

Textile oils are not simple lubricants, but important tools that affect the performance

of equipment, product quality and economic efficiency of the enterprise. Choosing the right oil, taking into account technological requirements, the type of material being processed and the characteristics of the equipment, significantly extends the service life of machines and increases the competitiveness of the finished product.

The main functions of textile oils are: to reduce friction between equipment parts and the materials being processed; to prevent sticking of moving parts of machines; to reduce static electricity in the processing of synthetic fibers; to maintain the quality of the fibers – smoothness, softness, brightness; to protect equipment from rust; to increase the technological convenience of spinning, weaving, knitting and final processing processes.

The composition of motor oil mainly consists of two components (Pentin, 2003):

1. Base oil (70–90%). Mineral (derived from petroleum) – produced by boiling direct petroleum and then separating the alkanes. This product consists of up to 90% branched saturated hydrocarbons. It is characterized by high dispersion of paraffins (non-uniformity of molecular chain masses). The lubricant is thermally unstable and does not retain its viscosity indicators during operation. Synthetic – a product of petrochemical synthesis. Ethylene is used as a raw material, from which a certain molecular mass and a long-chain polymer base are obtained by catalytic polymerization. Synthetic oil can also be obtained by hydrocracking mineral oils. It does not lose its properties during its service life (Abishek, 2024).

Semi-synthetic – a mixture of mineral (70–75%) and synthetic oil (up to 30%).

2. The proportion of modifiers in motor oil is about 10%. Ready-made "add-on packages" consist of a set of various components and are used to increase the necessary parameters of the lubricant: Antioxidant – slows down the wear of the oil; Forms a protective film against friction and adhesion; Detergent – prevents residue formation; Dispersant – keeps pollution in suspension; Antifoaming – reduces foaming; Viscosity modifiers – provide stability at different temperatures; Anti-corrosion – protects metal from rust. The general composition of lubricating oils is given in the table below.

Table 1. *Composition of lubricating motor fluids*

Components	Percentage amount
Basic base (saturated paraffins, polyalkylnaphthalenes, polyalphaolefins, linear alkylbenzenes, as well as complex ethers)	~90%
Additives package (sticky stabilizers, protective and antioxidant additives	Up to 10%

The strict technological and operational requirements for oils used in the textile industry include:

1. Low viscosity – so that they spread evenly throughout the material and do not weigh it down.

2. Easy washability – the ability to remove the oil from the fiber without damaging the fabric.

3. Chemical stability – resistance to oxidation and decomposition. 4. Odorless and non-toxic – safety for workers and the end user.

5. Colorless and non-staining – especially important for light fabrics.

6. Antistatic properties – especially relevant when working with synthetic materials.

Table 2. *Main properties of lubricant*

Property	Description
Viscosity	Determines the oil's fluidity; measured by SAE (e.g., 5W-40).
Ignition temperature	The temperature at which oil vapors ignite (usually 200–250 °C).

Property	Description
Solidification temperature	The temperature at which the oil loses its mobility (down to –50 °C for synthetic oils).
Alkalinity number	Indicates the acid-neutralizing ability (6–12 mg KOH/g).
Acidity number	Indicates the amount of acids in the oil; increases as the oil ages.
Sulphated ash content	Indicates the amount of solid residue left after combustion (0.5–1.5%).
Evaporation rate	Mass loss at high temperatures; the lower the better.

Among the various methods for studying the structure of organic and inorganic compounds, infrared spectroscopy (IRS), which is based on the absorption, reflection, and scattering of infrared radiation energy as it passes through a substance, occupies an important place (Tarasevich, 2012).

IR spectroscopy is based on the absorption of infrared radiation by oil molecules at certain frequencies, which correspond to the vibrations of chemical bonds. By comparing the spectra of motor oil and used oil, it is possible to determine the following: the degree of oxidation, the presence of decomposition products (organic metal compounds), the presence of water, fuel, and solid particles.

In the course of work, the composition of the oil was determined by IR spectra in the laboratory of the Center for Advanced Technologies of the Republic of Uzbekistan using equipment manufactured by Shimadzu (Japan).

Figure 1. *IR spectroscopic image of textile oil*

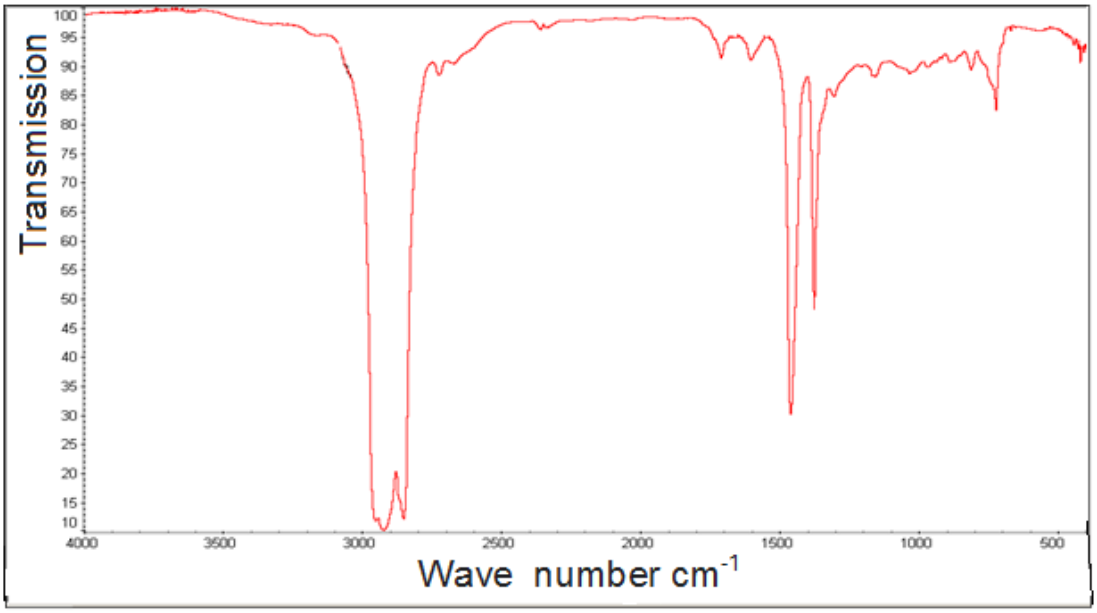

Analysis of the data presented in the figure shows that the main absorption lines are located at approximately 2850, 2925 cm^{-1} and 3000–3100 cm^{-1}. According to the characteristic frequency table, these vibrations correspond to the following: the valence vibration lines of the CH_2 group, characteristic of aliphatic hydrocarbons; the C=C bond vibrations of aromatic rings. The strong peak at approximately 700 cm^{-1} indicates the presence of four carbon atoms in the aliphatic chains. Thus, the main composition of the studied oil consists of saturated hydrocarbons and benzene class compounds. The IR-spectrum of the oil used for the comparative analysis was also obtained (Fig. 2), which made it possible to determine the changes in the composition – oxidation processes, accumulation of substances formed during wear and decomposition of additives.

Figure 2. *IR spectroscopic appearance of used textile oil*

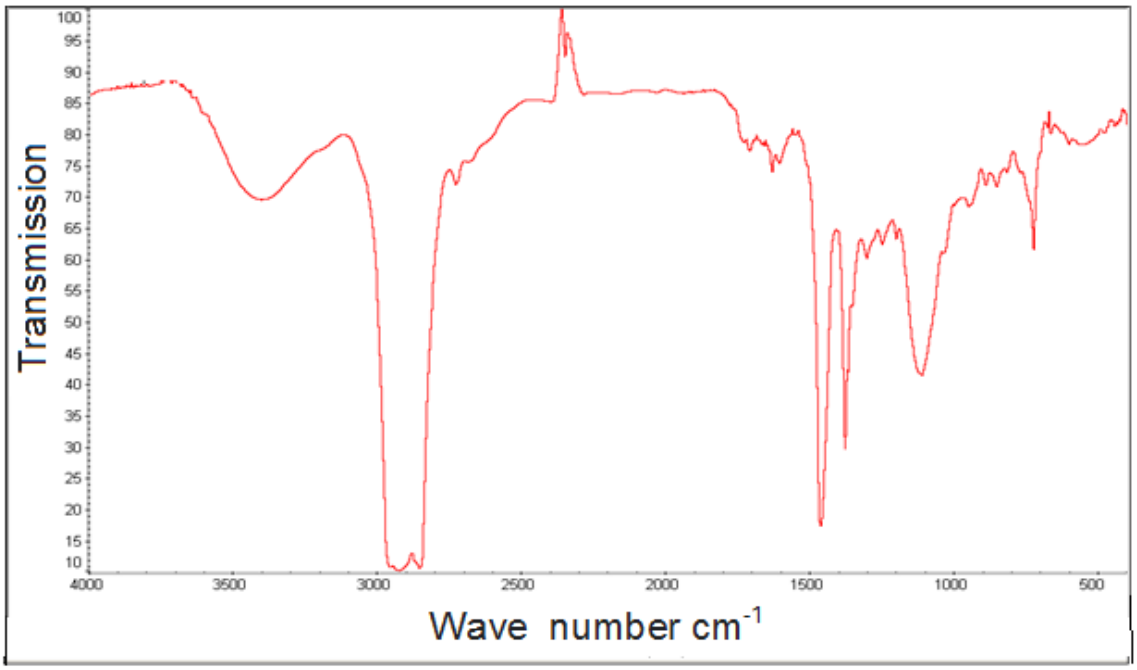

Analysis of the presented data shows that a broad peak around 3400–3450 cm^{-1} corresponds to the vibrations of the –OH (hydroxyl) group. This indicates that moisture or water was added to the oil during operation. Peaks around 1700–1750 cm^{-1} are characteristic of –C=O (carbonyl) groups, indicating the formation of aldehydes or ketones as a result of oil oxidation. Peaks in the range of 1100–1150 cm^{-1} belong to –S=O (sulfoxide or sulfate) groups, indicating the accumulation of metals or oil additives (detergent, antioxidant). A change in the ratio of the CH_2 and CH_3 vibration peaks around 2850–2950 cm^{-1} may indicate the presence of fuel residues or organic substances in the oil. Additional peaks in the range of 600–800 cm^{-1} may originate from mineral particles or metal oxides. Peaks around 3000–3100 cm^{-1} and 1600 cm^{-1} are characteristic of aromatic C–H and C=C vibrations, indicating benzene-like substances or heavy hydrocarbons accumulated in used oils.

The analysis shows that infrared spectroscopy is an effective and rapid tool for determining the composition and condition of both new and used motor oils. By comparing the spectra, it is possible to identify characteristic changes associated with oxidation, the accumulation of additives, the presence of moisture and friction products.

This allows an objective assessment of the suitability of oils for reuse in the textile industry. After cleaning and regeneration, used motor oils can be used as lubricants for mechanisms in the textile industry, anti-corrosion coatings, anti-dust compositions and auxiliary technical means. The use of regenerated oils reduces the cost of purchasing new lubricants, reduces the volume of industrial waste and reduces the impact on the environment.

Conclusion

An analysis of a sample of motor oil was performed using the Fourier transform infrared spectroscopy (FTIR) method, and characteristic spectra were obtained, including absorption lines characteristic of hydrocarbon oils and additives. The IR spectroscopy method allowed us to confirm the type of oil and determine its chemical composition without damaging the sample. The use of IR spectral analysis in combination with oil regeneration processes is an economically viable and environmentally sound solution that ensures the uninterrupted operation of textile enterprises.

References

Majidov A.Kh., Sharipov K. A. Osnovy ochistki masel. Tashkent, Science. 2000. – 140 p.
Pentin Yu. A., Vilkov L. V. Fizicheskie metody issledovaniya v khimii. –M.: Mir, 2003. –683 p.
Tarasevich B. N. IR spectrum osnovnykh klasov organicheskikh soedineniy. Reference material. – Moscow, 2012. – 55 p.
Abhishek Kumar, Avinish Kumar. Performance Characterization of Lubricants. CRC Press, Boca Raton FL USA-2024.

submitted 12.08.2025;
accepted for publication 27.08.2025;
published 29.09.2025

Contact: nodirbekdoc2020@gmail.com

The Austrian Journal of Technical and Natural Sciences, No 7–8
ISSN 2310-5607

PREMIER Publishing
ppublishing.org

DOI:10.29013/AJT-25-7.8-126-130

OPERATING CHARACTERISTICS OF OILS USED IN THE TEXTILE INDUSTRY AND METHODS OF THEIR REGENERATION

Davletov Zafar [1], Kobilov Nodirbek [2], Nasullaev Khikmatullo [2], Gulomov Shuxratqodir [2], Igamkulova Nargisa [1]

[1] Tashkent Institute of Chemical Technology, Tashkent, Uzbekistan

[2] Uzbekistan scientific research of chemical-pharmaceutical institute, Tashkent, Uzbekistan

Cite: *Davletov Z., Kobilov N., Nasullaev Kh., Gulomov Sh., Igamkulova N. (2025). Operating Characteristics of Oils Used in the Textile Industry and Methods of Their Regeneration. Austrian Journal of Technical and Natural Sciences 2025, No 7–8.* https://doi.org/10.29013/AJT-25-7.8-126-130

Abstract

The article presents the main operational characteristics of oils used in the textile industry and methods of their recovery. methods of oil recovery used in the textile industry, technological processes and their comparative descriptions are given.

Keywords: *oil, technology, properties, description, operation, method*

Introduction

The frictional properties of working parts in the textile industry lead to their wear, overheating and shortening of their service life. Therefore, it is necessary to constantly lubricate the rubbing surfaces. This task is performed by the lubrication system. A certain amount of mechanical energy is spent on overcoming friction. As a result of lubrication, the power required to overcome friction decreases, the wear of the rubbing surfaces slows down, and the heat released during the friction process is removed. At the same time, the oil washes away crushed particles and various contaminants from the rubbing surfaces, protects the surfaces from rust, and in some cases prevents the formation of deposits on neighboring moving surfaces (Zagidullin et al., 2016).

During the operation of machines, the quality of the oil deteriorates due to metal particles, oxidation and contamination. Also, a decrease in the amount of additives that provide good lubricating properties of the oil leads to a decrease in its quality. Mechanical impurities are metal particles and additives that are formed when two friction surfaces slide.

Mineral impurities (sand, dust) enter the engine through the air and reduce the lubricating properties of the oil. The amount of mechanical impurities in the oil composition should not exceed 0.2% (Rylyakin E. G. and Voloshin A. I., 2015).

Quantitative changes in the oil include the loss of light fractions due to evaporation, combustion and dispersion. Qualitative changes are associated with chemical

changes in the substances in the oil, oxidation products and polymerization, combustion products of fuel and oil, dust, water and other contaminants.

Under operating conditions, textile oil must maintain sufficient fluidity and high colloidal stability at low temperatures. High fluidity at low temperatures ensures good flow of the oil into the friction nodes, sealing gaps, forming a film separating the friction surfaces and, as a result, reducing friction and wear (Abishek, 2024).

The need to operate in low-temperature regions and store equipment for long periods of time requires attention to the low-temperature properties of motor oils and their behavior in conditions of high humidity condensation. Condensation of water in the oil leads to its loss of stability and deterioration of its quality. The high colloidal stability of the oil, especially in the presence of water, ensures its performance, minimizes rust and corrosion (including corrosion-mechanical wear), as well as oxidation and the formation of various deposits (Majidov and Sharipov, 2000).

Materials and methods

In the textile industry, oils and lubricants are used for the following purposes: lubrication of bearings, shafts, chains and guides; protection of fibers from static electricity and improvement of their fluid movement; protection of metal parts from rust.

Mineral, synthetic or emulsion oils are often used, with the addition of SFM, anti-rust and antistatic additives. During operation, such oils are contaminated with fibers, dust, water, paints, oxidation products and form emulsions, which reduces their performance. In order to extend the service life and reduce costs, oils are regenerated – their properties are restored and the possibility of further use is created.

Used lubricating oil (ULO) is considered hazardous as it is able to cause pollution and affect the environment. The presence of degraded additives, contaminants, and by-products of degradation render ULO more toxic and harmful to health and environment than virgin base oils. Recovery of ULO generally comprises cleaning, drying, and adsorption in order to eliminate water, sludge, and impurities. As the ULO is one of the hazardous wastes generated in various industries, such as industrial and automotive, it should not be used or disposed of in ways that are harmful for the environment. Recovery of ULO carries out many advantages which includes lower environmental impact, higher energy saving and lower risks. The main objective of this paper was to thoroughly review various recovery process principles and treatment methods for ULO. Importance of ULO recycling and various techniques along with their limitations were also discussed. The significance of this study lies in reviewing the roles of adsorbent and adsorption reclamation processes of ULO and few promising adsorbents were earmarked for further study (Anisuzzaman S. M. et al., 2021).

The contamination characteristics of textile oils are such that, compared to motor oils, they contain fewer metal particles; more organic fibers and dust; paints and pre-treatment chemicals; water and emulsions; SFM and tarry deposits.

Results and discussion

In this regard, we have developed methods for cleaning oils used in the textile industry.

The main methods of regeneration of textile oils:

1. Mechanical cleaning. Filtration through fabric, paper or fine-mesh filters – removal of fibers, dust and large mechanical impurities. Centrifugation – separation of water and fine dispersed particles. Sedimentation – used as a preliminary stage.

2. Physico-chemical cleaning. Coagulation and flotation – removal of emulsified water droplets and surfactants (PAVs). Sorption cleaning – activated clays, silica gel or zeolites are used to remove coloring substances, resins and oxidation products. Demulsification – heating and adding special reagents to destroy stable emulsions.

3. Heat treatment. Vacuum drying – removal of moisture and volatile substances under reduced pressure. Inert gas (nitrogen) blowing and heating – prevents oxidation during heating.

4. Chemical re-purification. Treatment with alkaline solutions – neutralization of acid products formed as a result of oxidation.

Adsorption on activated carbon – improvement of the color and odor of the oil. Additives – addition of additives to restore antistatic and anti-corrosion properties.

The figure and table below show regeneration methods for reusing motor oils in the textile industry.

Figure 1. *Used oil purification methods*

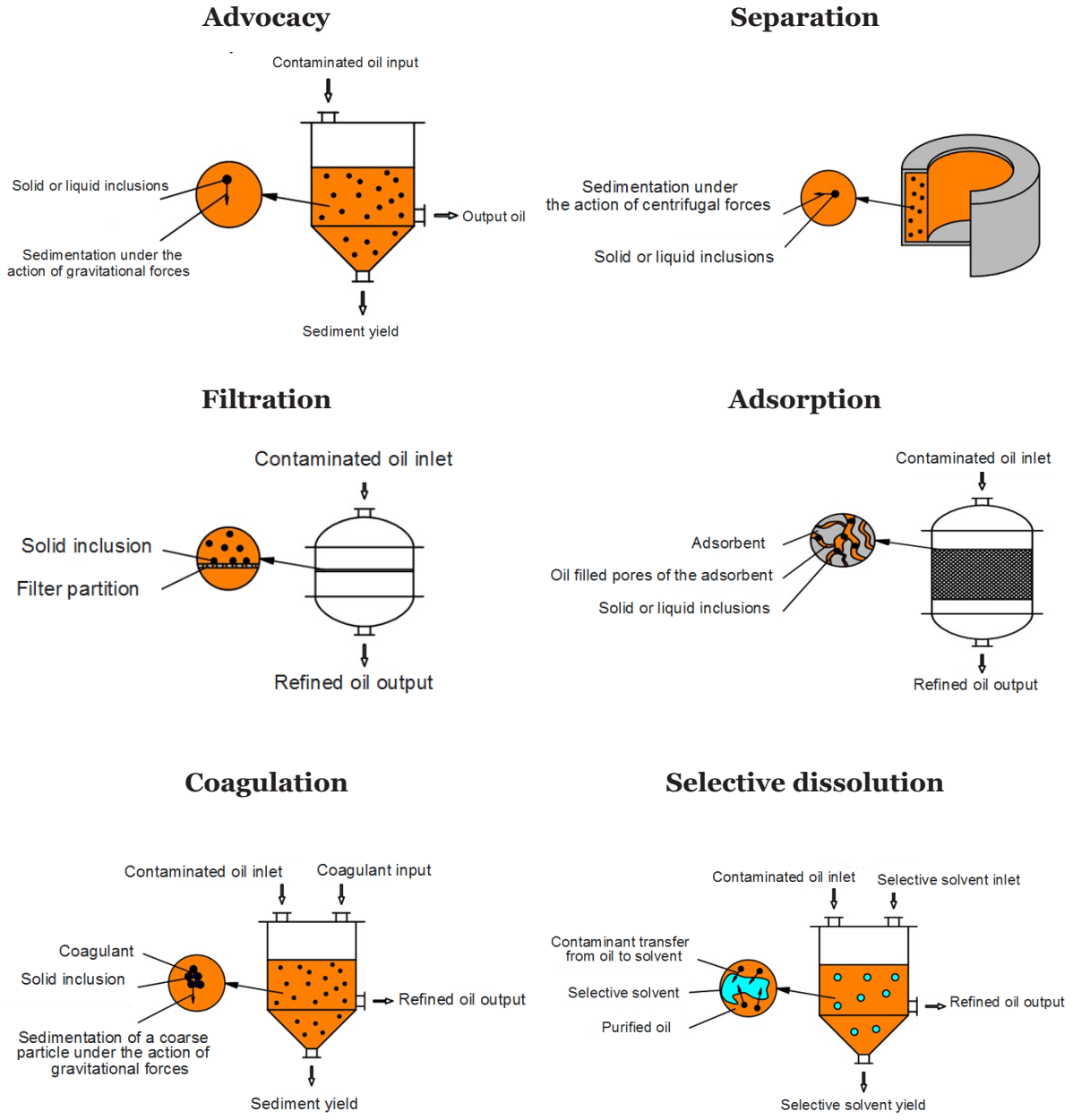

Thus, the regeneration of oils used in the textile industry is an important element of efficient and environmentally friendly production. The analysis shows that the best results can be achieved when using a complex cleaning scheme that includes mechanical, physicochemical, thermal and chemical methods, followed by the addition of additives. This approach allows: to remove up to 90–95% of contaminants of various nature, restore the main operational properties of the oil, reduce the cost of purchasing new lubricants by 30–60%, and reduce the negative impact on the environment by reducing the volume of hazardous waste.

Table 1. *Comparative descriptions of used oil regeneration methods in the textile industry*

Methods	Contamination	Cleaning efficiency	Costs	Advantages	Disadvantages	Applications
Landing	Large particles, sediment	40–50%	Low	Simplicity, no complex equipment	Requires a long time, ineffective for fine particles	Initial cleaning
Filtration	Fibers, dust, mechanical particles	50–70%	Low-medium	Simplicity, possibility of automation	Filter replacement required	Initial and intermediate cleaning
Centrifuge	Fine particles, water	70–85%	Medium–high	High speed, good water separation	Requires expensive equipment	Primary cleaning in enterprises using large volumes of oil
Coagulation and flotation	Emulsions, SFM, water	75–90%	Medium	Effective breaking of stable emulsions	Reagents and pH control required	Basic and additional purification
Sorption purification	Dyes, resins, oxidation products	80–95%	Medium	Improves color, odor, stability	Requires regeneration or disposal of the sorbent	Final purification
Vacuum drying	Water, volatile matter	85–95%	Medium–high	Removes moisture without strong heating	Consumes a lot of energy	After mechanical or chemical cleaning
Chemical neutralization	Acidic oxidation products	90–95%	Medium	Restores average pH and stability	Produces alkaline wastewater	Final cleaning before adding additives
Additive addition	Lack of functional properties	-	Medium	Fully restores operational properties	Does not remove impurities	Final stage

Conclusion

Regeneration of oils used in the textile industry is not only economically acceptable, but also an important environmental safety measure. Modern technologies allow recovery of 70–90% of the original oil resource, which reduces the need for processing of petroleum products, reduces the amount of hazardous waste, and plays an important role in protecting the environment.

References

Abhishek Kumar, Avinish Kumar. Performance Characterization of Lubricants. CRC Press, Boca Raton FL USA-2024.

Zagidullin S.Kh., Dolganov V. L., Lykov A. N., Kiselyov A. M. Development of a new method of thermal mineralization problem. Chemical technology and biotechnology. Vestnik PNIPU. – No. 4. 2016. – P. 129–137.

Rylyakin E. G., Voloshin A. I. Ochistka i vosstanovlenie masel. “Molodoy uchyonyy” Ejemesyachnyy nauchnyy journal. g. Kazan. – No. 1 (81). January, 2015. – P. 92–94.
Anisuzzaman S. M., Muhammad Hazaruddin, N. N. M. Nasir. Used lubricating oil recovery process and treatment methods: A review. 2021. IOP Conference Series Materials Science and Engineering 1195(1):012031
Majidov A. H., Sharipov K. A. Osnovy ochistki masel. – Tashkent, Science. 2000. – 140 p.

submitted 08.06.2025;
accepted for publication 22.06.2025;
published 29.09.2025

Contact: nodirbekdoc2020@gmail.com

The Austrian Journal of Technical and Natural Sciences, No 7–8
ISSN 2310-5607

PREMIER Publishing
ppublishing.org

DOI:10.29013/AJT-25-7.8-131-135

PHYSICAL AND CHEMICAL STUDY OF SAPROPEL OF KUSHKANATAU FIELD OF KARAKALPAKSTAN

Tajibaev Turganbay Ansatbaevich [1], Allaniyazov Davran Orazimbetovich [2], Erkayev Aktam Ulashevich [3], Ochilov Siroj Urazboy uli [2], Kurbiyazov Dilshodbek Kuanishbay uli [2]

[1] Applicant Karakalpak Research Institute of Natural Sciences, Karakalpak Branch Academy of Sciences of the Republic of Uzbekistan,

[2] Karakalpak Research Institute of Natural Sciences, Karakalpak branch of Ruz

[3] Department of Chemical Technology of Inorganic Substances, Tashkent Institute of Chemical Technology, Tashkent

[4] Chemistry Laboratory, Karakalpak Research Institute of Natural Sciences, Karakalpak branch of Ruz

Cite: *Tajibaev T.A., Allaniyazov D.O., Erkayev A.U., Ochilov S.U., Kurbiyazov D.K. (2025). Physical and Chemical Study of Sapropel of Kushkanatau Field of Karakalpakstan. Austrian Journal of Technical and Natural Sciences 2025, No 7–8.* https://doi.org/10.29013/AJT-25-7.8-131-135

Abstract

This paper examines the chemical composition and properties of the sapropel of the Kushkanatau field located in the territory of Karakalpakstan. Sapropel is a widespread deposit with a large number of micro and macro elements. The article shows the possible uses of the mineral sapropel and their role in the agricultural sector. The results of the existing experience in the use of sapropel in agriculture show that sapropel has the property of restoring soil fertility due to the content of various trace elements that increase soil fertility. Along with this, the water-retaining property of sapropel will allow more rational use of water.

Keywords: *Karakalpakstan, Kushkanatau, sapropel, fertilizers, trace elements, agriculture, crop production*

Introduction

Sapropel – bottom sediments of various freshwater reservoirs. The name came from the Greek words sapros – "rotten" and pelos – "dirt." Natural coloration varies from pink to dark brown. In the air, the natural color disappears. Sapropel forms the remains of animals and plants, as well as mineral and organic impurities brought by wind and water (Wildflush I. R., Kukresh S. P., Ionas V. A., 2001). It contains at least 15% organic matter, including ligninohumus complex, carbohydrates, bitumens, and other substances in a colloidal state. Sapropel

can range in color from pink to dark brown, and hardens when dried. Sapropel mud is used in medicine to treat various diseases, including atherosclerosis, chronic hepatitis, peptic ulcer disease and others (Kama sapropel http://sapropel.su).

Sapropel is a valuable organic fertilizer that improves soil structure, provides plants with nutrients and increases yields. It can be used as a pre-sowing fertilizer, when planting trees and shrubs, as well as in greenhouses (Kireicheva L. V., Khokhlova O. B., 2004).

In agriculture, sapropel is used as a fertilizer (after freezing, water is separated, the structure is a loose state). Especially effective is the use on acidic and light sandy and sandy loamy soils, as well as to increase the humus content in soils (dose for crops 30–40 t/ha; for vegetable, potato and fodder root crops 60–70 t/ha), for compost preparation (Sapropel. 1991).

The use of sapropel as a fertilizer improves the mechanical structure of soils, moisture-absorbing and water-retaining ability and aeration, gives an increase in humus soil, activates soil processes. Sapropel fertilizer helps to mobilize the soil composition, leads to self-purification from pathogenic plants, fungi and harmful microorganisms. Studies of scientists have found that the mineral part of sapropels contains a large number of vitamins macro and trace elements, such as: Co, Mn, Cu, B, Br, Mo, V, Cr, Be, Ni, Ag, Sn, Ba, Sr, Ti (Dubinina L. F., 1974; Mishin G. M., 1966).

Sapropel is used for direct application to the soil as well as for land reclamation, sanitation and restoration (Wildflush I. R., Kukresh S. P., Ionas V. A., 2001; Kama sapropel http://sapropel.su; Kireicheva L. V., Khokhlova O. B., 2004; Sapropel // 1991).

The organic matter of sapropel is a combination of plant and animal residues, as well as their decay products. It includes products of hydrolysis of biopolymers, polymer compounds formed in the process of biotic and abiotic destruction, products of synthesis of organic substances, as well as products of microorganisms. The organic matter of sapropel is characterized by a low carbon content (4,7–6,0%) and a fairly high oxygen content (23–39%) (Lishtvan I. I., Lopotko M. Z., 1976; Plaksin G. V., Likholobov V. A., Krivonos O. I., 2008).

According to L. R. Mukina, studies show that sapropel-based fertilizers support a positive balance of nitrogen and phosphorus. After the test experiments, the content of mobile phosphorus increased compared to the control (version without fertilizers). A particularly significant accumulation of the element was observed during the application of fresh and activated sapropel, vermicompost and granulated peat zeolite fertilizers. The maximum increase in the yield of barley green mass on floodplain soil was obtained by saturating the additives with mineral fertilizers in the version using a vermicompost and fresh sapropel mined from a depth of 2–2,5 m (Mukina L. R., 2008).

The chemical composition and properties of sapropels of various deposits differ significantly and are determined by the conditions of formation, as well as the diversity of the flora and fauna of the lakes. Also classification of sapropel type is Carbonate, silica, organic, ferrous

Biologically active components include nitrogenous and hormone-like compounds, enzymes, vitamins, carotenes and pigments. The mineral part consists of compounds of iron, magnesium, potassium and other elements.

Research objects and methods

The object of the study in this study is the sapropel of the Kushkanatau field of Karakalpakstan, located 130 km from Nukus in the Bozatau region. It is a calcareous raw material often found in lakes and under peat beds. When choosing sapropel for fertilizers, acidity indicators, nitrogen, calcium and other trace elements are important. These characteristics may vary depending on the location of production. Fresh sapropel from a great depth contains more nutrients, but has low ash content.

Research results and their analysis:

These raw materials were subjected to X-ray phase analysis. From Fig. 1. it can be seen that the following diffraction band peaks are observed in the sapropel composition; calcium strontium aluminosilicate 28%, Code Reference 01-075-9267, chemical formula $Na_{0.84}Ca_{0.16}Al_{1.16}Si_{2.84}O_8$;

Figure 1. *Diffractogram of sapropella in Kushkanatau field*

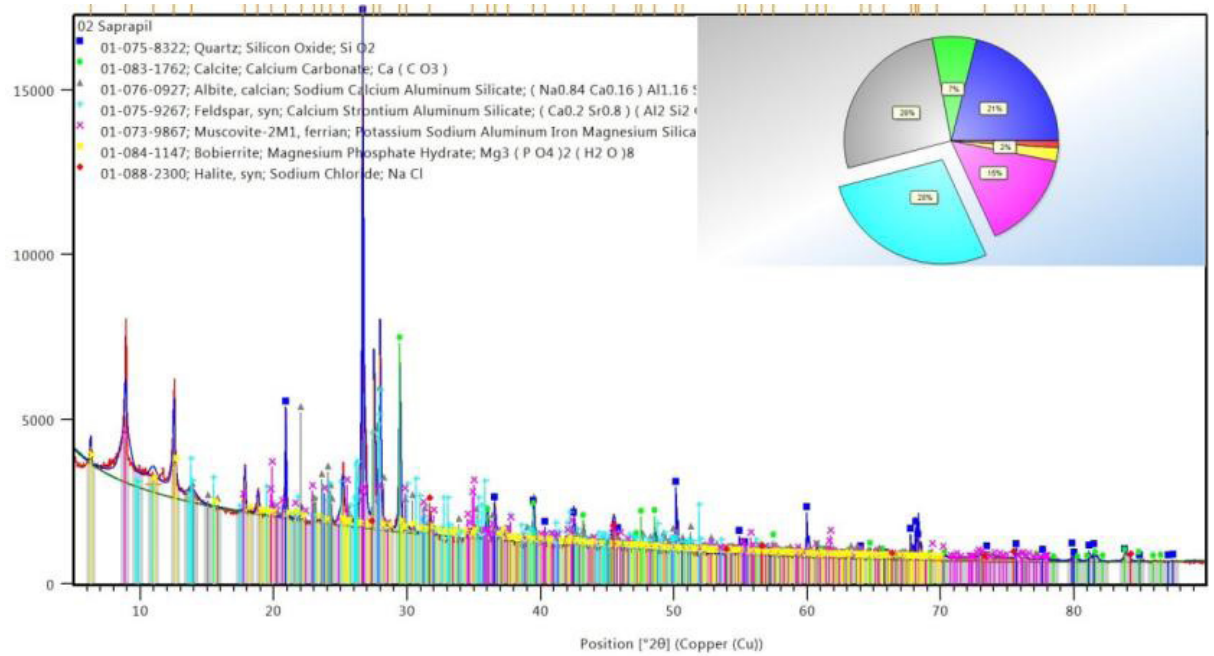

Figure 2. *SEM Micrographs and EDR analysis of Sapropel of the Kushkanatau Field*

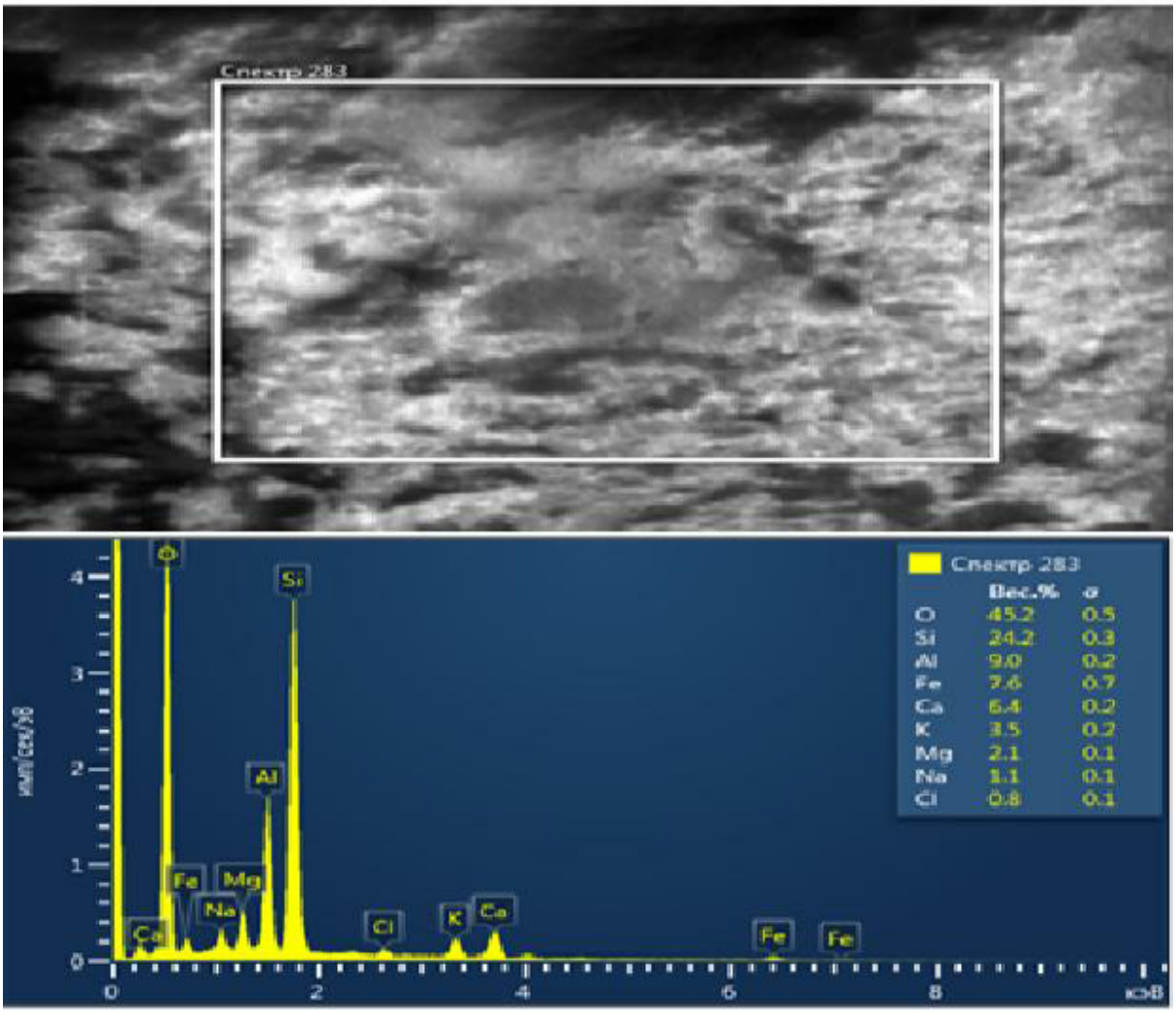

Sodium calcium aluminosilicate 26%, reference 01–076–0927 chemical formula $Ca_{0.2}Sr_{0.8}Al_2Si_2O_8$; silicon oxide 21%, reference 01–075–8322, chemical formula SiO_2, Potassium, Sodium, Aluminum, Iron, Magnesium, Silicate, Hydroxide 15%, reference 01–073–9867, chemical formula $K_{0.93}Na_{0.07}Al_{1.66}Fe_{0.18}Mg_{0.16}Al_{0.82}Si_{3.18}O_{10}(OH)_2$; Calcium carbonate 7%, 01–083–1762 formula $CaCO_3$, Magnesium phosphate hydrate 2%, 01–084–1147 formula $Mg_3(PO_4)_28H_2O$, sodium chloride 1%, 01–088–2300 formula NaCl; The sample consists mainly of calcium carbonate, aluminum, iron, sodium, magnesium, potassium, silicon (Allaniyazov D. O., 2019; Allaniyazov D. O., Erkaev A. U., 2019; Allaniyazov D. O., Tazhibaev T. A., Ochilov S. U., 2024; Allaniyazov D. O., Erkaev A. U., 2022).

Further, sapropel powders of the Kushkanatau deposit were analyzed using SEM, and elemental compositions of this sample were simultaneously determined using an energy dispersion analyzer. Electron microscopic images are shown in Fig.2.

The following chemical elements were recorded in the energy dispersion spectrum with the following percentage correspondences; oxygen 45.2; silicon 24.2; aluminum 9,0; iron 7,6; calcium 6,4; potassium 3,5; magnesium 2,1; sodium 1,1 and chlorine 0,8. Sapropel processing has the potential to increase agricultural yields. However, it is necessary to develop technologies to create competitive fertilizers.

Conclusions

Physical and mechanical characteristics and chemical composition of sapropel of Kushkanatau deposits are presented. Methods are described for determining the chemical composition, as well as conducting physicochemical studies of sapropel. For this, radiographic, electron microscopic studies were carried out on modern devices. According to our study, the sample consists mainly of calcium carbonate, aluminum, iron, sodium, magnesium, potassium, silicon.

Summing up, it should be noted that sapropel is widespread in most lakes in the regions of Karakalpakstan. This opens up great opportunities for using it to increase agricultural yields due to its unique properties. However, for this it is necessary to develop a comprehensive technology for the production of complex fertilizers, which is competitive with foreign counterparts.

References

Wildflush I. R., Kukresh S. P., Ionas V. A. Agrochemistry: Textbook – 2nd ed., Add. And revised. – Mn.: Urajai, 2001. – 488 p., Ill.

Kama sapropel http://sapropel.su

Kireicheva L. V., Khokhlova O. B. Fertilizing and reclamation mixtures based on sapropels // Fertility, 2004. – No. 4. – P. 26–28.

Sapropel // Encyclopedic reference book “Tver region.” Lake deposits of sapropel of the Tver region. – M., 1991.

Dubinina L. F. On the question of sources of accumulation of trace elements in sapropels / L. F. Dubinina, K. N. Telezhnikova, L. B. Datsuk // Theses of the 2nd Republic Scientific Conference. Problems of using sapropel in the national economy. – Minsk, 1974. – P. 40–41.

Mishin G. M. Physical and Chemical Qualities of Middle Ural Sapropels / G. M. Mishin // Second Inter-Branch Scientific Conf. on the use of sapropels in agriculture. – Sverdlovsk, 1966. – P. 83–85.

Lishtvan I. I., Lopotko M. Z. The use of sapropels in the national economy // Problems of the use of sapropels in the national economy. – Minsk: Science and Technology, 1976. – P. 5–13.

Plaksin G. V., Likholobov V. A., Krivonos O. I. Sapropel, as a source of chemical products // Sapropel and its processing products. International. scientific-prose. conf. – Omsk, 2008. – P. 5–7.

Mukina L. R. Efficiency of sapropel and sapropel-based organomineral fertilizers application on floodplain irrigated soils of Krasnoyarsk Krai//Sapropel and its processing products. International. scientific-prose. conf. – Omsk, 2008. – P. 17–20.

Allaniyazov D. O. Development of scientific foundations of processes for production and technology of complex fertilizers from glauconites and phosphorites of Karakalpakstan Diss. Ph D. – Tashkent IONH AN RUz, 2019. – 123 p.
Allaniyazov D. O., Erkaev A. U. Enrichment of Karakalpakstan glauconite by dry method. International Scientific Journal "National Association of Scientists" (NAU) ISSN 2413-5291, 2021. – Vol. 2. – No. (36_63). – P. 4–8.
Allaniyazov D. O., Erkayev A. U., Tajibayev T. A., Ochilov S. U., processing of local agro ores of Karakalpakstan for high-efficiency fertilizer. Journal of Survey in Fisheries Sciences 2023. – 10(3S). – P. 1225–1232.
Allaniyazov D. O., Tazhibaev T. A., Ochilov S. U. Application of agricultural ore of Karakalpakstan as complex fertilizers. Collection of materials of the V International Scientific and Theoretical Conference "Actual Issues of Natural Sciences". 2024. – P. 566–569.
Allaniyazov D. O., Erkaev A. U., Study of agrochemical effect of obtained new types of complex fertilizers based on Karakalpakstan agro-ore with various mineral fertilizers. International Journal of Advanced Research in Science and Technology, Int. J. Adv. Res. Sci. Technol. – Volume 11. – Issue 12. 2022. – P. 881–886.

submitted 10.08.2025;
accepted for publication 24.08.2025;
published 29.09.2025

Contact: tajibaevishturganbay@gmail.com; dauran_1985@mail.ru; dauran_1985@mail.ru;
sochilovs9777@gmail.com; dilshodbekkurbiyazov@gmail.com

Contents

Section 1. Chemistry